FLOW-FIELD CHARACTERISTICS AND AERODYNAMIC LOADS ON EXTERNAL STORES NEAR THE FUSELAGE AND WING-PYLON POSITIONS OF A SWEPT-WING/FUSELAGE MODEL AT MACH NUMBERS OF 0.4 AND 0.7 – PHASE V

R. H. Roberts and J. R. Myers

ARO, Inc.

March 1974

Approved for public release; distribution unlimited.

PROPULSION WIND TUNNEL FACILITY
ARNOLD ENGINEERING DEVELOPMENT CENTER
AIR FORCE SYSTEMS COMMAND
ARNOLD AIR FORCE STATION, TENNESSEE

NOTICES

When U. S. Government drawings specifications, or other data are used for any purpose other than a definitely related Government procurement operation, the Government thereby incurs no responsibility nor any obligation whatsoever, and the fact that the Government may have formulated, furnished, or in any way supplied the said drawings, specifications, or other data, is not to be regarded by implication or otherwise, or in any manner licensing the holder or any other person or corporation, or conveying any rights or permission to manufacture, use, or sell any patented invention that may in any way be related thereto.

Qualified users may obtain copies of this report from the Defense Documentation Center.

References to named commercial products in this report are not to be considered in any sense as an endorsement of the product by the United States Air Force or the Government.

FLOW-FIELD CHARACTERISTICS AND AERODYNAMIC LOADS ON EXTERNAL STORES NEAR THE FUSELAGE AND WING-PYLON POSITIONS OF A SWEPT-WING/FUSELAGE MODEL AT MACH NUMBERS OF 0.4 AND 0.7—PHASE V

R. H. Roberts and J. R. Myers
ARO, Inc.

FOREWORD

The work reported herein was conducted by the Arnold Engineering Development Center (AEDC) and sponsored by the Air Force Flight Dynamics Laboratory (AFFDL/FGC), Air Force Systems Command (AFSC), under Program Element 62201F, Project 8219.

The test results presented were obtained by ARO, Inc. (a subsidiary of Sverdrup & Parcel and Associates, Inc.), contract operator of AEDC, AFSC, Arnold Air Force Station, Tennessee. The test was conducted from July 13, 1972 through February 10, 1973, under ARO Project No. PA028. The manuscript was submitted for publication on April 12, 1973.

This technical report has been reviewed and is approved.

L. R. KISSLING
Lt Colonel, USAF
Chief Air Force Test Director
Directorate of Test

FRANK J. PASSARELLO
Colonel, USAF
Director of Test

ABSTRACT

Experimental data were obtained to aid in the prediction of aerodynamic loads and separation-trajectory characteristics on stores under the influence of an aircraft flow field. Four types of data were obtained in the vicinity of a generalized aircraft model: (1) flow field surveys, using a 40-deg cone probe, to determine the local velocity field, (2) force and moment data on four store models, (3) pressure distribution data on an ogive-cylinder model, and (4) captive-trajectory store separation data on one store model. The generalized aircraft model consisted of a swept-wing/fuselage combination with rectangular, flow-through engine ducts. Pylon locations were on the fuselage centerline and at the wing 1/3-semispan. The effect of a systematic variation of duct flow was investigated in each phase of testing. Testing was accomplished at Mach numbers 0.4 and 0.7, a Reynolds number of 3.6 million per foot, and aircraft and store angles of attack varying from 0 to 15 deg. Results of the test show that duct flow had little effect on the parameters investigated on all phases of testing, except at the higher Mach number where small variations in the coefficients or trajectories were evident. In general, the variations of parameters investigated for all test configurations followed an orderly pattern and should be amenable to the formulation of a generalized analytical store separation prediction method.

CONTENTS

APPENDIXES

I. ILLUSTRATIONS

Figure

Figure | Page

Figure | Page

II. TABLES

NOMENCLATURE

C_A Axial-force coefficient, (measured total axial force)/$q_\infty S$

C_m Pitching-moment coefficient referenced to the store midpoint, (pitching moment)/$q_\infty Sd$

C_N Normal-force coefficient, (normal force)/$q_\infty S$

C_n Yawing-moment coefficient referenced to the store midpoint, (yawing moment)/$q_\infty Sd$

C_Y	Side-force coefficient, (side force)/$q_\infty S$
cg	Center of gravity
d	Store reference diameter, ft
h	Altitude, ft
I_{xx}	Full-scale moment of inertia about the store longitudinal axis, slug-ft^2
I_{yy}	Full-scale moment of inertia about the store lateral axis, slug-ft^2
I_{zz}	Full-scale moment of inertia about the store vertical axis, slug-ft^2
ℓ_p	Location of duct-flow controller plug measured from duct-closed position, in.
M_∞	Free-stream Mach number
$\overline{m}$	Store mass, slugs
p_∞	Free-stream static pressure, psfa
q_∞	Free-stream dynamic pressure, $0.7p_\infty M_\infty^2$, psf
Re	Free-stream unit Reynolds number, per foot
S	Store maximum cross-sectional area, ft^2
t	Real trajectory time from initiation of trajectory, sec
V_{duct}	Velocity in the duct, ft/sec
V_∞	Free-stream velocity, ft/sec
W_1	Initial vertical downward velocity of the store cg, ft/sec
X	Axial displacement of the store cg relative to the carriage position on the pylon in the flight-axis coordinate system, ft, full scale
X′	Axial displacement of the store cg relative to the carriage position on the pylon in the fuselage coordinate system, in., model scale
X_{cg}	Longitudinal cg location from nose, ft, full scale
X_p	Axial displacement of the flow field probe tip relative to the fuselage nose station in the fuselage coordinate system, in.

Y Lateral displacement of the store cg relative to the carriage position on the pylon in the flight-axis coordinate system, ft, full scale

Y' Lateral displacement of the store cg relative to the carriage position on the pylon in the fuselage coordinate system, in., model scale

Y_p Lateral displacement of the flow field probe tip relative to the fuselage centerline in the fuselage coordinate system, in.

Z Vertical displacement of the store cg relative to the carriage position on the pylon in the flight-axis coordinate system, ft, full scale

Z' Vertical displacement of the store cg relative to the carriage position on the pylon in the fuselage coordinate system

Z_p Vertical displacement of the flow field probe tip relative to the fuselage centerline in the fuselage coordinate system, in.

α Angle of attack of the store model, flow field probe, or wing-fuselage model, deg

$\Delta\theta$ Angle between the store longitudinal axis and its projection in the X_{PY}-Y_{PY} plane, positive when the store nose is raised as seen by the pilot

$\Delta\phi$ Store model roll angle, positive in the clockwise direction looking upstream, deg

$\Delta\psi$ Angle between the projection of the store longitudinal axis in the X_{PY}-Y_{PY} plane and the X_{PY} axis, positive when the store nose is to the right as seen by the pilot

FLIGHT-AXIS-SYSTEM COORDINATES

X_F Parallel to the free-stream wind vector, positive in the upstream direction

Y_F Perpendicular to the free-stream wind vector in the horizontal plane, positive to the right looking upstream

Z_F Perpendicular to the X_F and Y_F directions, positive in the downward direction

FUSELAGE COORDINATE SYSTEM

X_{PY} Parallel to the fuselage axial centerline, positive in the downstream direction

X_{PY} Perpendicular to the fuselage centerline and parallel to the wing chord plane, positive to the left looking upstream

Z_{PY} Perpendicular to the wing chord plane, positive in the downward direction

SECTION I
INTRODUCTION

This investigation was conducted in the Aerodynamic Wind Tunnel (4T) to obtain data to aid in the development of a generalized theoretical method for predicting separation characteristics of stores from high-speed fighter-bomber aircraft. The large number of stores that may be carried at one time by present fighter-bomber aircraft poses a complex problem. To acquire a basic understanding of the nature of the problem and the related sources of difficulty that may arise during store separation under these circumstances, the flow-field characteristics in the vicinity of the store resulting from the aircraft fuselage, wing, pylons, racks, and adjacent stores must be known. This information, along with corresponding force data and pressure distribution data on the store model, should provide a reasonable foundation for the formulation of an accurate prediction method.

Four types of data were obtained in the vicinity of a generalized aircraft shape with and without pylons and simulated engine ducts installed. The data consisted of (1) flow-field surveys, using a 40-deg cone probe, to determine the local velocity field, (2) force and moment data on four store models, (3) pressure distribution data on an ogive-cylinder store model, and (4) captive-trajectory store-separation data on one model. The effect of a systematic variation of duct flow rate was investigated on each phase of testing. In addition to the tests with the store in the vicinity of the aircraft model, free-stream data were obtained on two of the store models.

The aircraft model consisted of a swept-wing/fuselage combination with rectangular flow-through engine ducts. Pylon locations were on the fuselage centerline and at the wing 1/3-semispan. This model represented a generalized aircraft shape and was installed on the main tunnel support system. Store models and the flow probe were supported from the Captive Trajectory Support (CTS) system.

Testing was accomplished at M_∞ = 0.4 and 0.7, Re = 3.6 million per foot, and aircraft angles of attack from 0 to 15 deg.

SECTION II
APPARATUS

2.1 TEST FACILITY

The Aerodynamic Wind Tunnel (4T) is a closed-loop, continuous flow, variable-density tunnel in which the Mach number can be varied from 0.1 to 1.3. At all Mach numbers, the stagnation pressure can be varied from 300 to 3700 psfa. The test section is 4 ft square and 12.5 ft long with perforated, variable porosity (0.5- to 10-percent open) walls. It is completely enclosed in a plenum chamber from which the air can be evacuated, allowing part of the tunnel airflow to be removed through the perforated walls of the test section.

Two separate and independent model support systems were used during the test. The parent model was inverted in the test section and supported by an offset sting attached to the main pitch sector. The flow probe and store models were supported by the CTS which extends down from the tunnel top wall. The CTS system provides store movement (six degrees of freedom) independent of the parent aircraft model. An isometric drawing of a typical store-parent installation is shown in Fig. 1, Appendix I.

Also shown in Fig. 1 is a block diagram of the computer control loop used during tests employing the CTS system. The analog system and the digital computer work as an integrated unit and, along with the required input information, control the CTS movement during testing. Store (or probe) positioning is accomplished by use of six individual d-c electric motors. Maximum translational travel of the CTS is ±15 in. from the tunnel centerline in the lateral and vertical directions and 36 in. in the axial direction. Maximum angular displacements are ±45 deg in pitch and yaw and ±360 deg in roll. A schematic showing the test section details and the location of the models in the tunnel is shown in Fig. 2.

2.2 TEST ARTICLES

The probe used to obtain the flow-field data was attached directly to the CTS and consisted of a single cone-cylinder with a 40-deg included-angle tip. There were four equally spaced static-pressure orifices on the surface of the cone and a total-pressure orifice at the apex of the cone. Details and dimensions of the probe are shown in Fig. 3, and a photograph of the probe is presented in Fig. 4. Details and dimensions of the force models are shown in Fig. 5, and a photograph of the models is shown in Fig. 6. The ESUU-41 model is an axisymmetric store with the same cross-sectional area distribution as the SUU-41. The force models were mounted on a six-component, internal strain-gage balance that was attached to the CTS.

The pressure distribution model used during the test was an ogive-cylinder model having the same external geometry as the unfinned large force model. The pressure distribution model and support sting were an integral unit that attached directly to the CTS. Nineteen axially aligned pressure orifices were located on the model surface at evenly spaced increments along the model length. Details and dimensions of the pressure model are shown in Fig. 7, and a photograph of the model is shown in Fig. 8.

A sketch of the wing/fuselage model used during the test is shown in Fig. 9. The wing had a 45-deg sweep at the quarter-chord line, an aspect ratio of four, a taper ratio of 0.3, and six-percent-thick uncambered airfoil sections parallel to the plane of symmetry. Coordinates of the model airfoil sections are tabulated in Fig. 9. During this investigation, combinations of two fuselage bodies and two noses were used. Details and dimensions of the long fuselage, short fuselage, cambered nose, and uncambered nose with canopy are shown in Fig. 10. Details and dimensions of the body add-on without ducts are shown in Fig. 11, and details of the body add-on with ducts are shown in Fig. 12. Each duct

was instrumented with five pressure orifices: static taps on the two side walls and the bottom wall, and two total-head probes in the duct opening. Figure 13 shows the duct flow controller assembly, which is used in conjunction with the body add-on with ducts. The assembly locates plugs at a specified distance from the duct exit in order to control the mass flow rate through the duct.

The model had provisions for mounting pylons at the fuselage centerline and on the left wing at the 1/3- and 2/3-semispan stations. Details of the pylons are shown in Fig. 14, and a photograph of the pylons is presented in Fig. 15. The touch wires shown on the pylons are discussed in the following sections. Tunnel installation photographs showing the wing/fuselage model, ducts, and store models are presented in Fig. 16.

2.3 INSTRUMENTATION

Static and total pressures on the cone probe were measured using 5-psid transducers, and all pressures on the pressure distribution model and in the ducts were measured using 15-psid transducers. A six-component, internal strain-gage balance was used to obtain the force and moment data on the force models. Translational and angular positions of the probe and store models were obtained from the CTS analog outputs. The aircraft-model angle of attack was set using the main sting support and readout system. The pylons were instrumented with touch wires, and the system was electrically wired to give a visual indication on the control console when contact between the store and touch wire was made. The system was also electrically connected to automatically stop the CTS movement if the store model or CTS inadvertently contacted the parent model, its support sting, or the test section walls.

SECTION III
TEST DESCRIPTION

3.1 TEST CONDITIONS

All data were obtained at Mach numbers of 0.4 or 0.7 at a Reynolds number of 3.6 million per foot. Tunnel conditions were held constant at the desired Mach number and Reynolds number while data were being recorded.

3.2 DATA ACQUISITION

Data were obtained in the following manner during the test. The probe tip or store cg was manually positioned to a reference point, relative to the pylon configuration being tested, after the desired test conditions were established. During all tests, the probe and store-model centerlines were aligned parallel to the aircraft-model centerline, and displacements were measured in directions parallel to, or perpendicular to, the aircraft model centerline. The axis systems defining the store forces and moments, and store displacements are shown in Fig. 17.

A complete pressure distribution was obtained on the pressure model by taking pressure data at 10-deg roll increments through 360 deg. Local force coefficients were calculated by numerically integrating the circumferential pressure distributions. Total force and moment coefficients were then obtained by summing the local contributions along the model length.

Data were obtained in the following manner during the captive trajectory phase of testing. Test conditions were established in the tunnel, and the parent model was positioned at the desired angle of attack. The store model was then oriented to an initial position relative to the store carriage location on the pylon (see Table I). After the store was set at the desired initial position, operational control of the CTS was switched to the digital computer which controlled the store movement during the trajectory through commands to the CTS analog system (see block diagram, Fig. 1). Data from the wind tunnel consisting of measured model forces and moments, wind tunnel operating conditions, and CTS rig positions, were input to the digital computer for use in the full-scale trajectory calculations.

The digital computer was programmed to sólve the six-degree-of-freedom equations to calculate the angular and linear displacements of the store relative to the parent aircraft pylon. In general, the program involves using the last two successive measured values of each static aerodynamic coefficient to predict the magnitude of the coefficients over the next time interval of the trajectory. These predicted values are used to calculate the new position and attitude of the store at the end of the time interval. The CTS is then commanded to move the store model to this new position and the aerodynamic loads are measured. If these new measurements agree with the predicted values, the process is continued over another time interval of the same magnitude. If the measured and predicted values do not agree within the desired precision, the calculation is repeated over a time interval one-half the previous value. This process is repeated until a complete trajectory has been obtained.

In applying the wind tunnel data to the calculations of the full-scale store trajectories, the measured forces and moments are reduced to coefficient form and then applied with proper full-scale store dimensions and flight dynamic pressure. Dynamic pressure was calculated using a flight velocity equal to the free-stream velocity component plus the components of store velocity relative to the aircraft, and a density corresponding to the simulated altitude. Full-scale store parameters used in the trajectory calculations are listed in Table II.

3.3 CORRECTIONS

During force-model testing, deflections of the balance, sting, and CTS supports, caused by aerodynamic forces, were accounted for in the data reduction program to calculate the true store-model angles. Corrections were also made for model weight tares to calculate the net aerodynamic forces on the store force models.

3.4 PRECISION OF DATA

Estimated uncertainties in model and probe positioning resulting from the ability of the CTS and main pitch sector to set on a specified value are as follows:

			Δα, deg	
ΔX, in.	ΔY, in.	ΔZ, in.	Store	Aircraft
±0.05	±0.05	±0.05	±0.15	±0.10

Uncertainties in the data on the force model were calculated taking into consideration probable inaccuracies in the balance measurements and tunnel conditions. The uncertainties in the coefficients are based on a 95-percent confidence level. Coefficient uncertainties along with Mach number variation in the portion of the test section occupied by the models and variations in free-stream dynamic pressure are as follows:

M_∞	YM_∞	Δq_∞	ΔC_N	ΔC_Y	ΔC_m	ΔC_n	ΔC_A
0.40	±0.005	±2.2	±0.02	±0.02	±0.03	±0.03	±0.05
0.70	±0.005	±1.4	±0.01	±0.01	±0.01	±0.01	±0.02

Considering the error in translational and angular placements, extrapolation tolerances, and balance accuracy, the maximum uncertainties in full-scale position coordinates for the store during captive-trajectory store-separation are as follows:

M_∞	Store Mass	t, sec	ΔX, ft	ΔY, ft	ΔZ, ft	Δθ, deg	Δψ, deg	Δφ, deg
0.4	3.8825	0.50	±0.27	±0.18	±0.08	±1.9	±4.0	±13.5
0.4	15.5300	0.50	±0.07	±0.04	±0.02	±0.5	±1.0	± 3.4
0.7	3.8825	0.50	±0.51	±0.33	±0.15	±3.6	±7.6	±25.2
0.7	15.5300	0.50	±0.13	±0.08	±0.04	±0.9	±1.9	± 6.3

SECTION IV
RESULTS AND DISCUSSION

The four types of data obtained during this investigation consisted of velocity-vector data, store force and moment data, store pressure distribution data, and captive-trajectory store-separation data. During each phase of testing, data were obtained to determine interference effects on the flow field and on the store forces and pressure distributions resulting from the aircraft fuselage, ducts, wing, and pylon. Data were obtained near the wing 1/3-semispan and fuselage centerline stations.

Only representative data obtained during the test are presented herein. Basic configuration nomenclature is shown in Table III, and locations at which data were obtained can be seen by referring to Table IV. Identification of configuration numbers used in the data presentation is presented in Table V. The reference position for the force-and-moment store data corresponds to the store model cg in the carriage position on the pylon. The cg was on the store centerline at the store midpoint for all cases. Sign conventions used in the data presentation are shown in Fig. 17. Figure 18 shows the average duct flow velocity ratios for test Mach numbers of 0.4 and 0.7.

4.1 FLOW-FIELD DATA

The flow-field data obtained during this test were used as a guide in selecting testing regions for the force- and pressure-model data and the trajectories. The large volume of flow-field data obtained during the test precludes making any significant presentation of flow-field tests results at this time. Consequently, this report contains the description of the test and serves as the key to these data. A summary of store configuration, store position, survey region, and test condition information is presented in Appendix II. Extensive flow-field data are available in Refs. 1 through 4 from previous testing with the models.

4.2 FORCE- AND PRESSURE-MODEL DATA

Data were obtained on the force and pressure store models in the presence of the wing/fuselage model with and without ducts and pylons installed. All pressure data were obtained on the ogive-cylinder pressure distribution model. Force data were obtained on the finned and unfinned large force model, the SUU-41 model, and the ESUU-41 model.

Figures 19 through 24 present parent-model duct flow influence on force and moment coefficients for the finned and unfinned large force models from the wing 1/3-semipsan and fuselage centerline stations. These data are presented showing the coefficient variations with Z' for $Y' = 0$ and -0.375 and for $\alpha = 0$, 6, and 15 deg. These data show that, in general, duct flow had little effect on the force and moment coefficients except for small variations at the higher angles of attack.

Figures 25 through 28 show the effect of the addition to the wing/fuselage model of the body add-on and 1/3-semispan pylon on force and moment coefficients for the finned and unfinned large force models. The body add-on had little effect on either model except for small variation in the coefficients for the finned model at the higher angles of attack. The addition of the 1/3-semispan pylon produced a nose down increment in the pitching-moment coefficient, with the effect more noticeable on the finned model and increasing with increasing angle of attack.

Force and moment coefficients for the SUU-41 and ESUU-41 models at the wing 1/3-semispan station are presented in Fig. 29. These data show that the effects of body cross-sectional shape were negligible at these test conditions.

Figures 30 through 33 present parent-model duct flow influence on force and moment coefficients for the pressure distribution model, and Figs. 34 and 35 show the effect on the coefficients of the addition of body add-on or pylon to the wing/fuselage model. These data exhibit the same trends as those previously mentioned for the unfinned large force model at a similar wing/fuselage station.

4.3 TRAJECTORY DATA

Data obtained during this test phase consisted of separation trajectories of the finned large model from the wing 1/3-semispan pylon. Data showing the linear and angular displacements of the store relative to the carriage position on the pylon are presented as functions of full-scale trajectory time in Figs. 36 through 40. Positive X, Y, and Z displacements (as seen by the pilot) are forward, to the right (inboard), and down, respectively. Positive changes in pitch and yaw (as seen by the pilot) are nose up and nose right (inboard), respectively.

These data show that duct-flow influence on trajectories is negligible, except for a slightly increased roll rate as the duct flow is decreased. An increase in Mach number causes more rapid pitch and yaw oscillation and more rapid roll rates. The effects of an initital downward velocity and a change in store mass on separation trajectories can be seen in Fig. 40. The larger mass and moment of inertia result in a decrease in the pitch and yaw oscillation frequencies, whereas the initial downward velocity causes a more rapid Z displacement.

APPENDIXES

I. ILLUSTRATIONS
II. TABLES

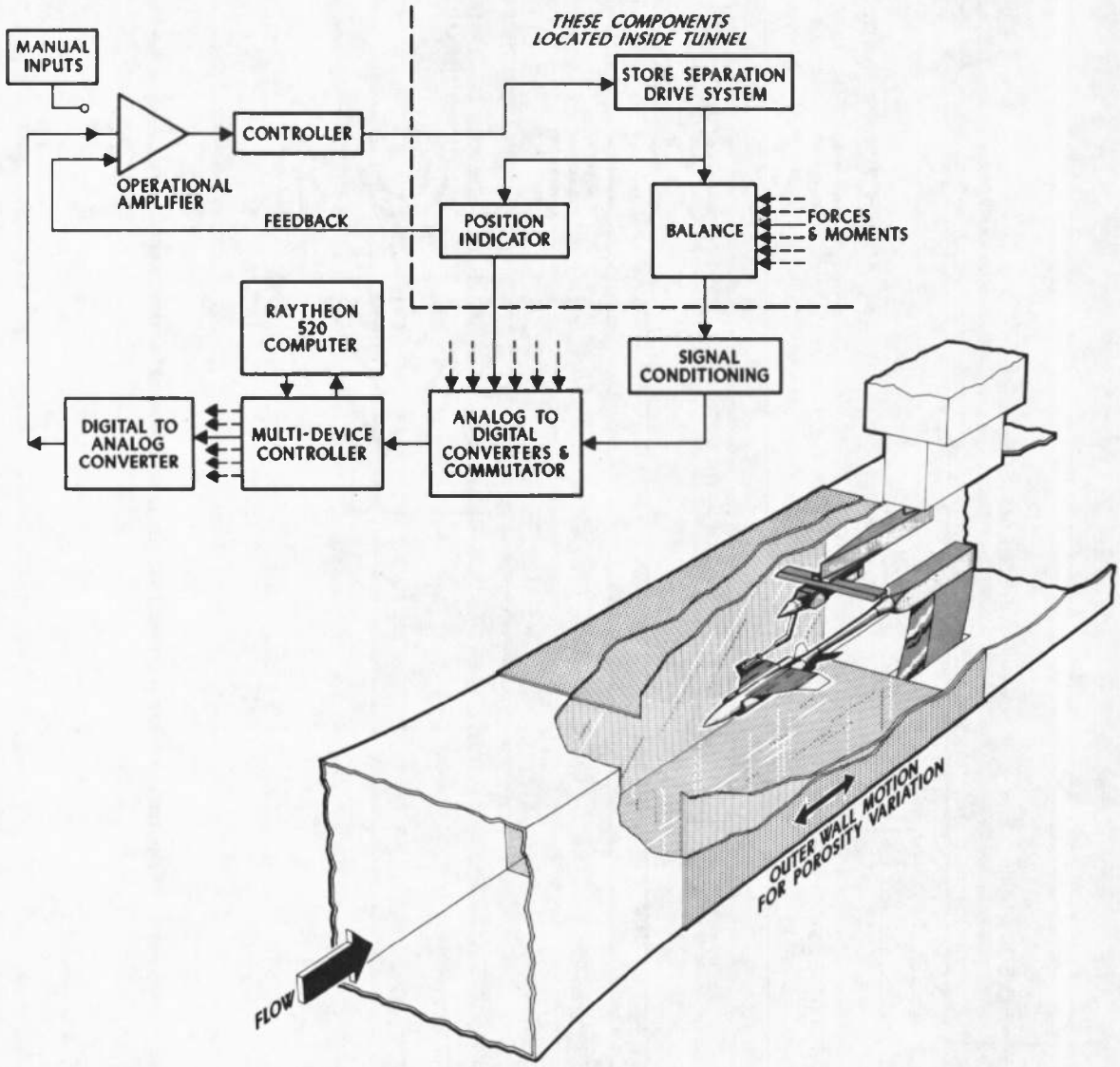

Fig. 1 Isometric Drawing of a Typical Store Separation Installation and a Block Diagram of the Computer Control Loop

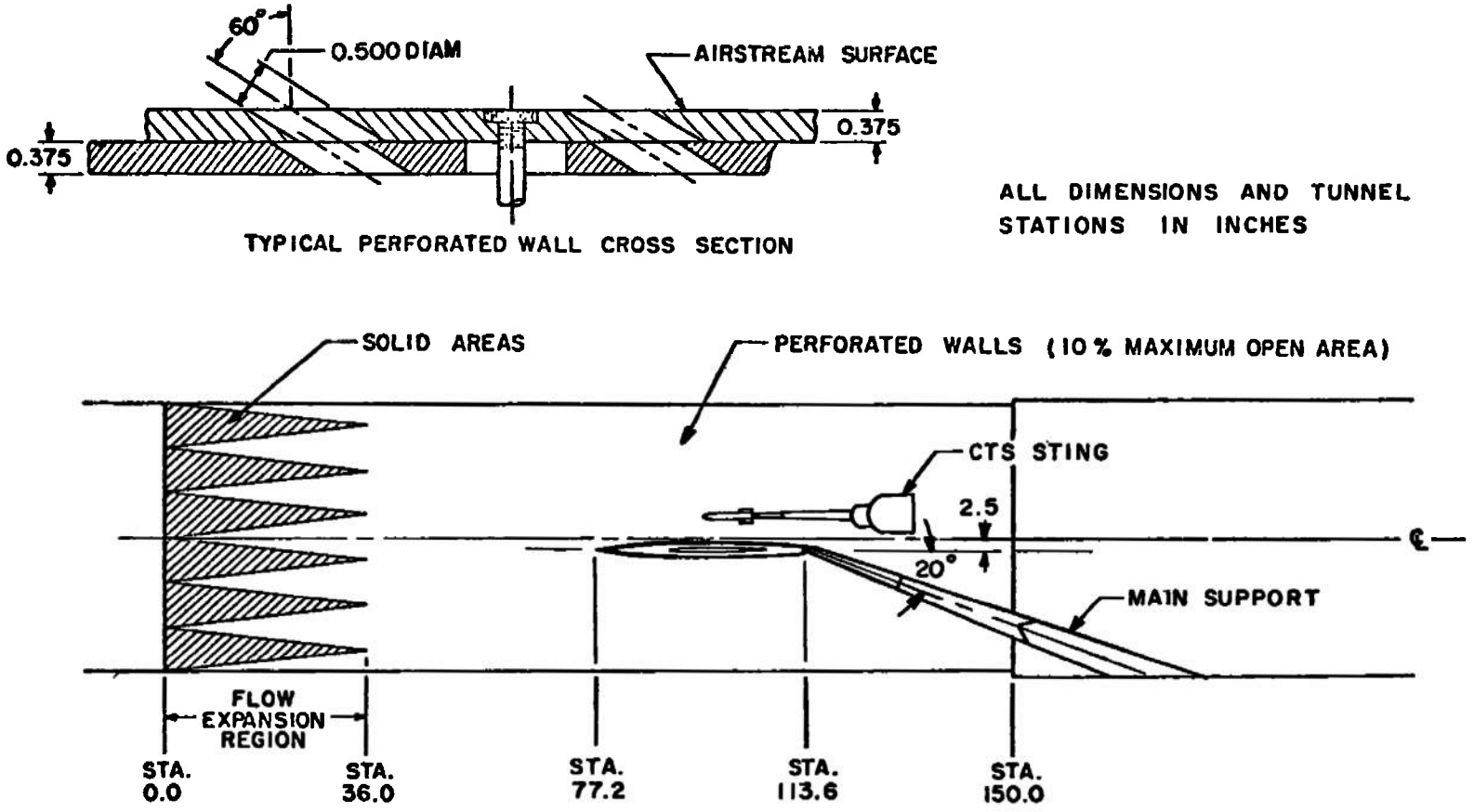

Fig. 2 Schematic of the Tunnel Test Section Showing Model Location

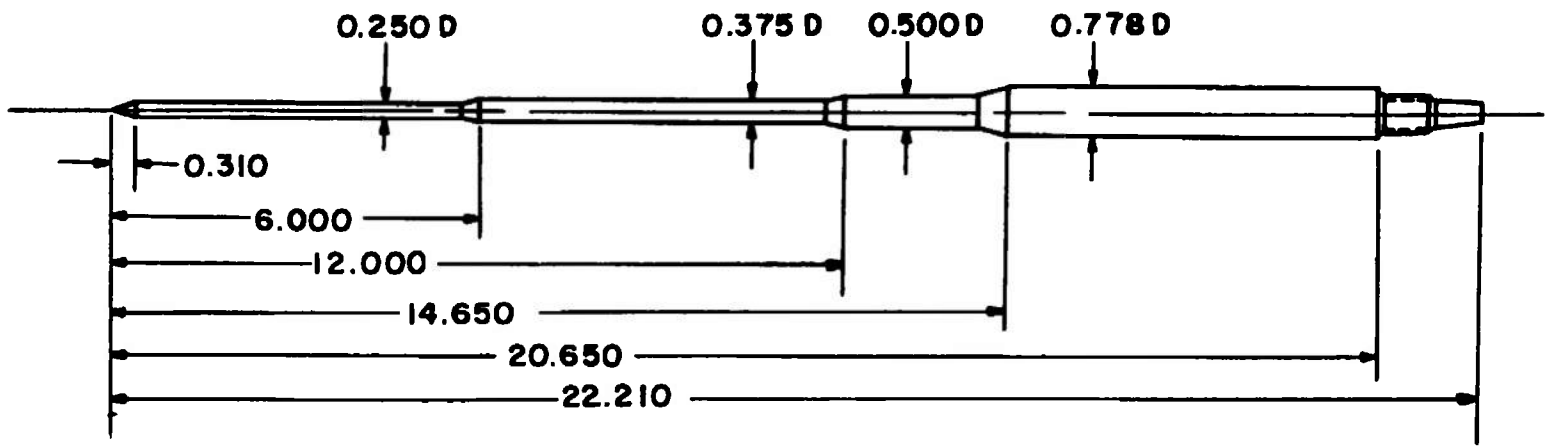

a. General Details

Fig. 3 Details and Dimensions of the 40-deg Cone Probe

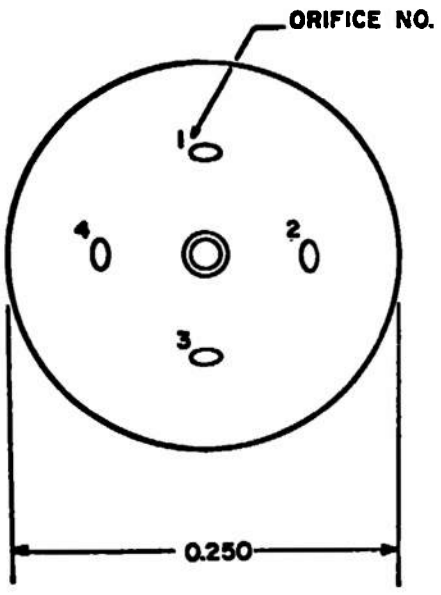

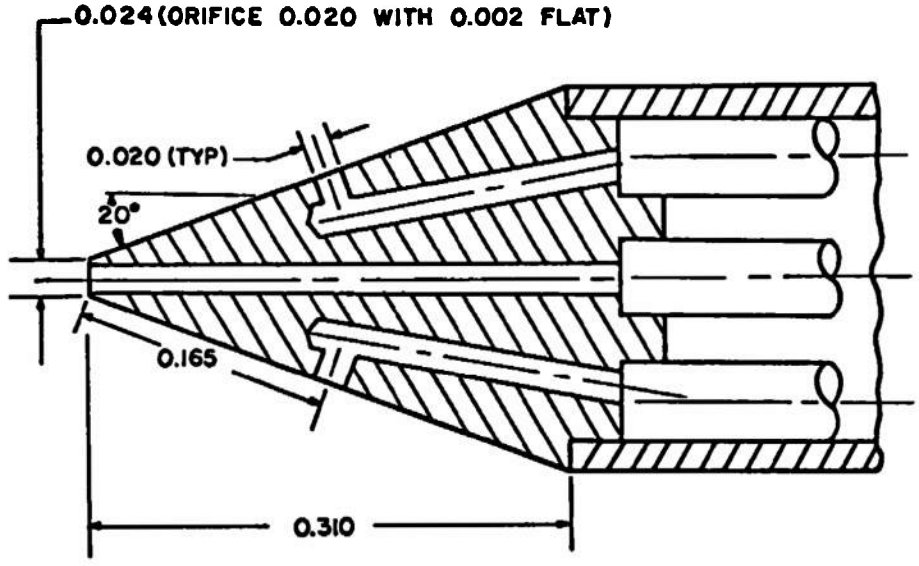

ALL DIMENSIONS IN INCHES

b. Probe Tip Details
Fig. 3 Concluded

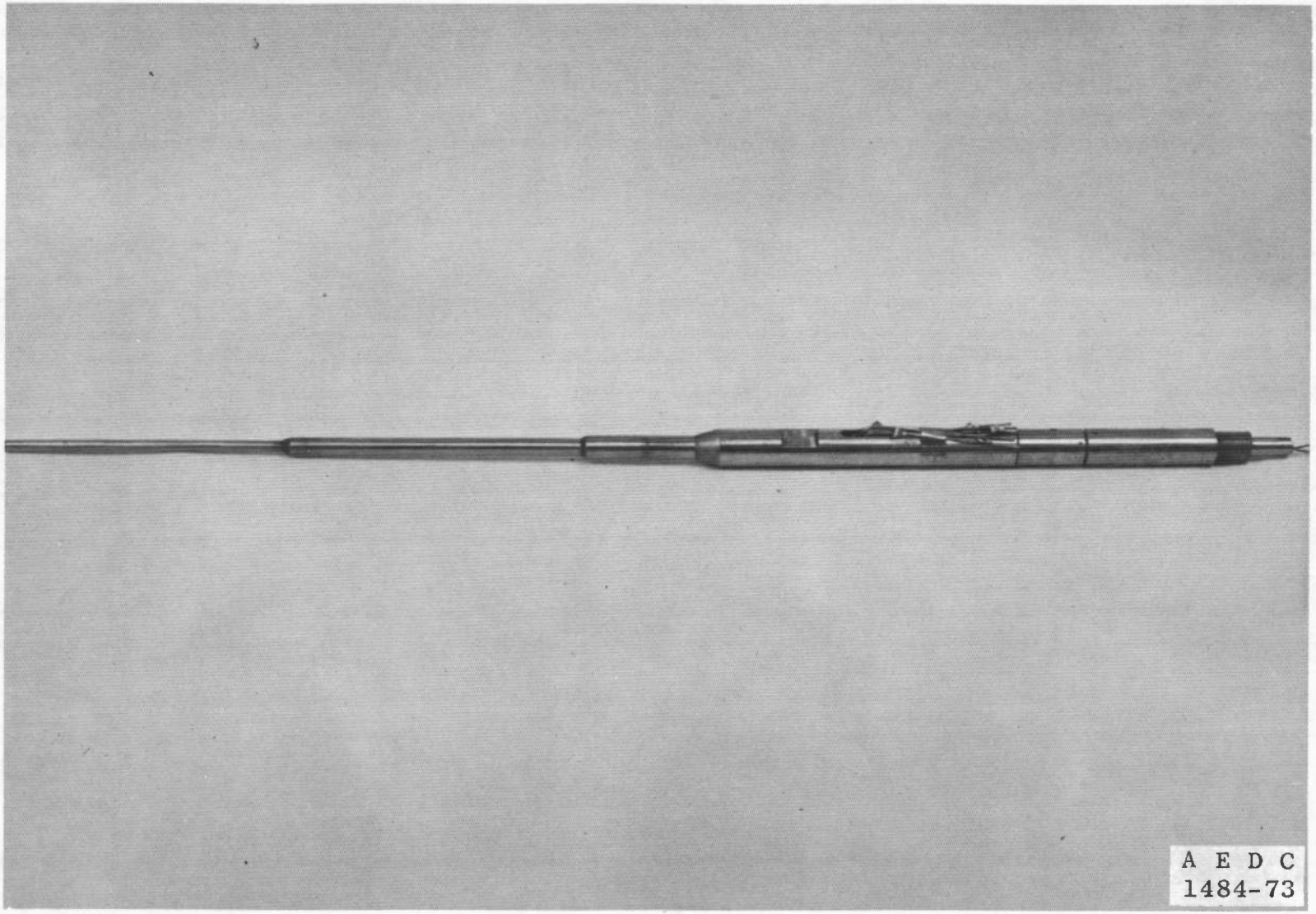

Fig. 4 Photograph of the 40-deg Cone Probe

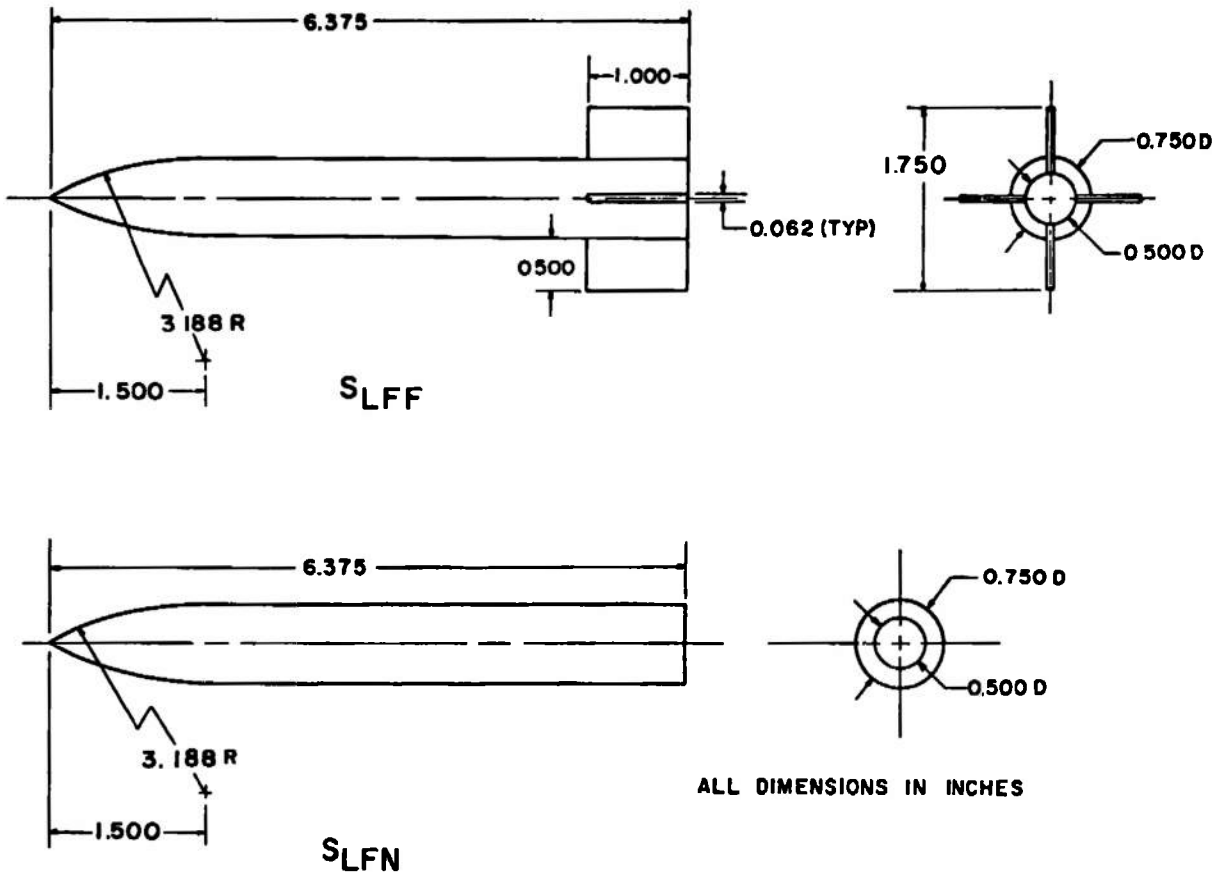

a. Large Force Models

Fig. 5 Details and Dimensions of the Force Models

STATION	Y_1	Y_2	Y_3	R_1	R_2
0	0	0	0	0	0
0.100	0.064	0.064	0.058	0.117	0.065
0.200	0.095	0.099	0.088	0.203	0.098
0.300	0.127	0.132	0.110	0.287	0.131
0.400	0.158	0.162	0.134	0.370	0.164
0.500	0.188	0.191	0.156	0.452	0.198
0.600	0.218	0.216	0.178	0.530	0.227
0.700	0.247	0.240	0.199	0.610	0.256
0.800	0.273	0.261	0.218	0.668	0.282
0.900	0.297	0.282	0.238	0.765	0.307
1.000	0.319	0.301	0.264	0.842	0.331
1.100	0.340	0.318	0.272	0.920	0.353
1.200	0.360	0.336	0.289	0.985	0.374
1.300	0.378	0.349	0.306	1.070	0.395
1.400	0.397	0.360	0.321	1.148	0.414
1.500	0.413		0.335	1.215	0.432
1.600	0.427		0.347	1.280	0.446
1.700	0.440		0.357	1.357	0.460
1.800	0.451		0.366	1.426	0.473
1.900	0.461		0.372	1.490	0.483
2.000	0.469		0.379	1.555	0.493
2.070	0.475		0.383	1.600	0.500
4.980	0.475		0.383	1.600	0.500
5.080	0.469		0.379	1.555	0.493
5.180	0.461		0.372	1.490	0.483
5.280	0.451		0.366	1.425	0.473
5.380	0.440		0.357	1.357	0.460
5.480	0.427		0.347	1.280	0.446
5.580	0.413		0.335	1.215	0.432
5.680	0.397	0.350	0.321	1.148	0.414
5.780	0.378	0.349	0.306	1.070	0.395
5.880	0.360	0.336	0.289	0.883	0.374
5.927	0.350	0.323	0.276	0.937	0.358

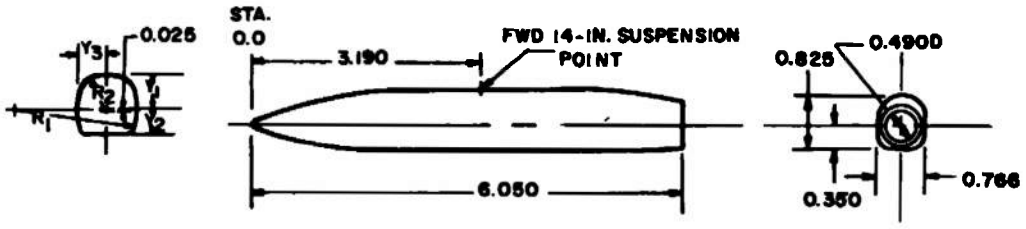

ALL DIMENSIONS IN INCHES

b. SUU-41 Model
Fig. 5 Continued

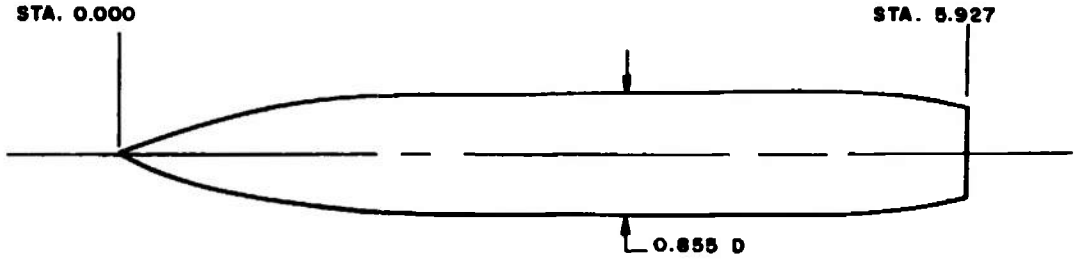

ALL DIMENSIONS IN INCHES

STA.	DIAM
0.000	0. 000
0.100	0. 128
0.200	0 192
0 300	0.252
0.400	0.310
0.500	0 365
0.600	0.418
0.700	0.468
0.800	0.514
0.900	0 557
1.000	0.599
1.100	0.639
1 200	0.678
1.300	0.714
1.400	0.741
1.500	0.766
1.600	0.788
1 700	0.806
1.800	0.822
1.900	0.835
2.000	0.847
2.070	0.855
4.980	0.855
5.050	0.847
5.150	0.835
5.250	0.821
5.350	0.806
5.450	0.788
5.550	0.766
5.650	0.741
5.750	0.714
5.850	0.678
5.927	0.644

c. ESUU-41 Model
Fig. 5 Concluded

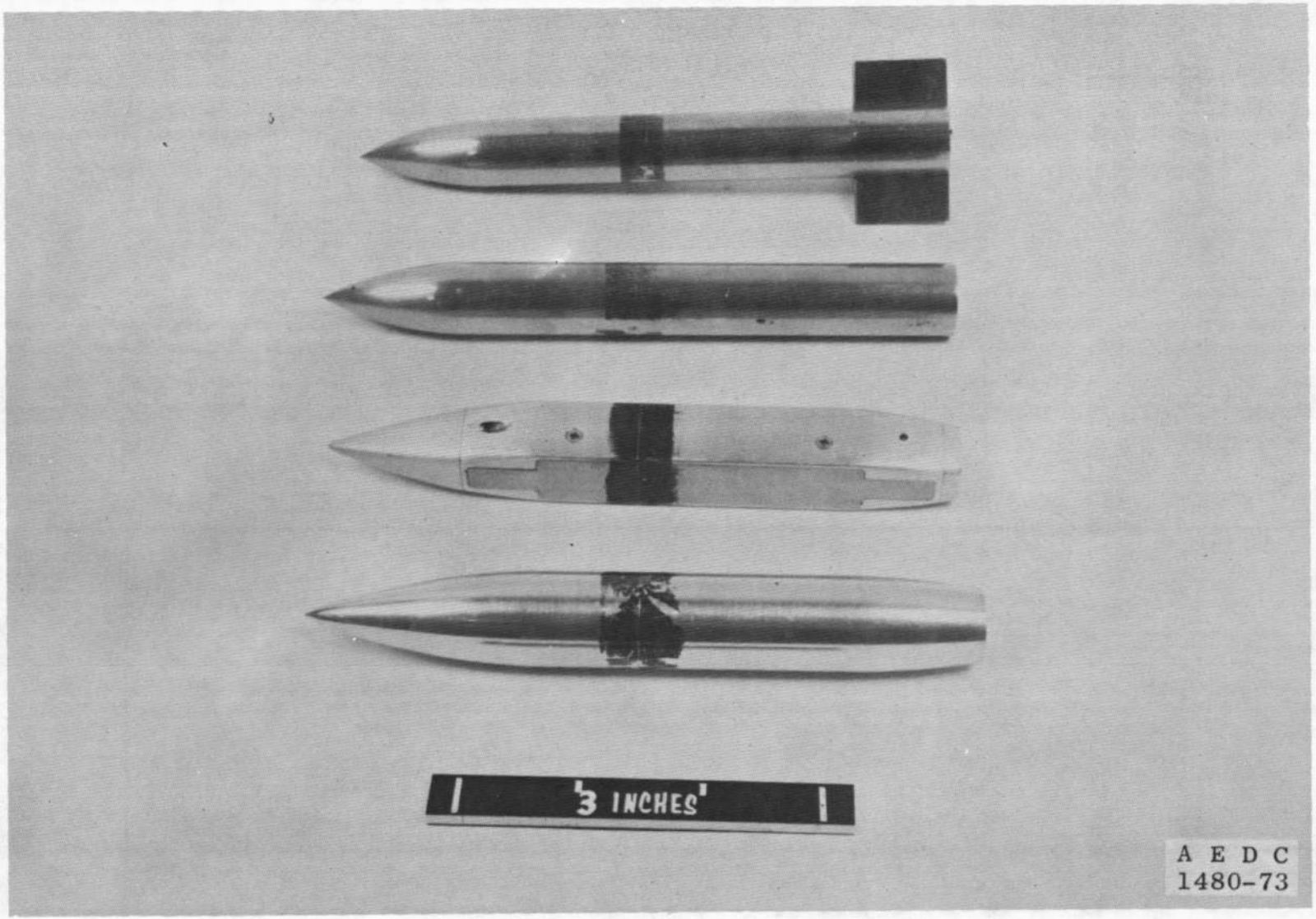

Fig. 6 Photograph of the Force Models

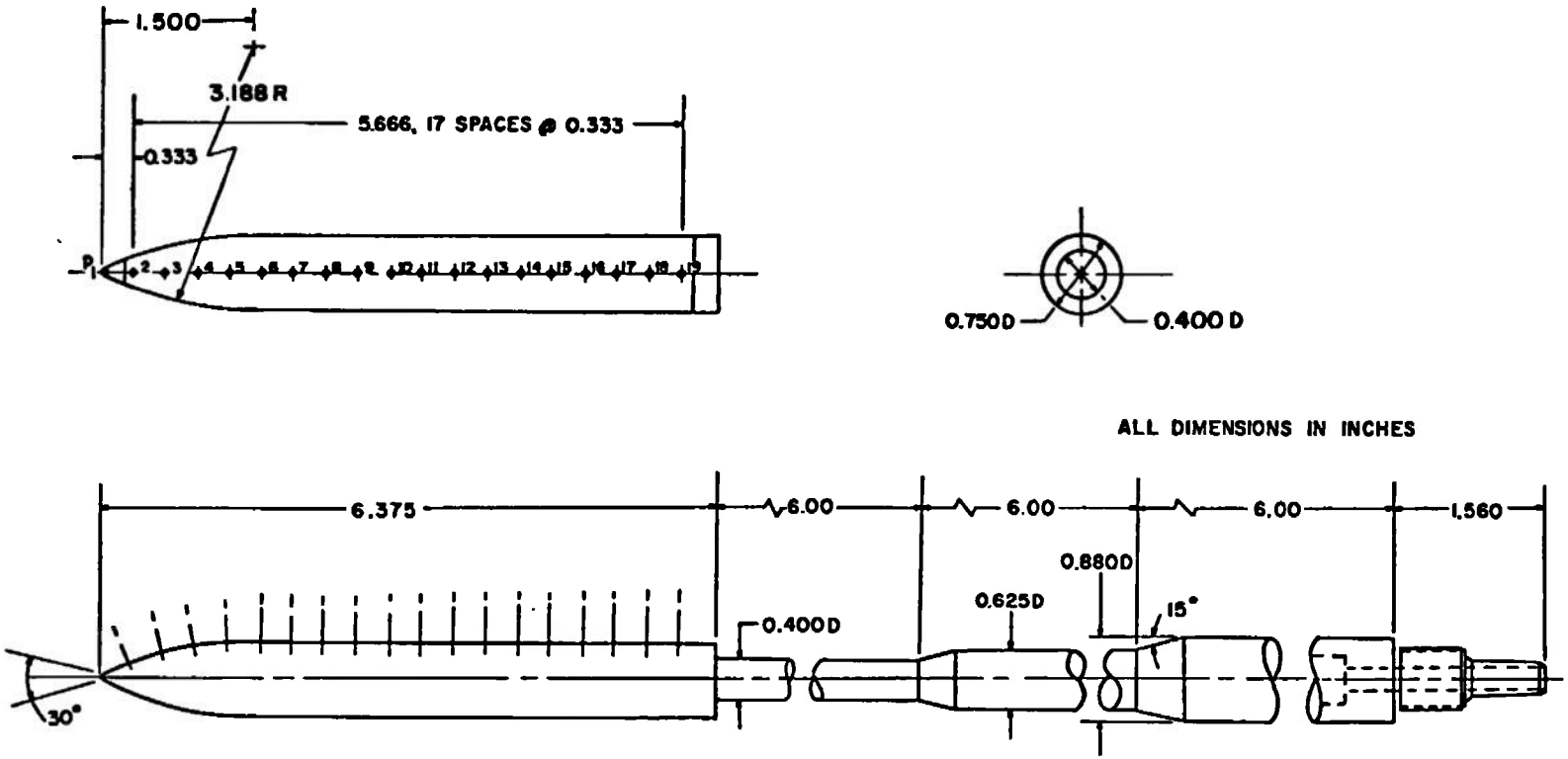

Fig. 7 Details and Dimensions of the Pressure Distribution Model

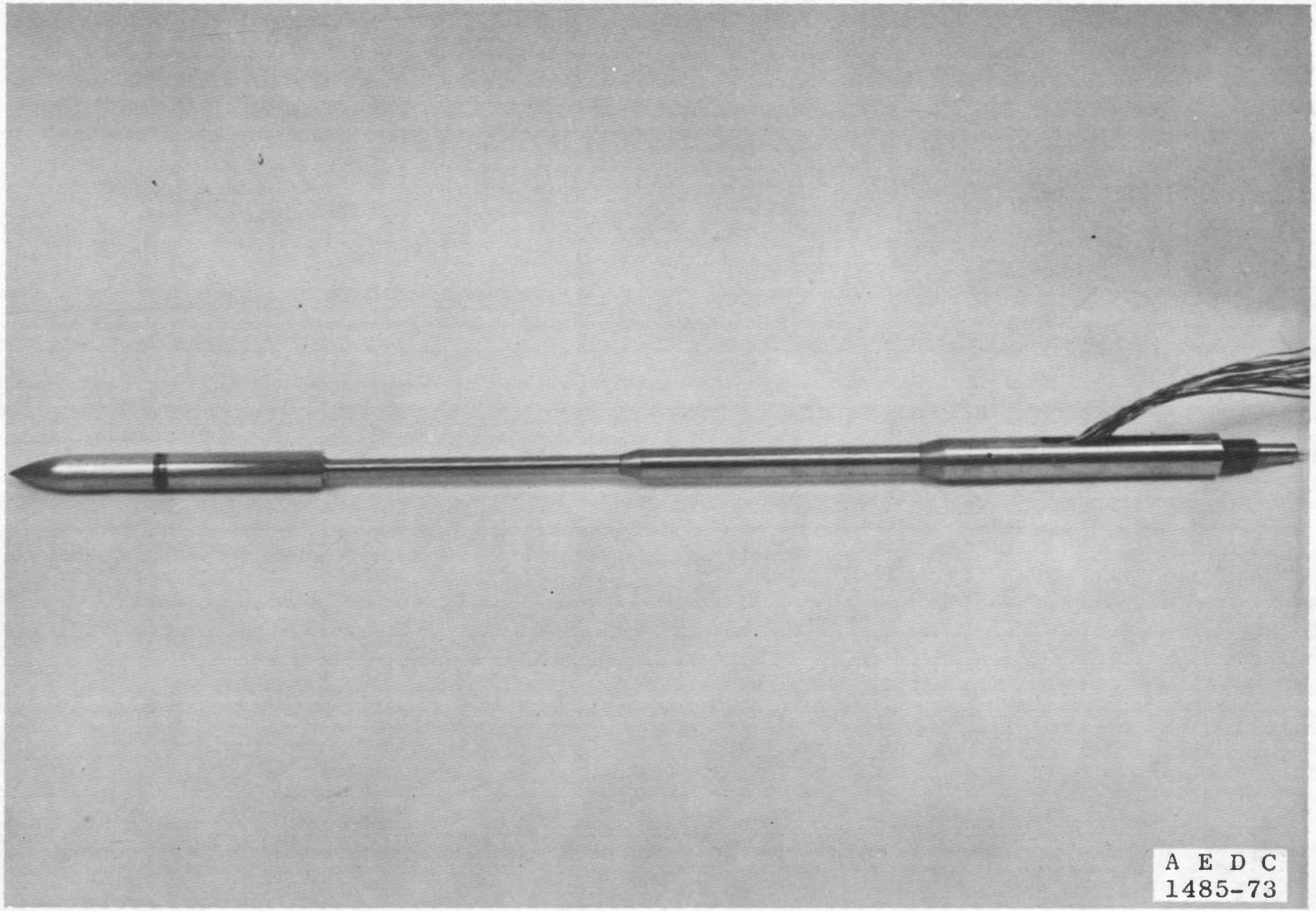

Fig. 8 Photograph of the Pressure Distribution Model

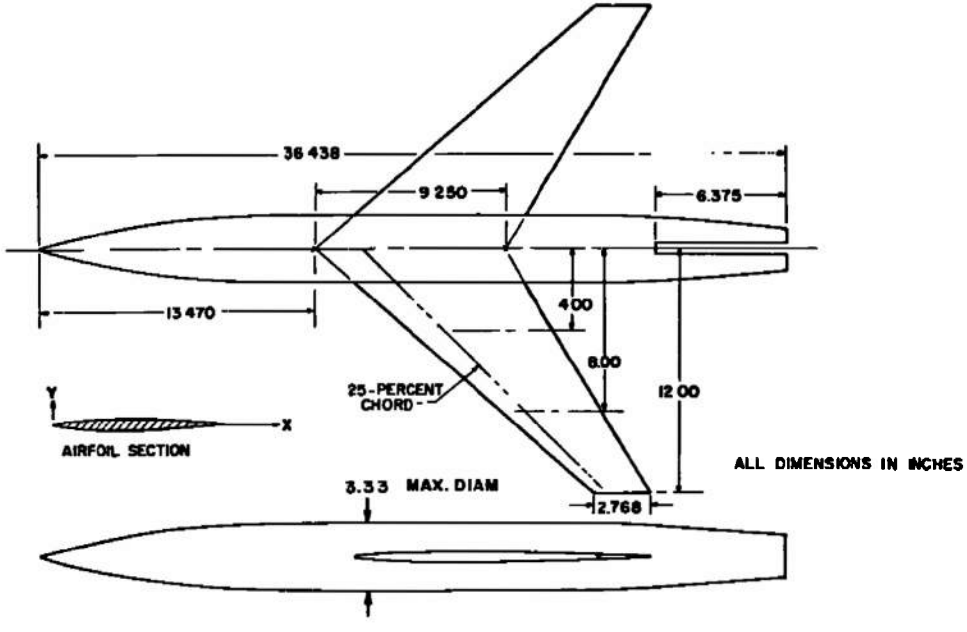

BODY COORDINATES

STATION PERCENT LENGTH	RADIUS PERCENT LENGTH
0.00	0.00
3.28	0.91
6.57	1.71
9.86	2.41
13.15	3.00
16.43	3.50
19.72	3.90
23.01	4.21
26.29	4.43
29.58	4.53
32.00	4.57
75.34	4.57
76.69	4.54
79.98	4.38
83.26	4.18
86.55	3.95
89.84	3.72
93.13	3.49
96.41	3.26
100.00	3.02

AIRFOIL COORDINATES

X, % CHORD SEE SEC.	Y, % CHORD SEE SEC.
0.00	0.000
0.50	0.464
0.75	0.563
1.25	0.718
2.50	0.981
5.00	1.313
7.50	1.591
10.00	1.824
15.00	2.194
20.00	2.474
25.00	2.667
30.00	2.842
35.00	2.945
40.00	2.996
45.00	2.992
50.00	2.925
55.00	2.793
60.00	2.602
65.00	2.364
70.00	2.087
75.00	1.775
80.00	1.437
85.00	1.083
90.00	0.727
95.00	0.370
100.00	0.013
L.E. RADIUS 0.229% CHD	
T.E. RADIUS 0.014% CHD	

Fig. 9 Sketch of the Wing/Fuselage Model (N_1B_2W)

BODY COORDINATES

STATION	RADIUS
14.558	4.57
27.452	4.57
27.944	4.54
29.143	4.38
30.338	4.18
31.537	3.95
33.736	3.72
33.934	3.49
35.129	3.26
36.438	3.02

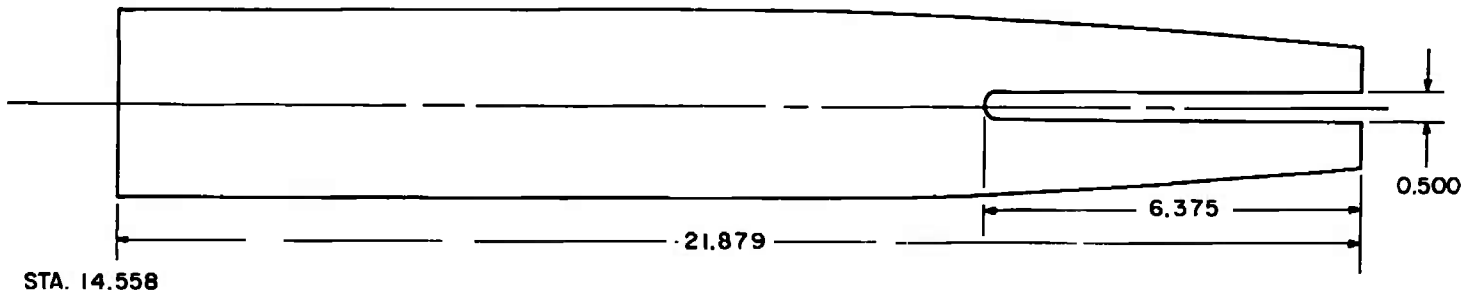

ALL STATIONS AND DIMENSIONS IN INCHES

a. Long Body (B_2)

Fig. 10 Details and Dimensions of the Fuselage Components for the Wing/Fuselage Model

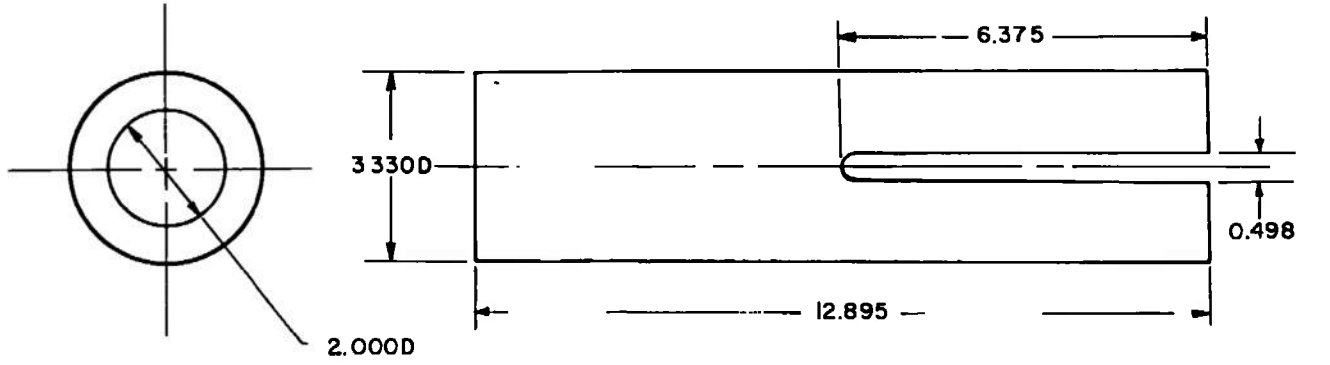

b. Short Body (B_2)
Fig. 10 Continued

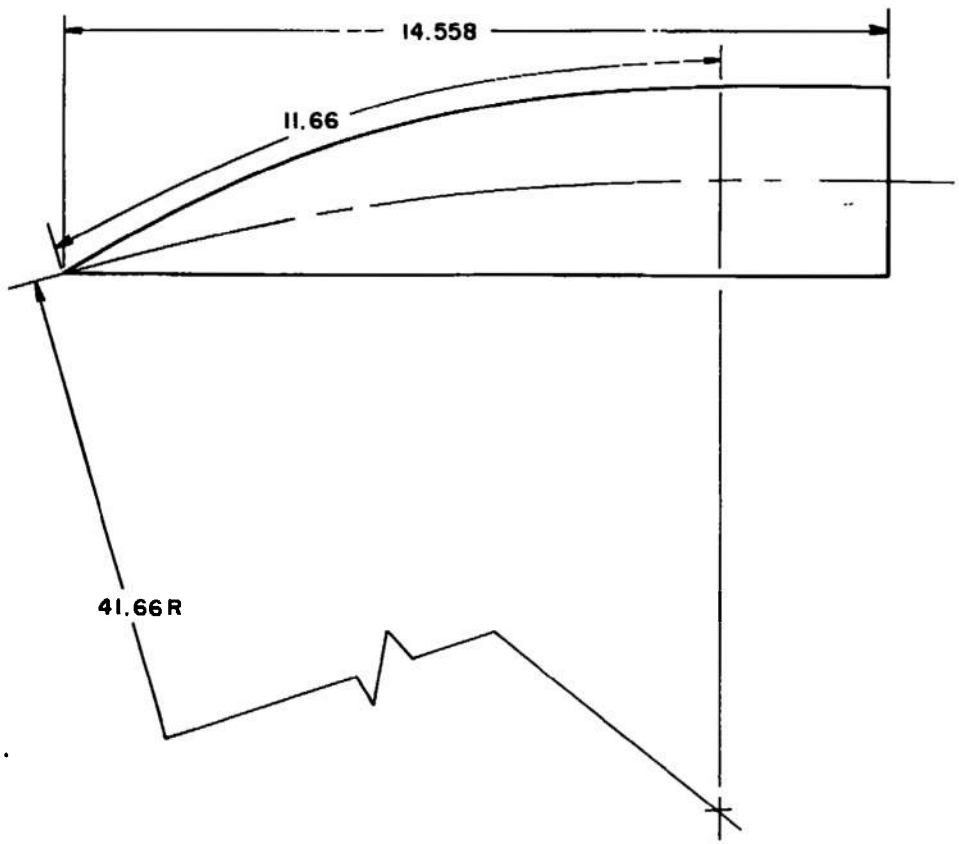

STATION*	OUTSIDE DIAM
0.75	0.422
1.50	0.814
2.25	1.177
3.00	1.510
3.75	1 814
4 50	2 090
5.25	2.338
6.00	2.557
6.75	2 749
7.50	2.914
8.25	3.050
9 00	3 160
9.75	3.242
10.50	3.298
11.25	3.326
11.66	3330

* STATION DIMENSIONS ARE MEASURED ALONG 3/8 DIAM ROD ℄ AND NORMAL TO 41.66R ARC

ALL STATIONS AND DIMENSIONS IN INCHES

c. Cambered Nose (N_2)
Fig. 10 Continued

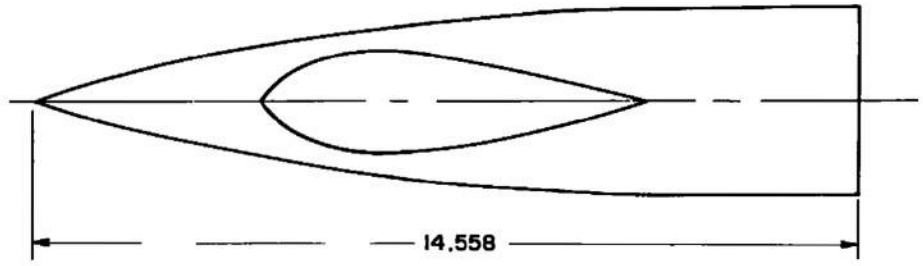

ALL STATIONS AND DIMENSIONS IN INCHES

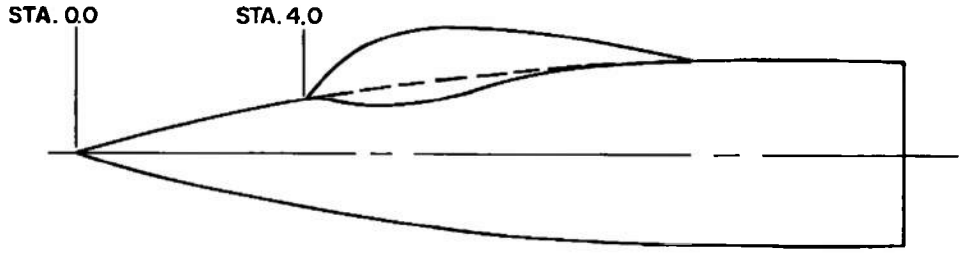

DISTANCE FROM NOSE TIP BODY STA.	UNCAMBERED NOSE RADIUS	CANOPY BULKHEAD DIAM
4.00	0.955	0
4.50	1.045	0.962
5.00	1.129	1.469
5.50	1.207	1.768
6.00	1.279	1.873
6.53	1.348	1.829
7.00	1.404	1.709
8.00	1.504	1.358
9.00	1.580	0.986
10.00	1.632	0.515
10.83	1.657	0

d. Uncambered Nose with Canopy ($N_1 C_1$)

Fig. 10 Concluded

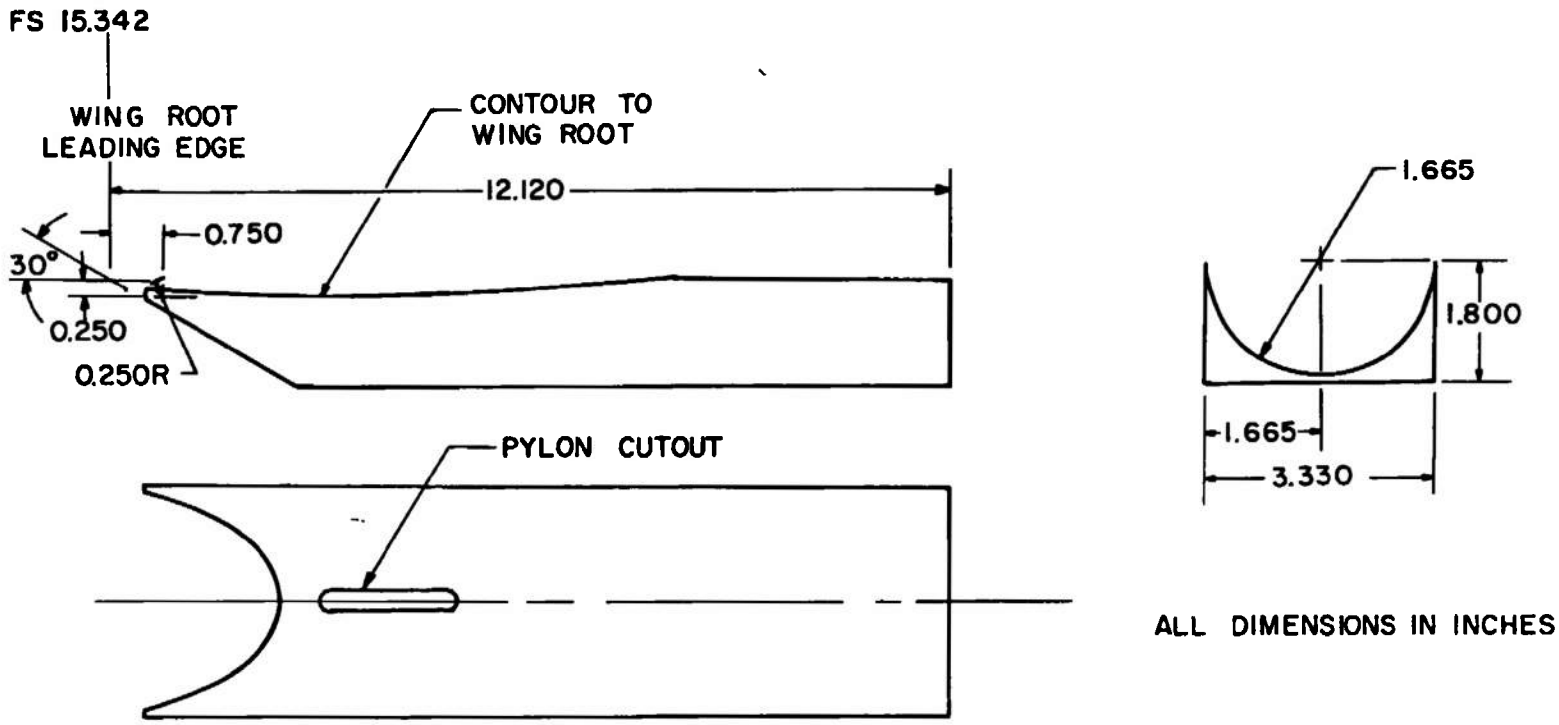

Fig. 11 Details and Dimensions of the Body Add-On without Ducts (A_1)

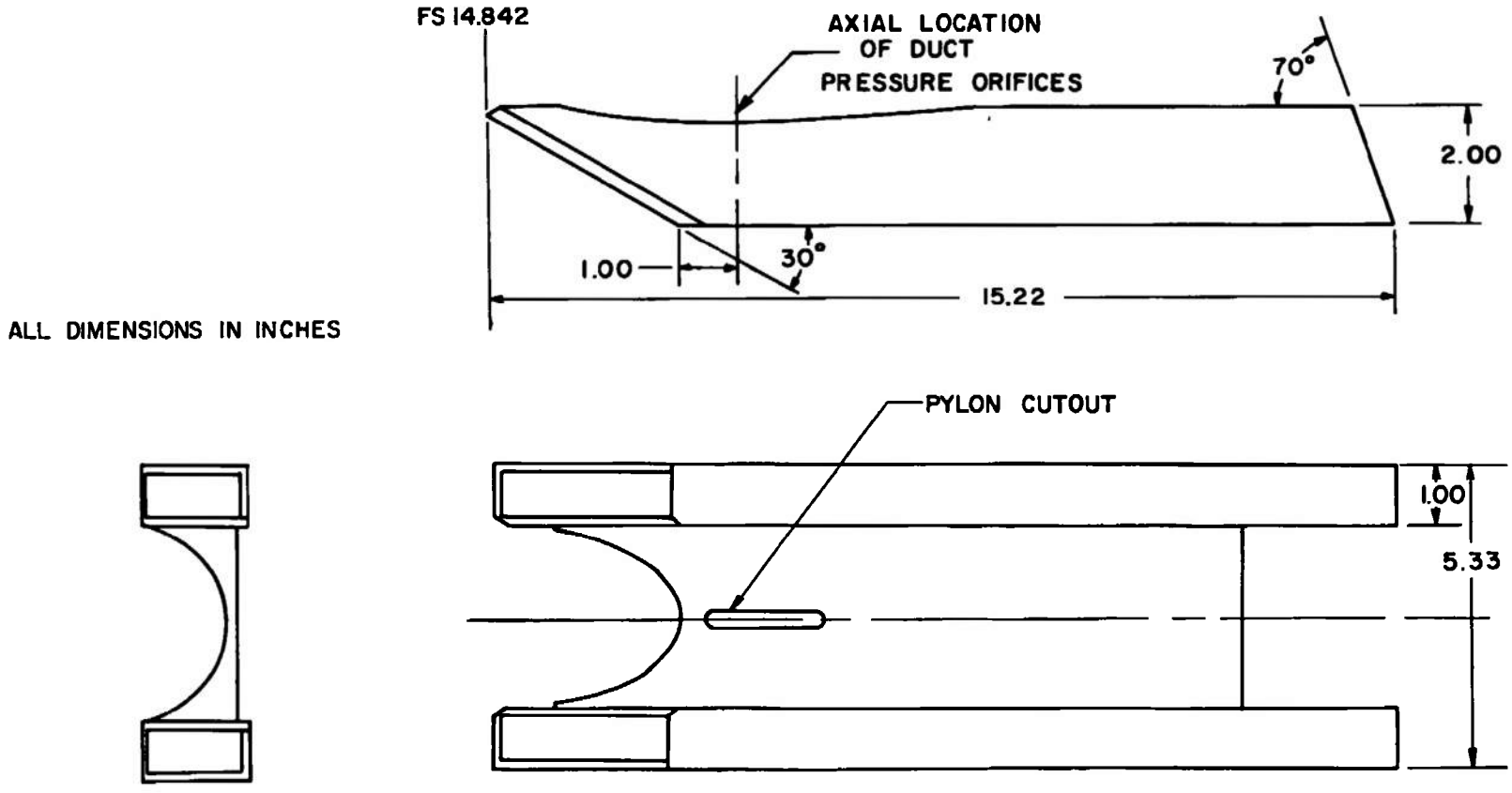

Fig. 12 Details and Dimensions of the Body Add-On with Ducts (A_2)

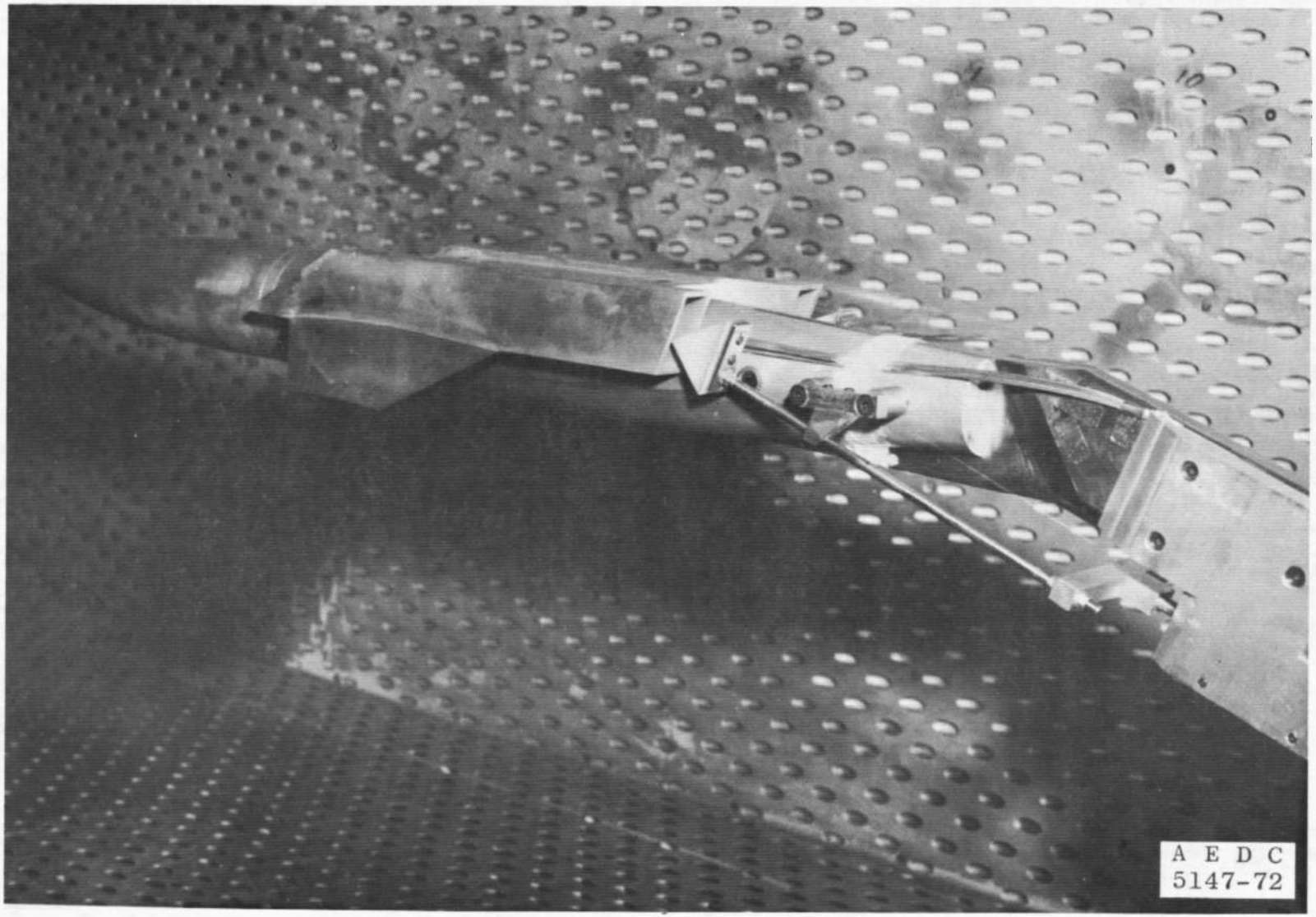

Fig. 13 Photograph of the Wing/Fuselage Model with Ducts and Duct Flow Controller Installed

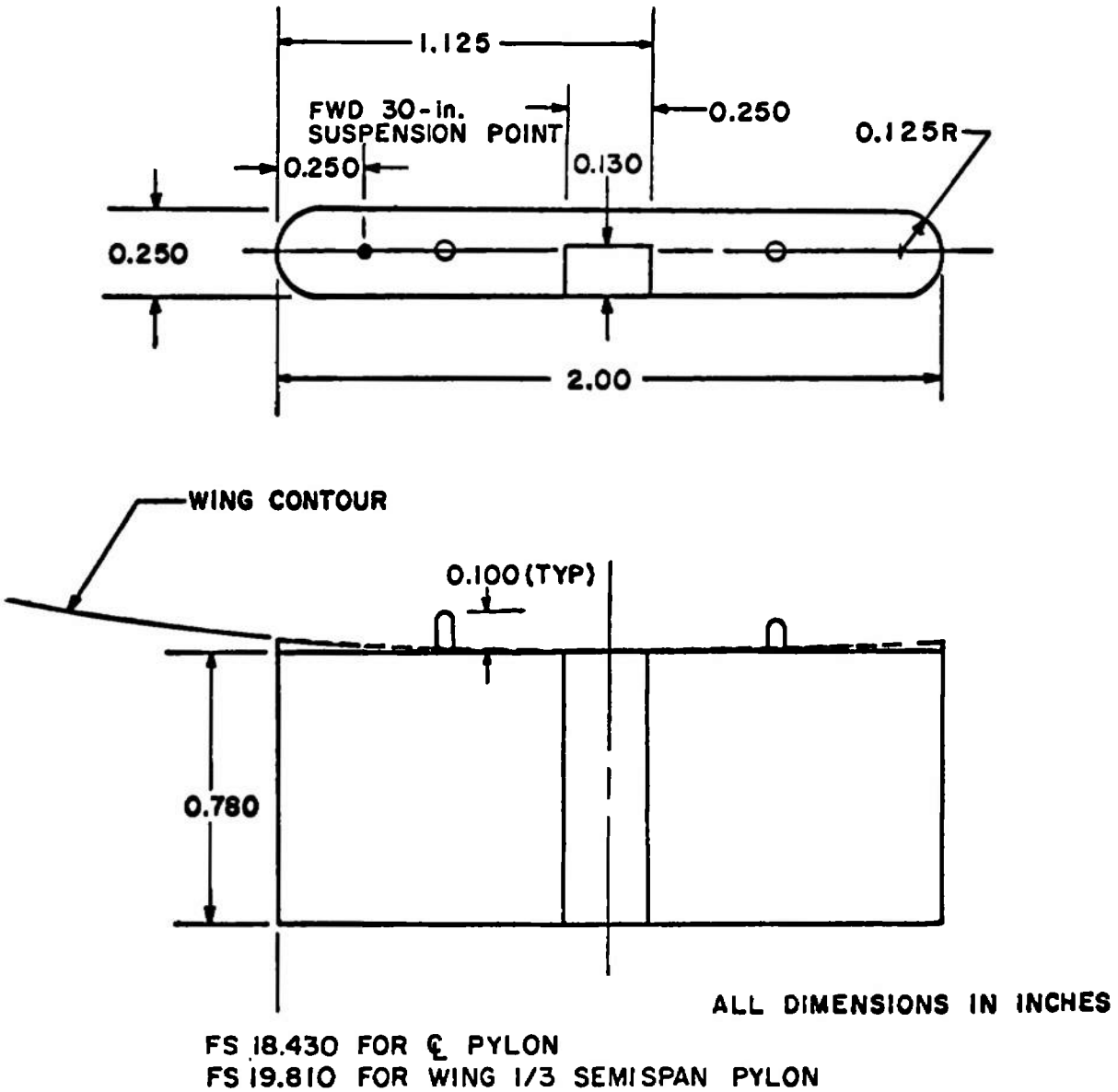

Fig. 14 Details and Dimensions of the Pylons

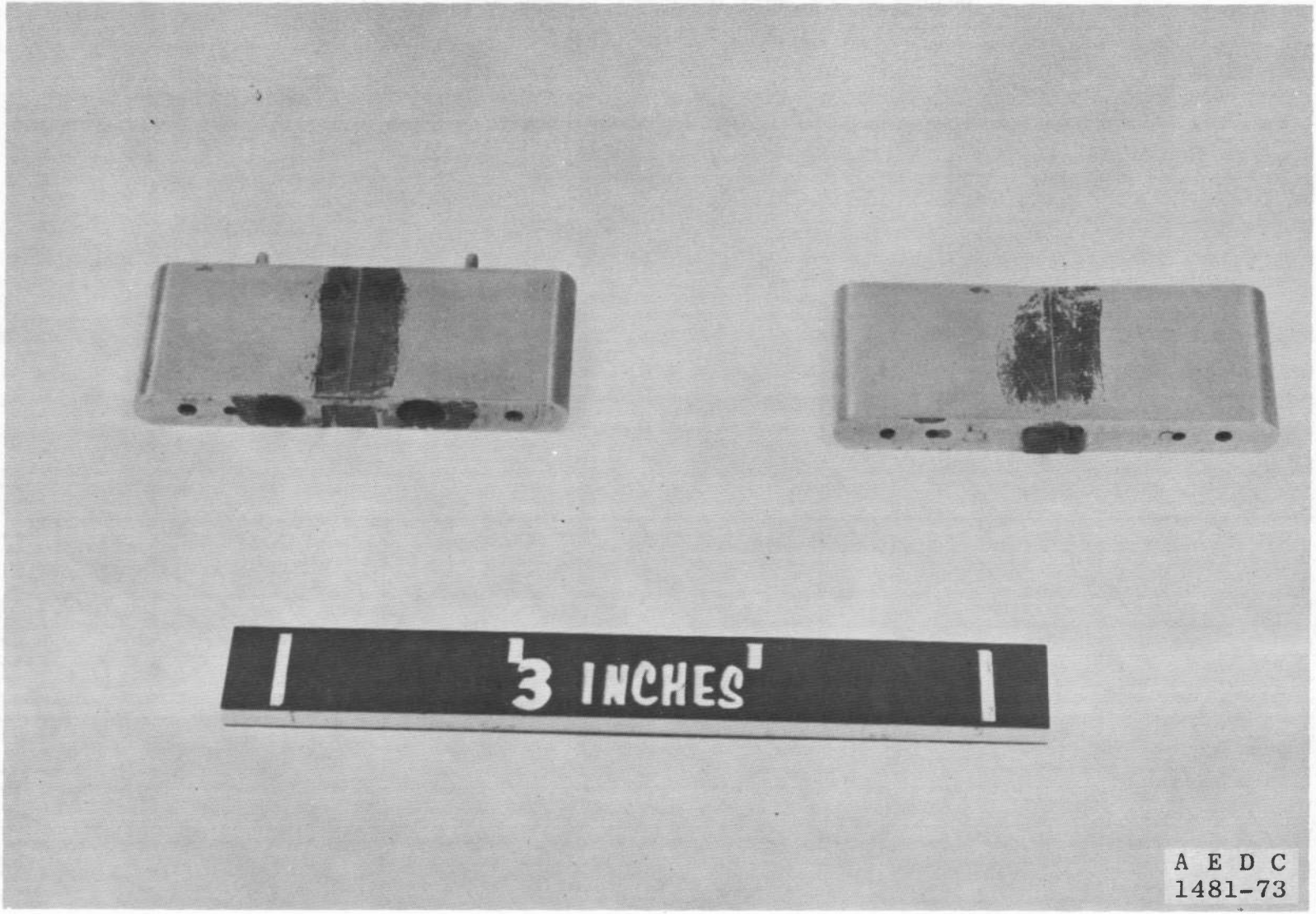

Fig. 15 Photograph of the Pylons

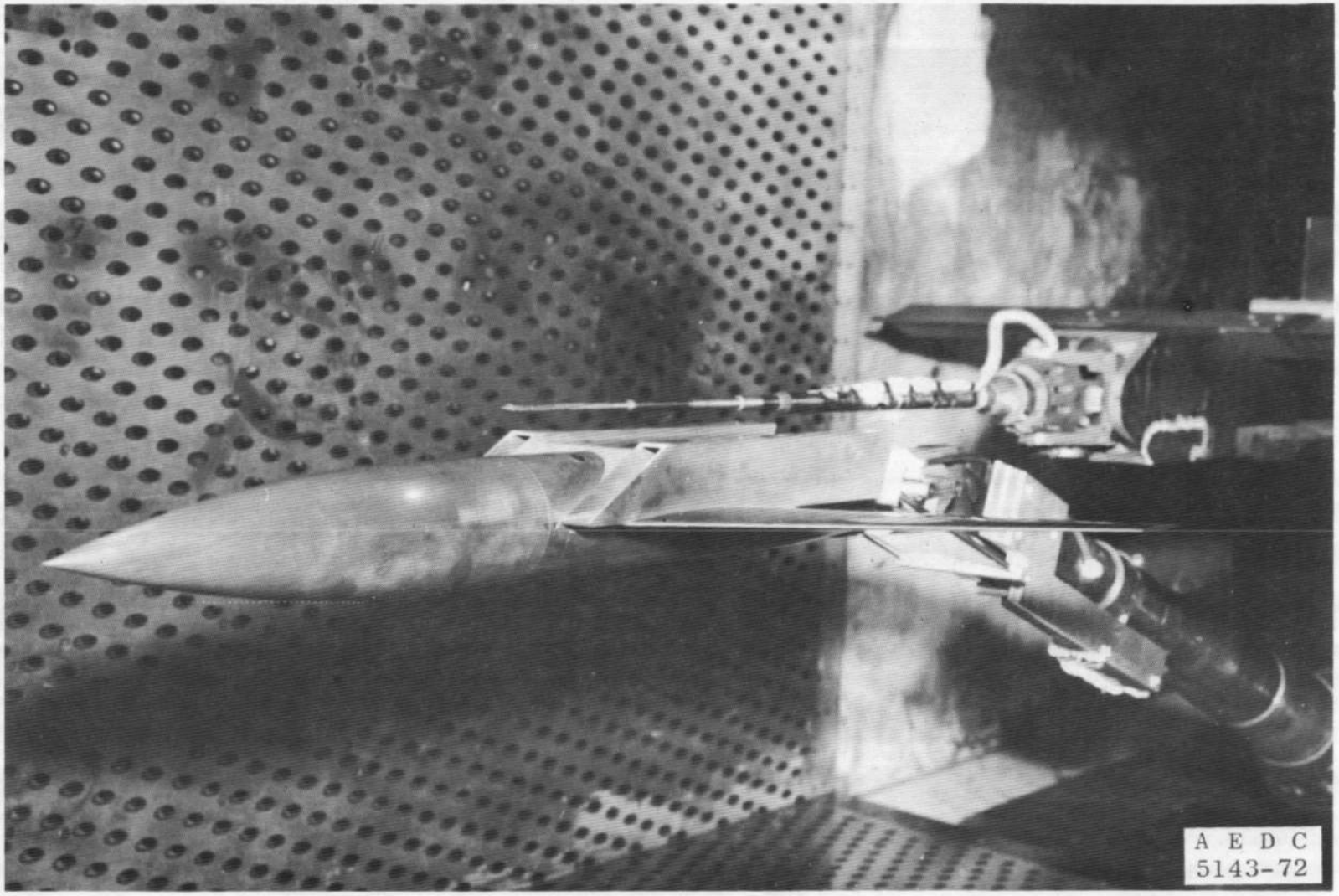

a. 40-deg Cone Probe

Fig. 16 Photograph of the Models Installed in the Tunnel

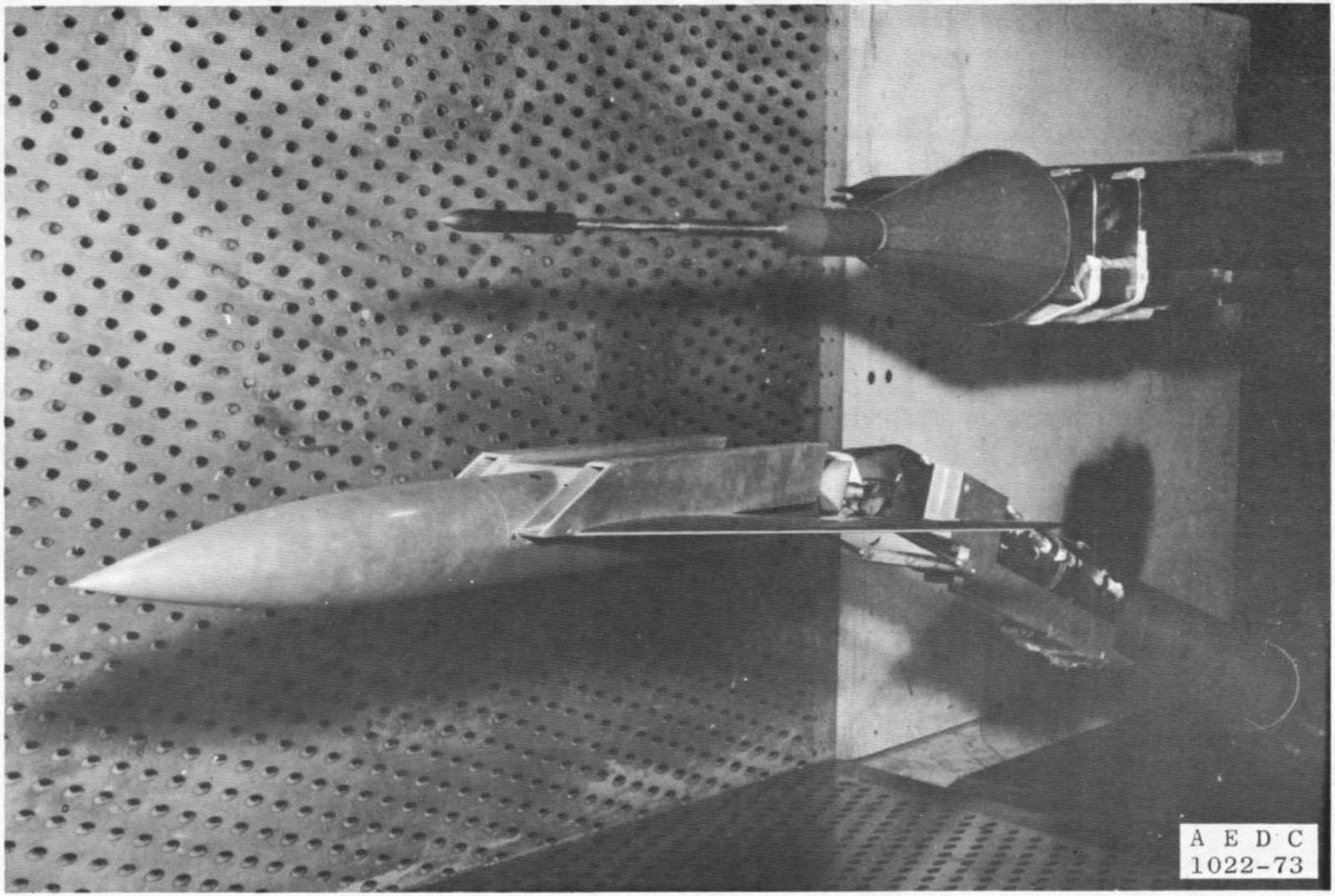

b. Pressure Distribution Model
Fig. 16 Concluded

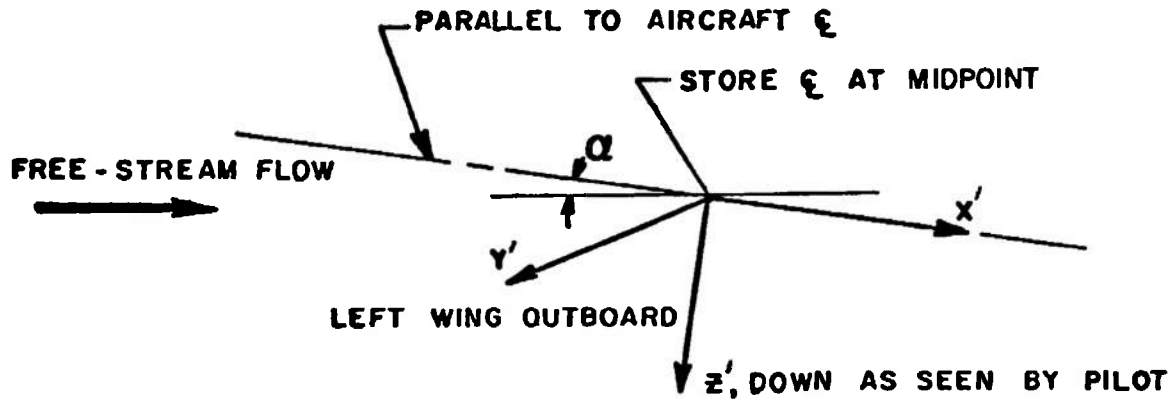

DISPLACEMENTS

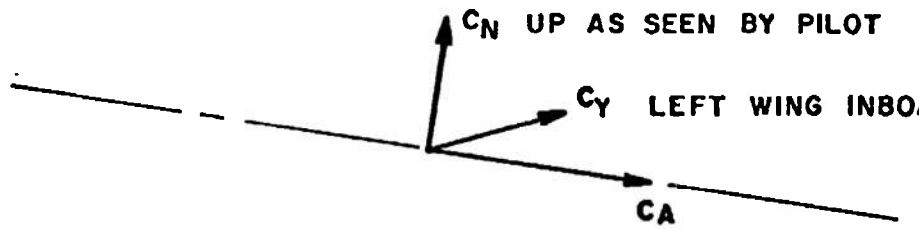

C_m and C_n POSITIVE NOSE UP AND NOSE RIGHT MOMENTS, RESPECTIVELY, AS SEEN BY THE PILOT. MOMENT REFERENCE AT THE STORE MIDPOINT.

FORCES AND MOMENTS

Fig. 17 Axis Systems Defining Displacement and Coefficient Directions

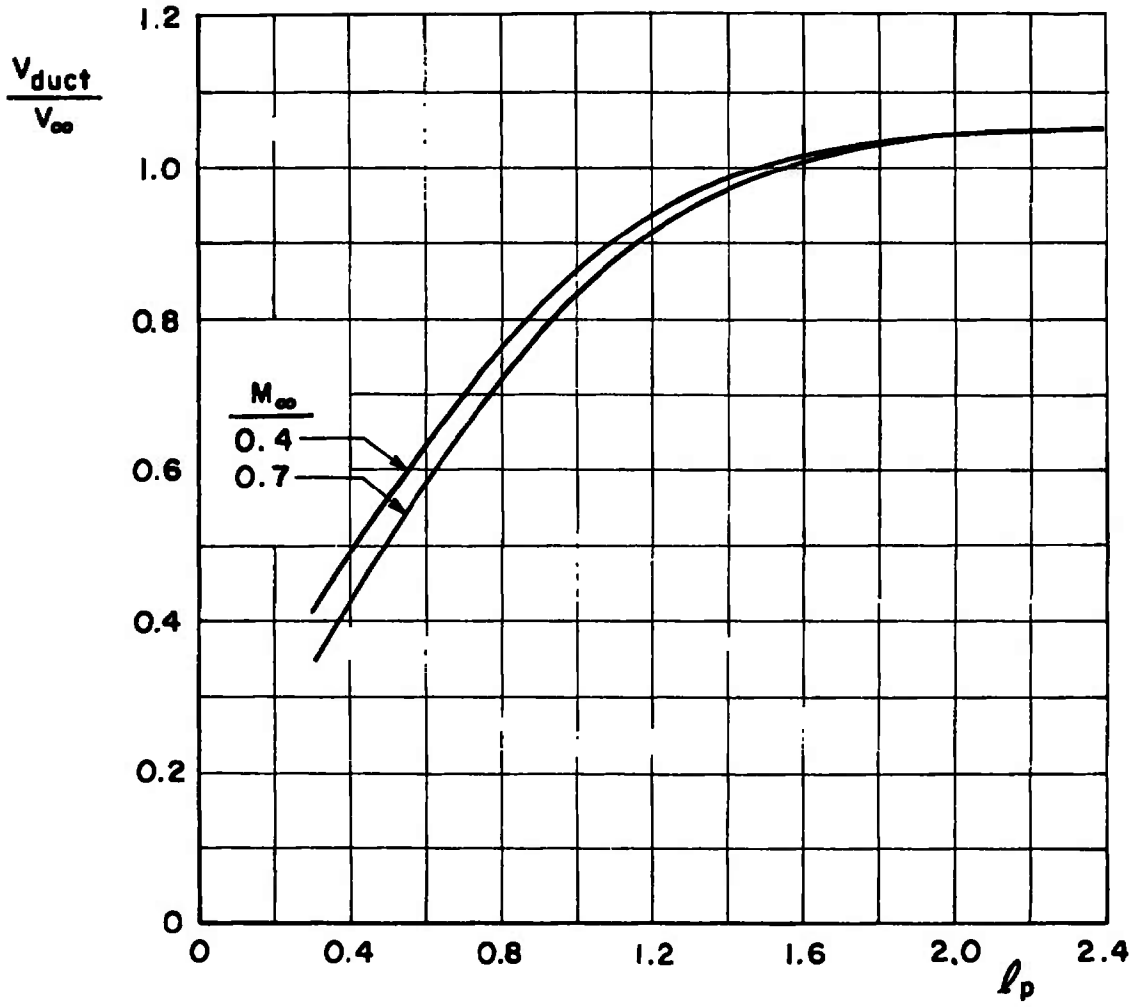

Fig. 18 Average Duct Flow Velocity Ratios for Test Mach Numbers of 0.4 and 0.7

SYMBOL	CONF	α	ℓ_p
○	7	0	0.375
□	7	0	0.750
△	7	0	2.400

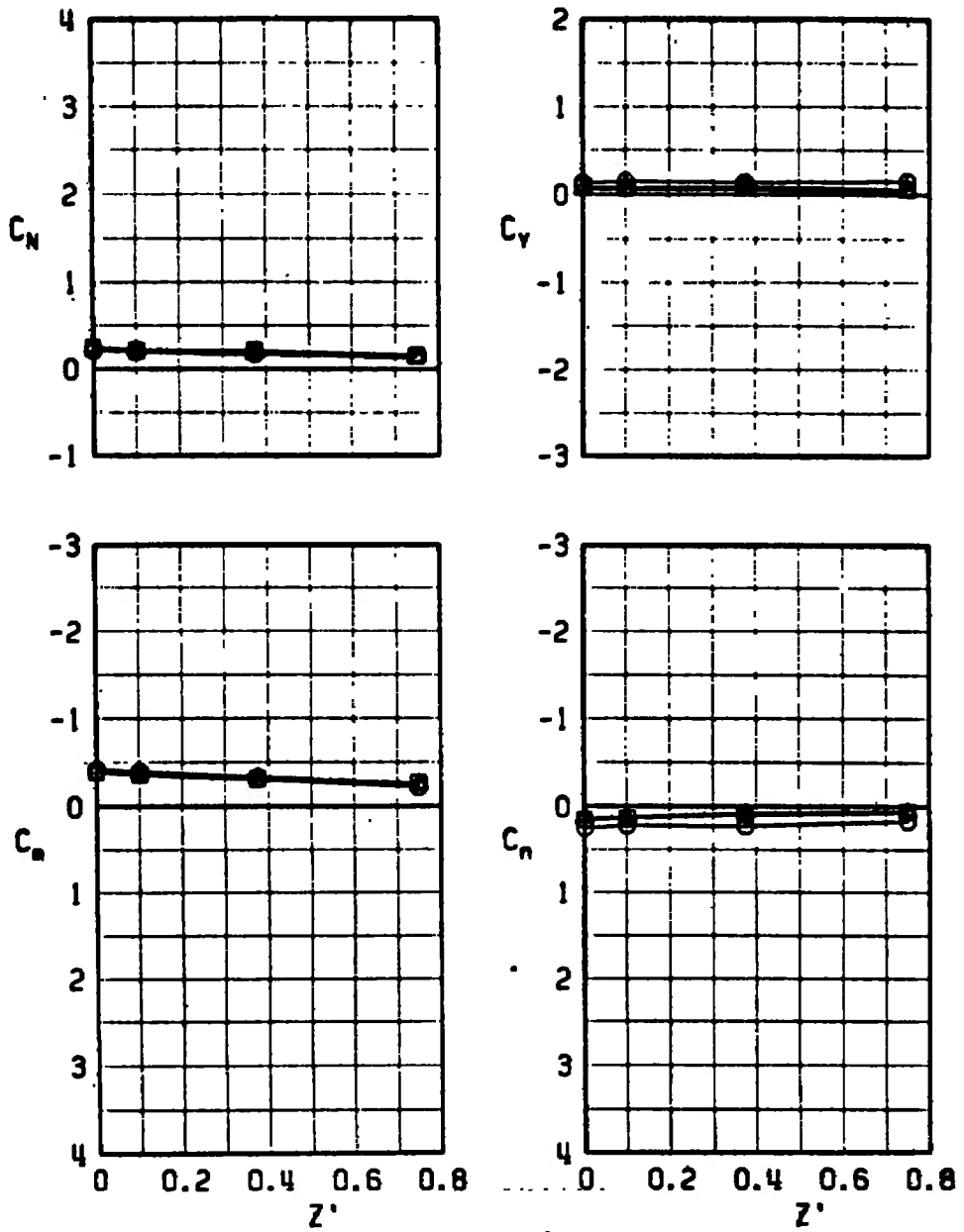

a. $\alpha = 0$, $Y' = 0$

Fig. 19 Parent-Model Duct Flow Influence on Force and Moment Coefficients for the Unfinned Large Model at the Wing 1/3-Semispan Station, $N_1B_2WA_2D$, $M_\infty = 0.4$

SYMBOL	CONF	α	ℓ_p
⊙	7	0	0.375
⊡	7	0	0.750
△	7	0	2.400

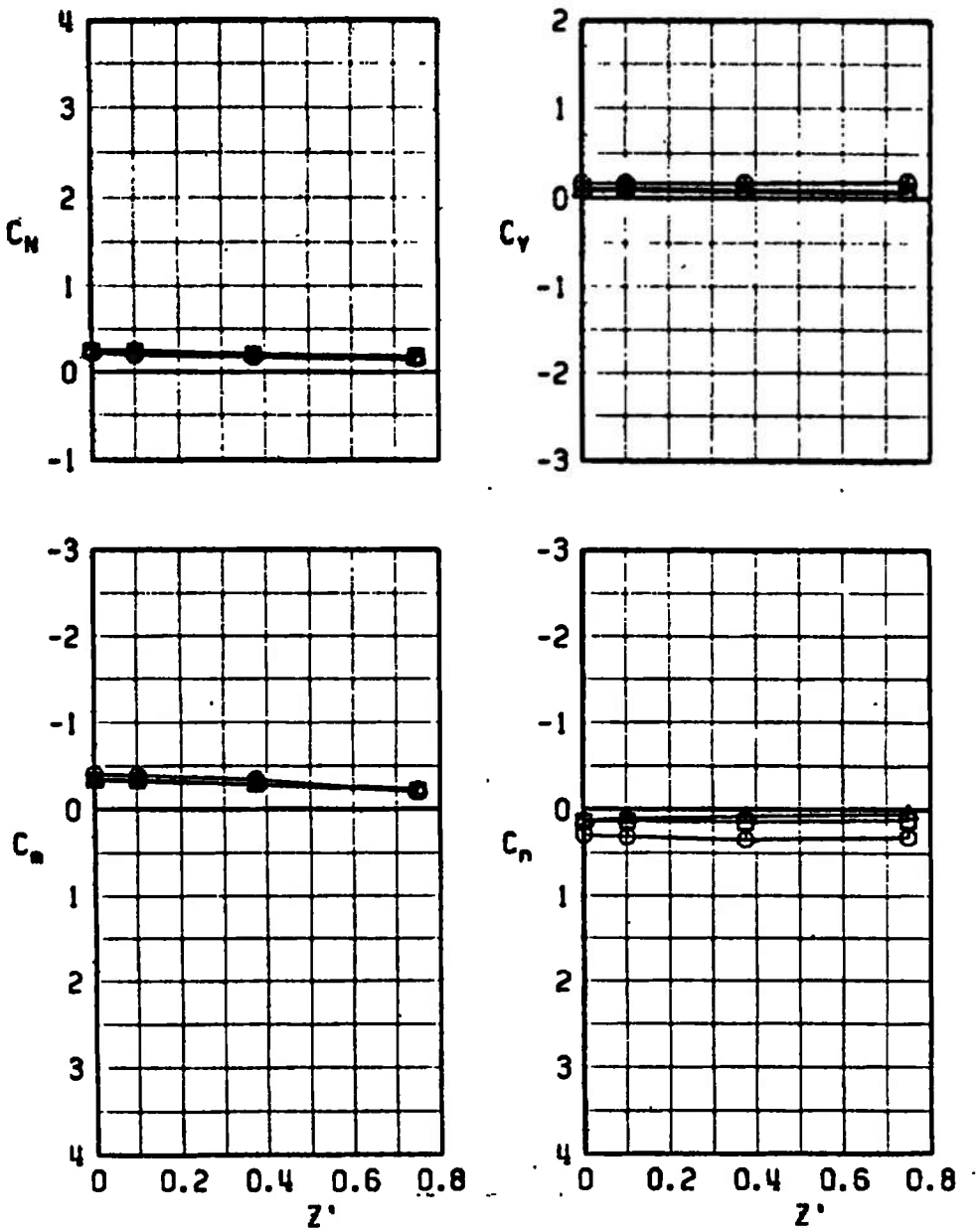

b. $\alpha = 0$, $Y' = -0.375$

Fig. 19 Continued

SYMBOL	CONF	α	ℓ_p
⊙	7	6	0.375
⊡	7	6	0.750
△	7	6	2.400

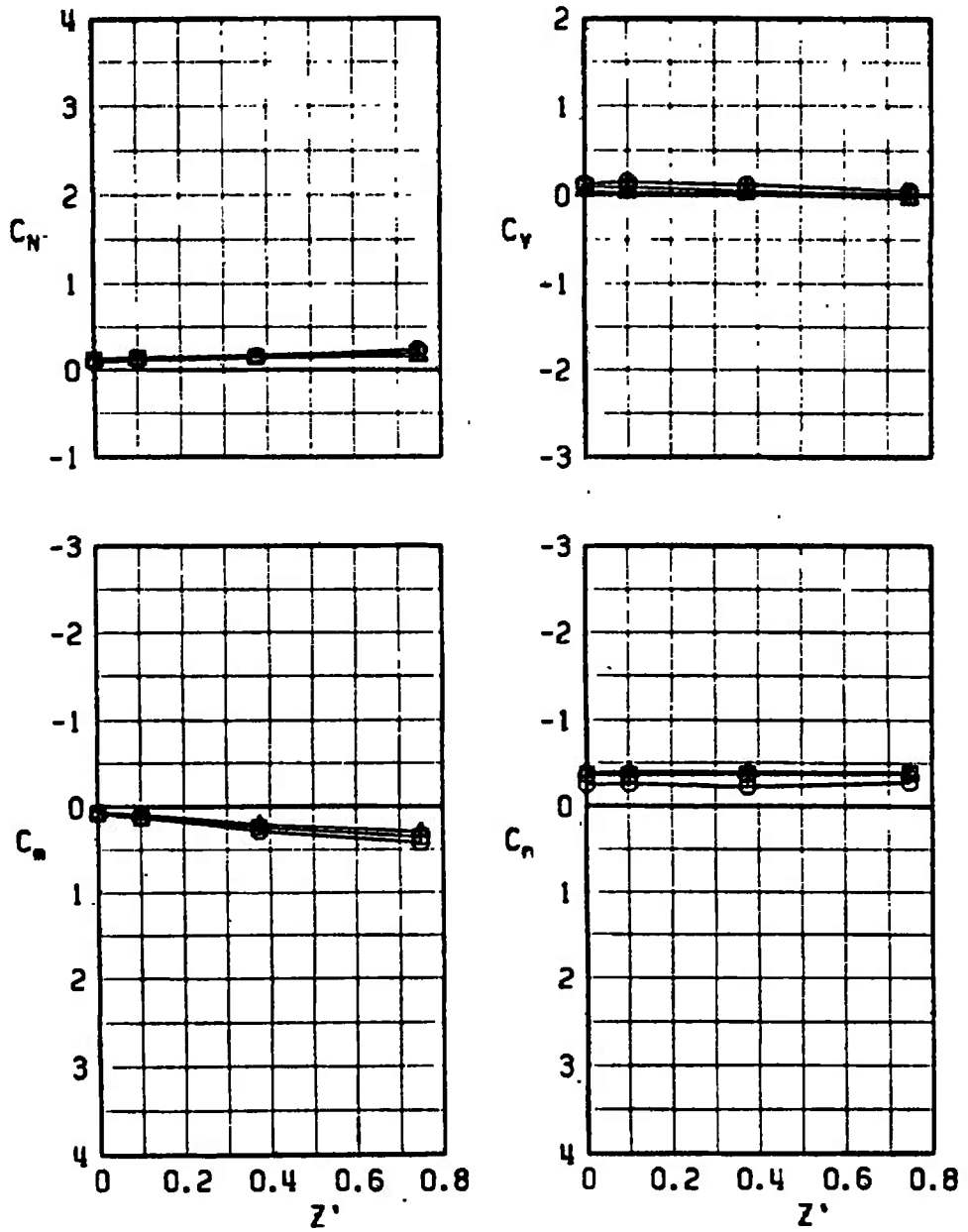

c. $\alpha = 6$, $Y' = 0$

Fig. 19 Continued

SYMBOL	CONF	α	ℓ_p
○	7	6	0.375
□	7	6	0.750
△	7	6	2.400

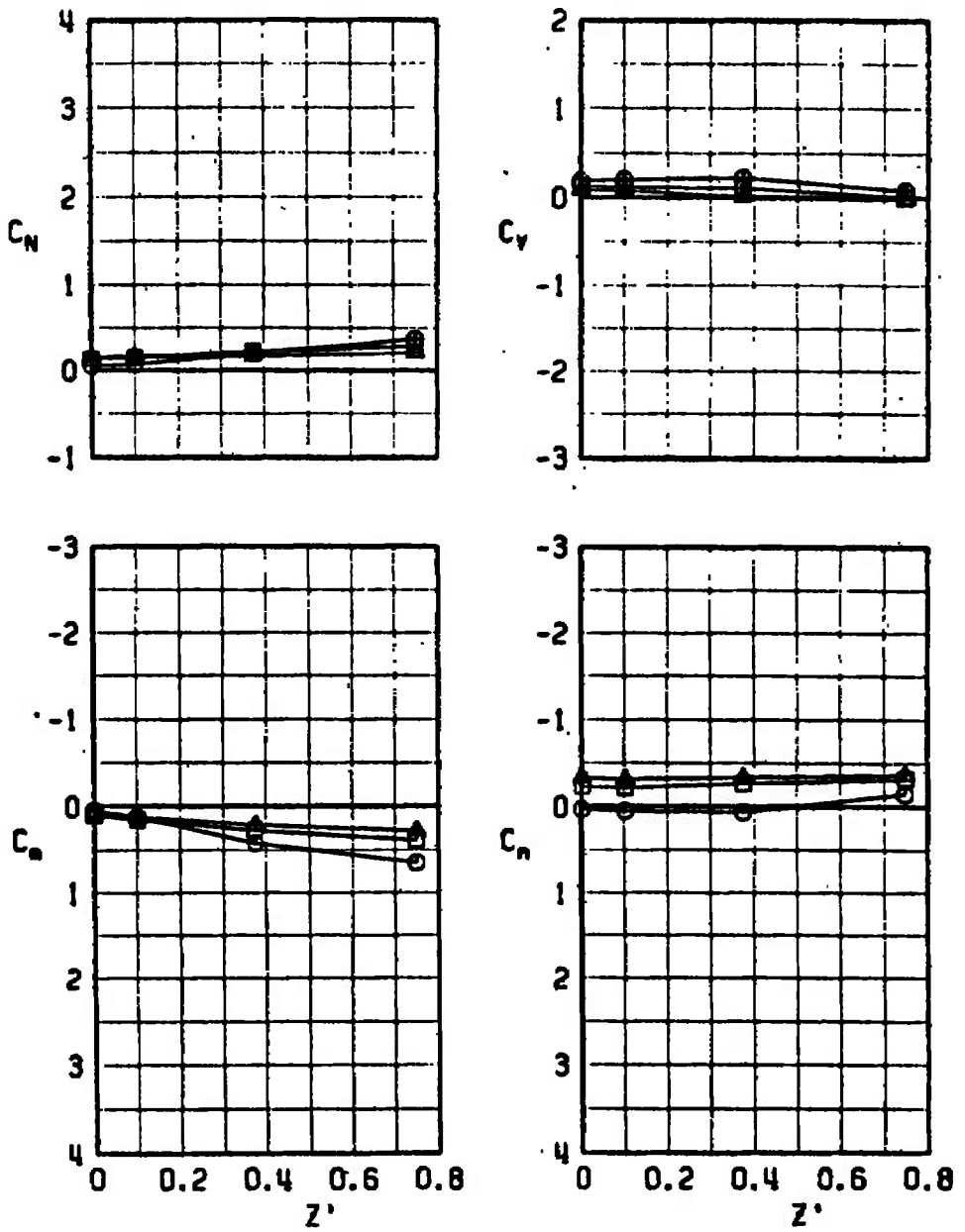

d. $\alpha = 6$, $Y' = -0.375$

Fig. 19 Continued

SYMBOL	CONF	α	ℓ_p
⊙	7	15	0.375
□	7	15	0.750
△	7	15	2.400

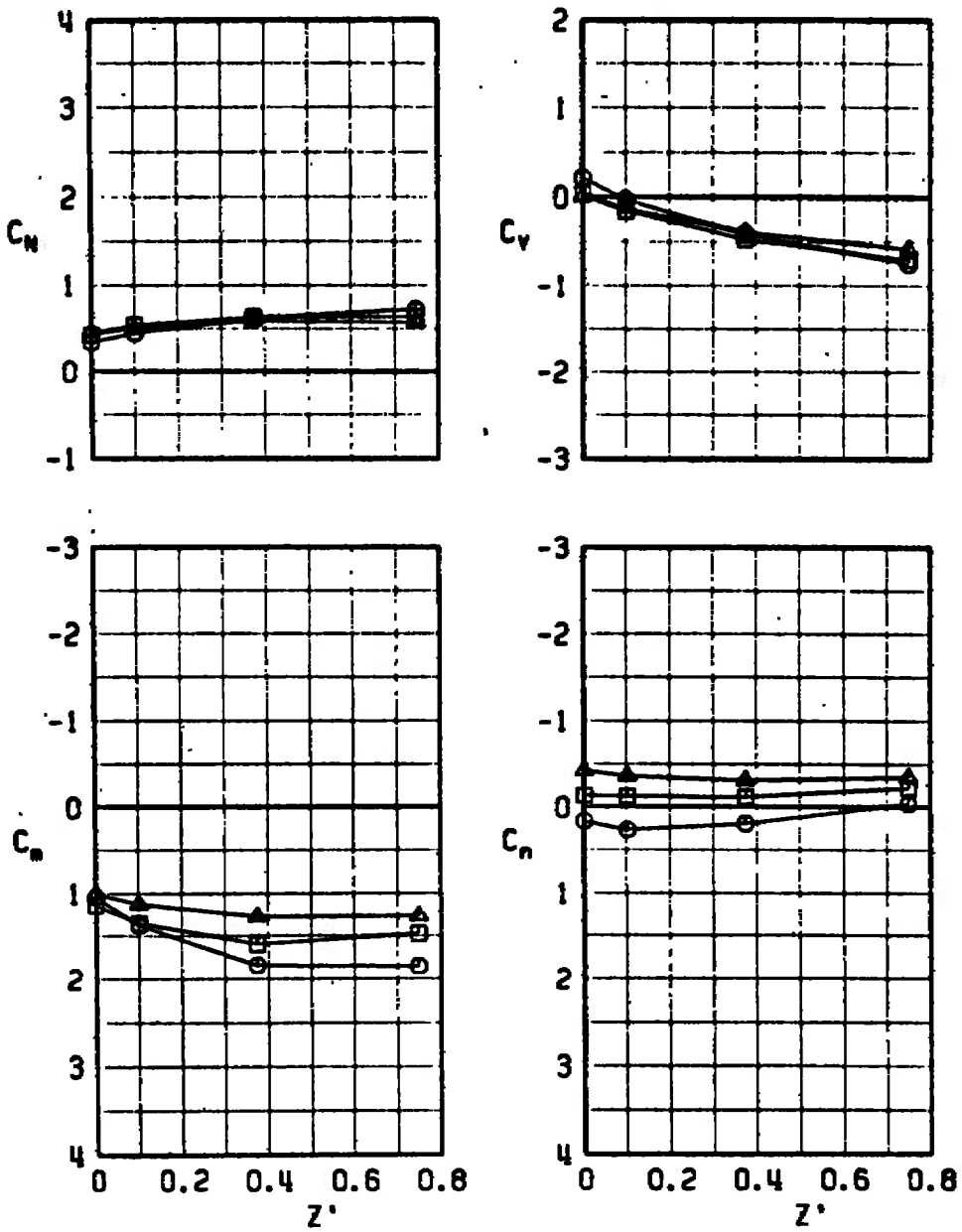

e. $\alpha = 15$, $Y' = 0$

Fig. 19 Continued

SYMBOL	CONF	α	ℓ_p
○	7	15	0.375
□	7	15	0.750
△	7	15	2.400

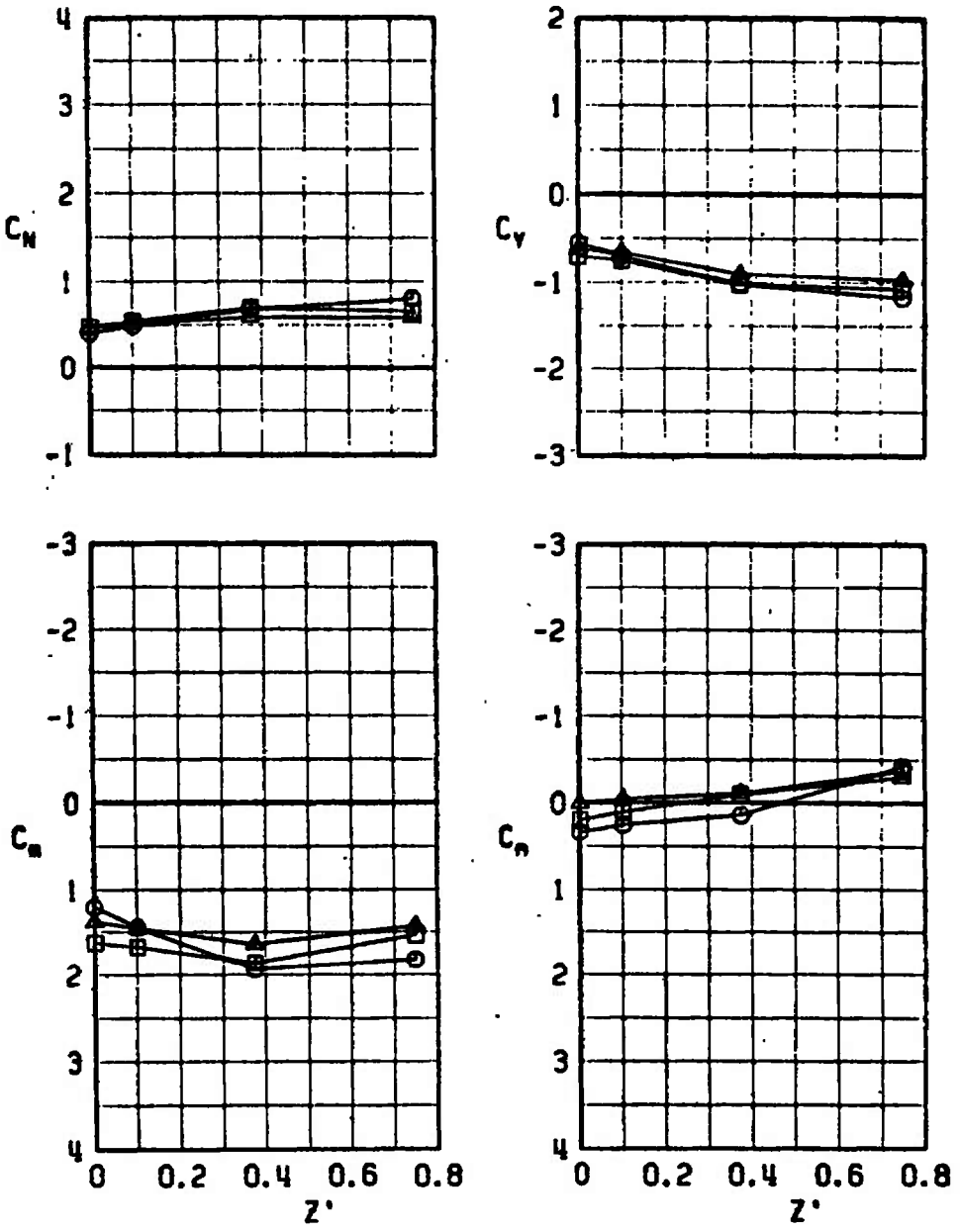

f. α = 15, Y' = -0.375
Fig. 19 Concluded

SYMBOL	CONF	α	ℓ_p
○	12	0	0.375
□	12	0	0.750
△	12	0	2.400

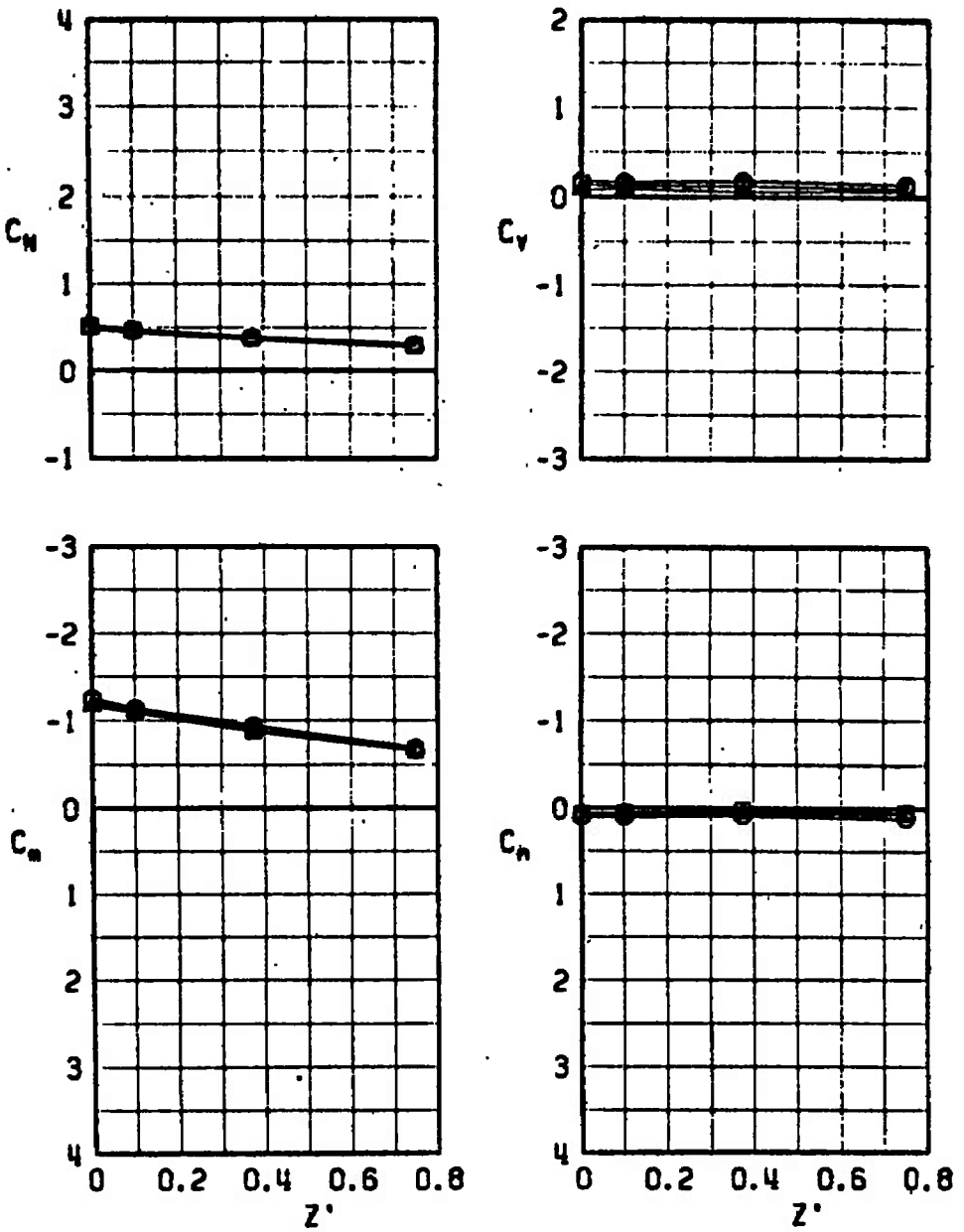

a. $\alpha = 0$, $Y' = 0$

Fig. 20 Parent-Model Duct Flow Influence on Force and Moment Coefficients for the Finned Large Model at the Wing 1/3-Semispan Station, $N_1B_2WA_2D$, $M_\infty = 0.4$

SYMBOL	CONF	α	ℓ_p
○	12	0	0.375
□	12	0	0.750
△	12	0	2.400

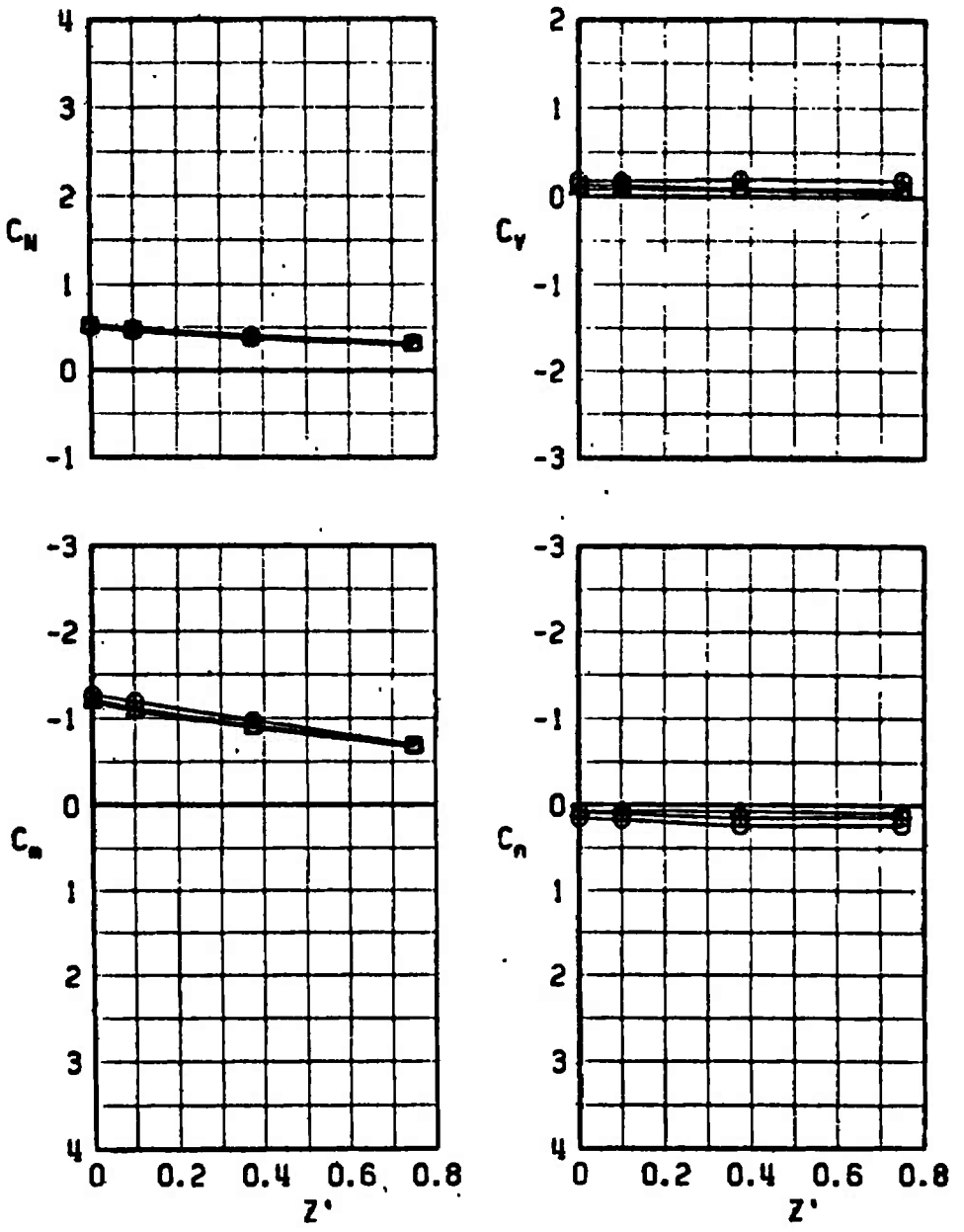

b. $\alpha = 0$, $Y' = -0.375$

Fig. 20 Continued

SYMBOL	CONF	α	ℓ_p
○	12	6	0.375
□	12	6	0.750
△	12	6	2.400

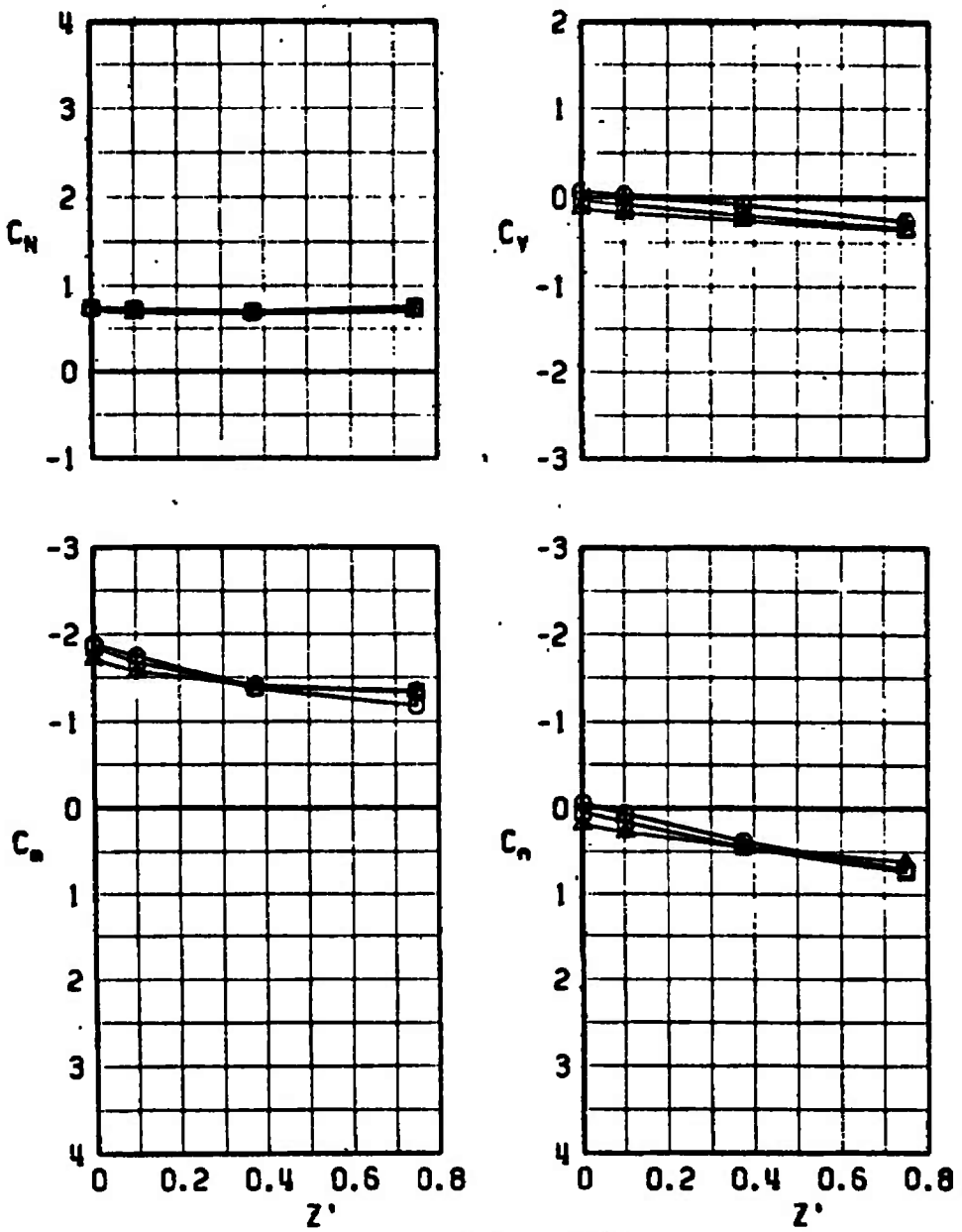

c. $\alpha = 0$, $Y' = -0.375$

Fig. 20 Continued

SYMBOL	CONF	α	ℓ_p
○	12	6	0.375
□	12	6	0.750
△	12	6	2.400

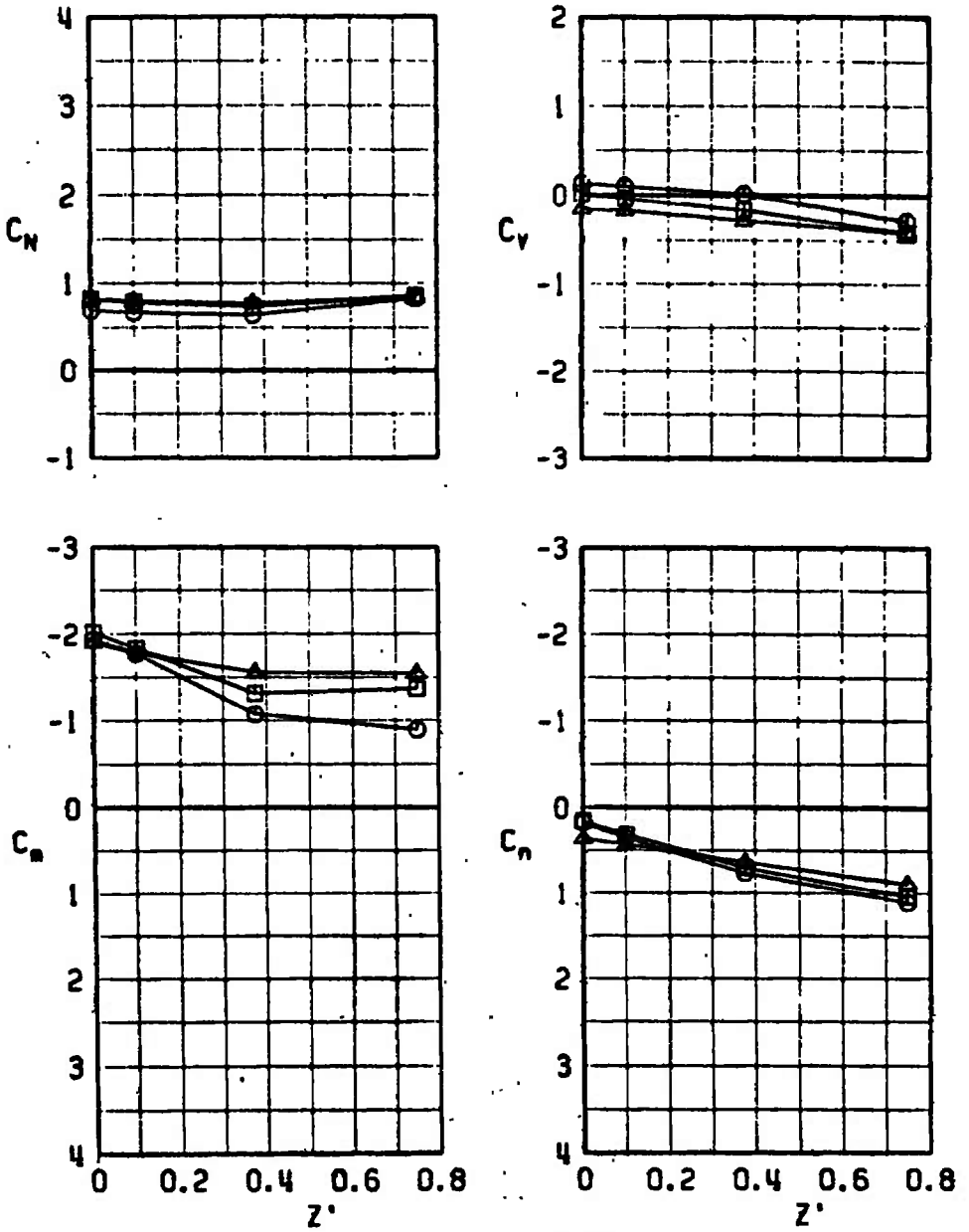

d. α = 6, Y' = -0.375
Fig. 20 Continued

SYMBOL	CONF	α	ℓ_p
○	12	15	0.375
□	12	15	0.750
△	12	15	2.400

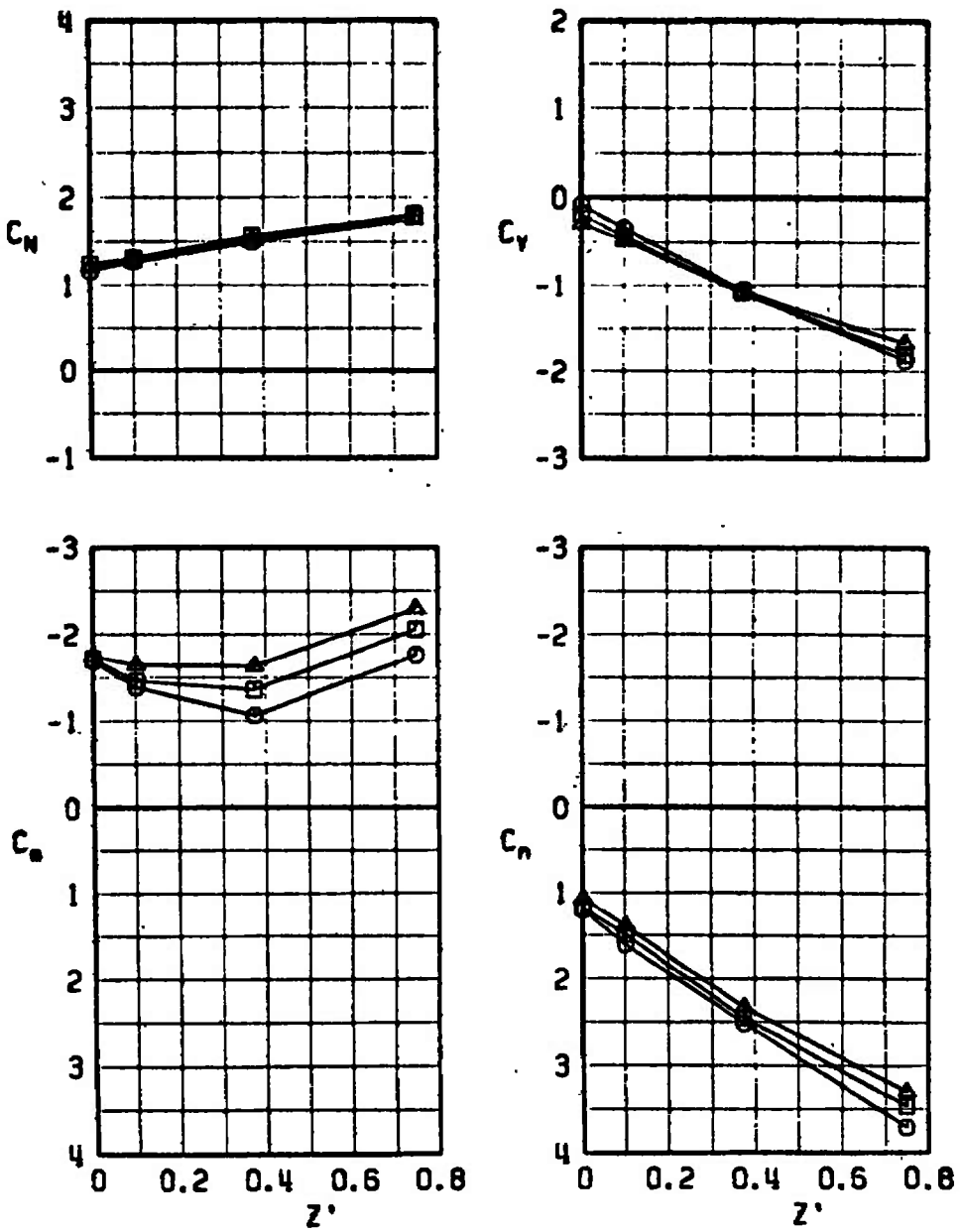

e. $\alpha = 15$, $Y' = 0$

Fig. 20 Continued

SYMBOL	CONF	α	ℓ_p
○	12	15	0.375
□	12	15	0.750
△	12	15	2.400

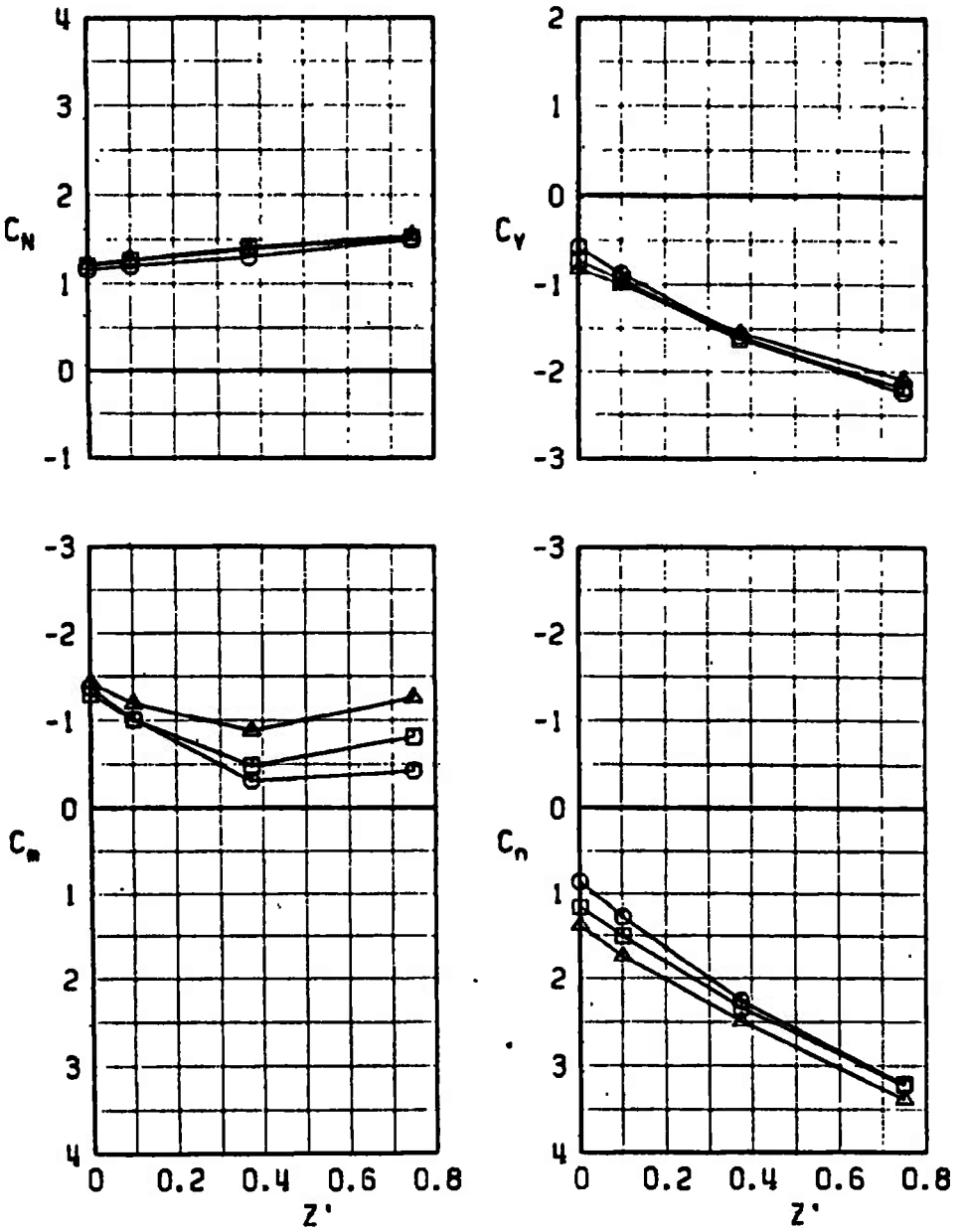

f. α = 15, Y' = -0.375

Fig. 20 Concluded

SYMBOL	CONF	α	ℓ_p
⊙	8	0	0.375
□	8	0	0.750
△	8	0	2.400

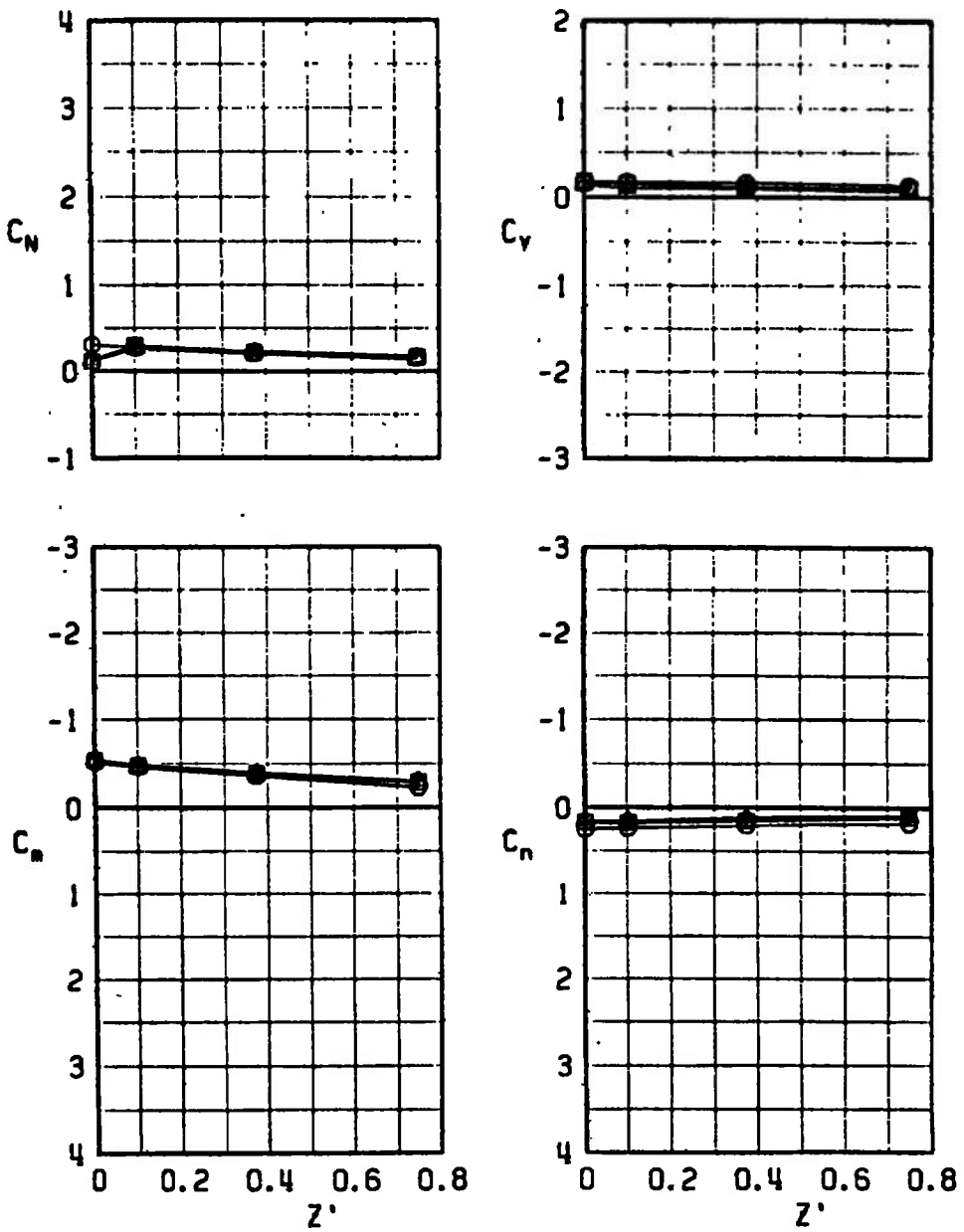

a. $\alpha = 0$, $Y' = 0$

Fig. 21 Parent-Model Duct Flow Influence on Force and Moment Coefficients for the Unfinned Large Model at tha Wing 1/3-Semispan Station, $N_1B_2WP_{1/3}A_2D$, $M_\infty = 0.4$

SYMBOL	CONF	α	ℓ_p
⊙	8	0	0.375
⊡	8	0	0.750
△	8	0	2.400

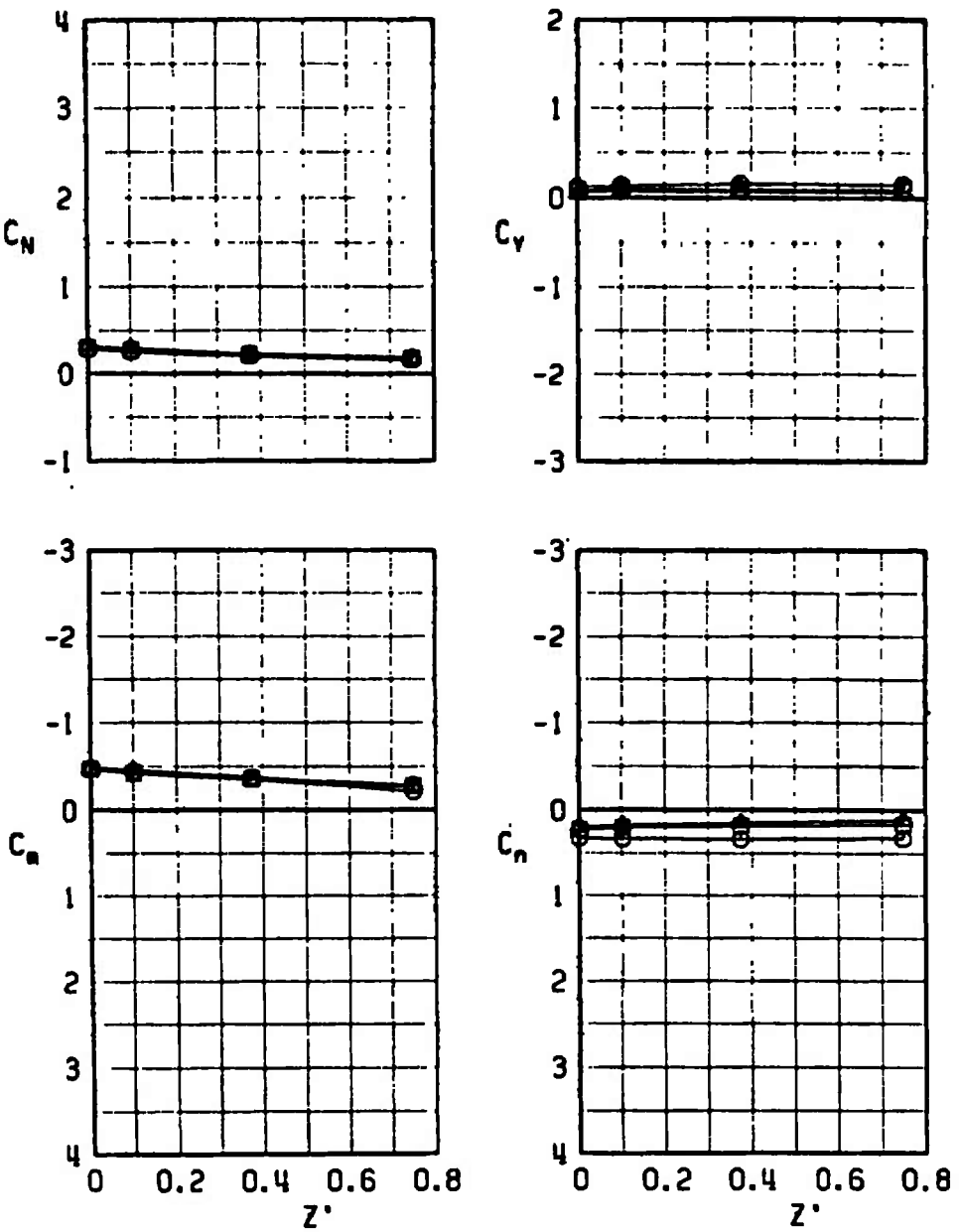

b. α = 0, Y' = -0.375
Fig. 21 Continued

SYMBOL	CONF	α	ℓ_p
○	8	6	0.375
□	8	6	0.750
△	8	6	2.400

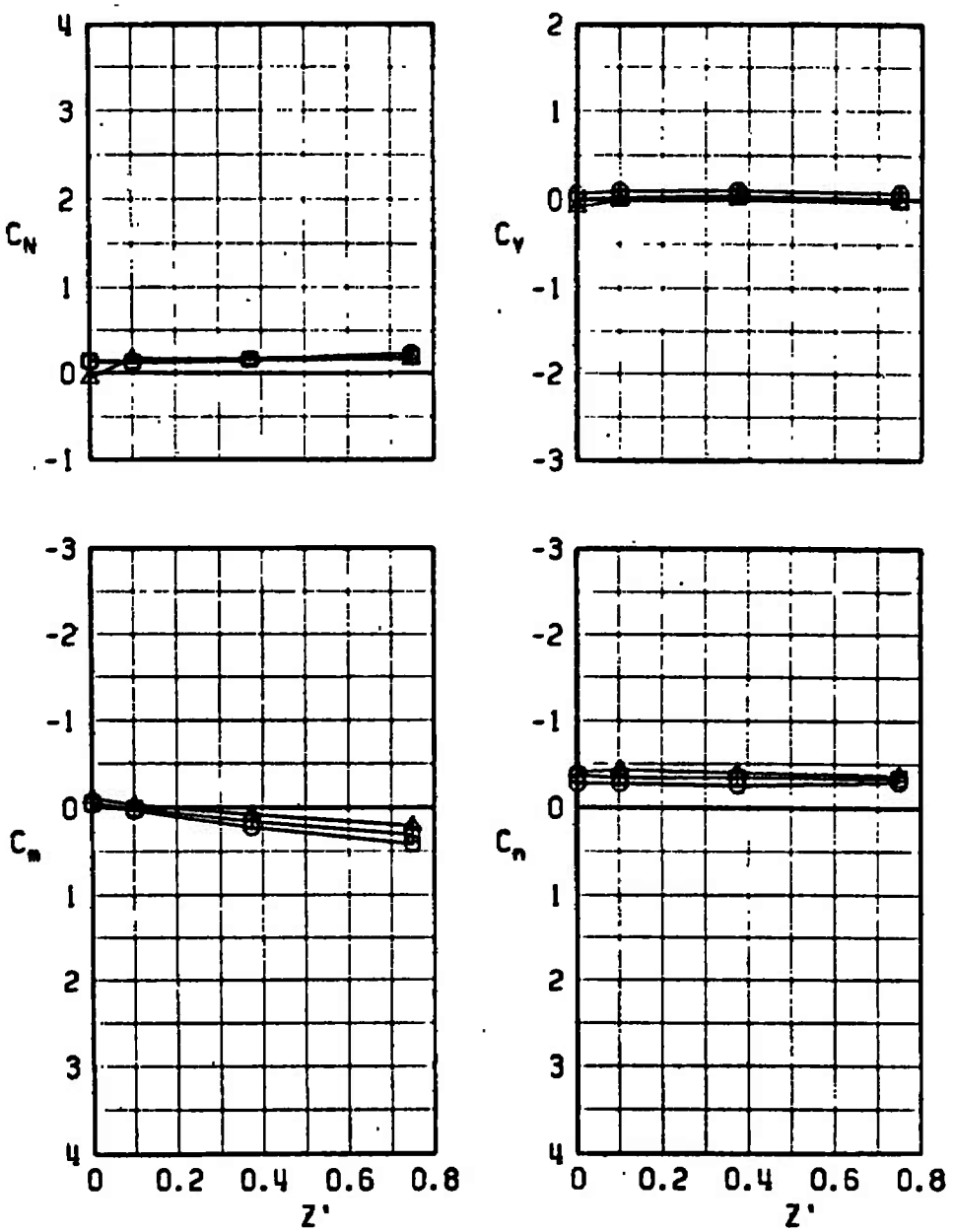

c. $\alpha = 6$, $Y' = 0$

Fig. 21 Continued

SYMBOL	CONF	α	ℓ_p
○	8	6	0.375
□	8	6	0.750
△	8	6	2.400

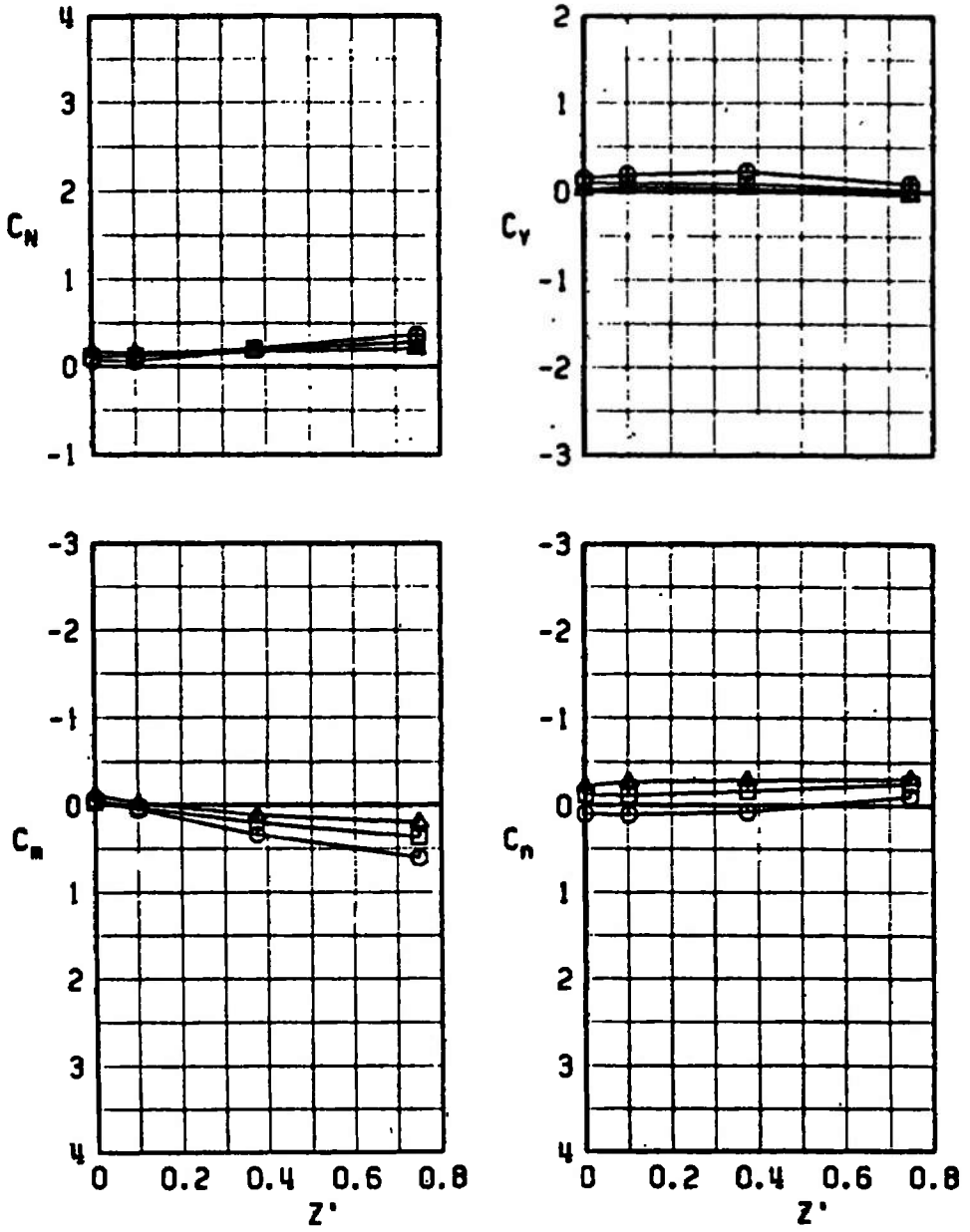

d. α = 6, Y' = -0.375
Fig. 21 Continued

SYMBOL	CONF	α	ℓ_p
○	8	15	0.375
□	8	15	0.750
△	8	15	2.400

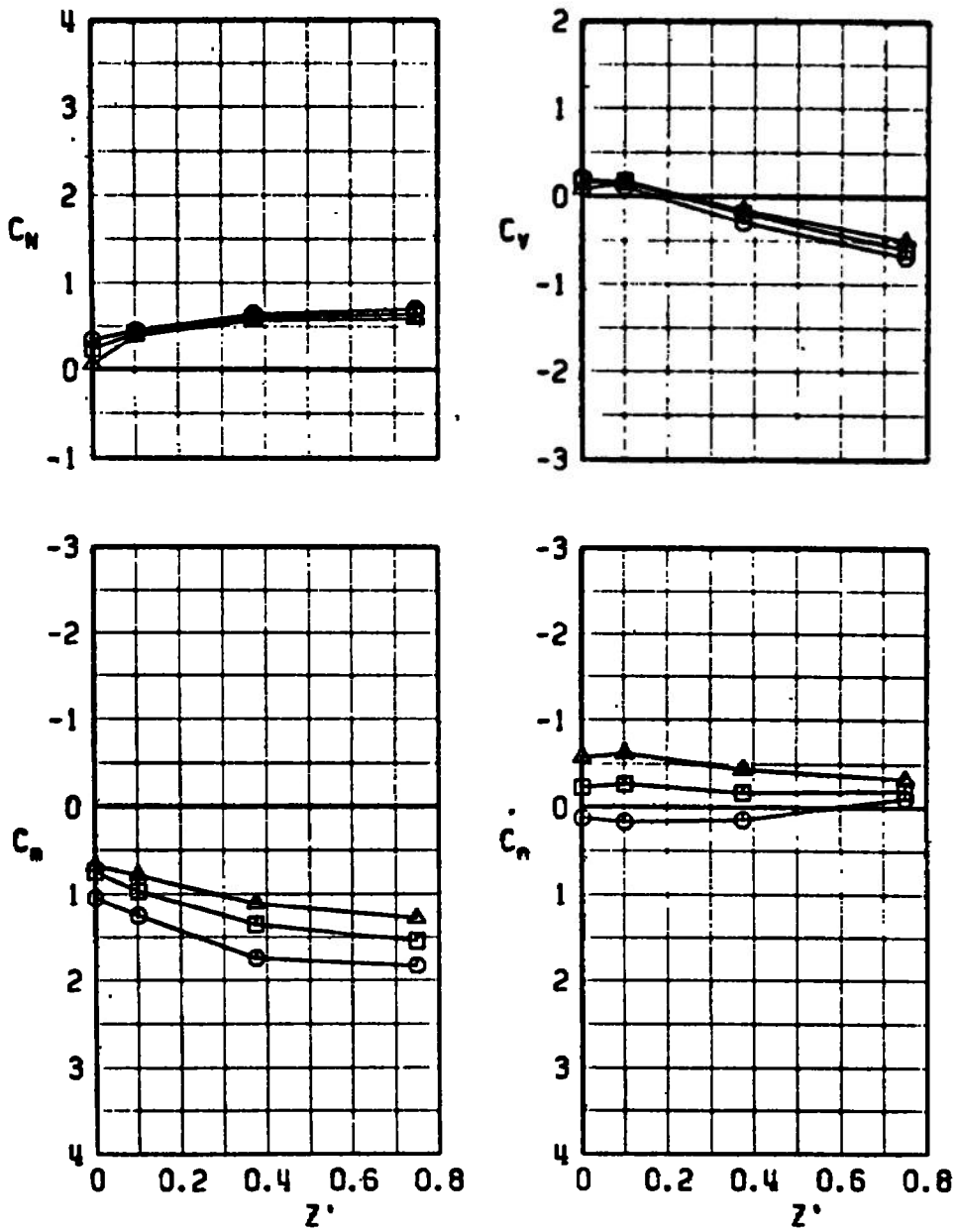

a. $\alpha = 15$, $Y' = 0$

Fig. 21 Continued

SYMBOL	CONF	α	ℓ_p
○	8	15	0.375
□	8	15	0.750
△	8	15	2.400

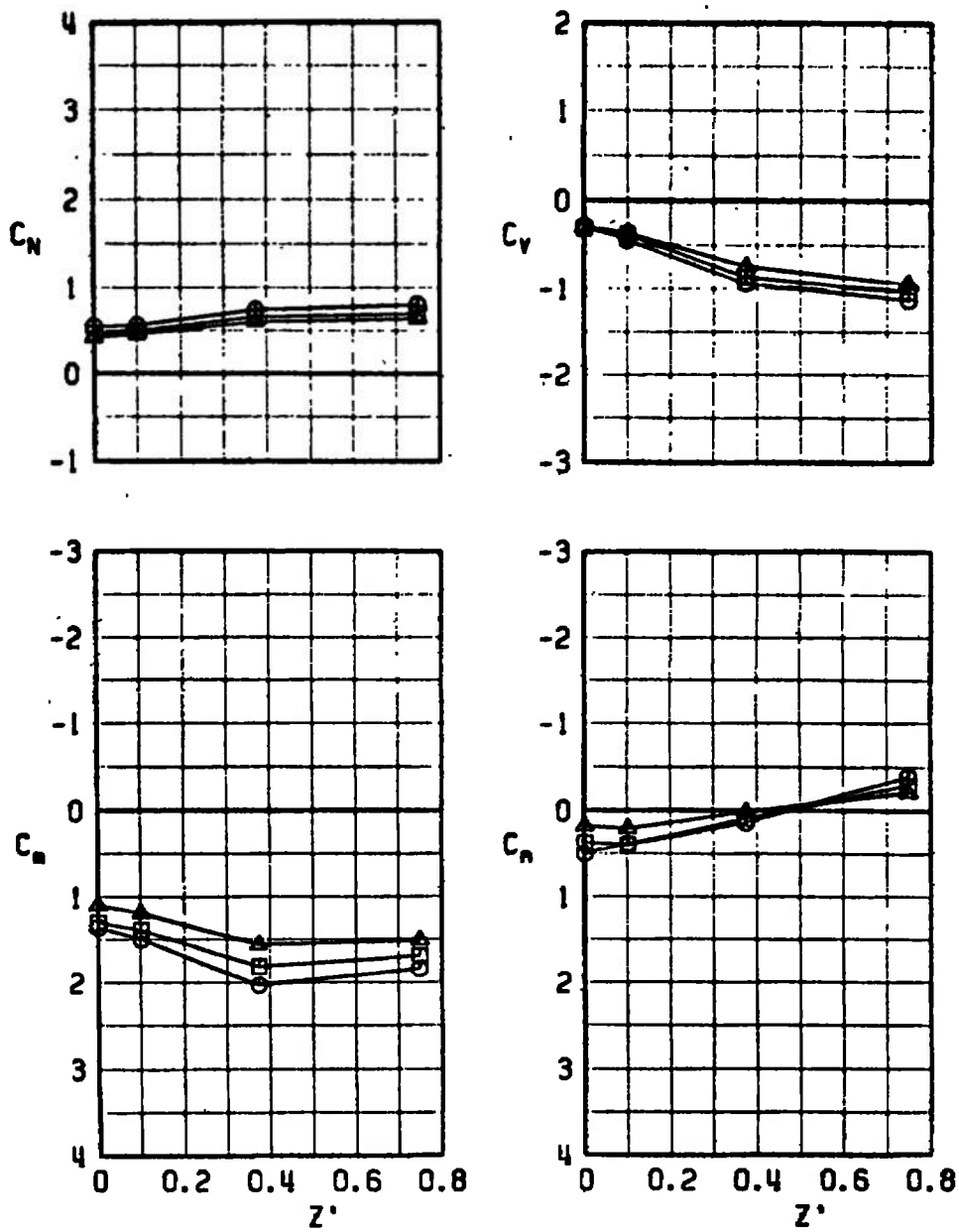

f. α = 15, Y' = -0.375
Fig. 21 Concluded

SYMBOL	CONF	α	ℓ_p
⏲	13	0	0.375
⊡	13	0	0.750
△	13	0	2.400

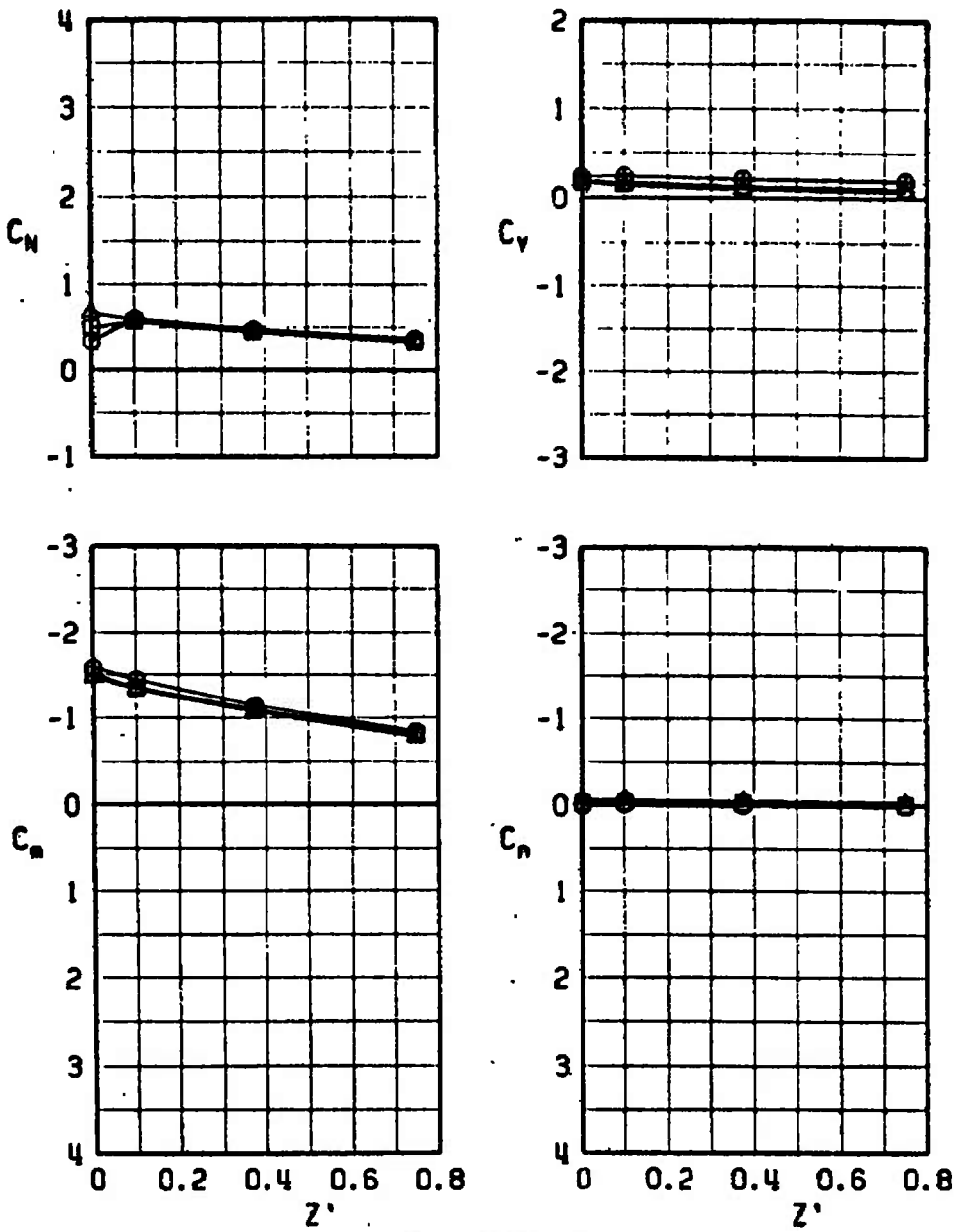

a. $\alpha = 0$, $Y' = 0$

Fig. 22 Parent-Model Duct Flow Influence on Force and Moment Coefficients for the Finned Large Model at the Wing 1/3-Semispan Station, $N_1 B_2 WP_{1/3} A_2 D$, $M_\infty = 0.4$

SYMBOL	CONF	α	ℓ_p
○	13	0	0.375
□	13	0	0.750
△	13	0	2.400

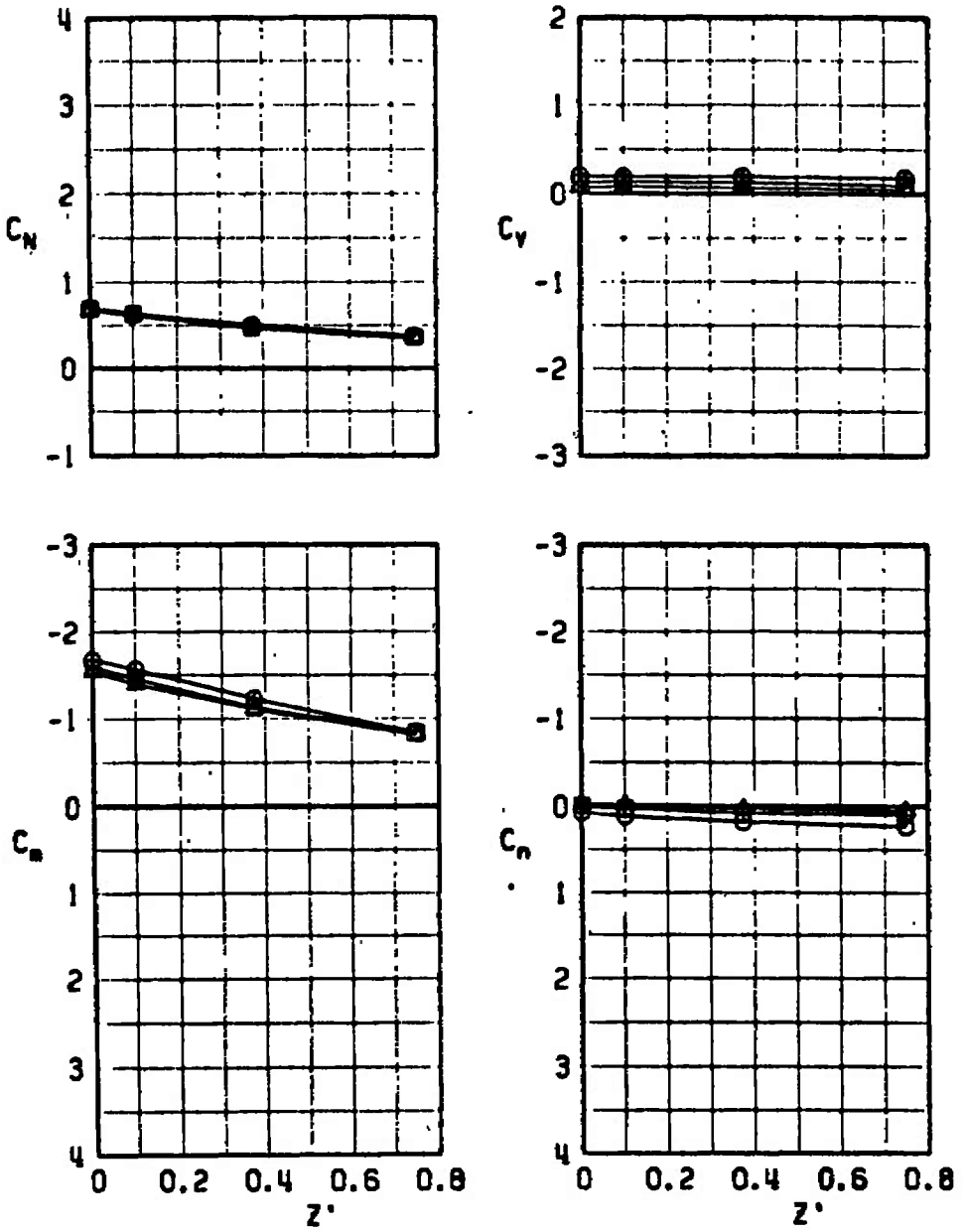

b. $\alpha = 0$, Y' = -0.375

Fig. 22 Continued

SYMBOL	CONF	α	ℓ_p
⊙	13	6	0.375
□	13	6	0.750
△	13	6	2.400

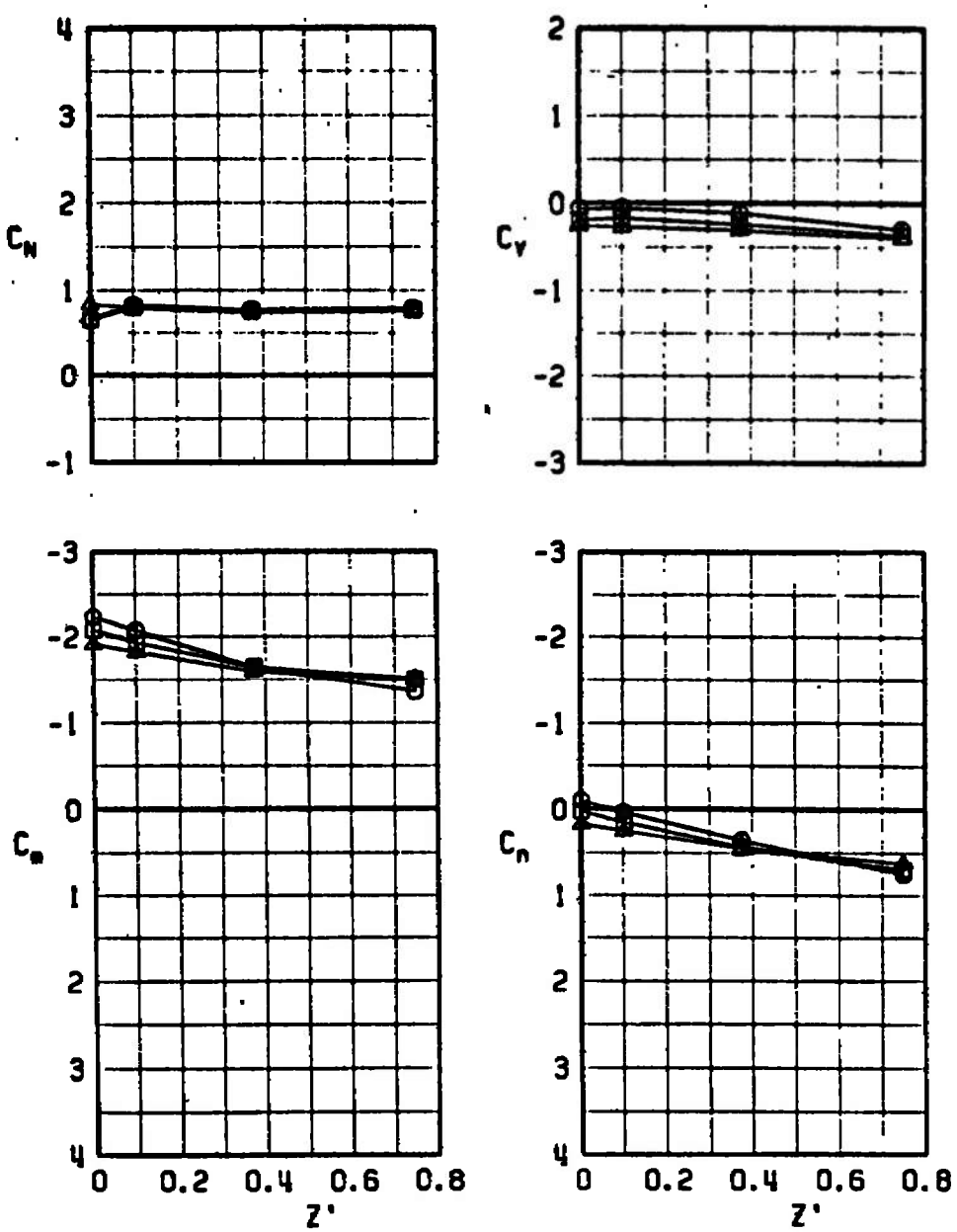

c. $\alpha = 6$, $Y' = 0$

Fig. 22 Continued

SYMBOL	CONF	α	ℓ_p
○	13	6	0.375
□	13	6	0.750
△	13	6	2.400

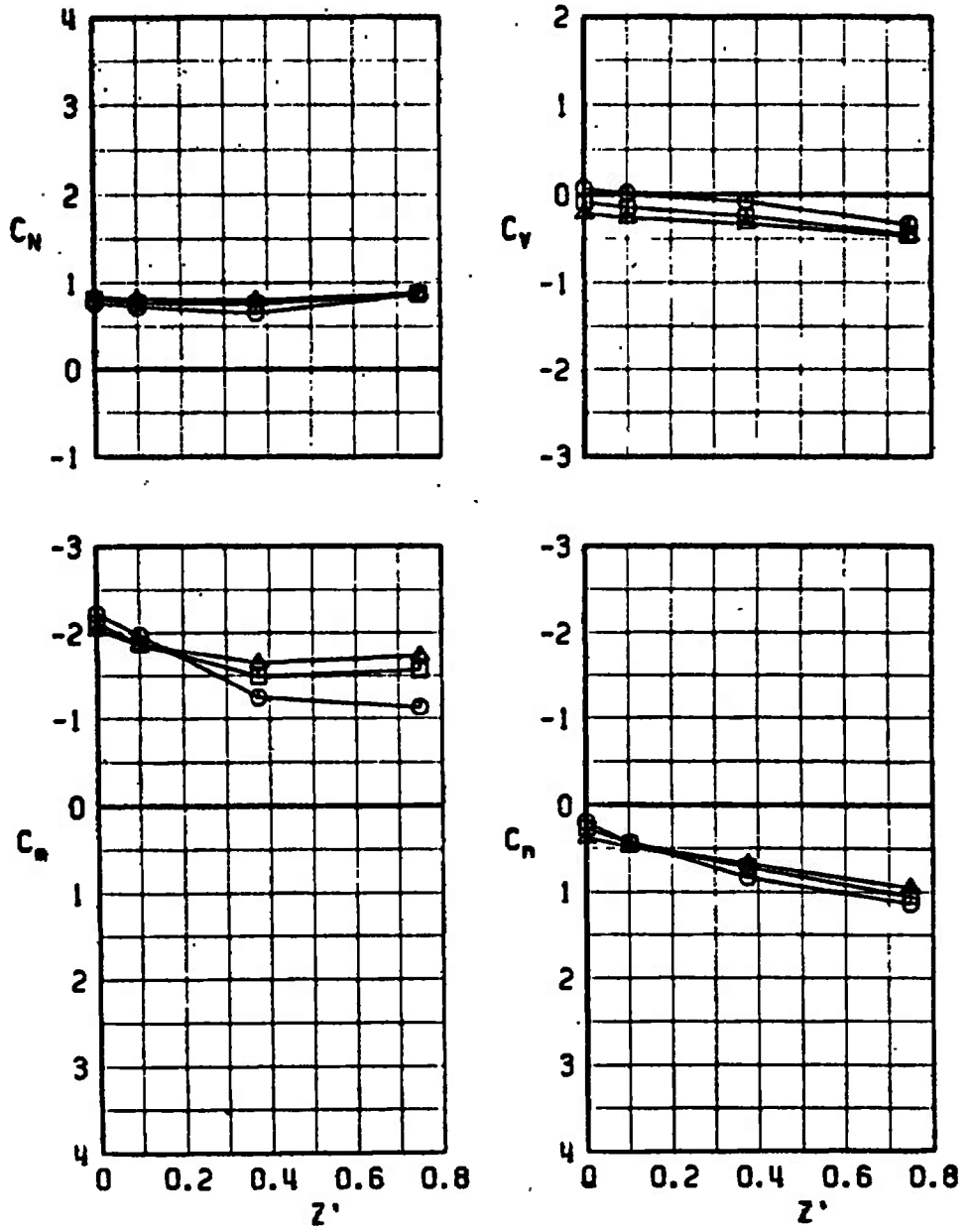

d. $\alpha = 6$, $Y' = -0.375$

Fig. 22 Continued

SYMBOL	CONF	α	ℓ_p
⊙	13	15	0.375
□	13	15	0.750
△	13	15	2.400

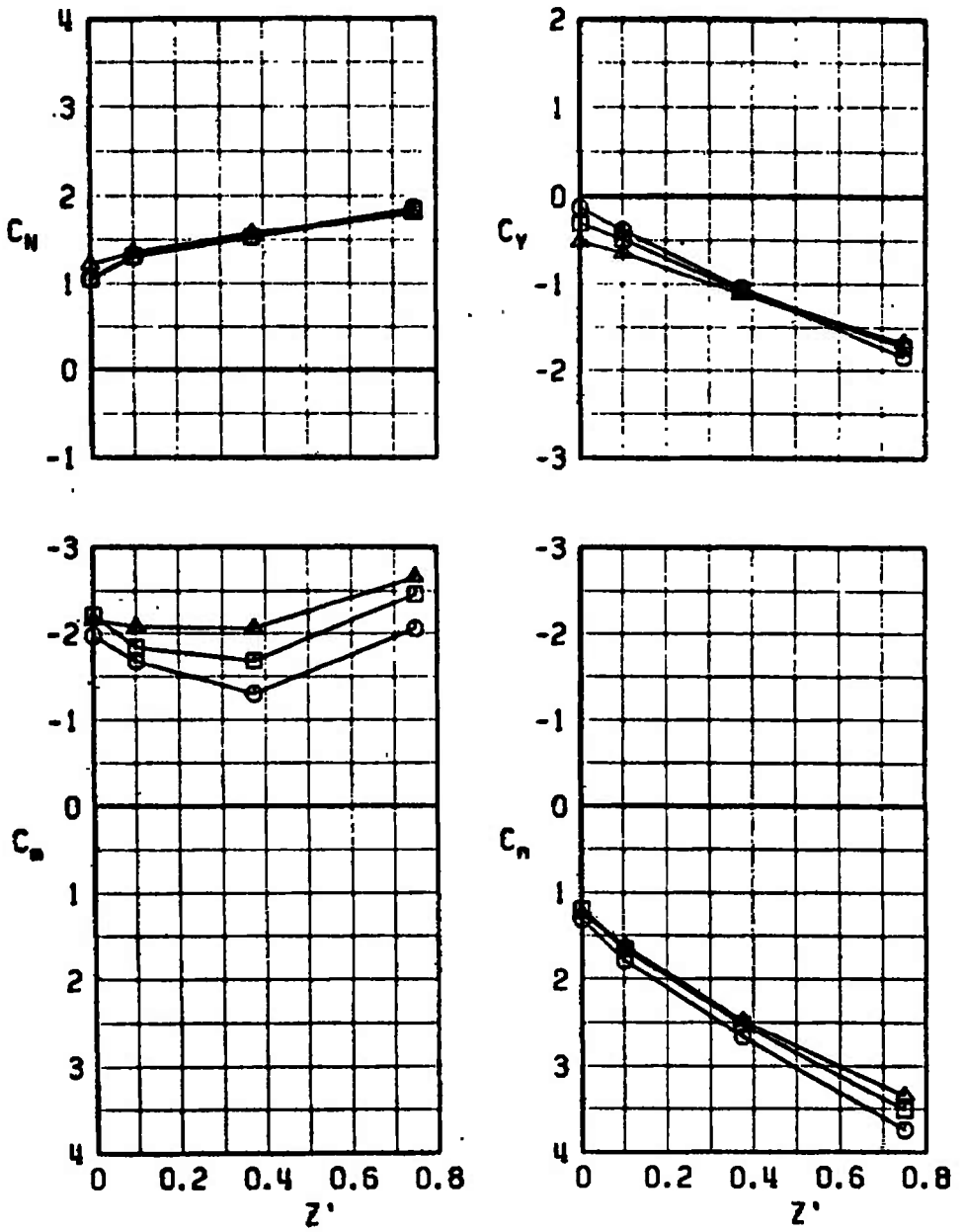

e. α = 15, Y' = 0

Fig. 22 Continued

SYMBOL	CONF	α	ℓ_p
○	13	15	0.375
□	13	15	0.750
△	13	15	2.400

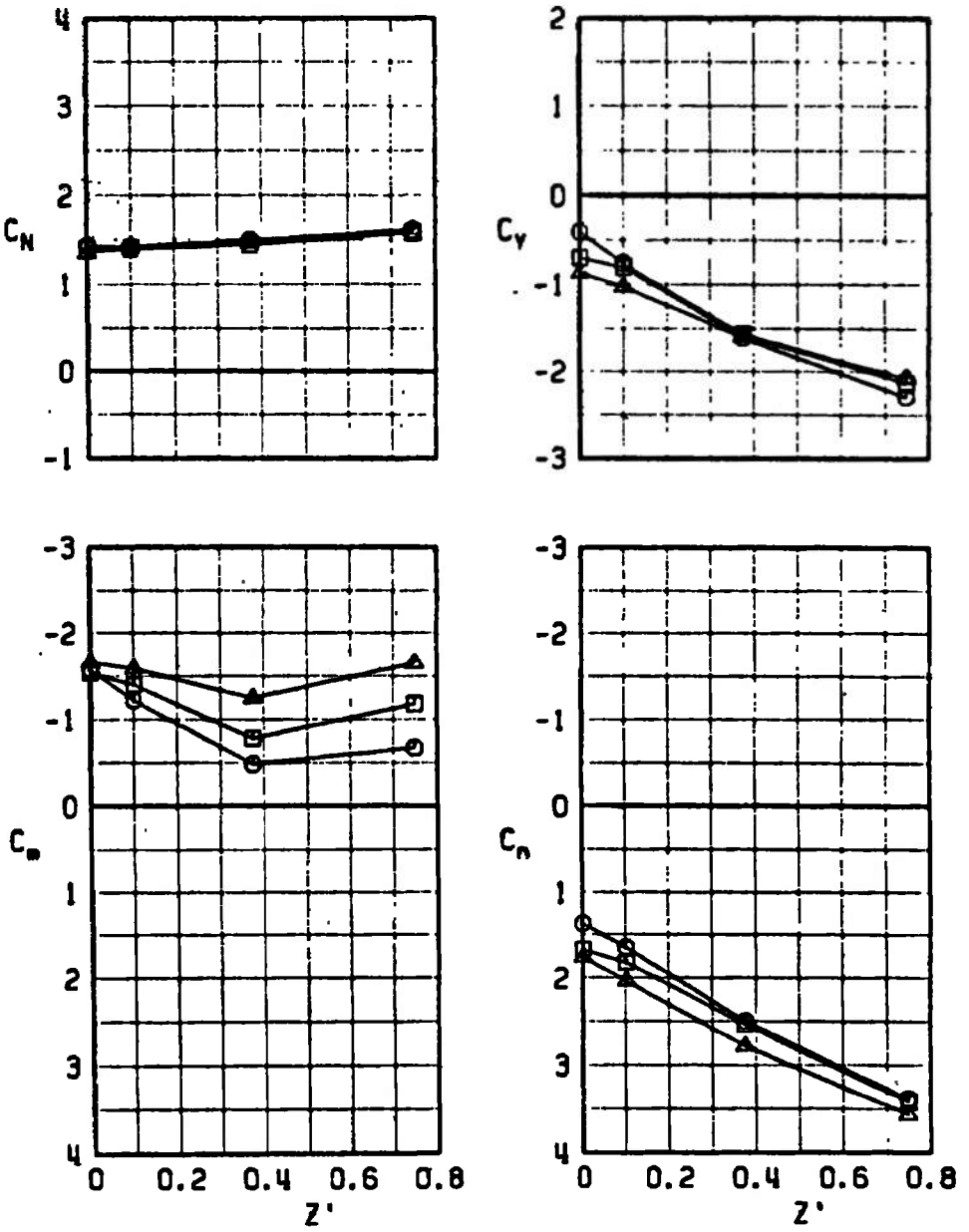

f. $\alpha = 15$, $Y' = -0.375$

Fig. 22 Concluded

SYMBOL	CONF	α	ℓ_p
○	9	0	0.375
□	9	0	0.750
△	9	0	2.400

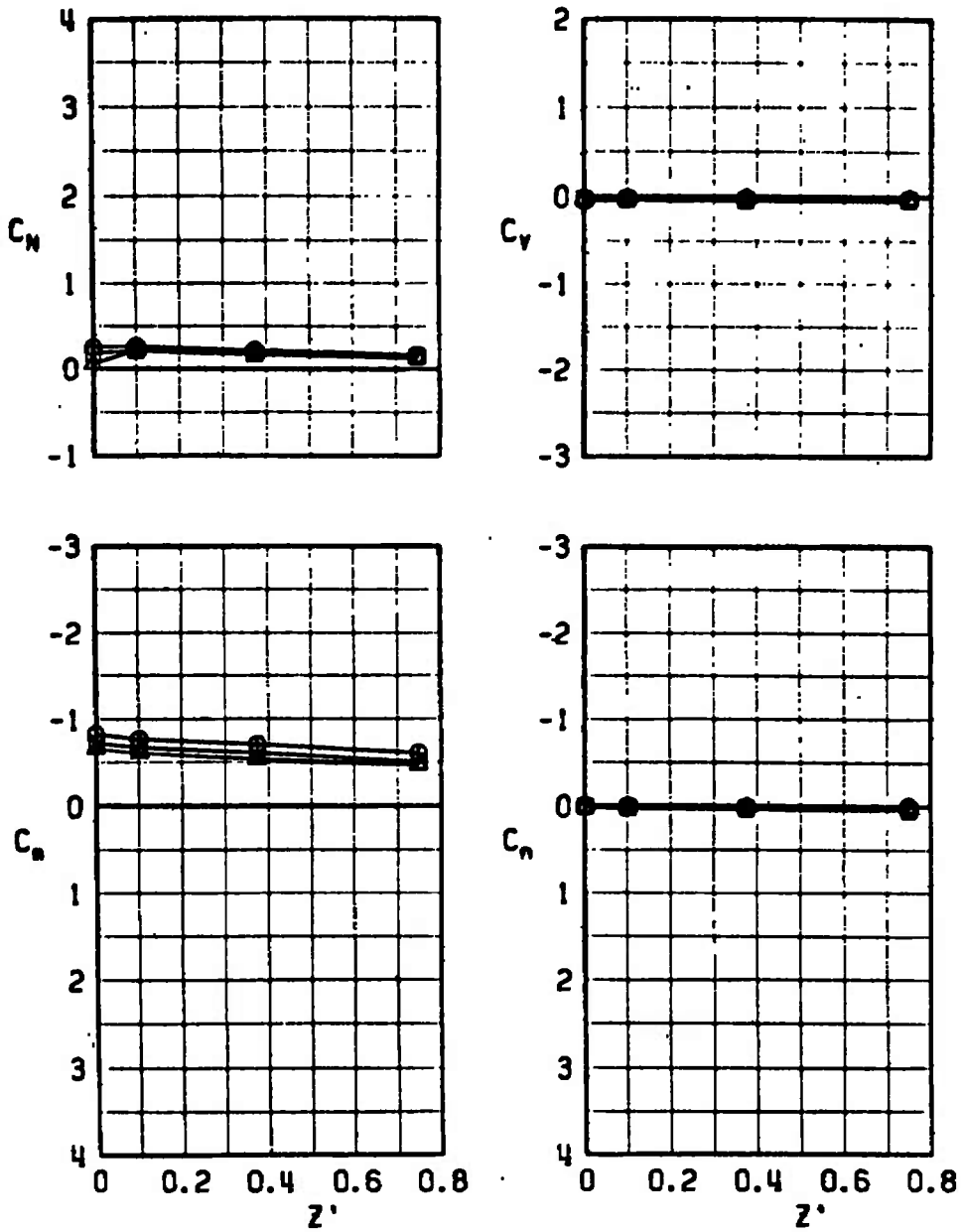

a. $\alpha = 0$

Fig. 23 Parent-Model Duct Flow Influence on Force and Moment Coefficients for the Unfinned Large Model at the Fuselage-Centerline Pylon Position, $N_1B_2WP_eA_2D$, $M_\infty = 0.4$

SYMBOL	CONF	α	ℓ_p
○	9	6	0.375
□	9	6	0.750
△	9	6	2.400

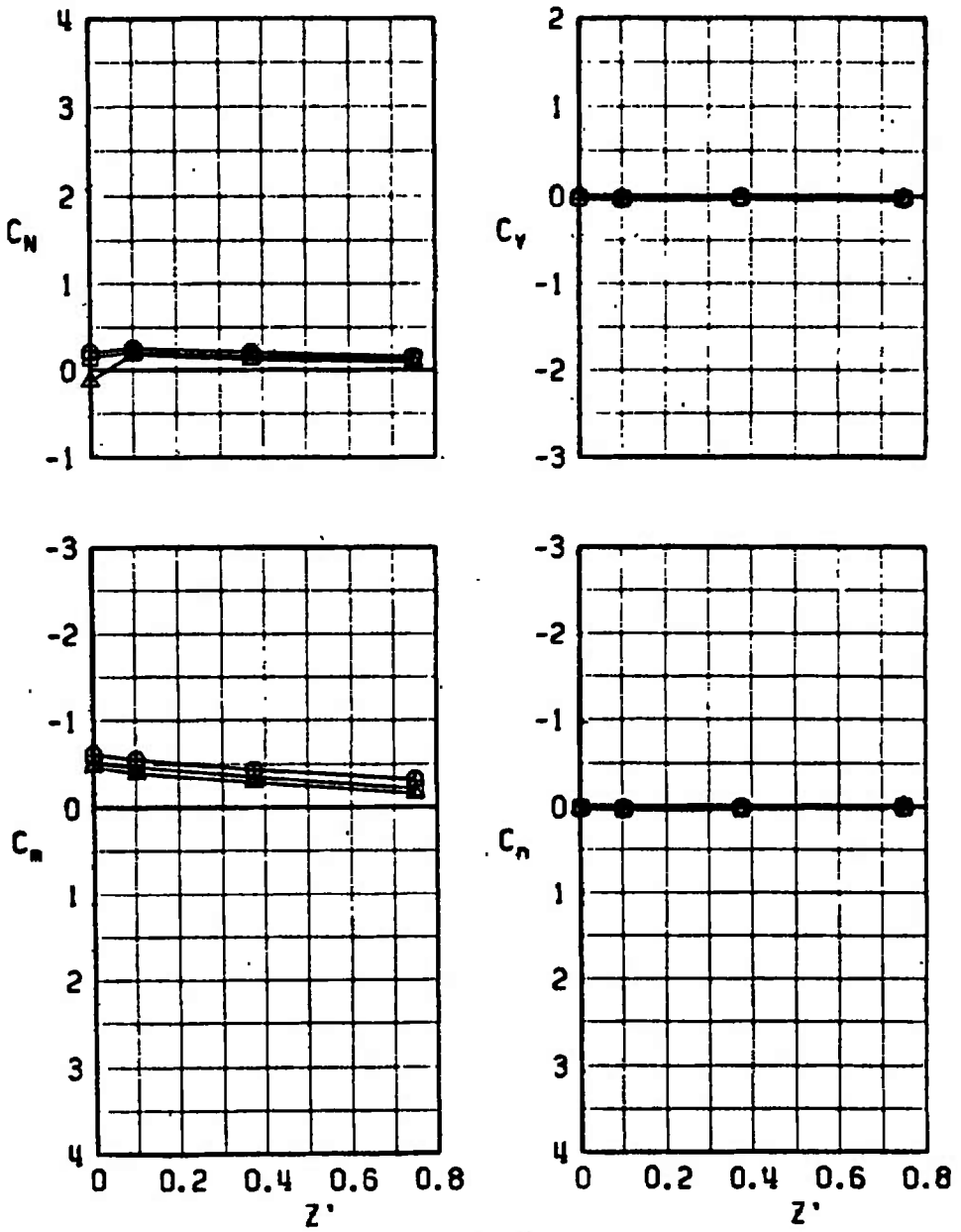

b. $\alpha = 6$

Fig. 23 Continued

SYMBOL	CONF	α	ℓ_p
⊙	9	15	0.375
⊡	9	15	0.750

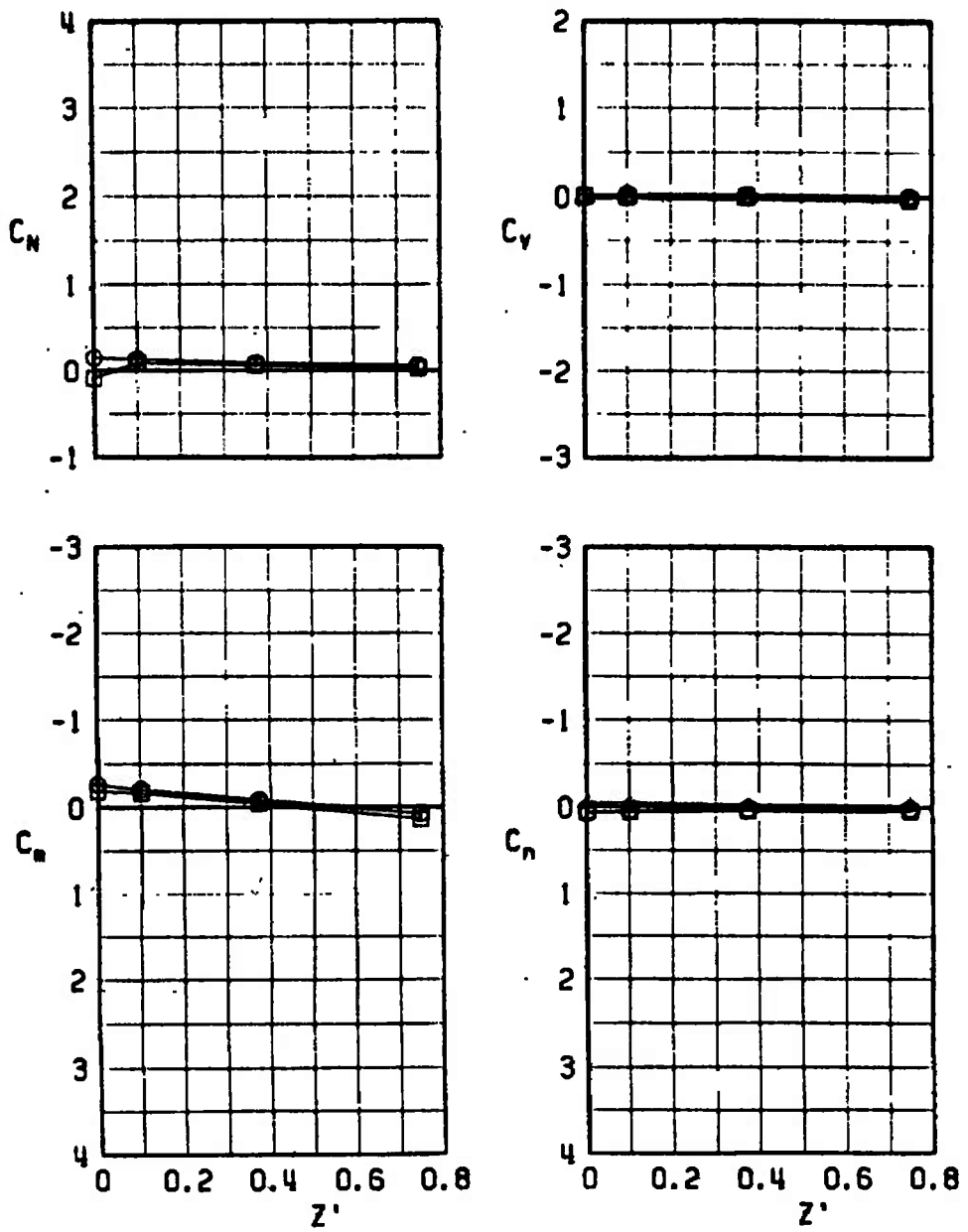

c. α = 15

Fig. 23 Concluded

SYMBOL	CONF	α	ℓ_p
⊙	14	0	0.375
□	14	0	0.750
△	14	0	2.400

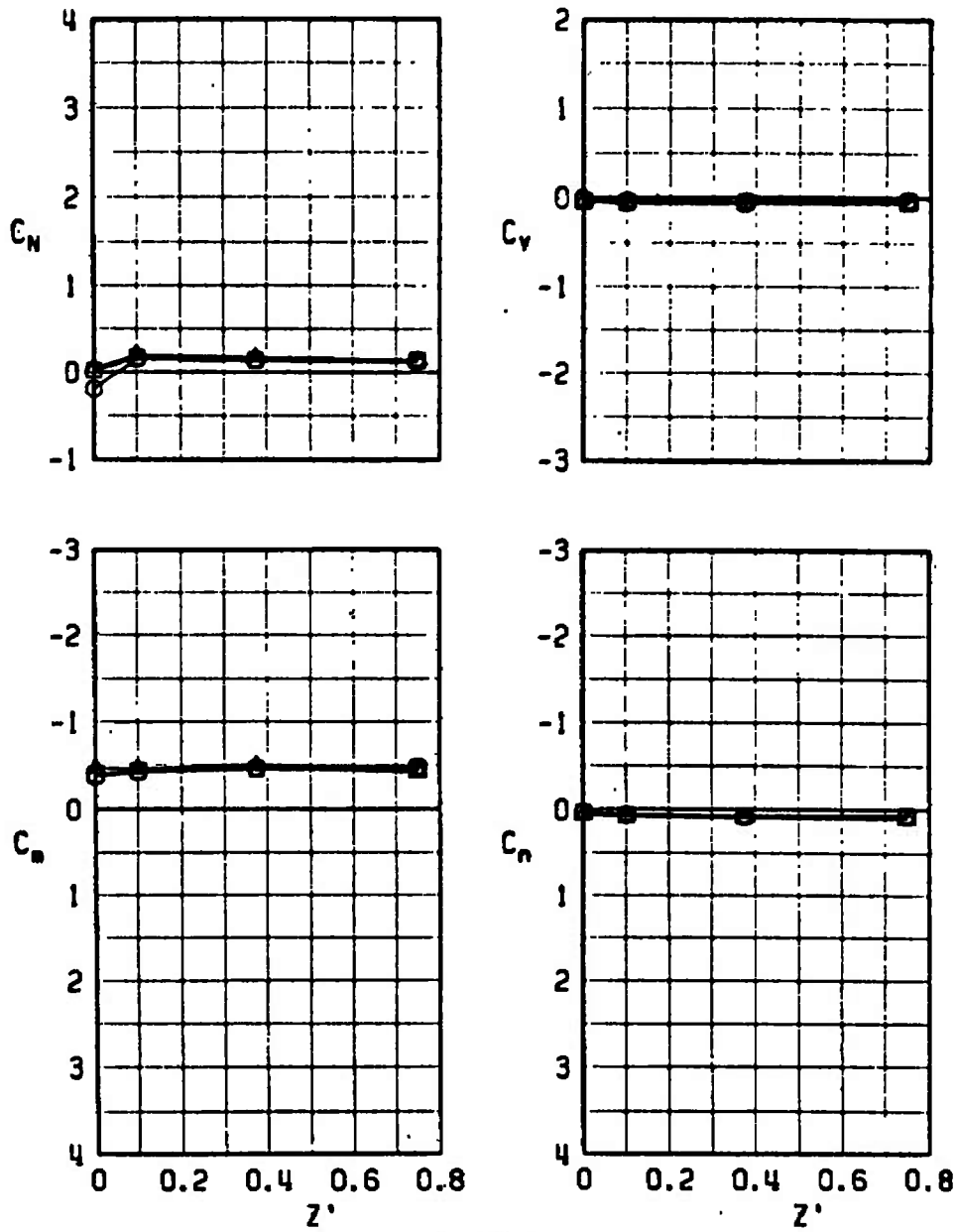

a. $\alpha = 0$

Fig. 24 Parent-Model Duct Flow Influence on Force and Moment Coefficients for the Finned Large Model at the Fuselage-Centerline Pylon Position, $N_1B_2WP_cA_2D$, $M_\infty = 0.4$

SYMBOL	CONF	α	ℓ_p
○	14	6	0.375
□	14	6	0.750
△	14	6	2.400

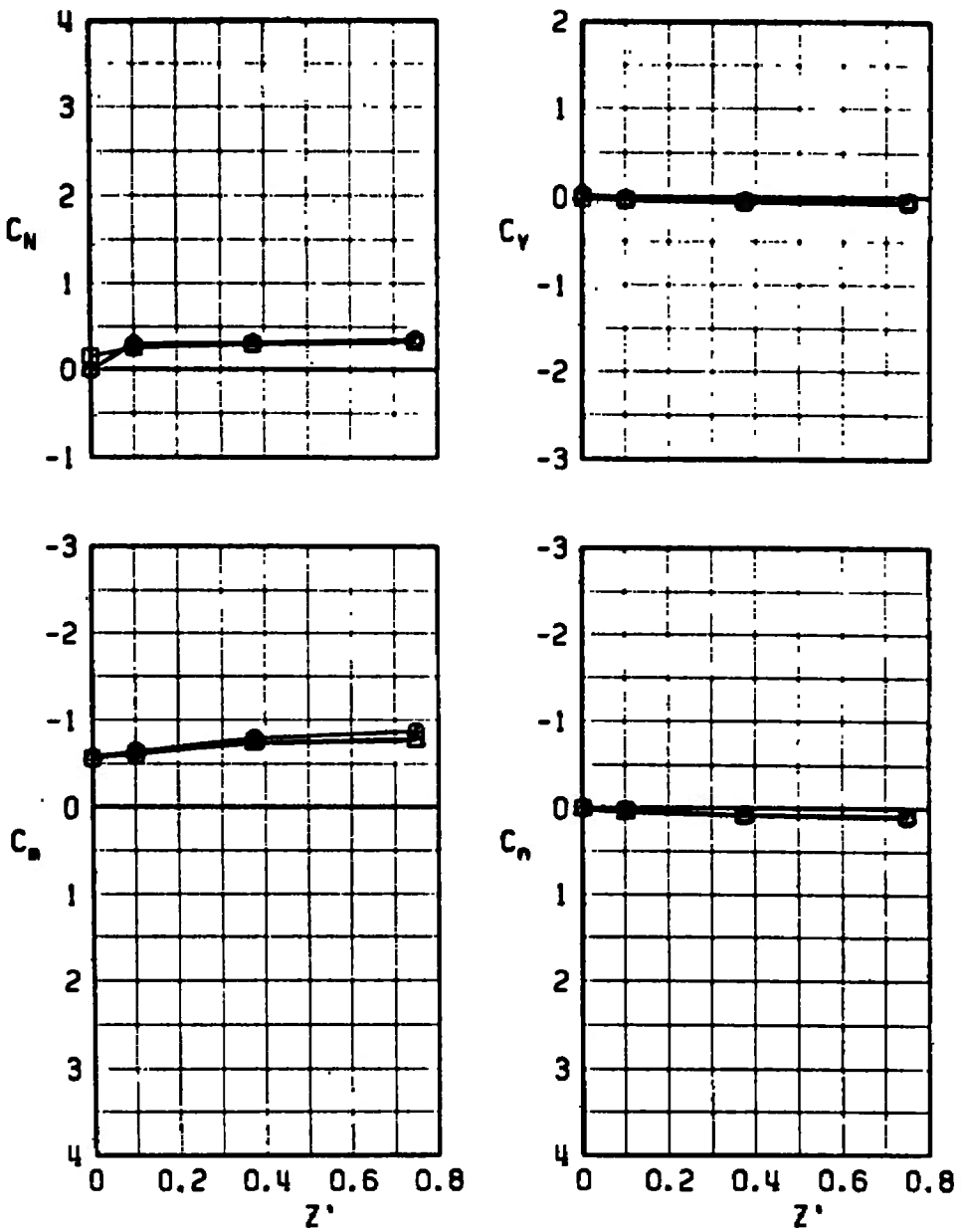

b. $\alpha = 6$

Fig. 24 Continued

SYMBOL	CONF	α	ℓ_p
⊙	14	15	0.375
□	14	15	0.750
△	14	15	2.400

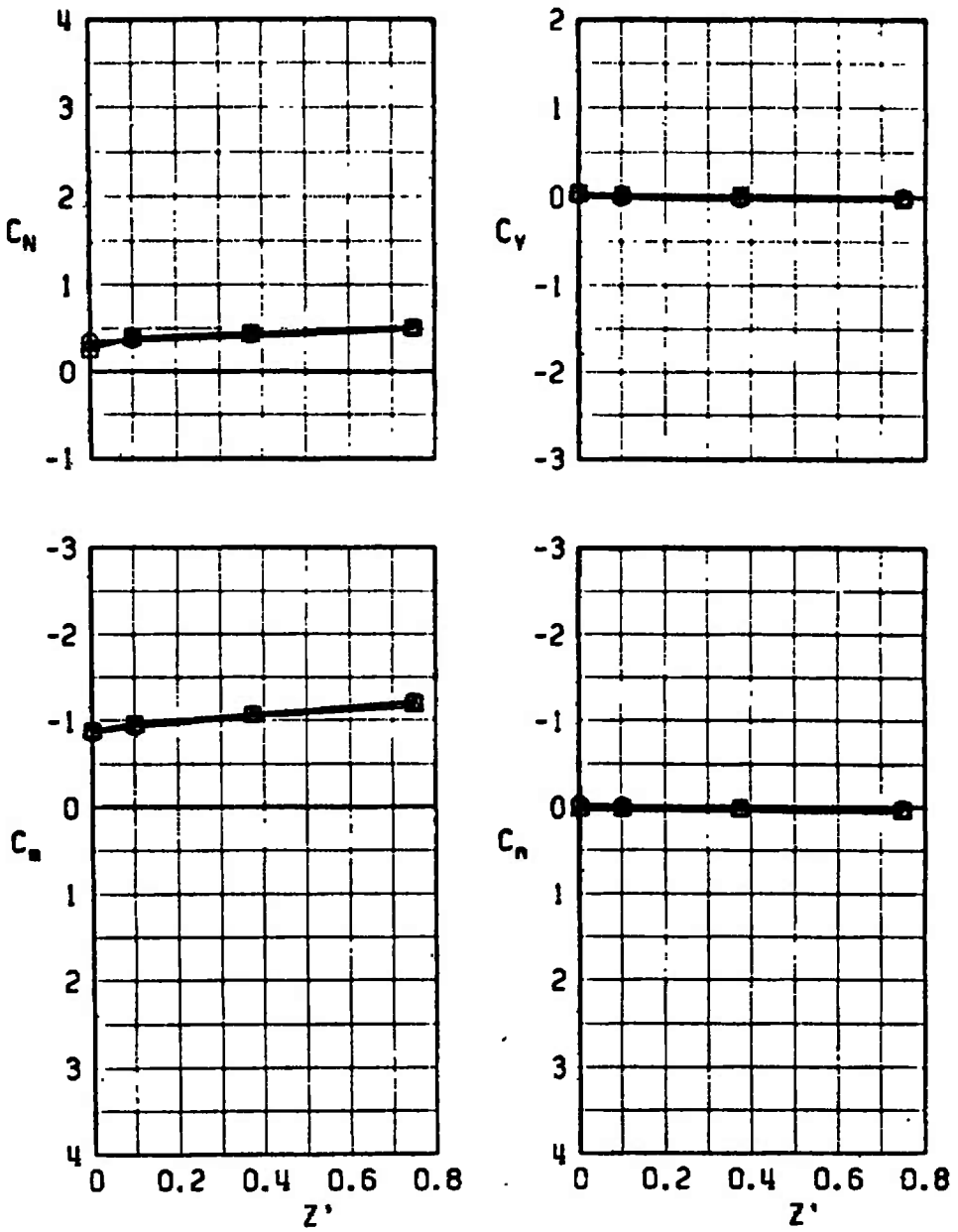

c. $\alpha = 15$

Fig. 24 Concluded

SYMBOL	CONF	α
○	5	0
□	6	0

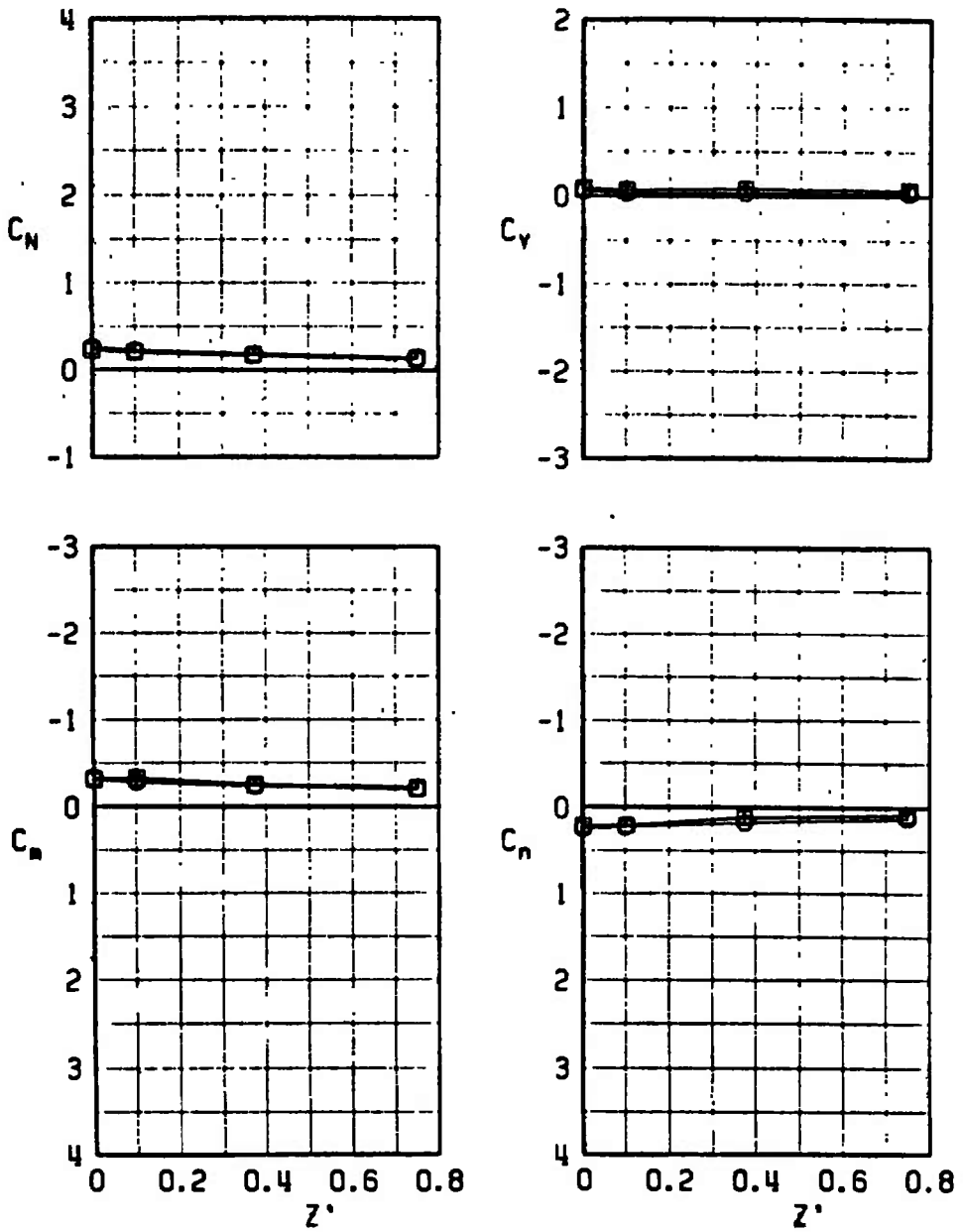

a. $\alpha = 0$, $Y' = 0$

Fig. 25 Force and Moment Coefficients for the Unfinned Large Model at the Wing 1/3-Semispan Station, N_1B_2W and $N_1B_2WA_1$, $M_\infty = 0.4$

SYMBOL	CONF	α
○	5	0
□	6	0

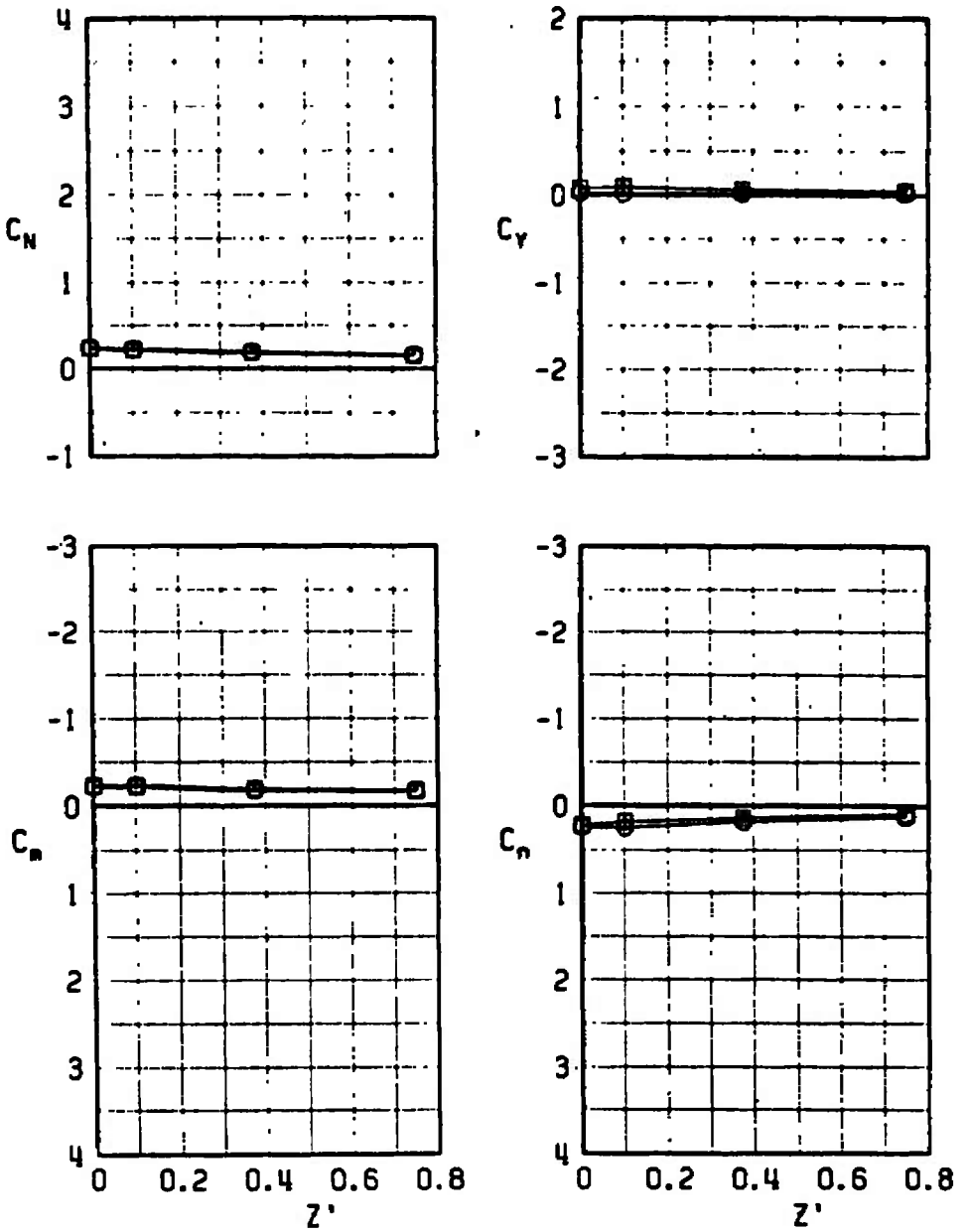

b. α = 0, Y' = -0.375
Fig. 25 Continued

SYMBOL	CONF	α
○	5	6
□	6	6

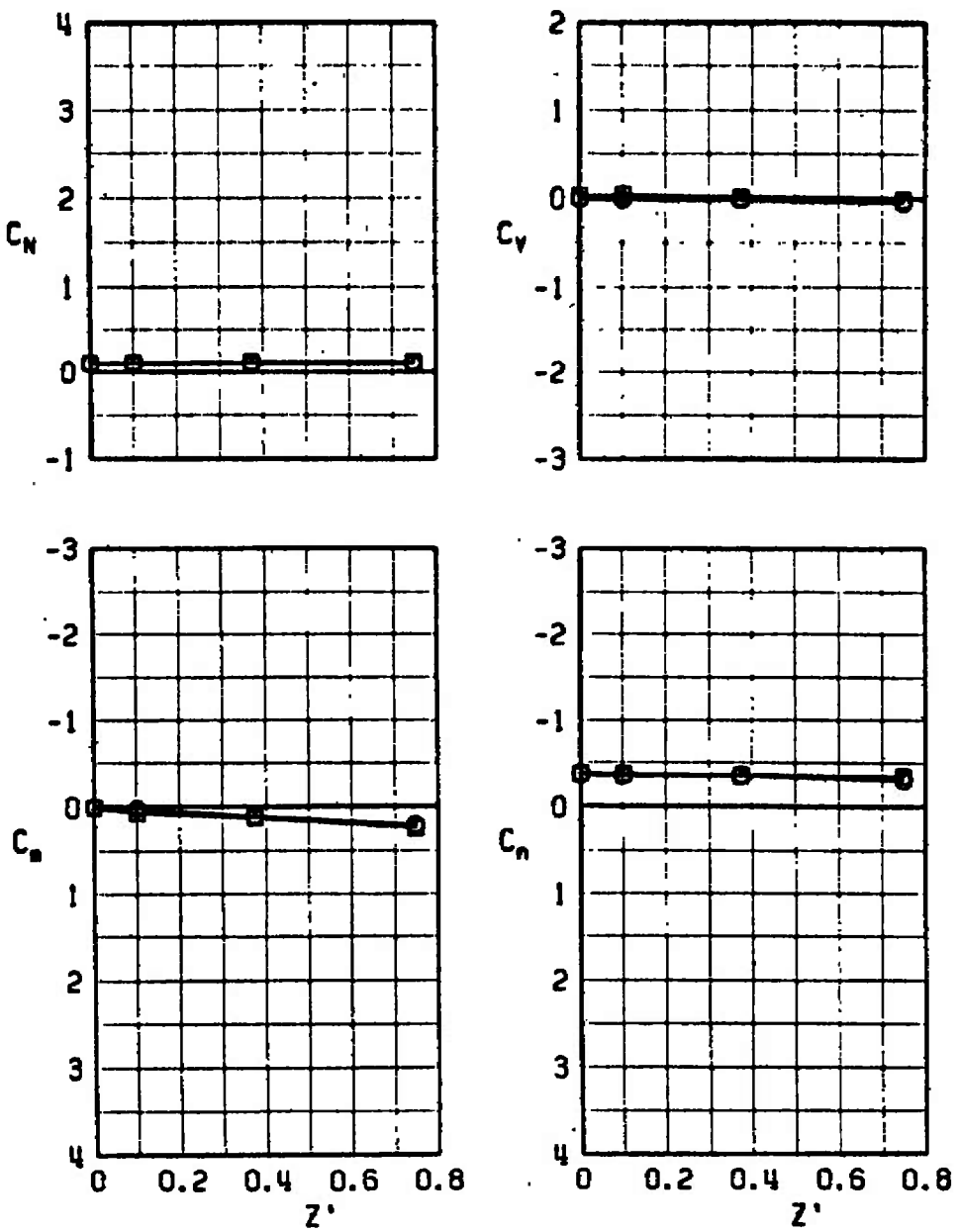

c. $\alpha = 6$, $Y' = 0$

Fig. 25 Continued

SYMBOL	CONF	α
⊙	5	6
⊡	6	6

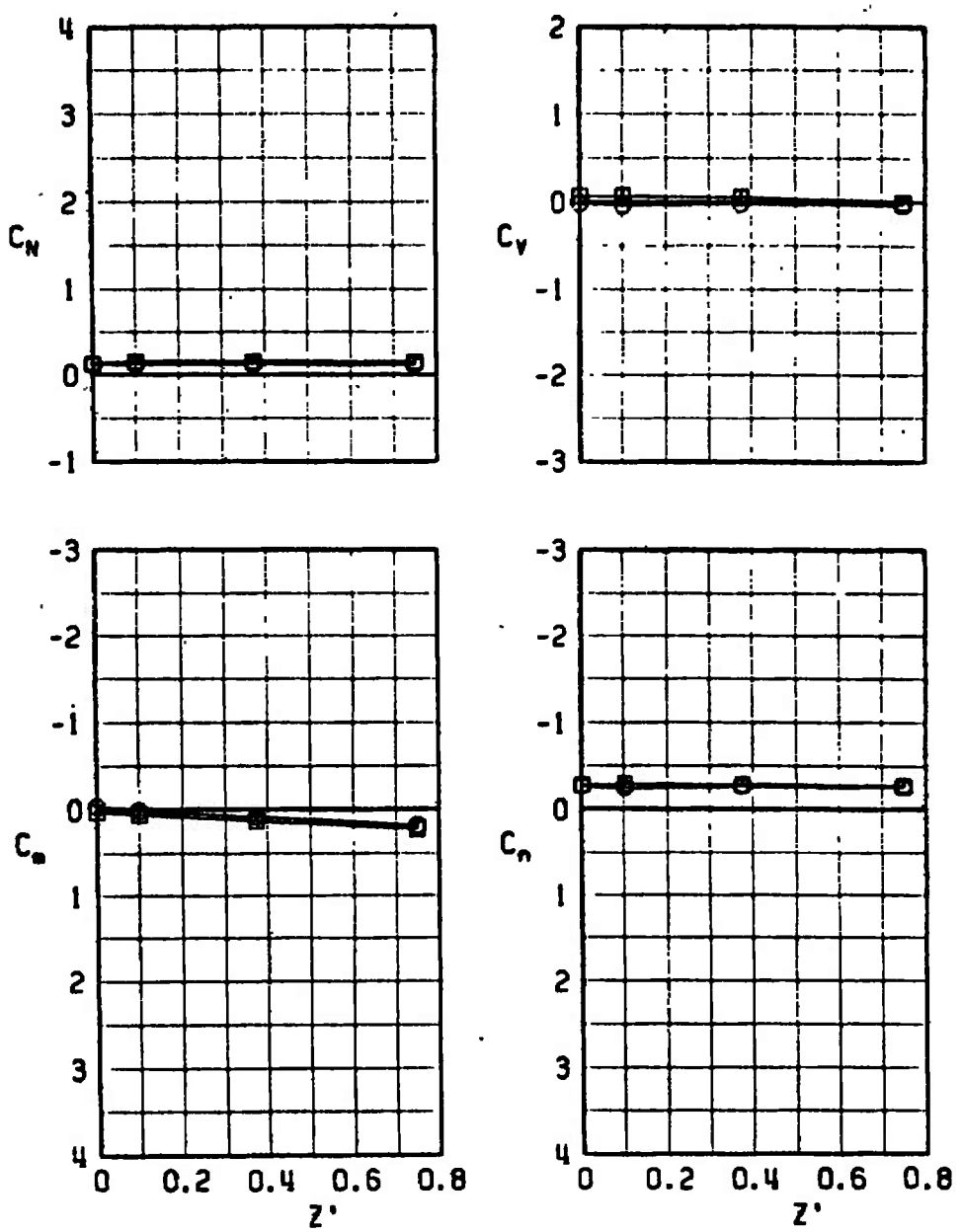

d. $\alpha = 6$, $Y' = -0.375$

Fig. 25 Continued

SYMBOL	CONF	α
○	5	15
□	6	15

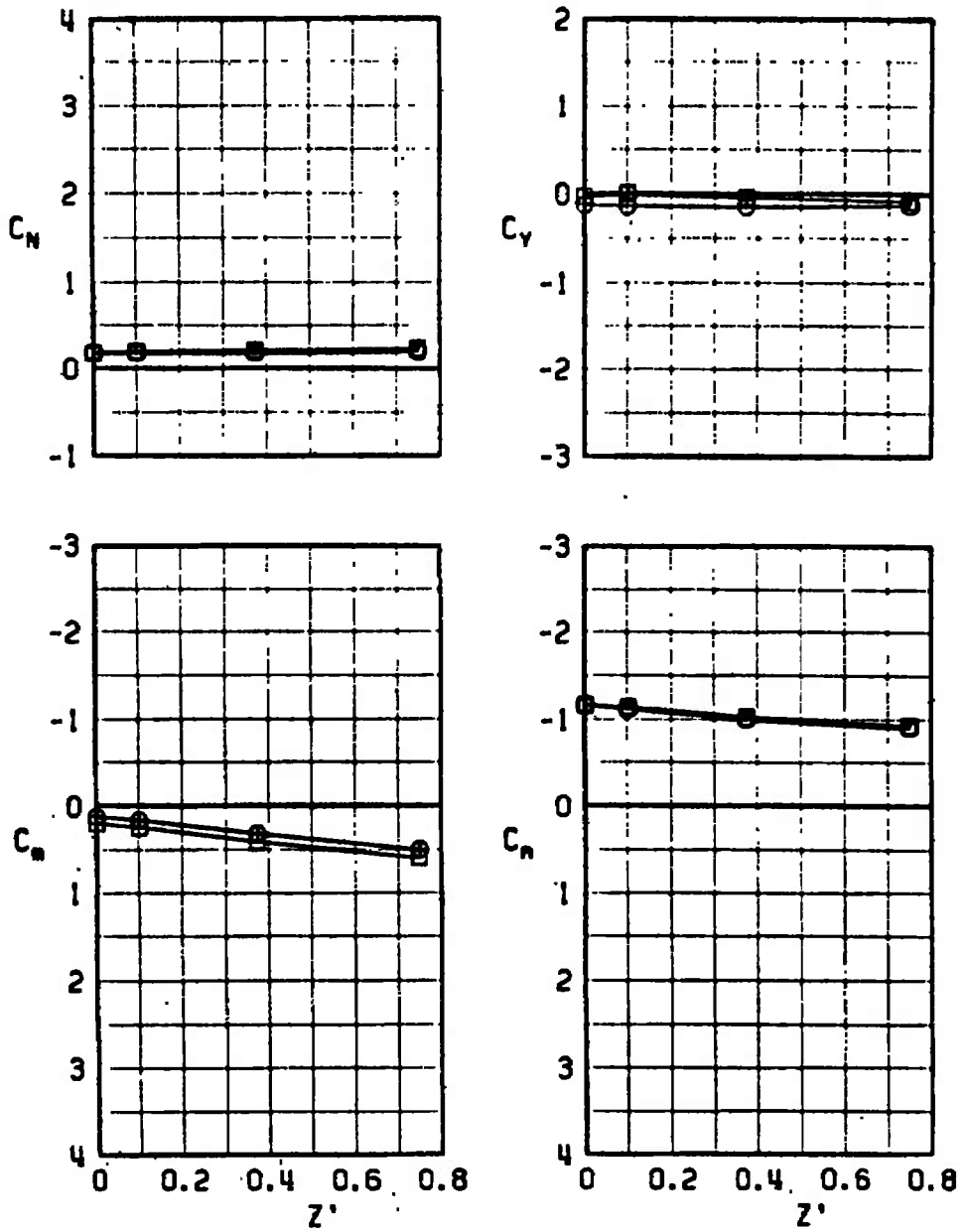

e. $\alpha = 15$, $Y' = 0$

Fig. 25 Continued

SYMBOL	CONF	α
○	5	15
□	6	15

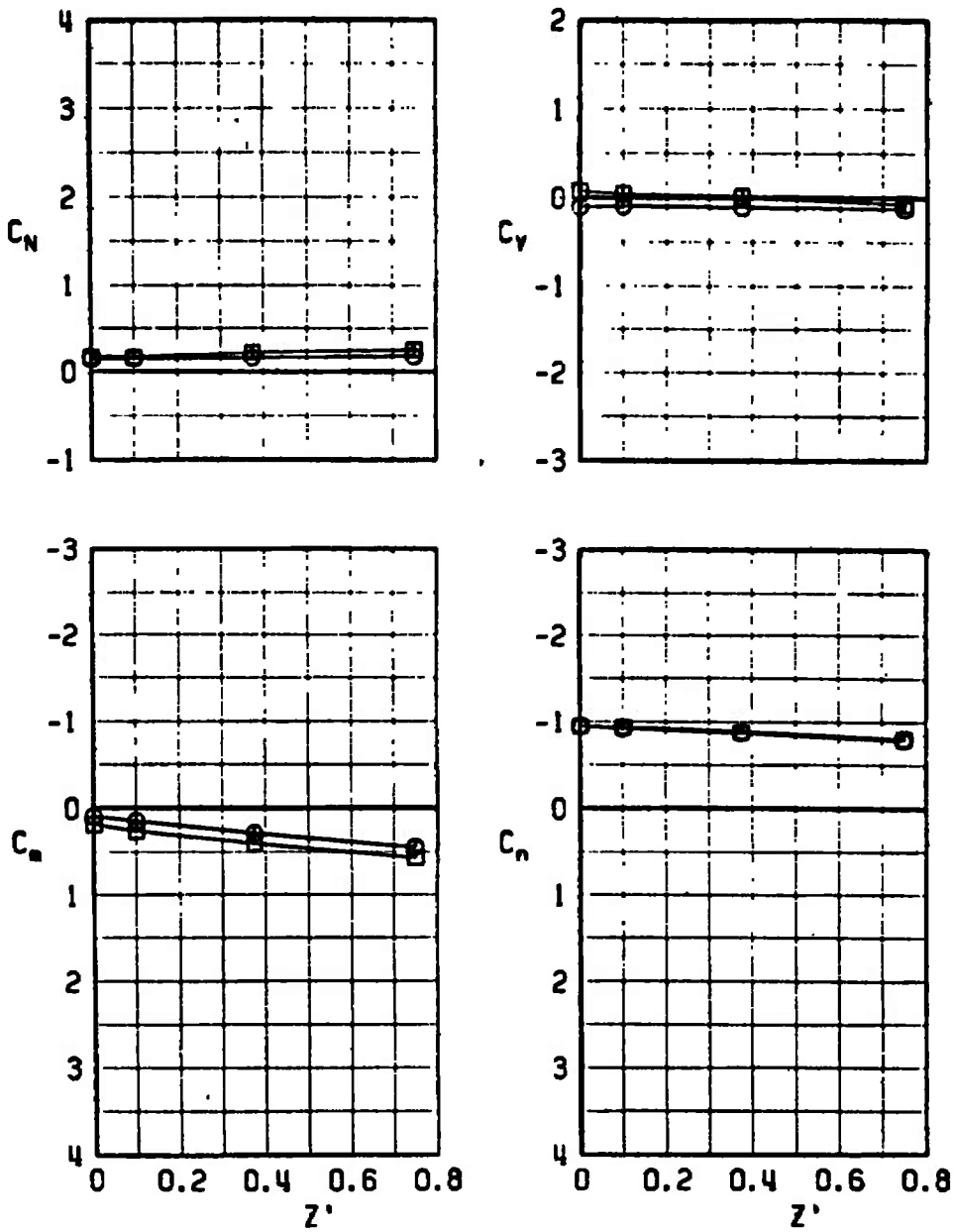

f. α = 15, Y' = -0.375
Fig. 25 Concluded

SYMBOL	CONF	α
⊙	10	0
⊡	11	0

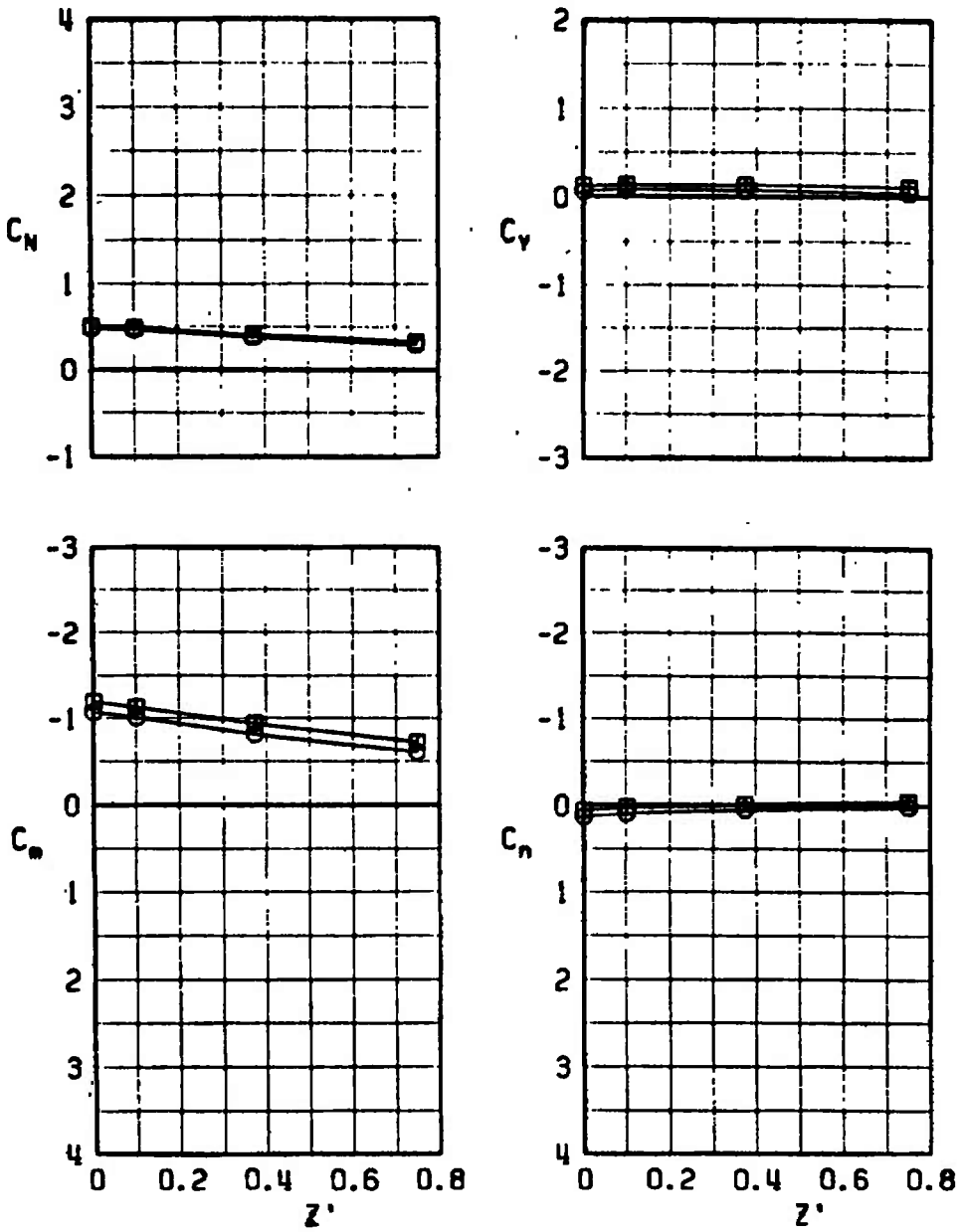

a. $\alpha = 0$, $Y' = 0$

Fig. 26 Force and Moment Coefficients for the Finned Large Model at the Wing 1/3-Semispan Station, N_1B_2W and $N_1B_2WA_1$, $M_\infty = 0.4$

SYMBOL	CONF	α
⊙	10	0
⊡	11	0

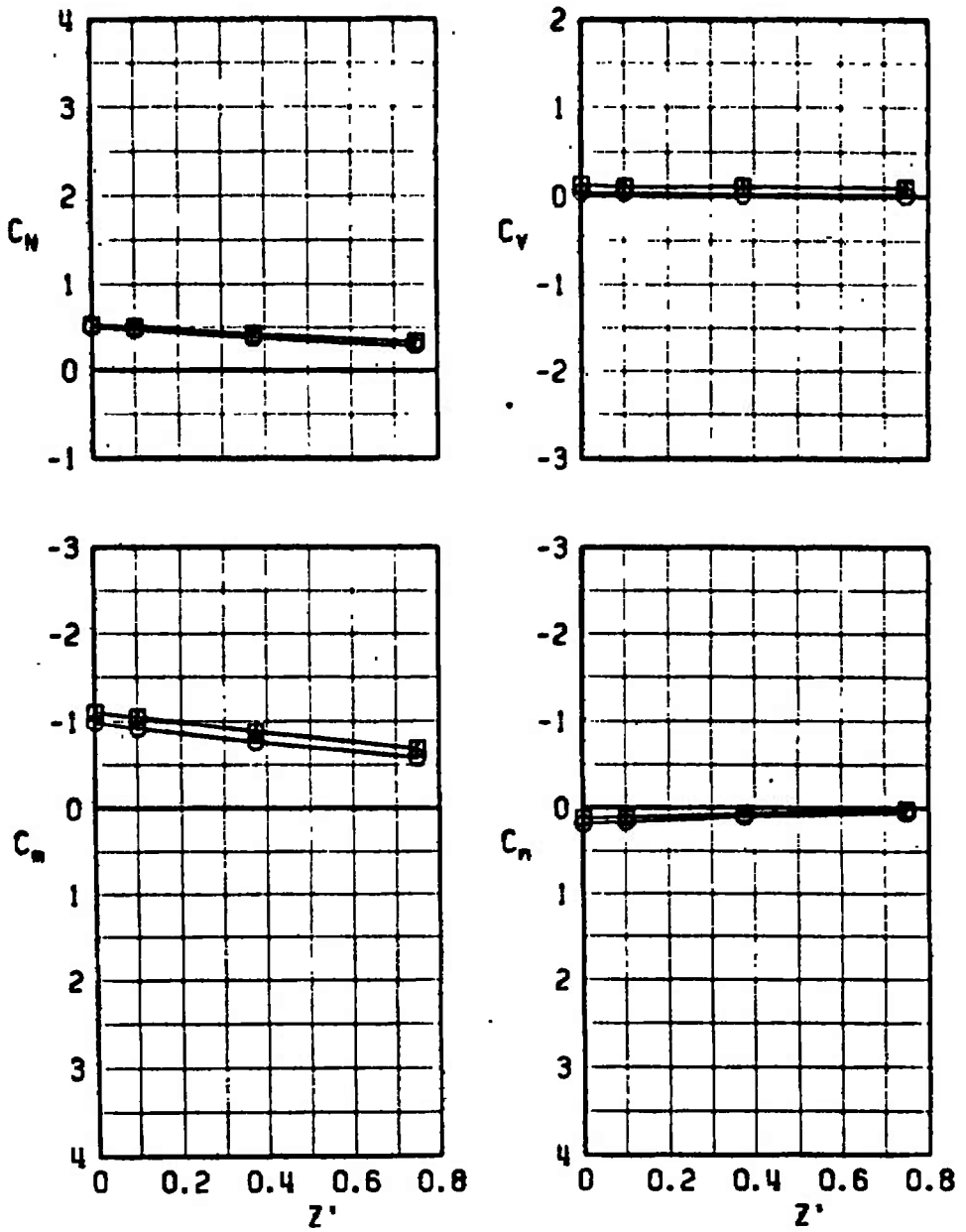

b. $\alpha = 0$, $Y' = -0.375$
Fig. 26 Continued

SYMBOL	CONF	α
⊙	10	6
⊡	11	6

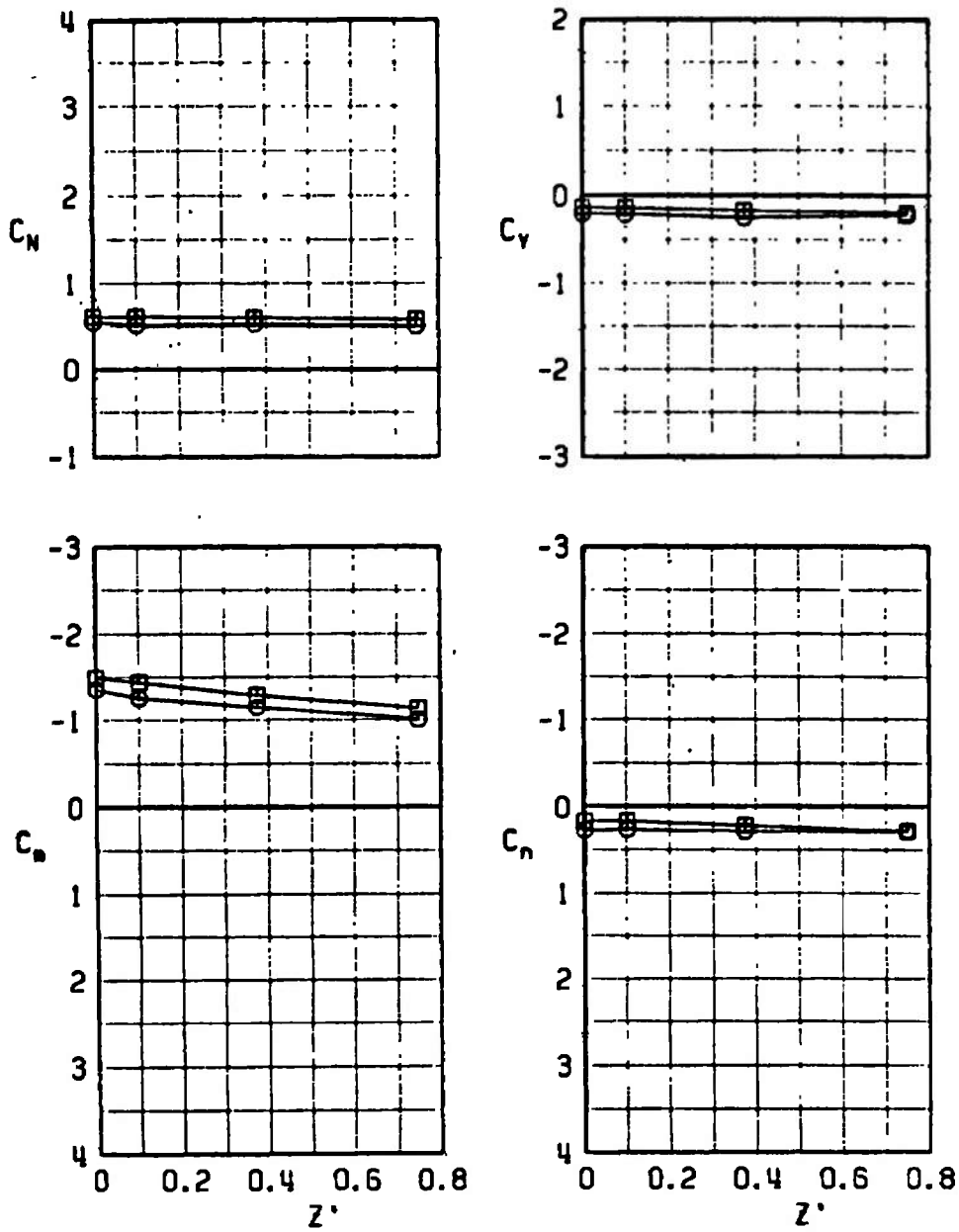

c. $\alpha = 6$, $Y' = 0$

Fig. 26 Continued

SYMBOL	CONF	α
○	10	6
□	11	6

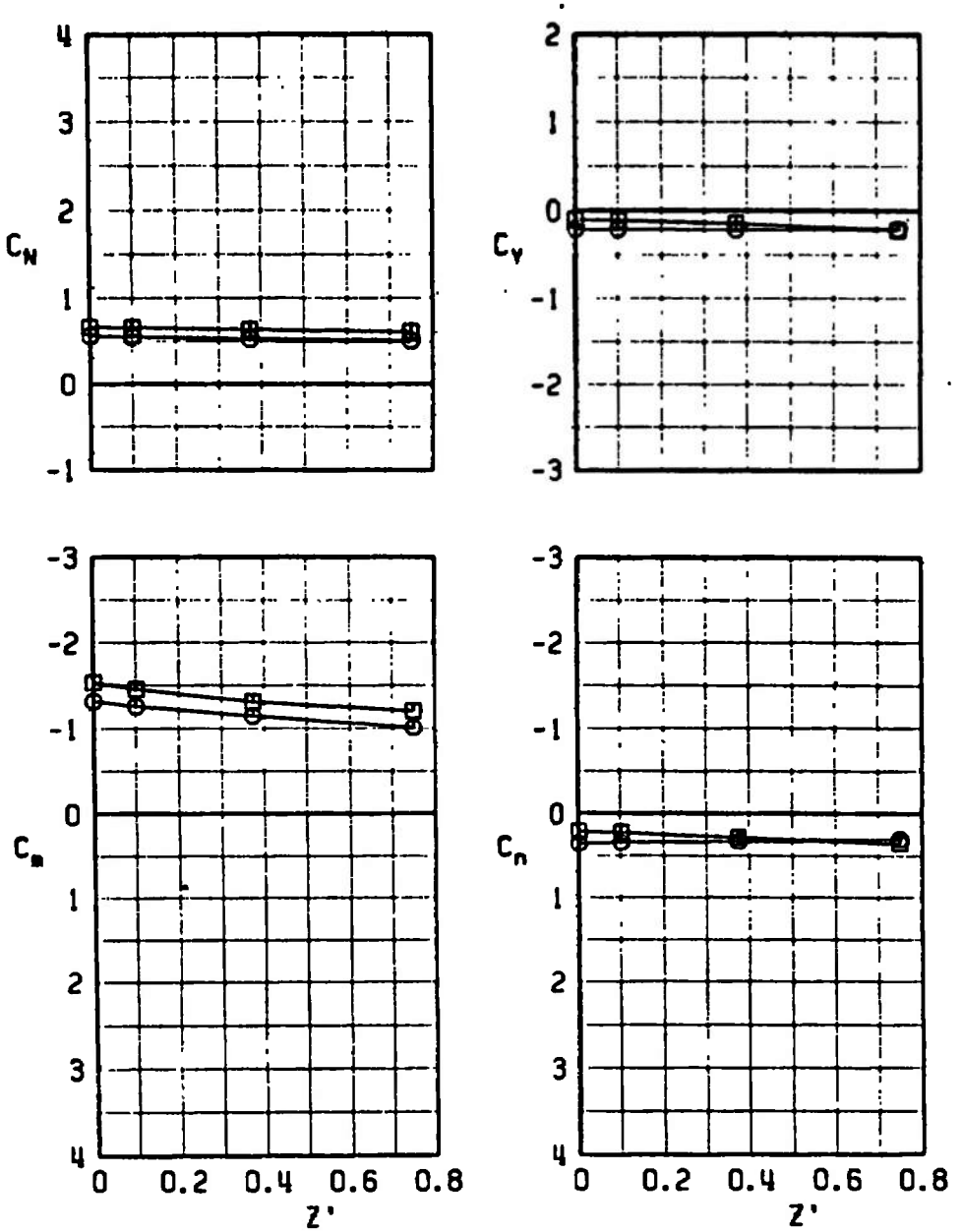

d. $\alpha = 6$, $Y' = -0.375$

Fig. 26 Continued

SYMBOL	CONF	α
○	10	15
□	11	15

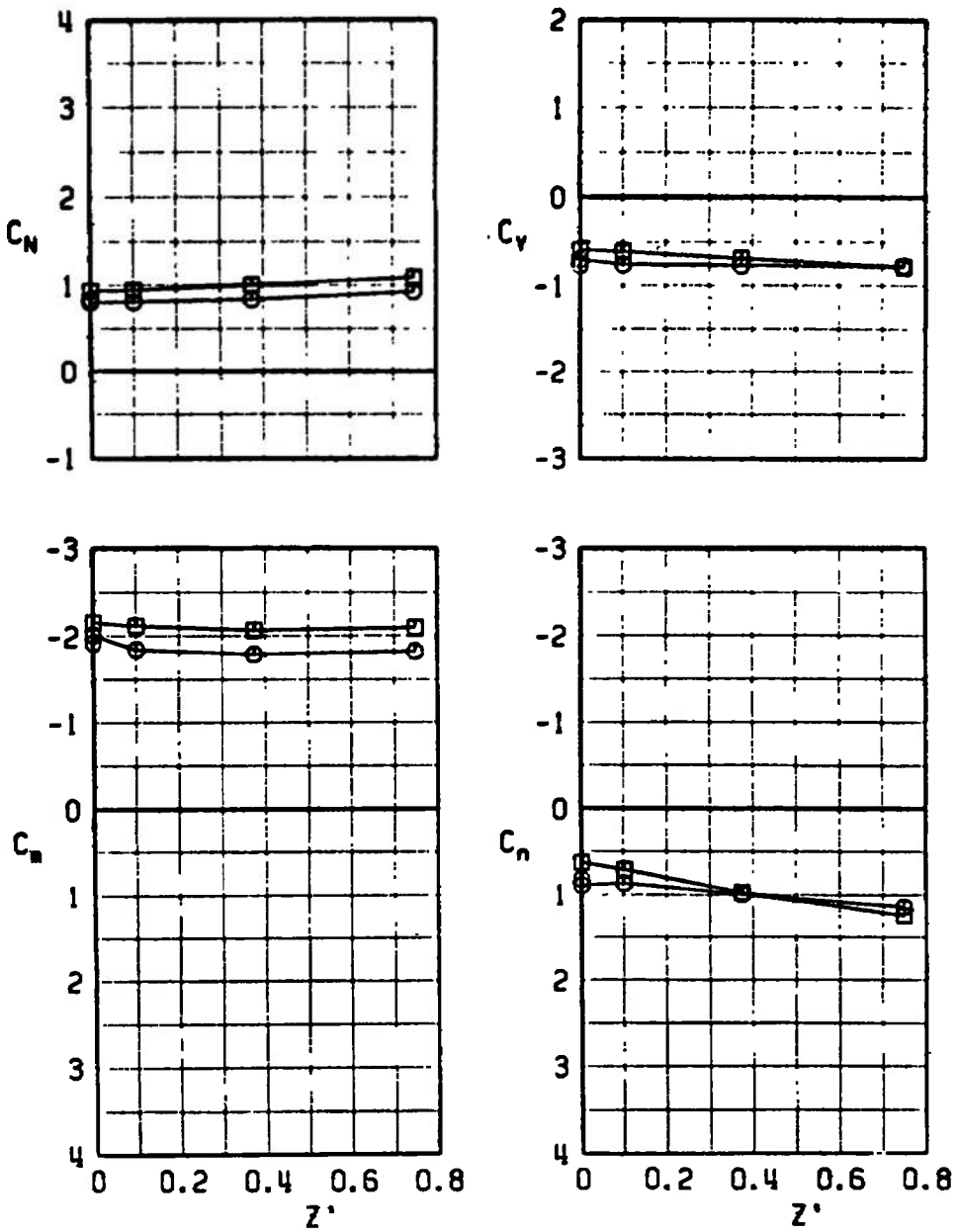

e. α = 15, Y' = 0

Fig. 26 Continued

SYMBOL	CONF	α
○	10	15
□	11	15

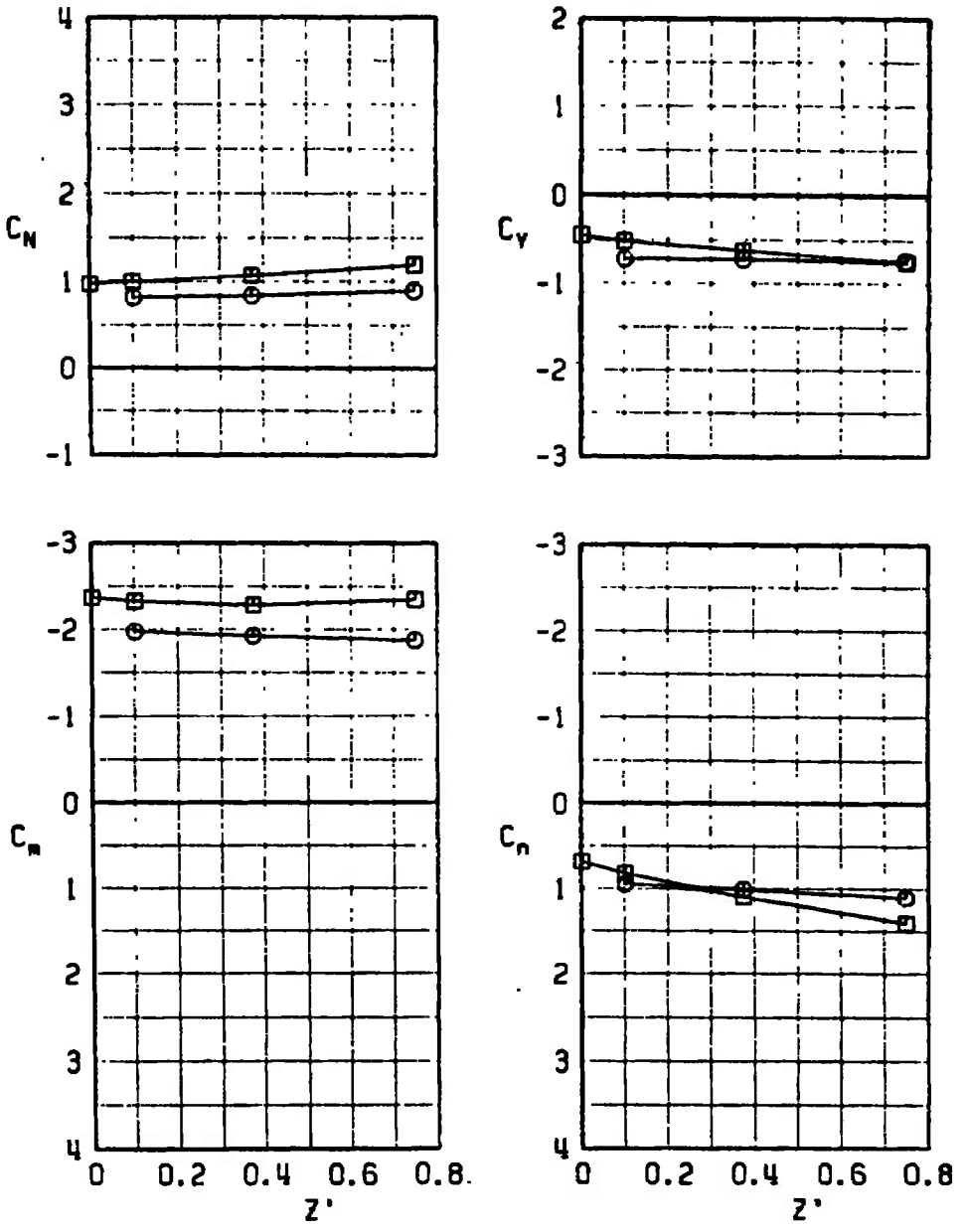

f. α = 15, Y' = -0.375
Fig. 26 Concluded

SYMBOL	CONF	α	ℓ_p
⊙	8	0	2.4
⊡	7	0	2.4

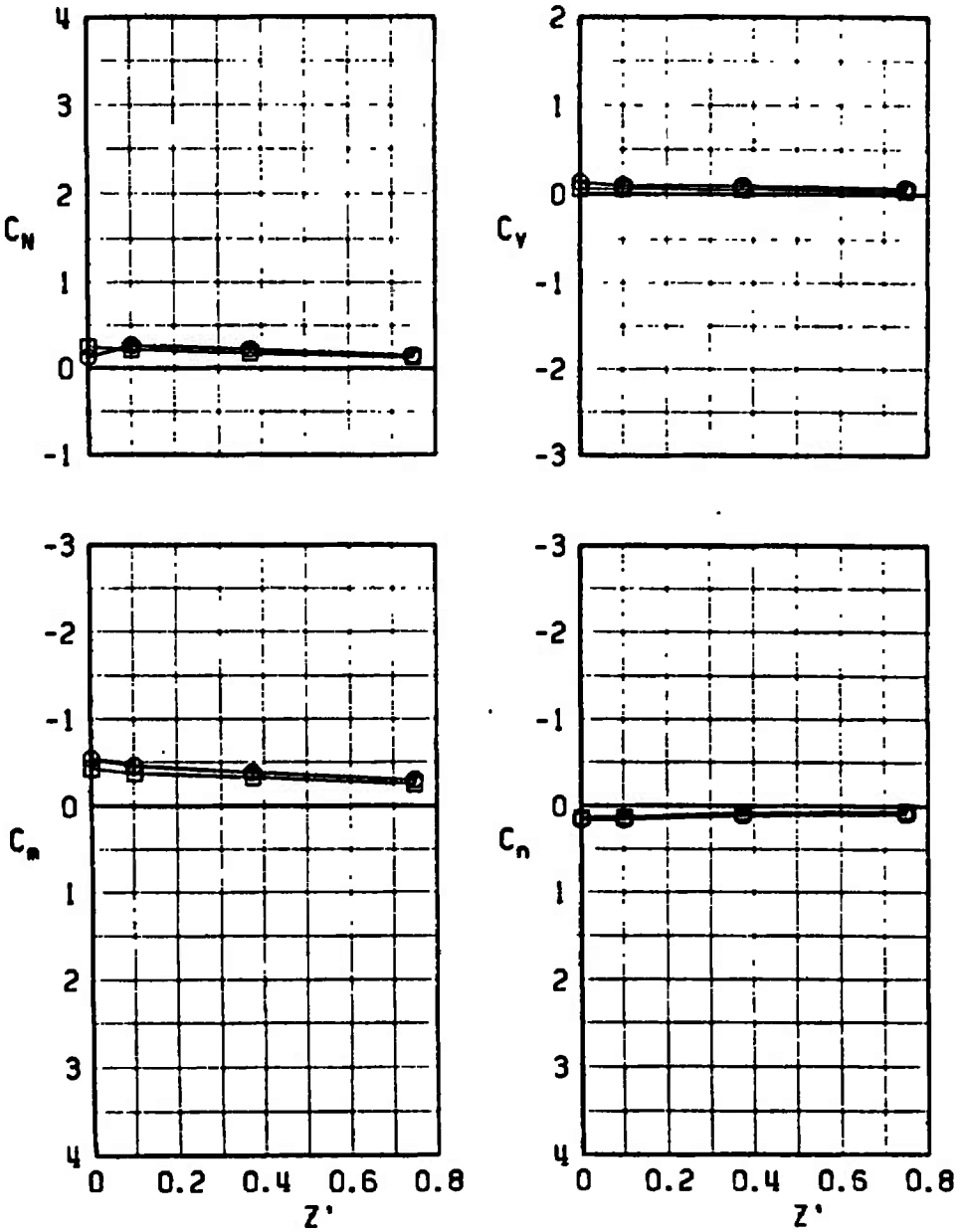

a. $\alpha = 0$, $Y' = 0$

Fig. 27 Force and Moment Coefficients for the Unfinned Large Model at the Wing 1/3-Semispan Station, $N_1B_2WA_2D$ and $N_1B_2WP_{1/3}A_2D$, $M_\infty = 0.4$

SYMBOL	CONF	α	ℓ_p
⊙	8	0	2.4
⊡	7	0	2.4

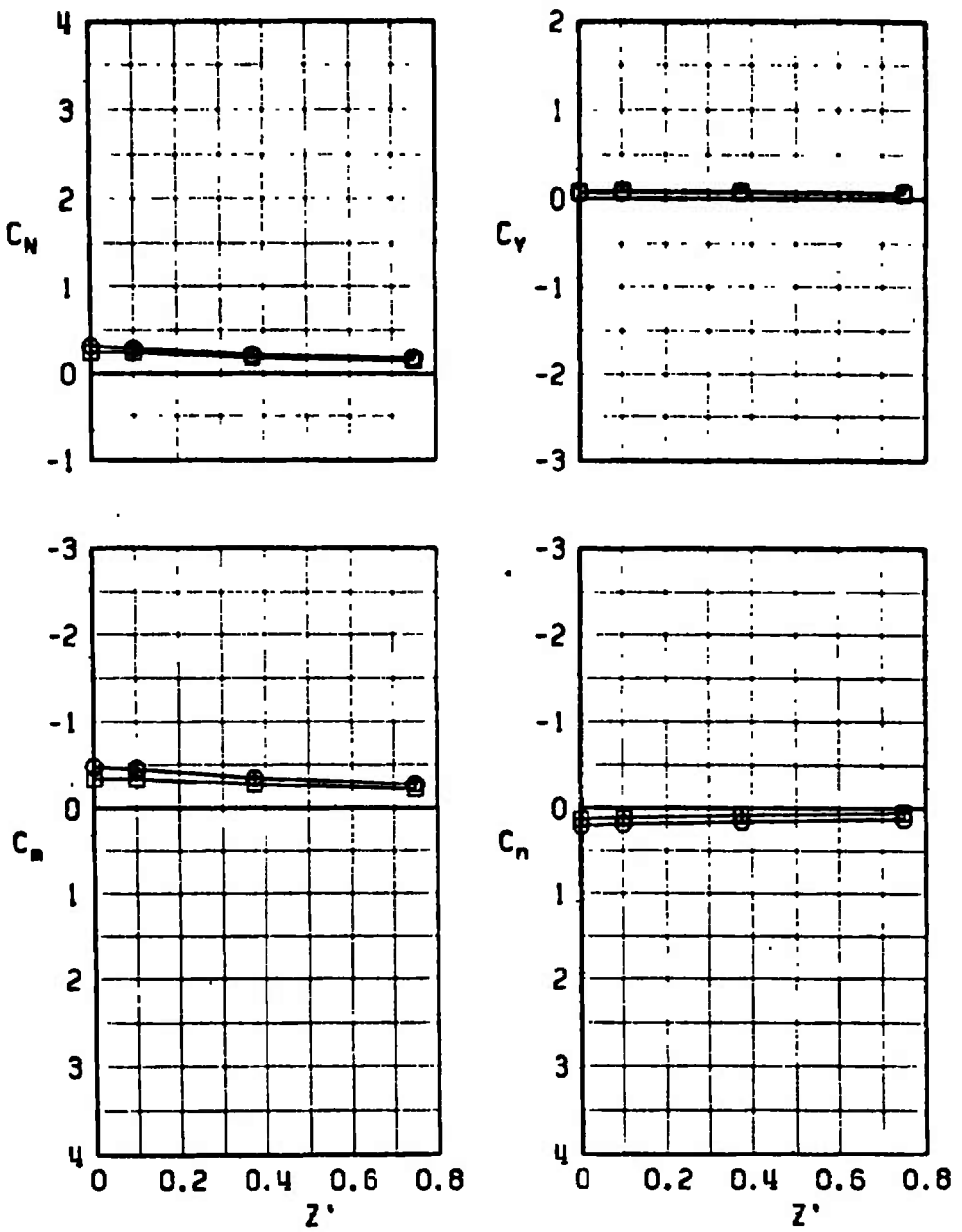

b. $\alpha = 0$, Y' = -0.375
Fig. 27 Continued

SYMBOL	CONF	α	ℓ_p
⊙	8	6	2.400
⊡	7	6	2.400

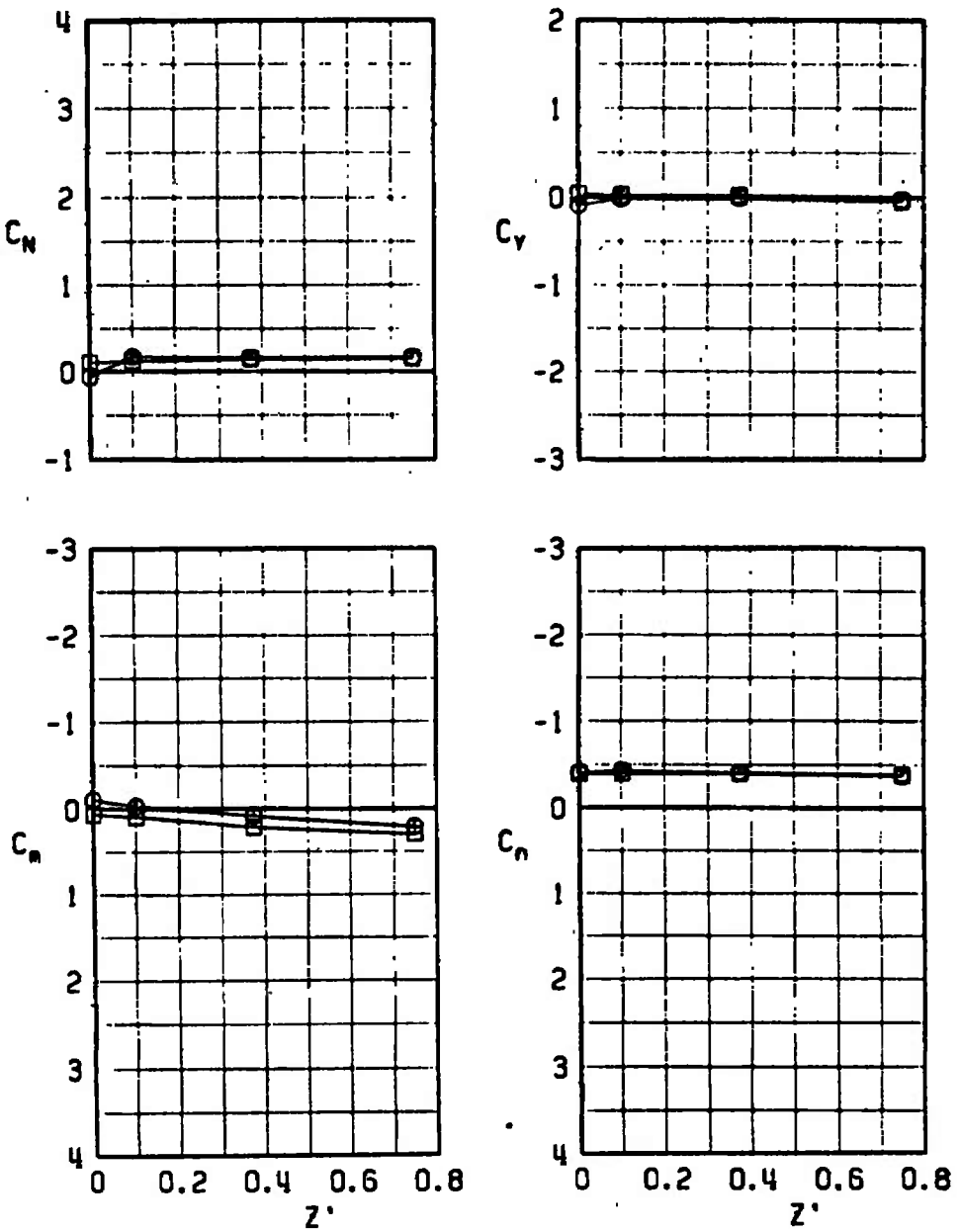

c. $\alpha = 6$, $Y' = 0$

Fig. 27 Continued

SYMBOL	CONF	α	ℓ_p
○	8	6	2.400
□	7	6	2.400

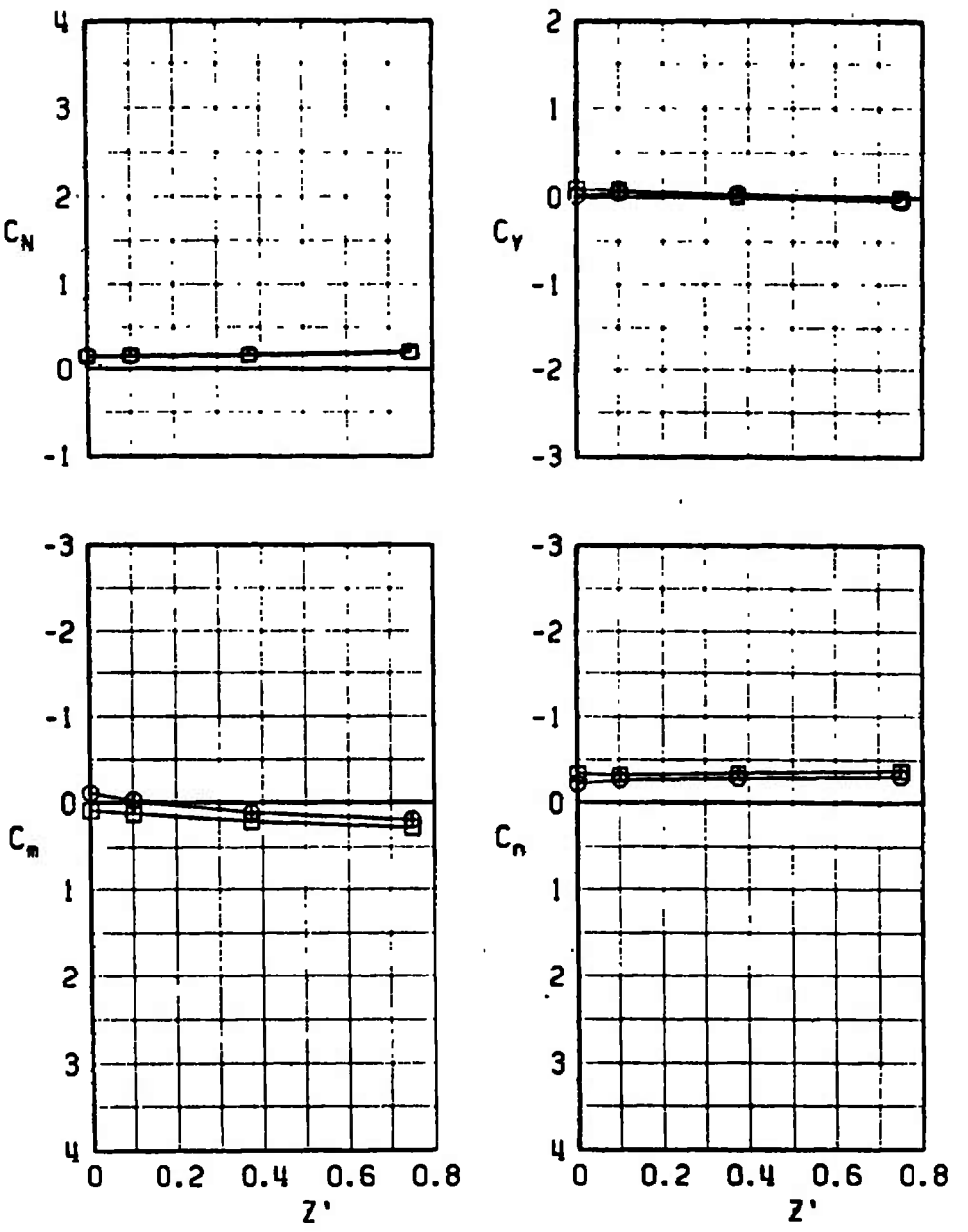

d. α = 6, Y' = -0.375
Fig. 27 Continued

SYMBOL	CONF	α	ℓ_p
○	8	15	2.4
□	7	15	2.4

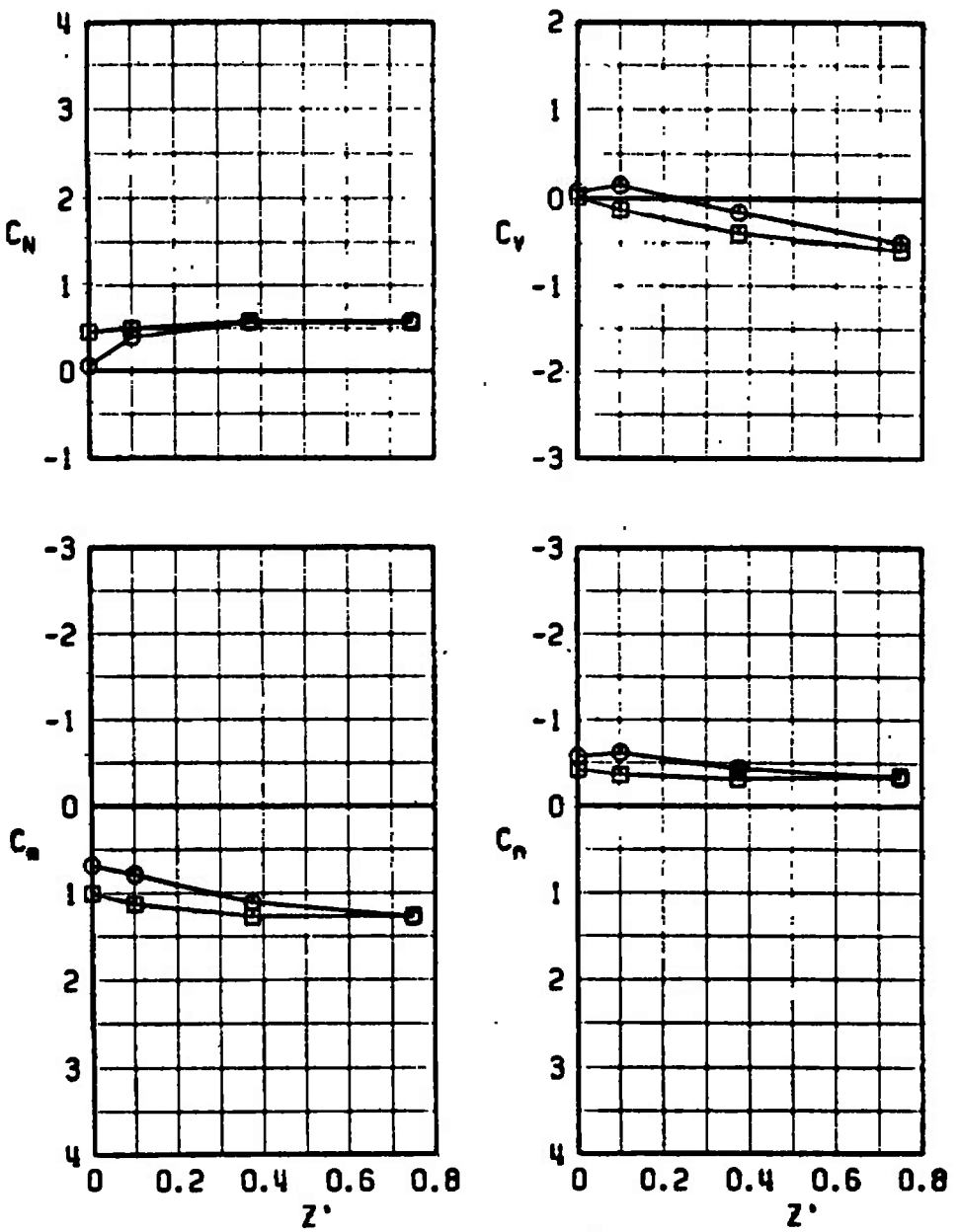

e. α = 16, Y' = 0

Fig. 27 Continued

SYMBOL	CONF	α	ℓ_p
○	8	15	2.4
□	7	15	2.4

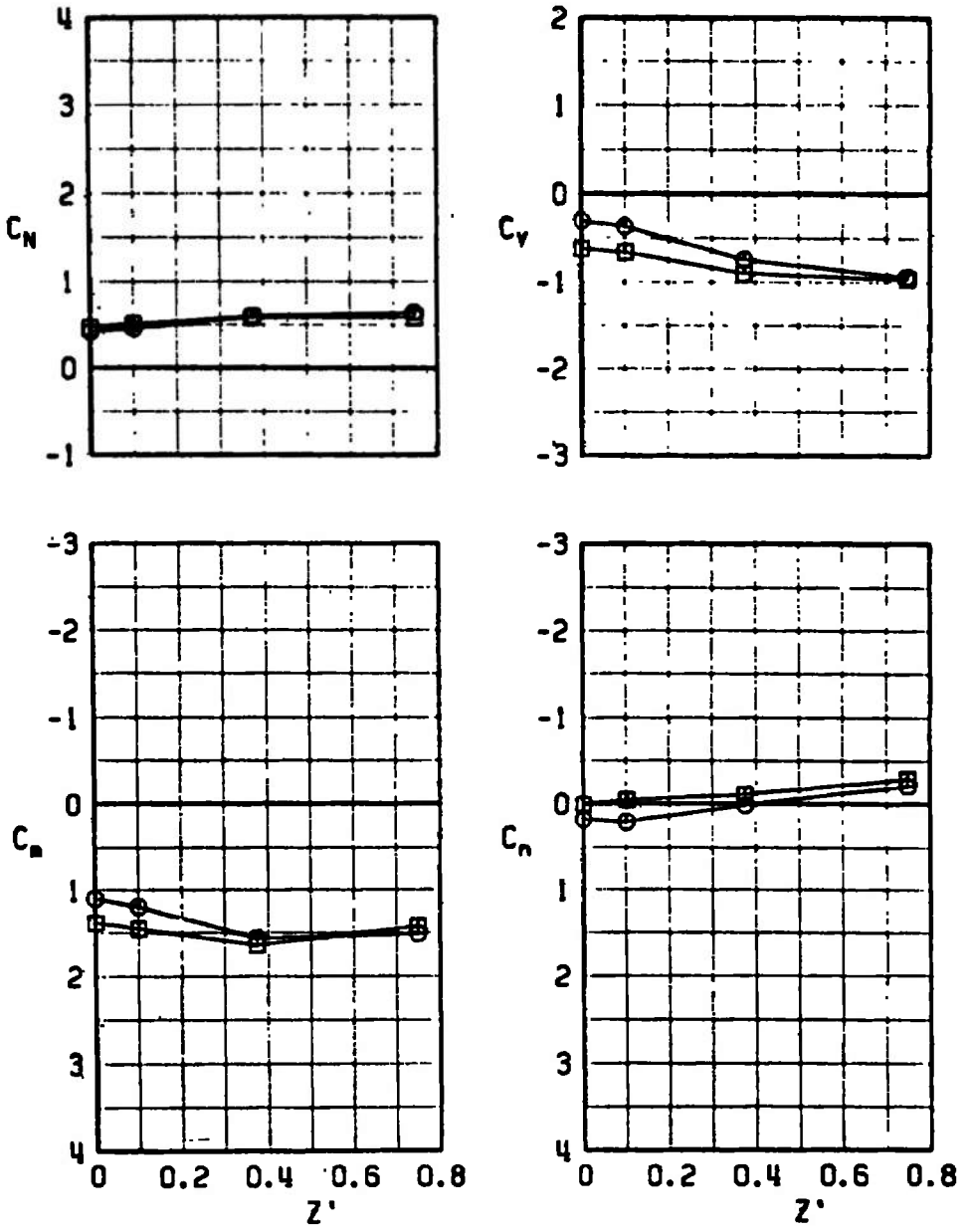

f. α = 15, Y' = -0.375
Fig. 27 Concluded

SYMBOL	CONF	α	ℓ_p
⊙	13	0	2.4
⊡	12	0	2.4

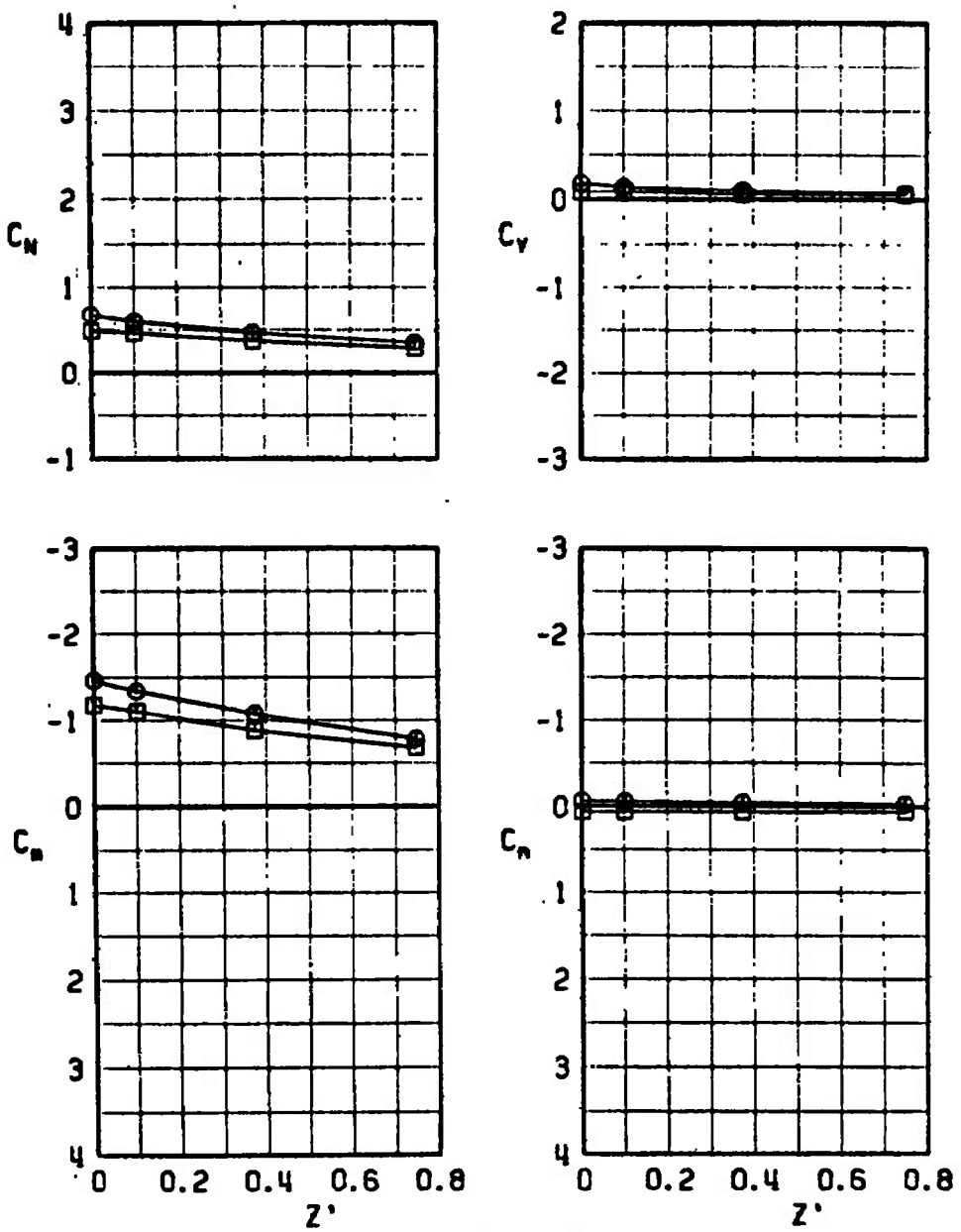

a. $\alpha = 0$, $Y' = 0$

Fig. 28 Force and Moment Coefficients for the Finned Large Model at the Wing 1/3-Semispan Station, $N_1B_2WA_2D$ and $N_1B_2WP_{1/3}A_2D$, $M_\infty = 0.4$

SYMBOL	CONF	α	ℓ_p
○	13	0	2.4
□	12	0	2.4

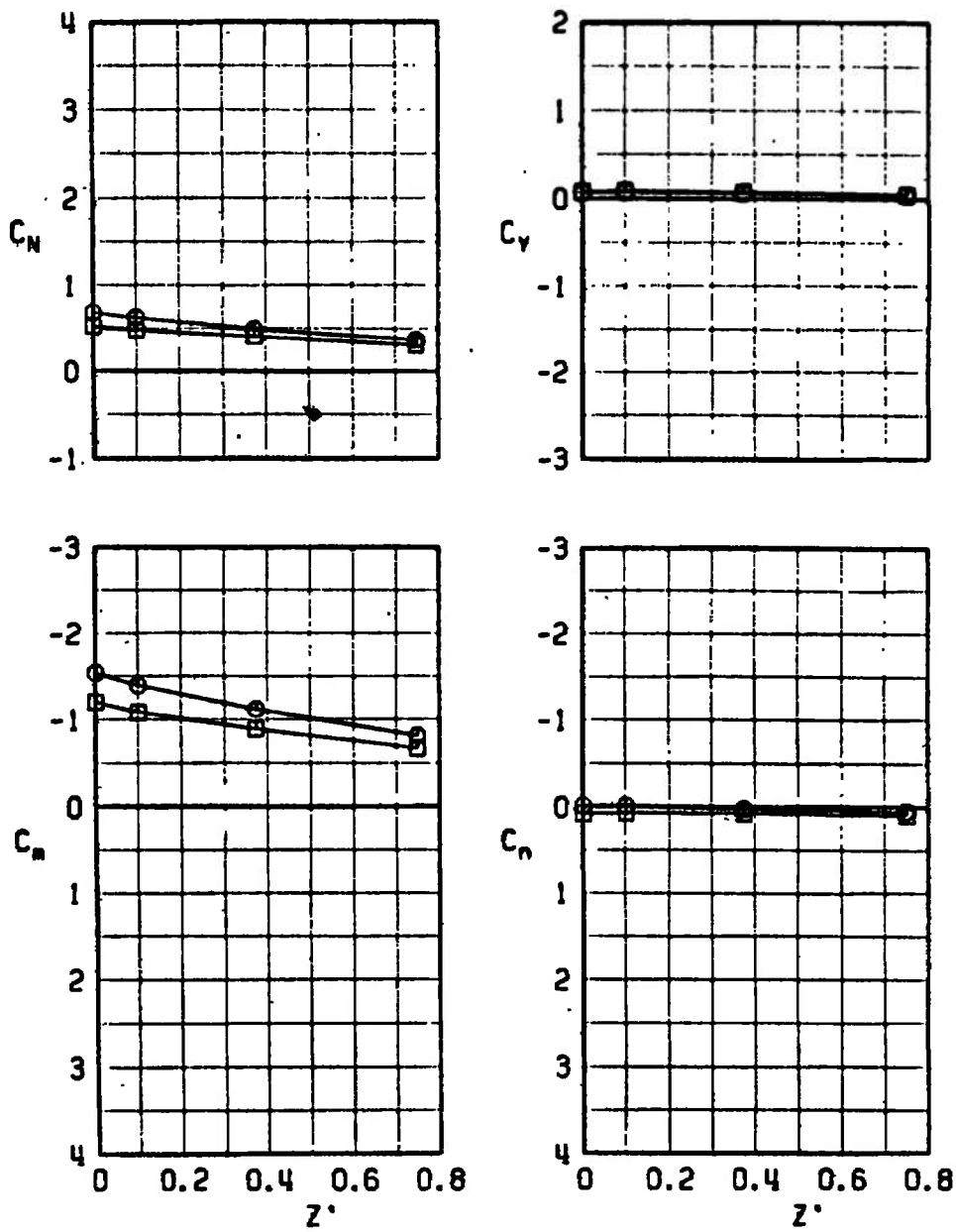

b. $\alpha = 0$, Y' = -0.375
Fig. 28 Continued

SYMBOL	CONF	α	ℓ_p
○	13	6	2.400
□	12	6	2.400

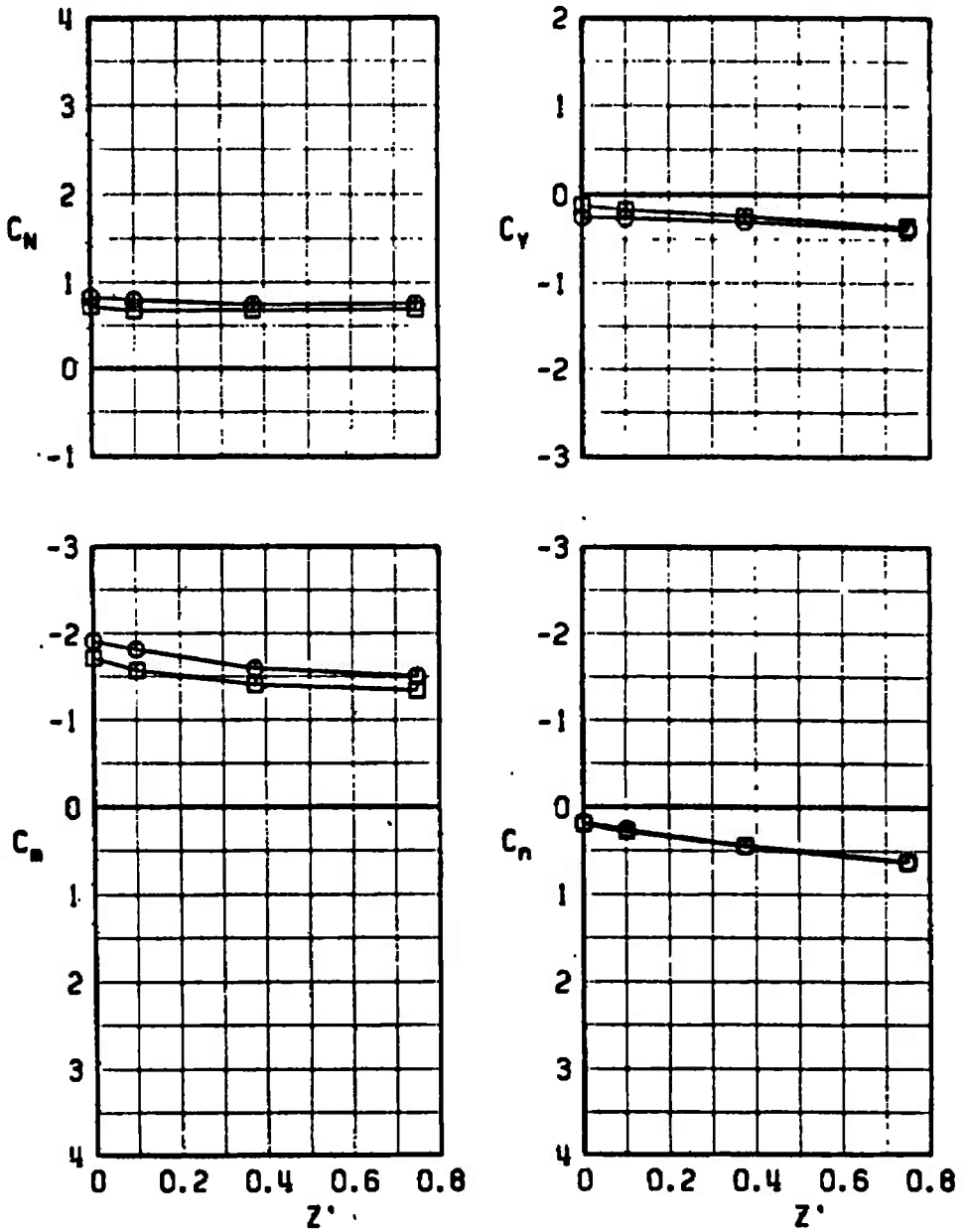

c. $\alpha = 6$, $Y' = 0$

Fig. 28 Continued

SYMBOL	CONF	α	ℓ_p
⊙	13	6	2.400
⊡	12	6	2.400

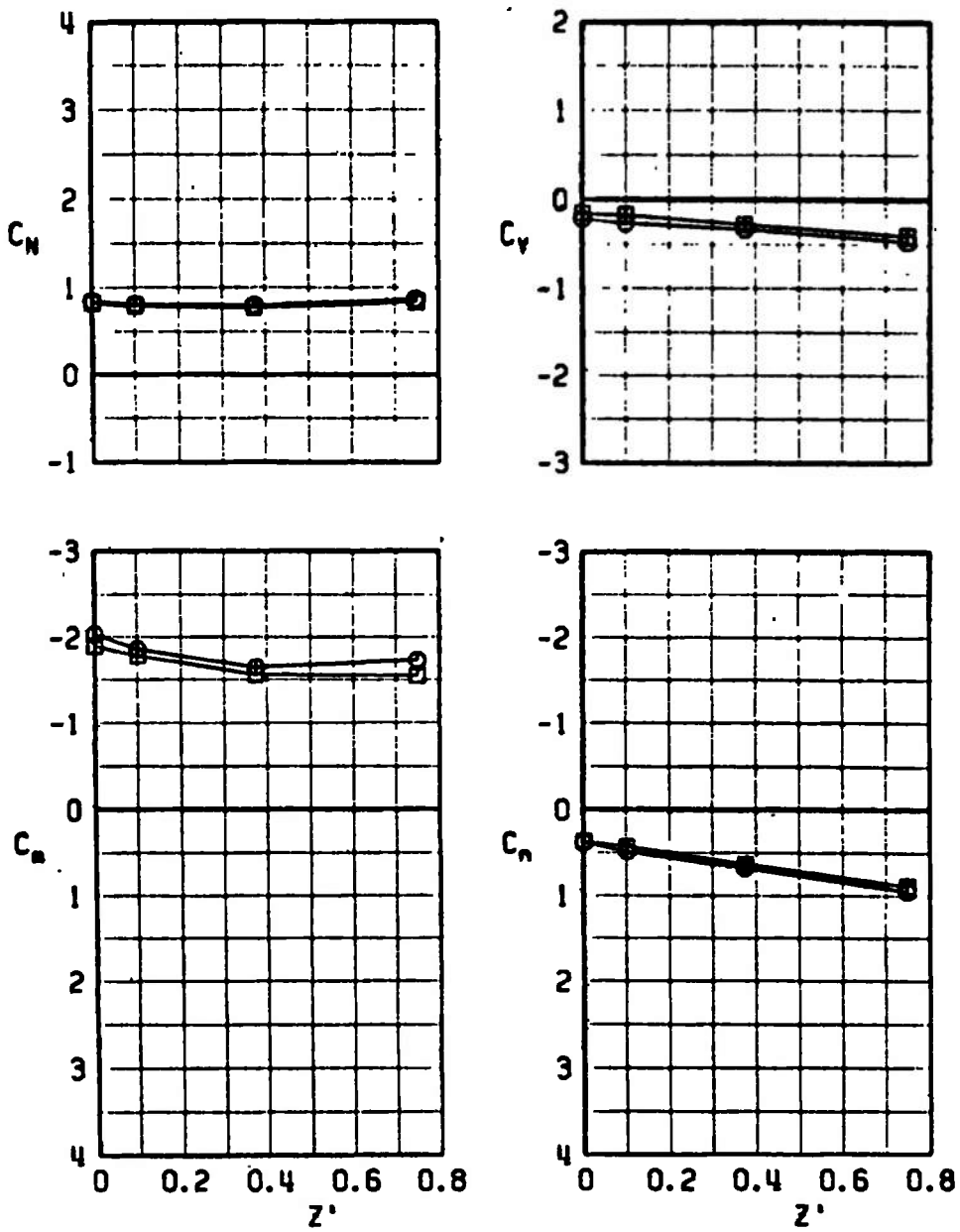

d. $\alpha = 6$, $Y' = -0.375$

Fig. 28 Continued

SYMBOL	CONF	α	ℓ_p
○	13	15	2.4
□	12	15	2.4

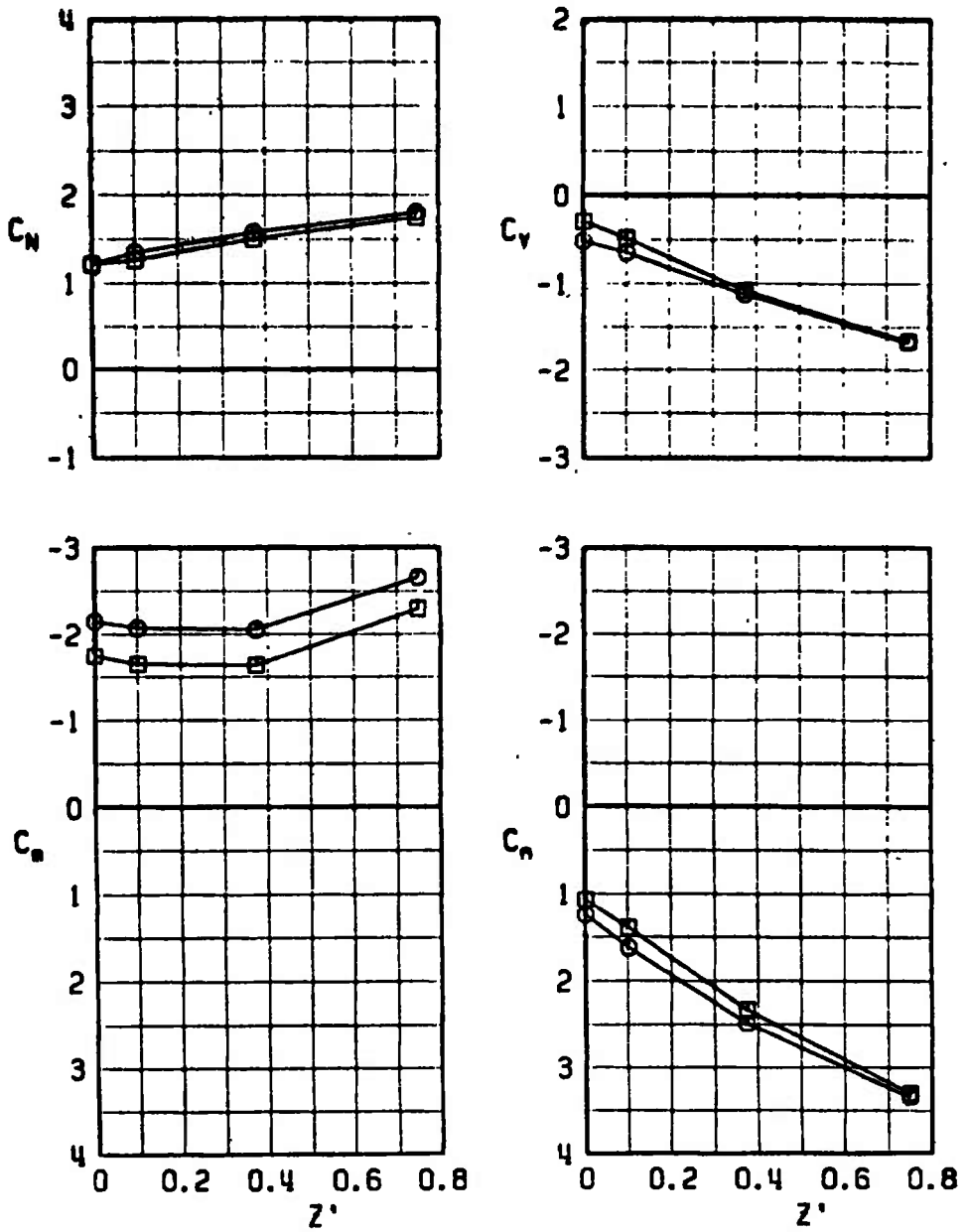

e. α = 15, Y' = 0
Fig. 28 Continued

SYMBOL	CONF	α	ℓ_p
○	13	15	2.4
□	12	15	2.4

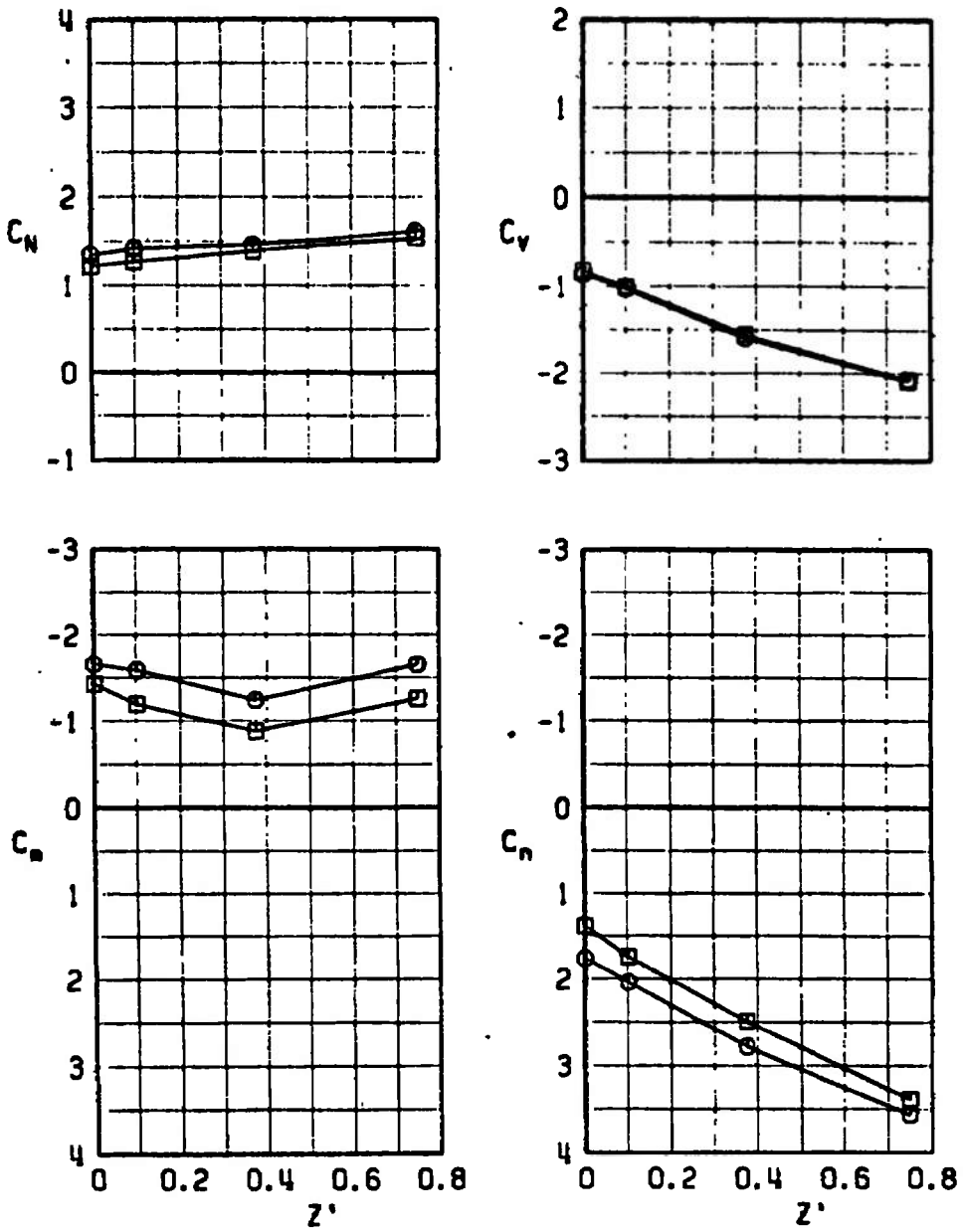

f. α = 15, Y' = -0.375
Fig. 28 Concluded

SYMBOL	CONF	α
○	3	0
□	4	0

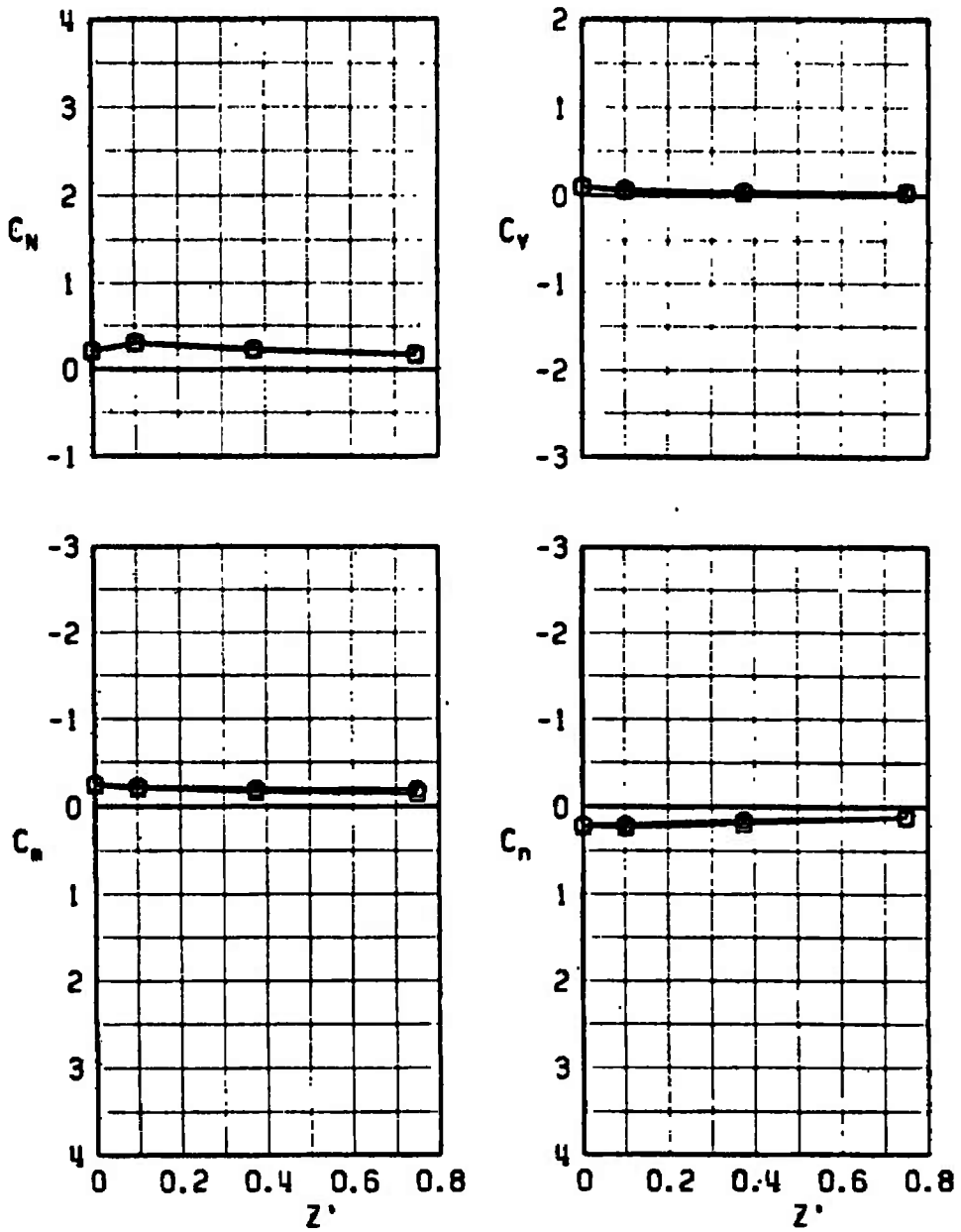

a. $\alpha = 0$; $Y' = 0$

Fig. 29 Force and Moment Coefficients for the SUU-41 and ESUU-41 Models at the Wing 1/3-Semispan Station, $N_1B_2WP_{1/3}$, $M_\infty = 0.4$

SYMBOL	CONF	α
⊙	3	6
⊡	4	6

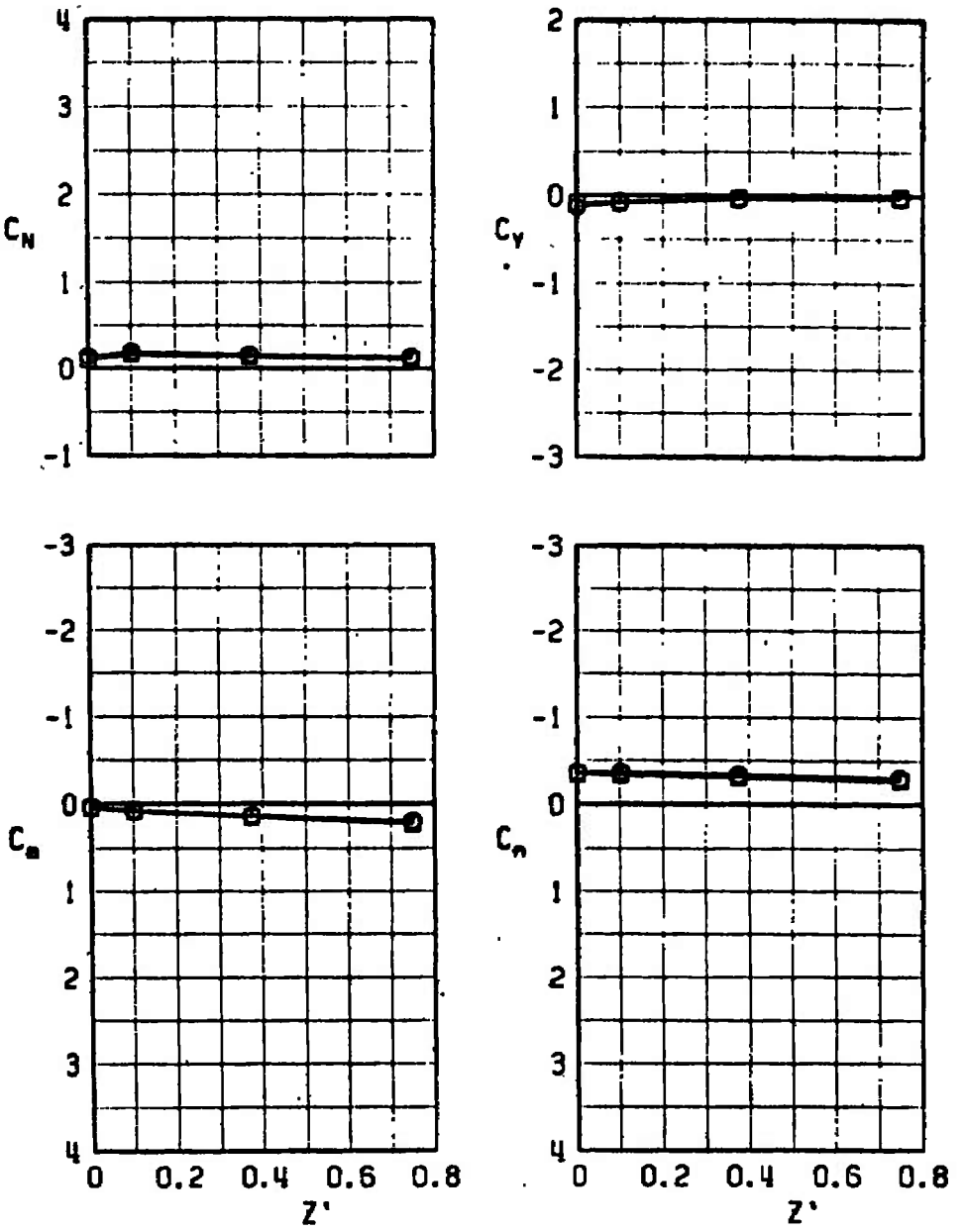

b. $\alpha = 6$, Y' = -0.375
Fig. 29 Continued

SYMBOL	CONF	α
⊙	3	15
⊡	4	15

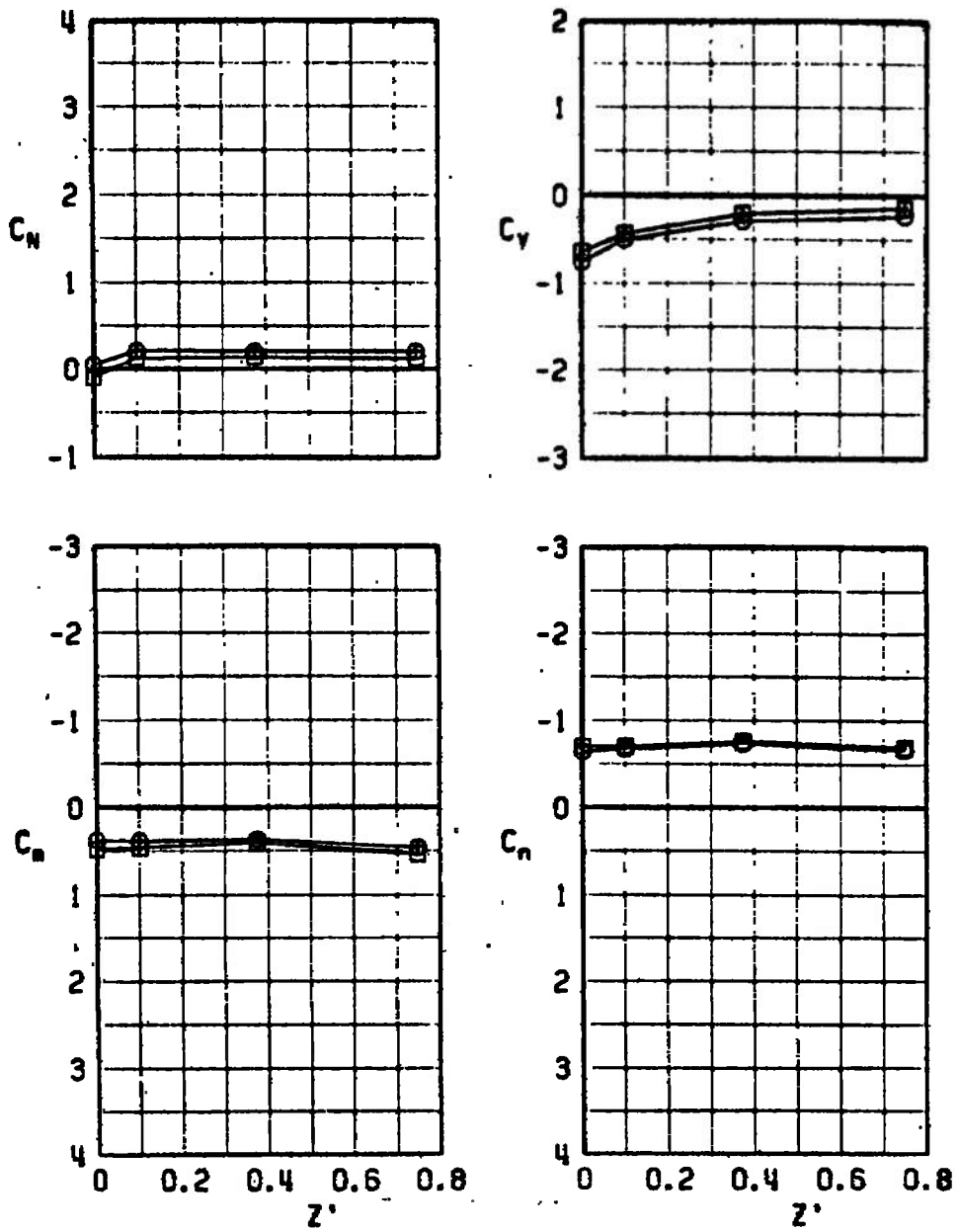

c. α = 15, Y' = 0
Fig. 29 Concluded

SYMBOL	CONF	α	ℓ_p
⊙	17	0	0.375
⊡	17	0	0.750
△	17	0	2.400

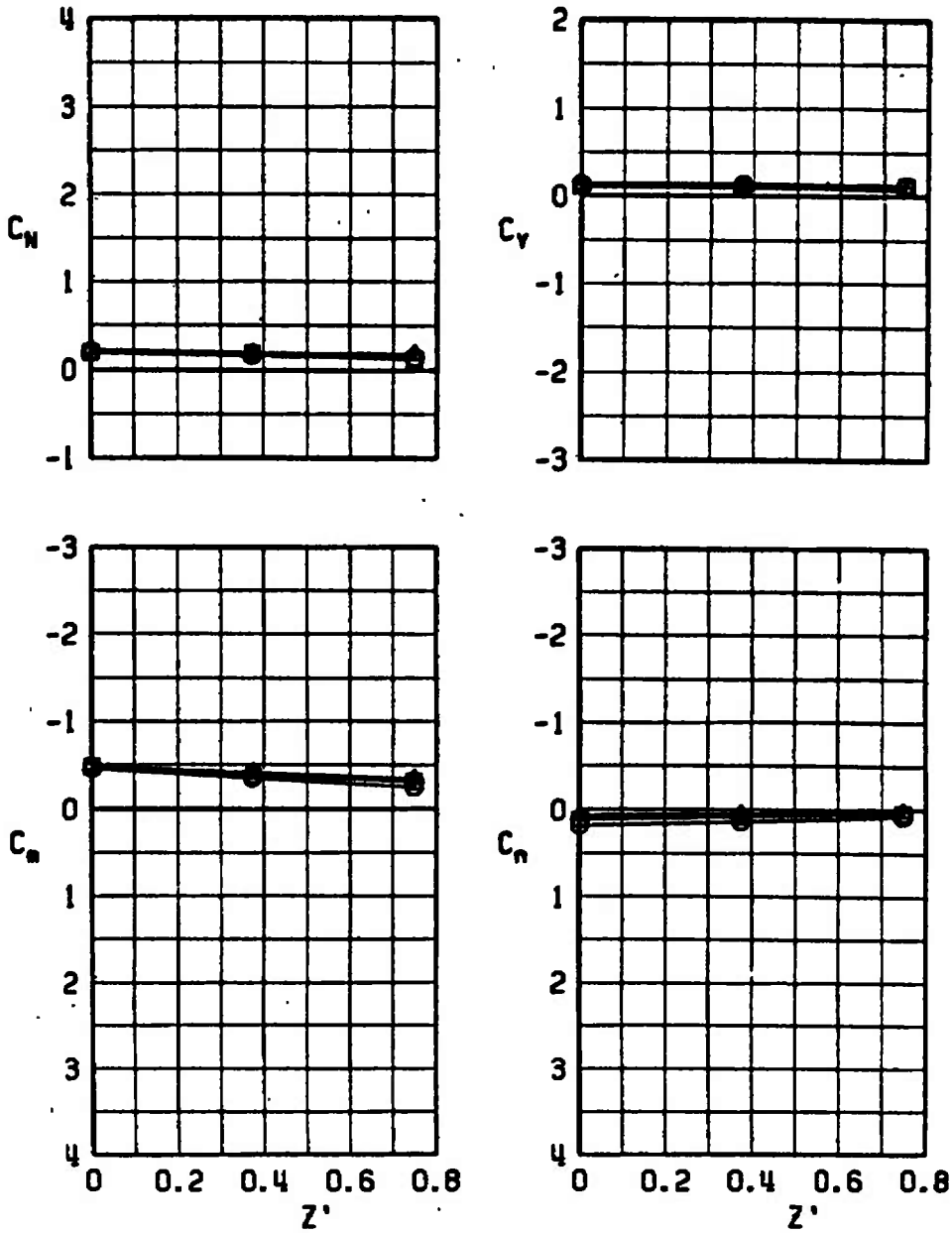

a. $\alpha = 0$, $Y' = 0$

Fig. 30 Parent-Model Duct Flow Influence on Force and Moment Coefficients for the Pressure Distribution Model at the Wing 1/3-Semispan Station, $N_1B_2WA_2D$, $M_\infty = 0.4$

SYMBOL	CONF	α	ℓ_p
⊙	17	0	0.375
⊡	17	0	0.750
△	17	0	2.400

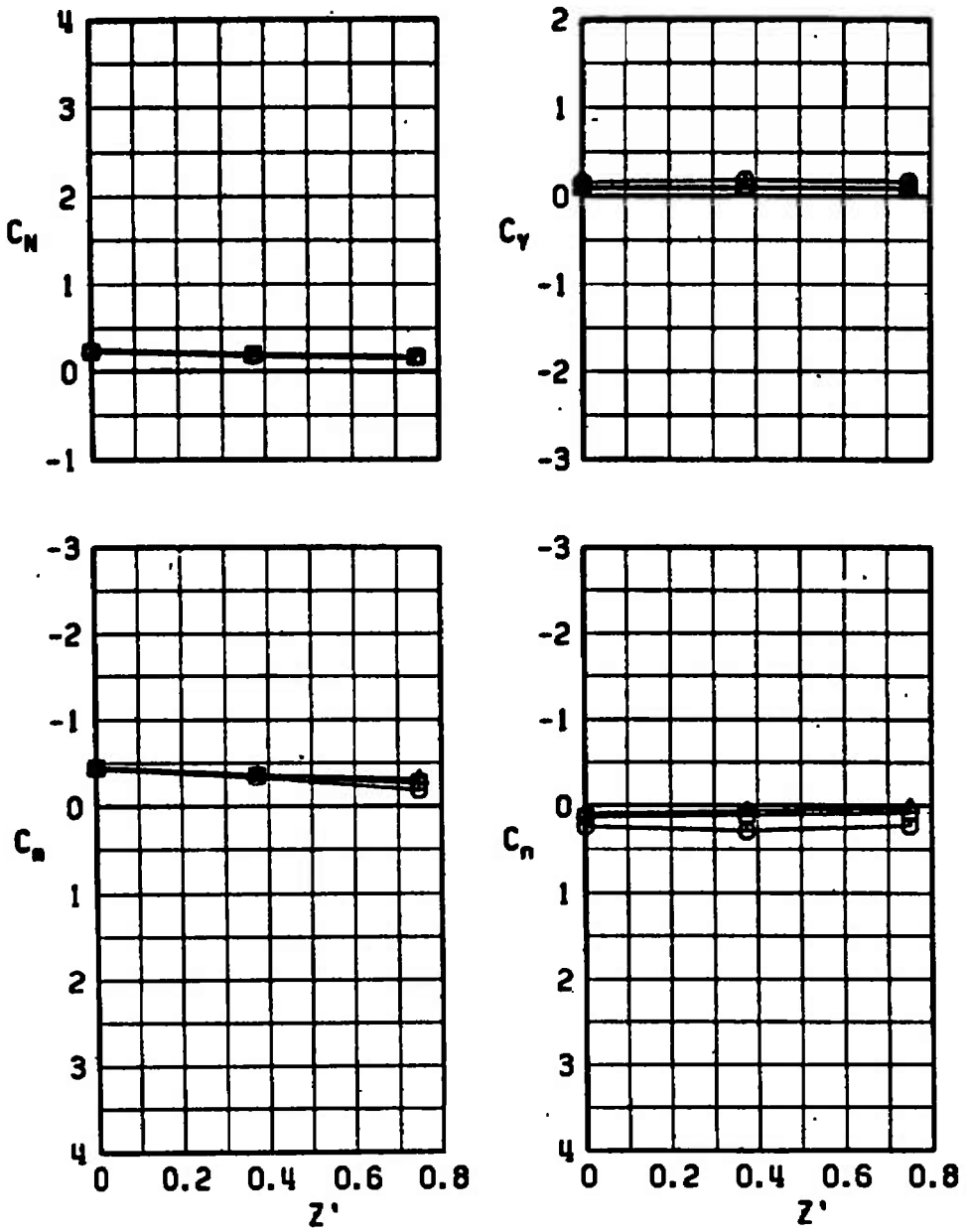

b. $\alpha = 0$, Y' = -0.375
Fig. 30 Continued

SYMBOL	CONF	α	ℓ_p
○	17	6	0.375
□	17	6	0.750
△	17	6	2.400

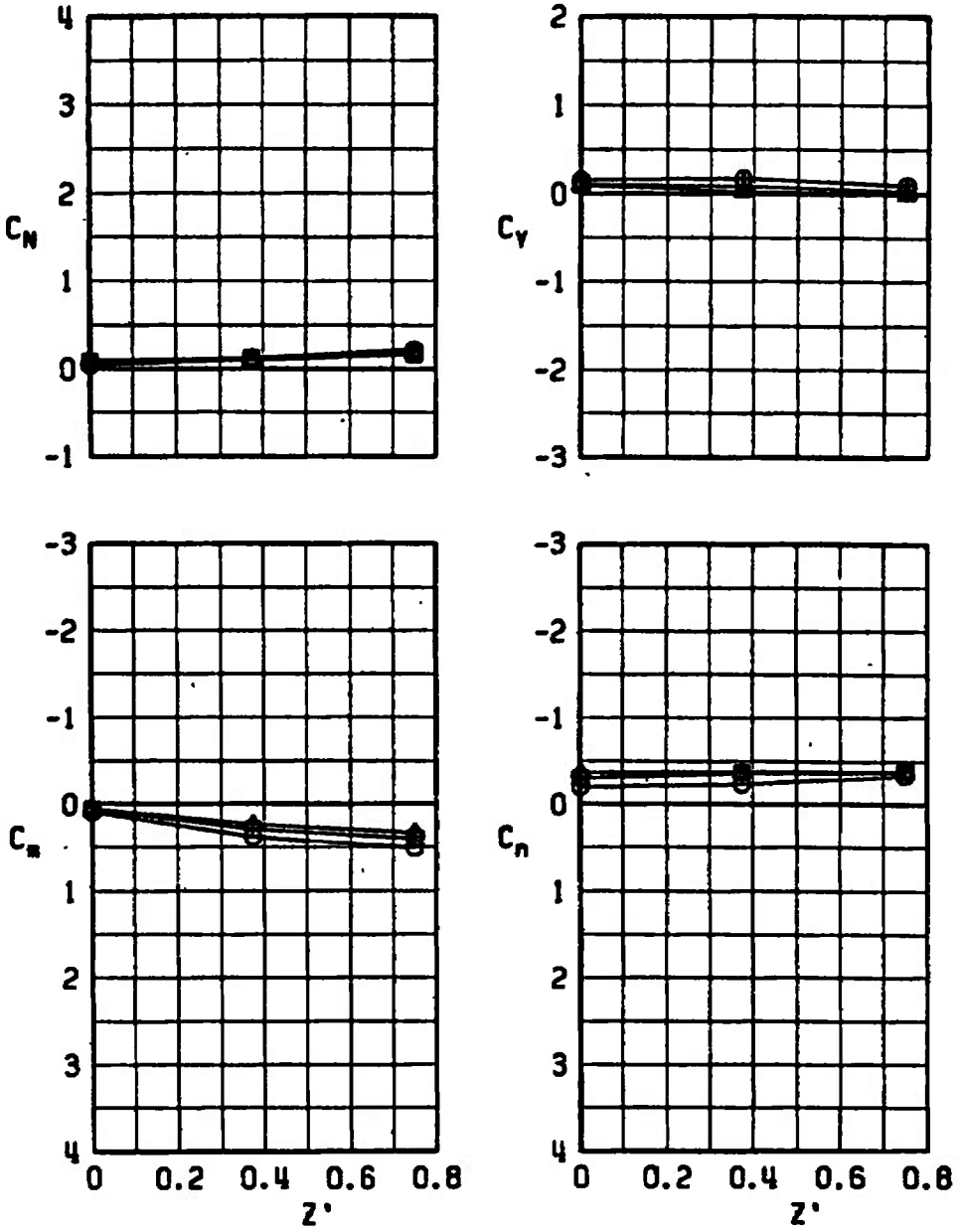

c. $\alpha = 6$, $Y' = 0$
Fig. 30 Continued

SYMBOL	CONF	α	ℓ_p
○	17	6	0.375
□	17	6	0.750
△	17	6	2.400

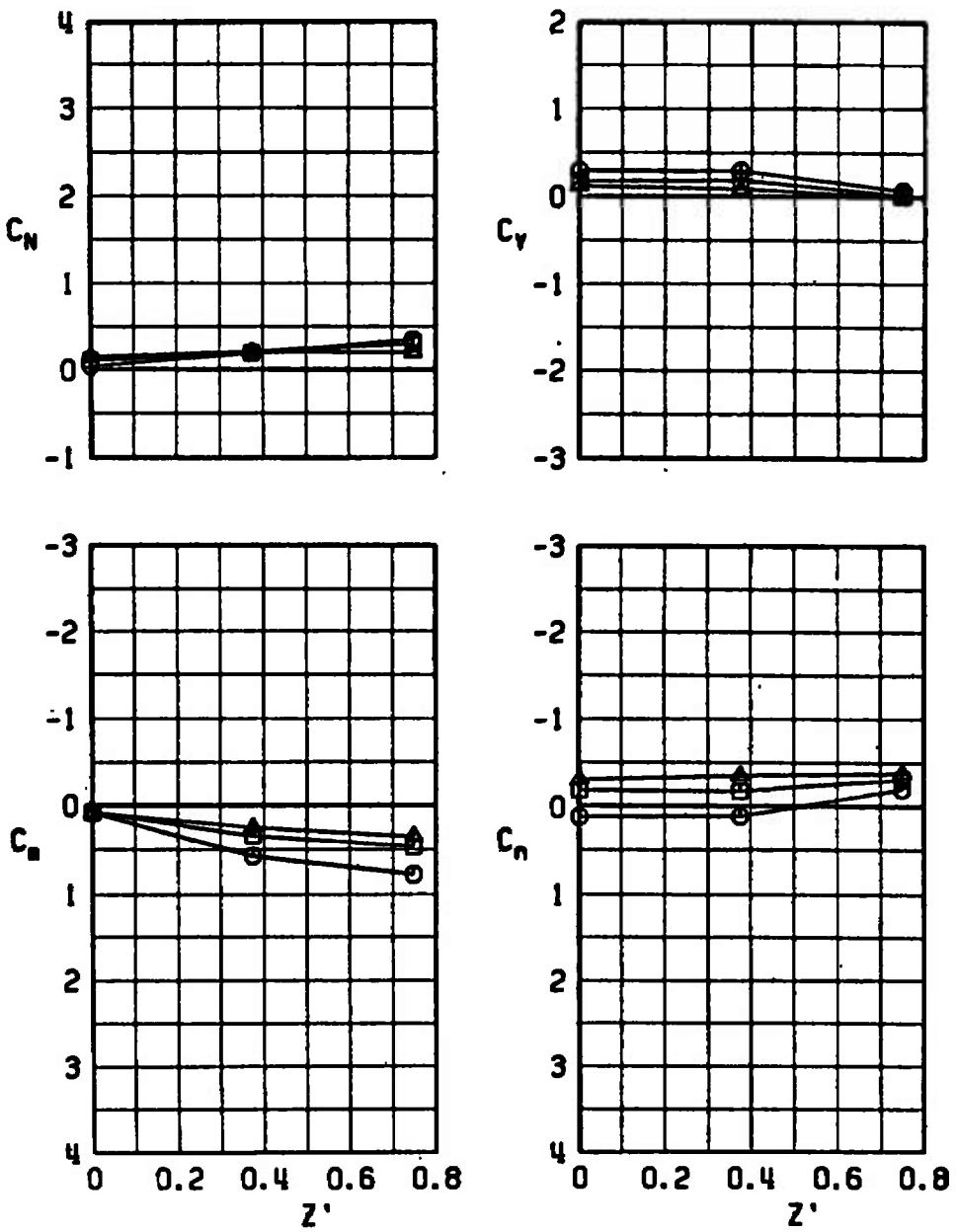

d. $\alpha = 6$, $Y' = -0.375$

Fig. 30 Concluded

SYMBOL	CONF	α	ℓ_p
⊙	18	0	0.375
⊡	18	0	0.750
△	18	0	2.400

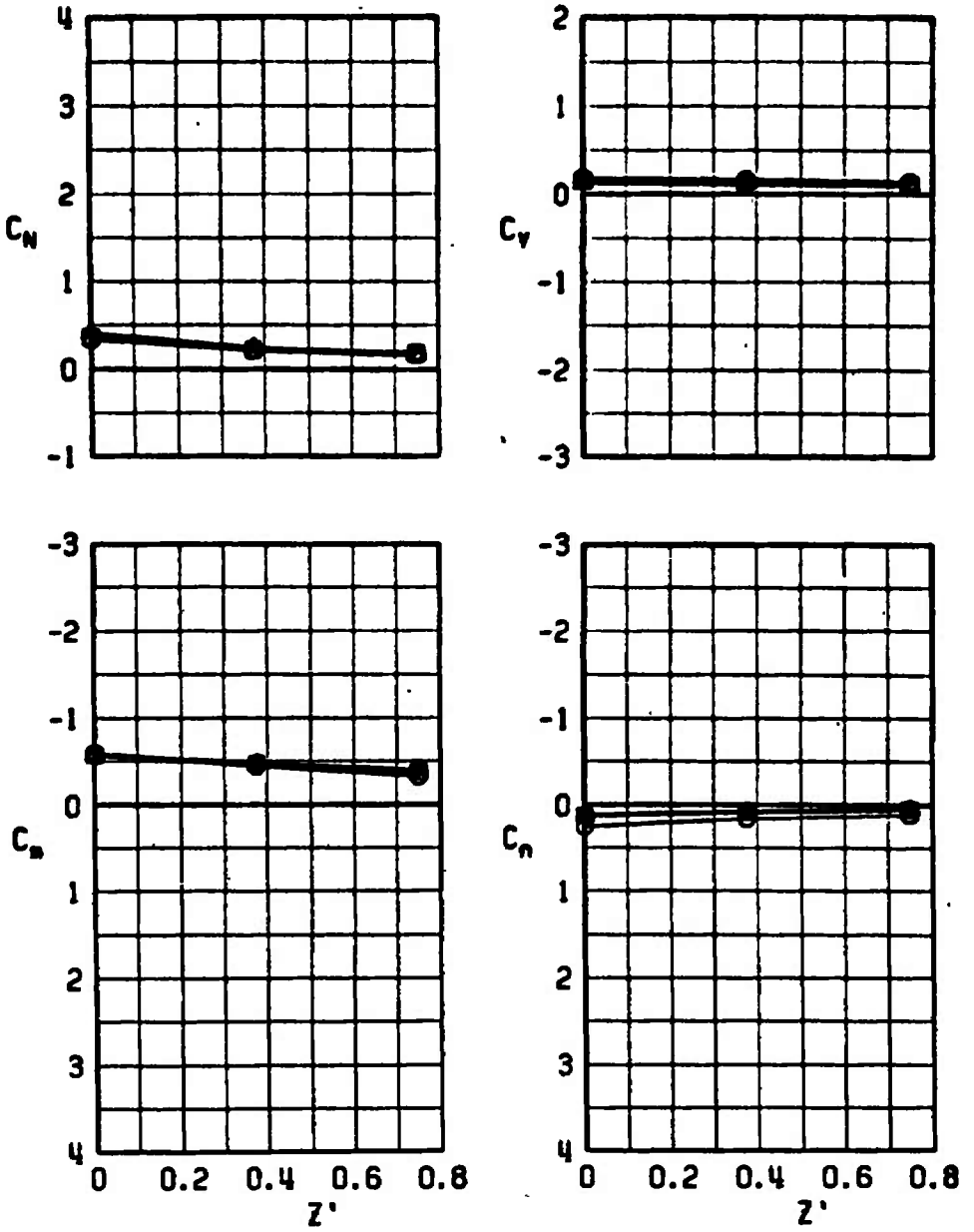

a. $\alpha = 0$, $Y' = 0$

Fig. 31 Parent-Model Duct Flow Influence on Force and Moment Coefficients for the Pressure Distribution Model at the Wing 1/3-Semispan Station, $N_1B_2WP_{1/3}A_2D$, $M_\infty = 0.4$

SYMBOL	CONF	α	ℓ_p
⊙	18	0	0.375
⊡	18	0	0.750
△	18	0	2.400

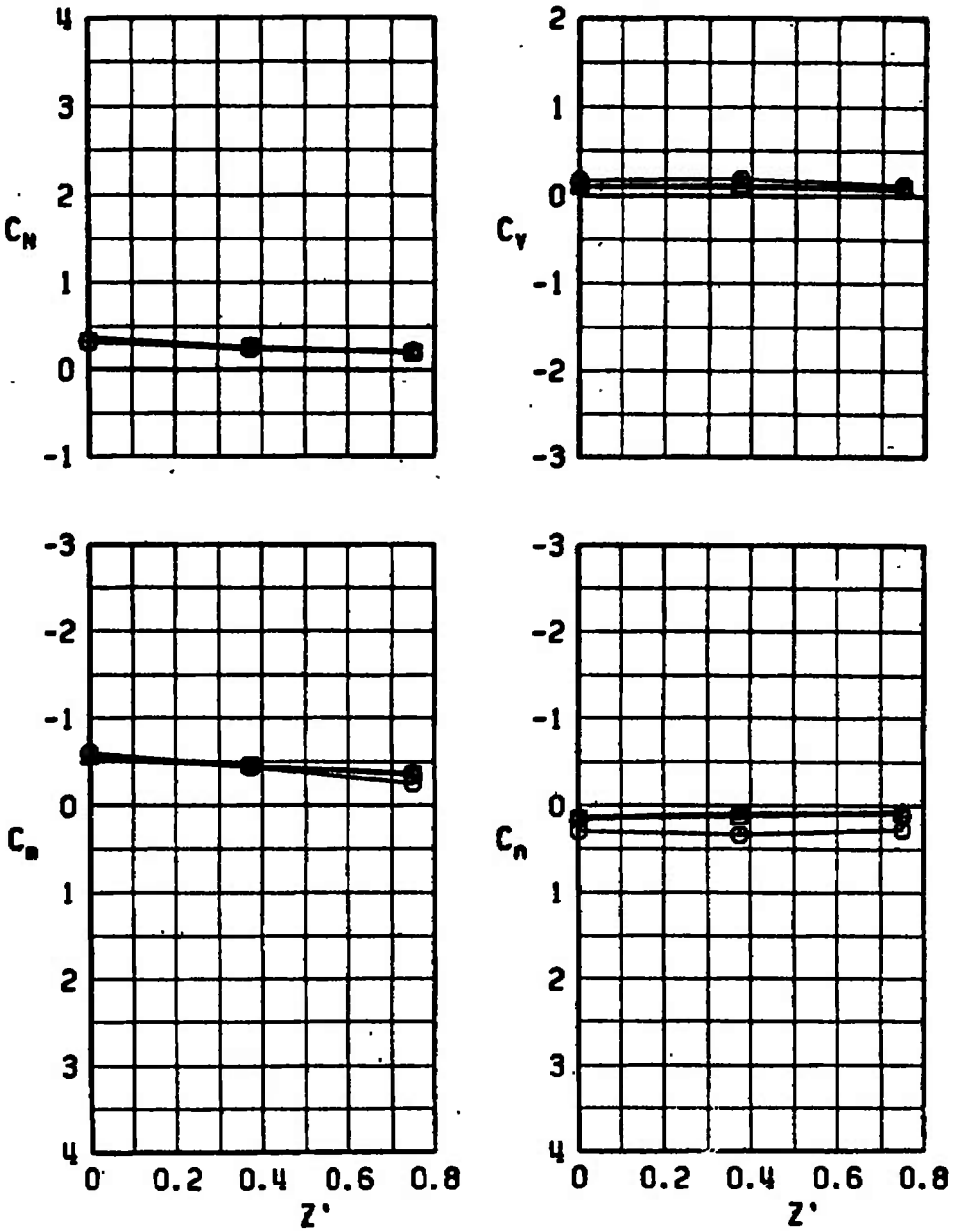

b. $\alpha = 0$, $Y' = -0.375$

Fig. 31 Continued

SYMBOL	CONF	α	ℓ_p
⊙	18	6	0.375
⊡	18	6	0.750
△	18	6	2.400

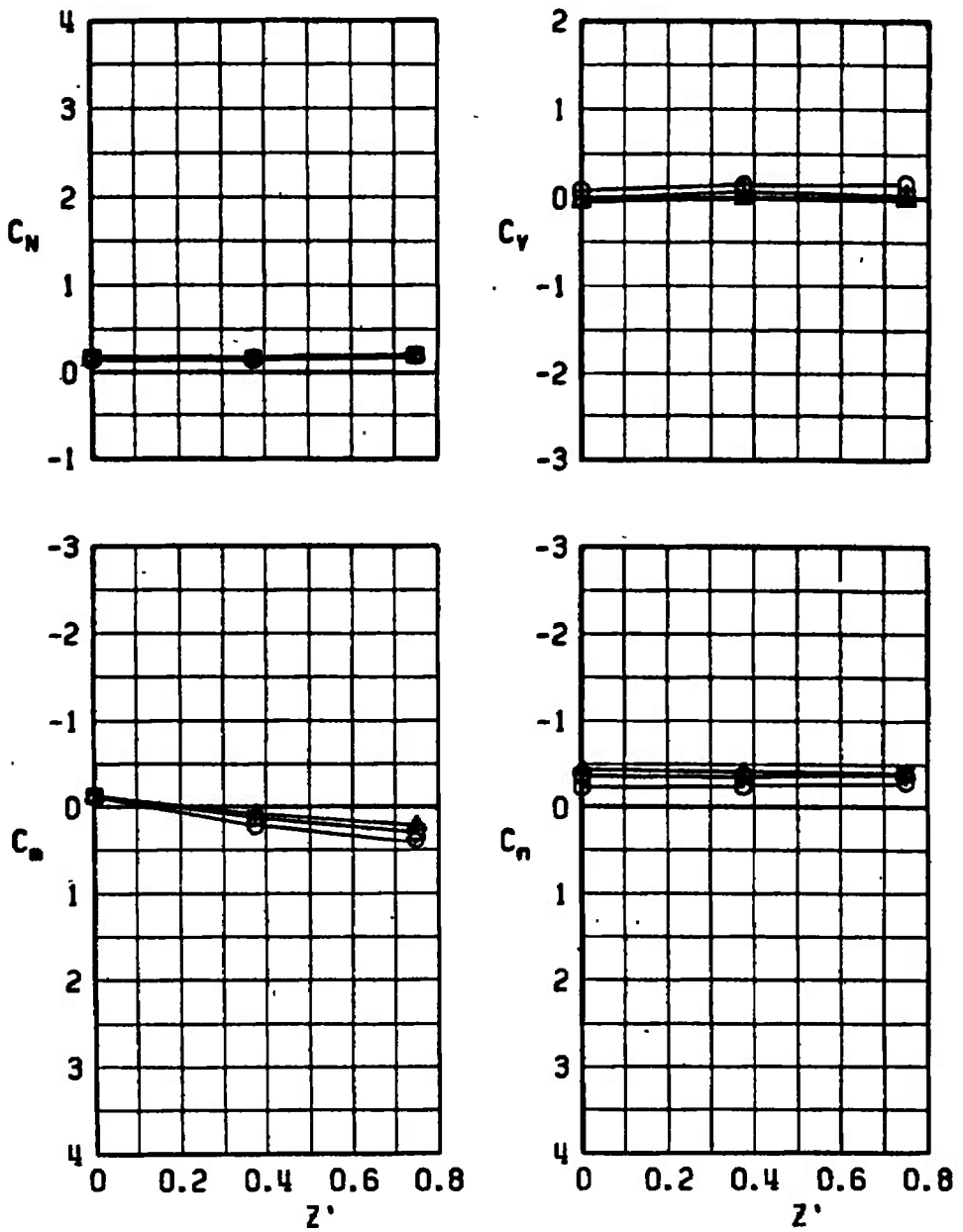

c. $\alpha = 6$, $Y' = 0$
Fig. 31 Continued

SYMBOL	CONF	α	ℓ_D
○	18	6	0.375
□	18	6	0.750
△	18	6	2.400

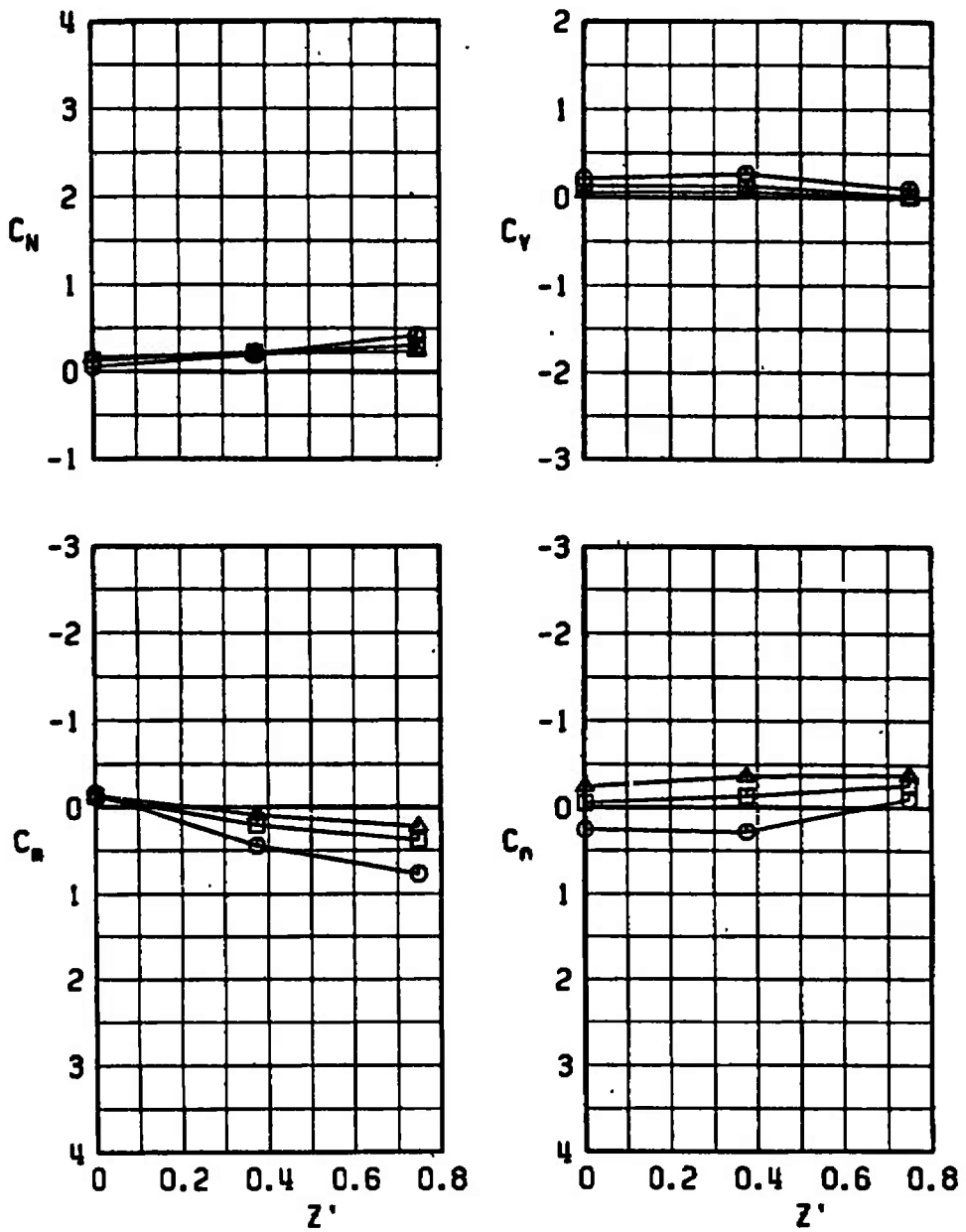

d. $\alpha = 6$, $Y' = -0.375$

Fig. 31 Concluded

SYMBOL	CONF	α	ℓ_p
⊙	18	0	0.375
□	18	0	0.750
△	18	0	2.400

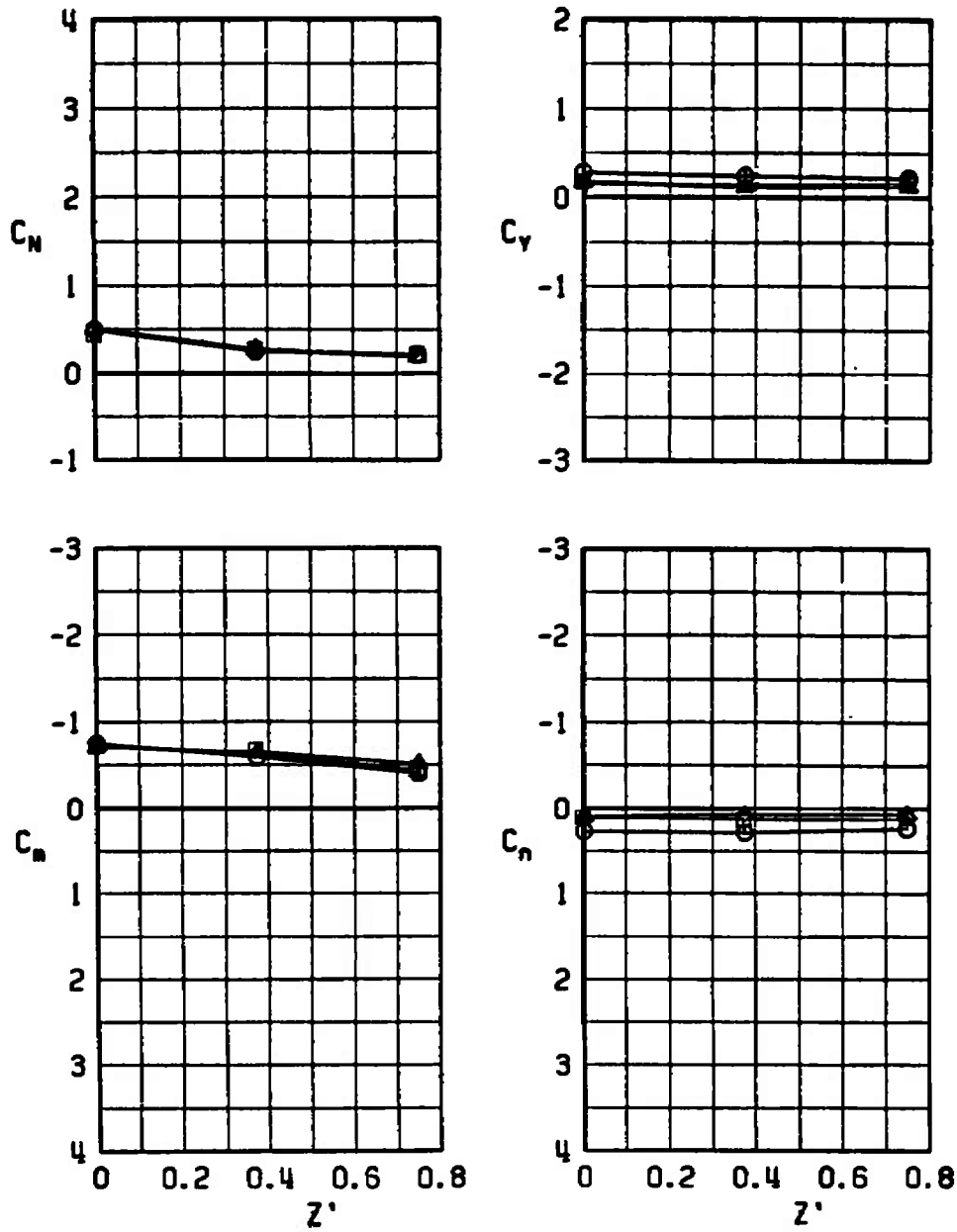

a. $\alpha = 0$, $Y' = 0$

Fig. 32 Parent-Model Duct Flow Influence on Force and Moment Coefficients for the Pressure Distribution Model at the Wing 1/3-Semispan Station, $N_1B_2WP_{1/3}A_2D$, $M_\infty = 0.7$

SYMBOL	CONF	α	ℓ_p
○	18	0	0.375
□	18	0	0.750
△	18	0	2.400

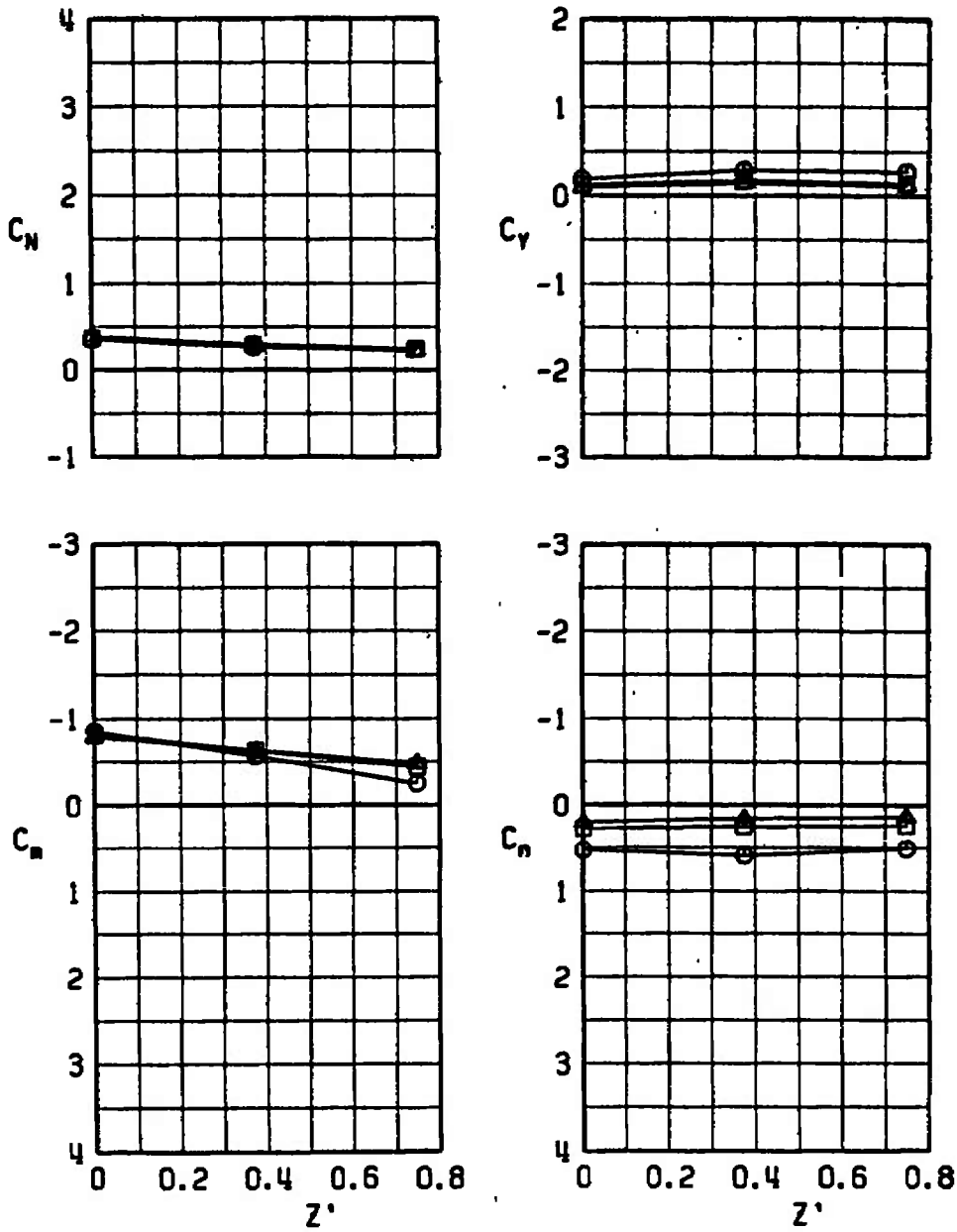

b. $\alpha = 0$, Y' = -0.375
Fig. 32 Continued

SYMBOL	CONF	α	ℓ_p
⊙	18	6	0.375
□	18	6	0.750
△	18	6	2.400

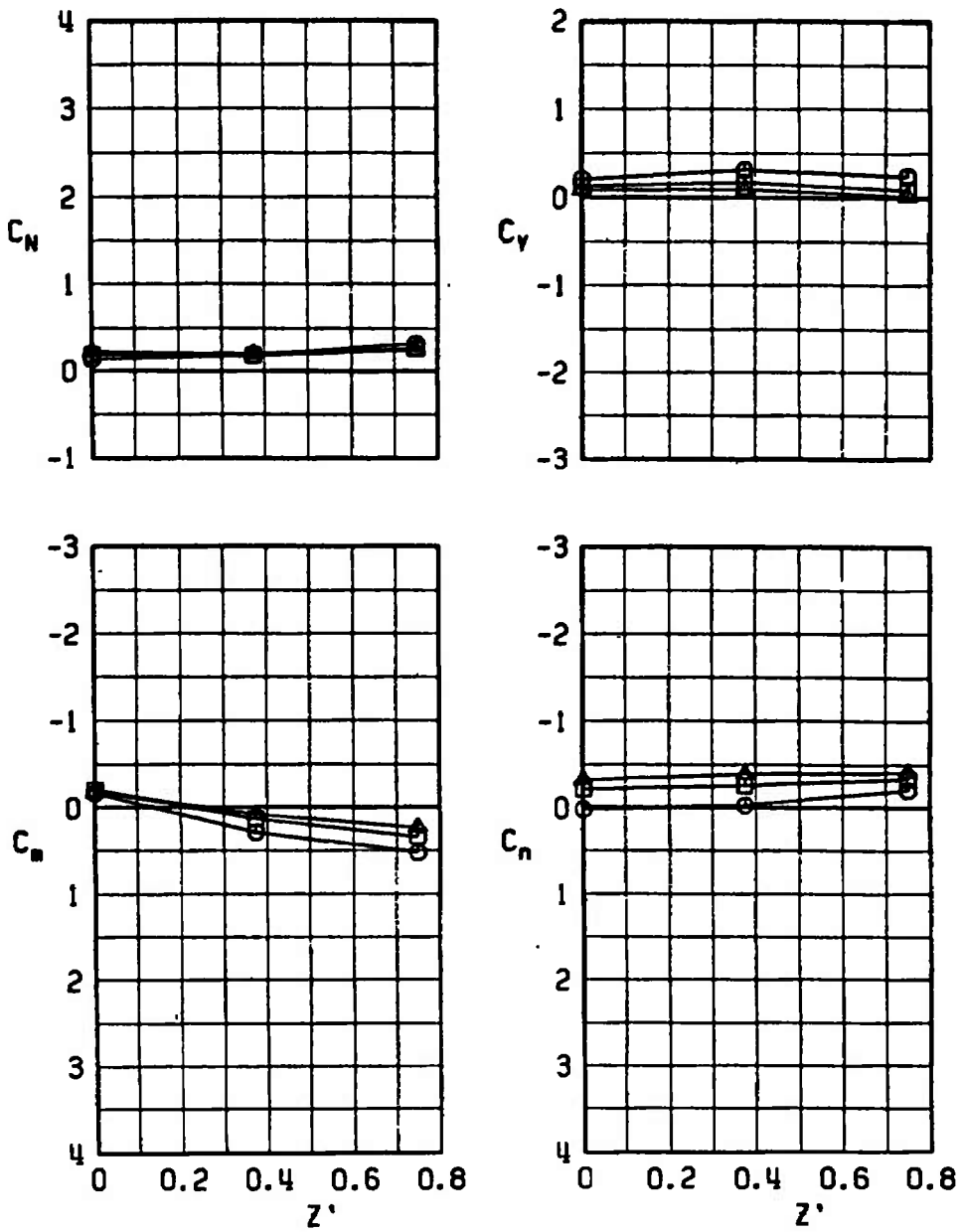

c. α = 6, Y' = 0
Fig. 32 Continued

SYMBOL	CONF	α	ℓ_p
⊙	18	6	0.375
□	18	6	0.750
△	18	6	2.400

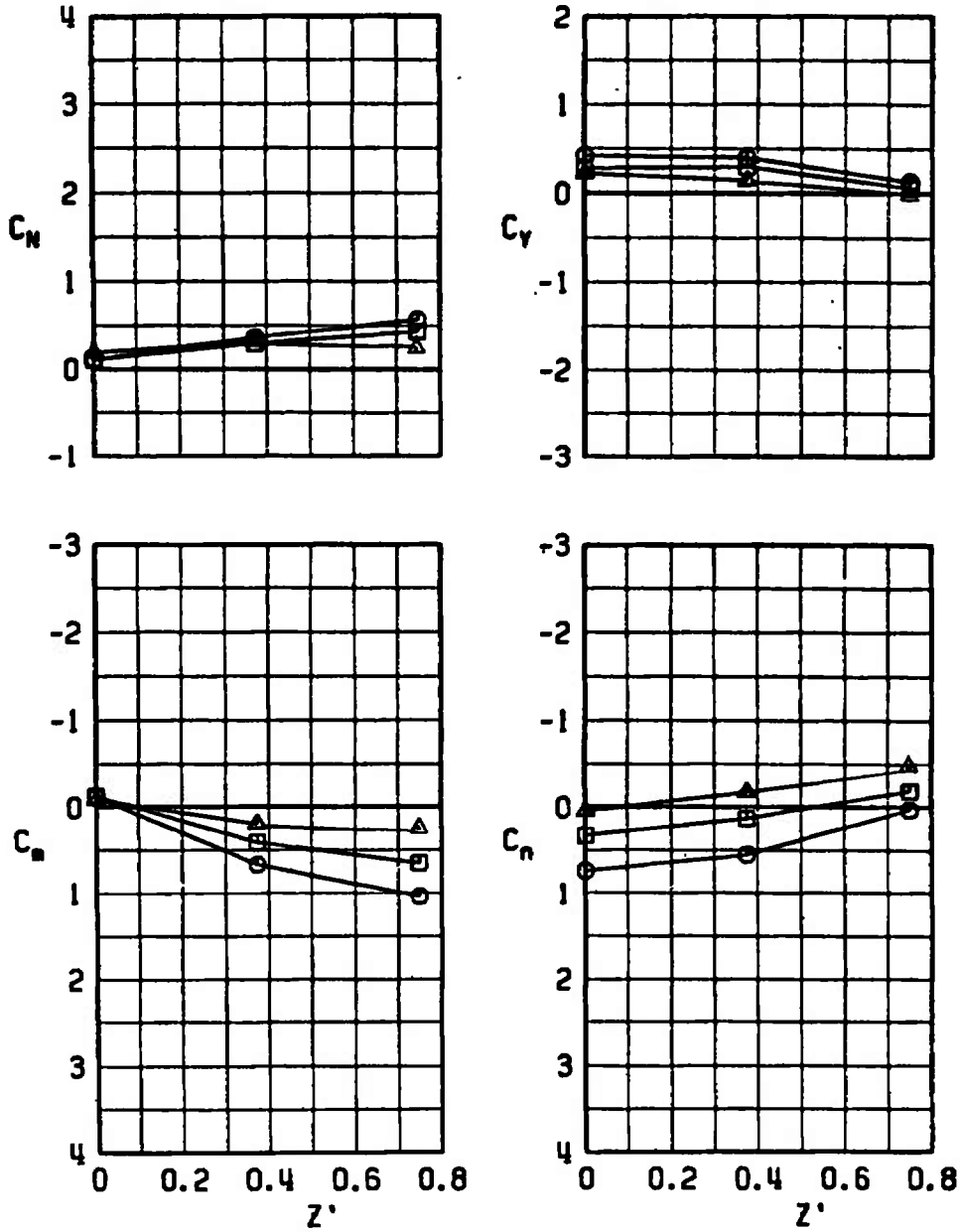

d. $\alpha = 6$, Y' = -0.375

Fig. 32 Concluded

SYMBOL	CONF	α	ℓ_p
⊙	19	0	0.375
⊡	19	0	0.750
△	19	0	2.400

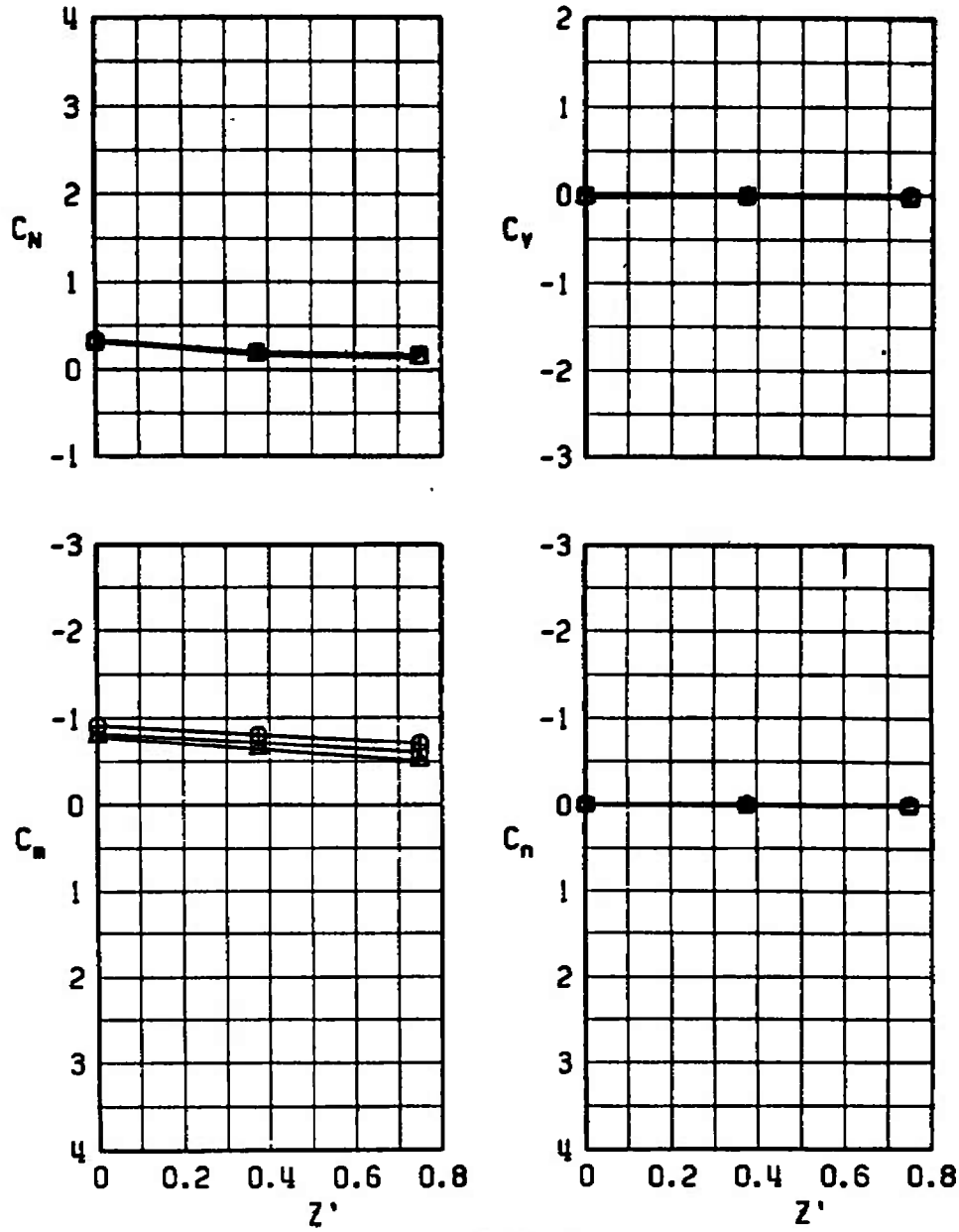

a. $\alpha = 0$, $Y' = 0$

Fig. 33 Parent-Model Duct Flow Influence on Force and Moment Coefficients for the Pressure Distribution Model at the Fuselage-Centerline Pylon Position, $N_1B_2WP_cA_2D$, $M_\infty = 0.4$

SYMBOL	CONF	α	ℓ_p
⊙	19	6	0.375
⊡	19	6	0.750
△	19	6	2.400

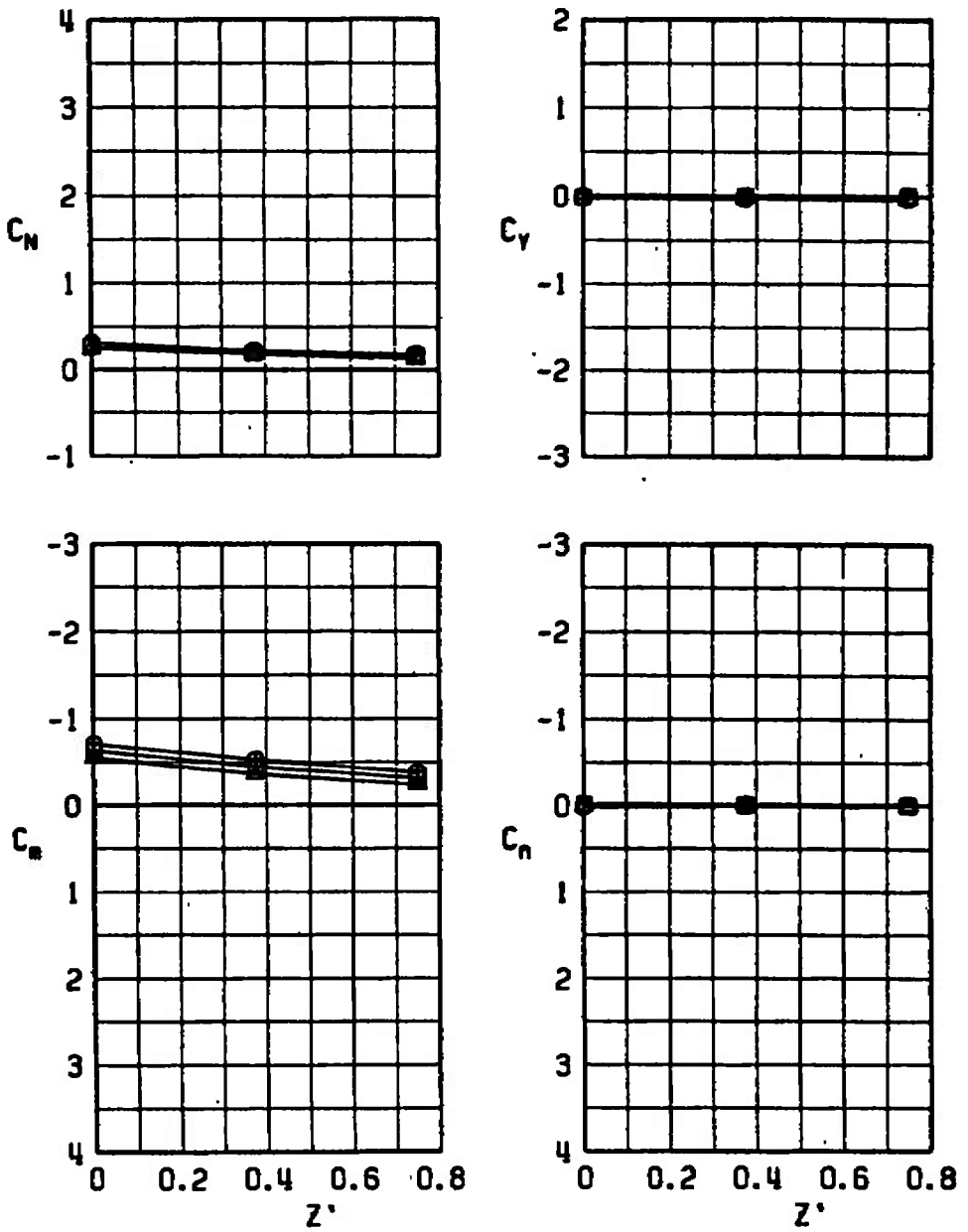

b. $\alpha = 6$, $Y' = 0$

Fig. 33 Concluded

SYMBOL	CONF	α
⊙	15	0
⊡	16	0

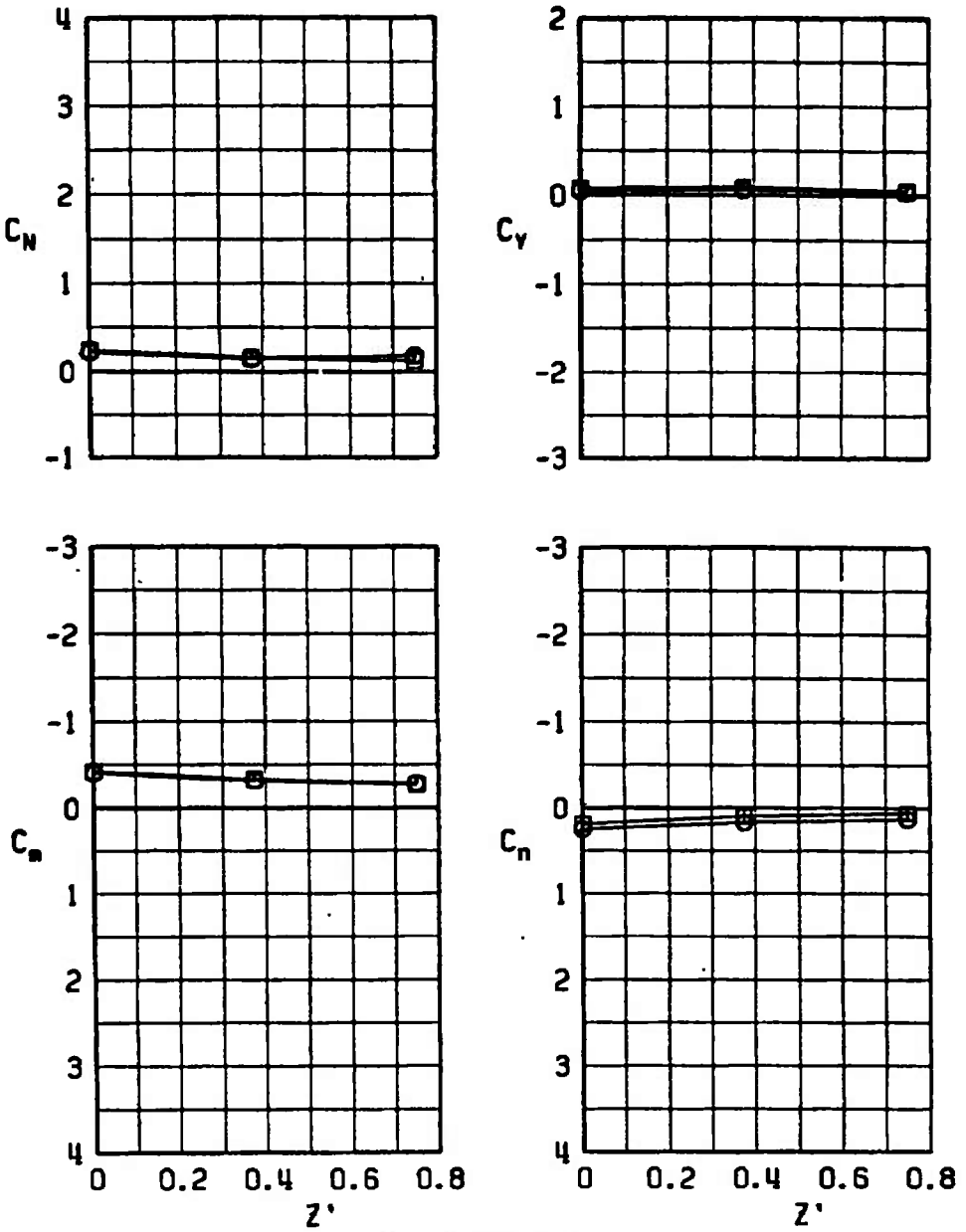

a. $\alpha = 0$, $Y' = 0$

Fig. 34 Force and Moment Coefficients for the Pressure Distribution Model at the Wing 1/3-Semispan Station, N_1B_2W and $N_1B_2WA_1$, $M_\infty = 0.4$

SYMBOL	CONF	α
⊙	15	0
⊡	16	0

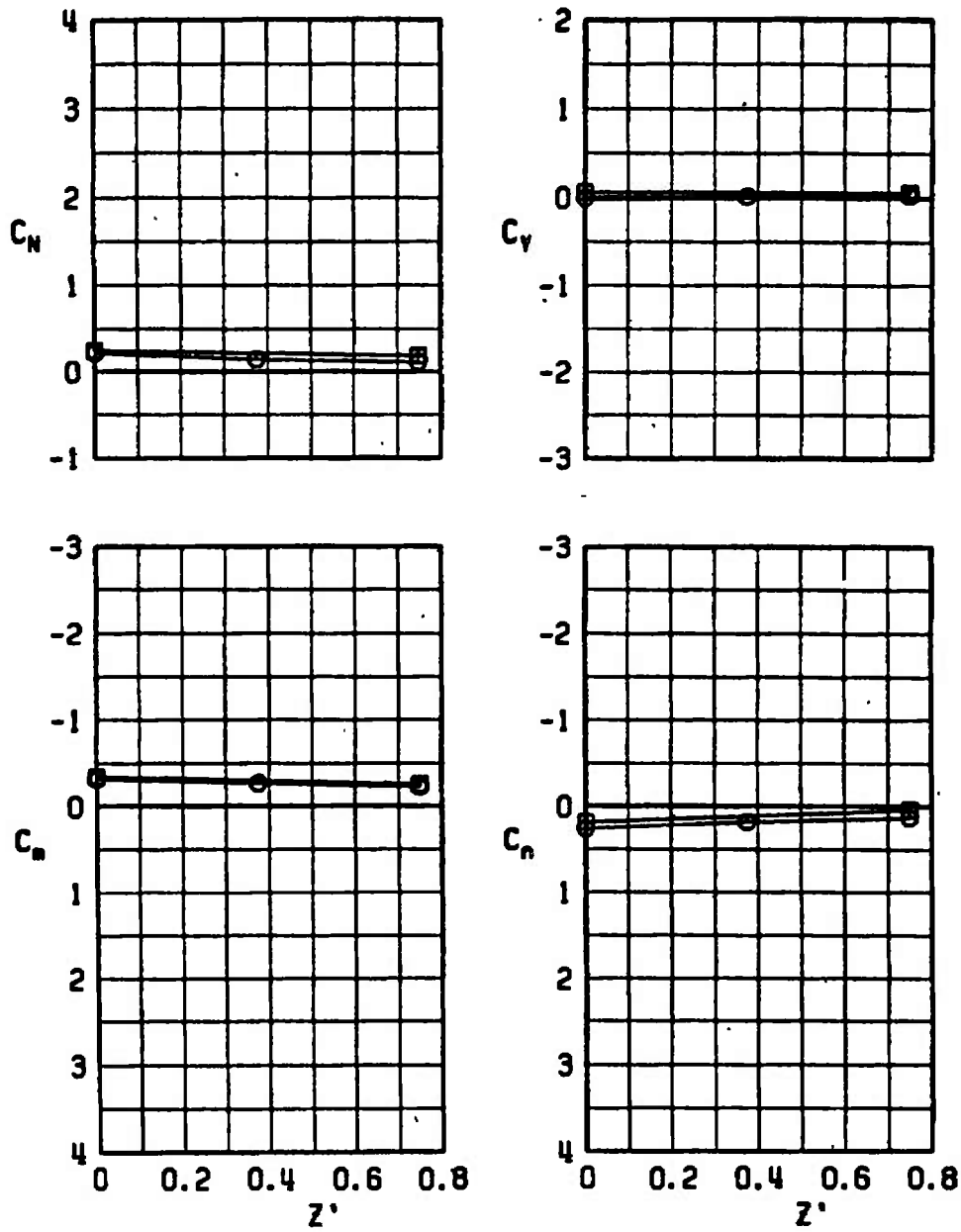

b. $\alpha = 0$, $Y' = -0.375$

Fig. 34 Continued

SYMBOL	CONF	α
⊙	15	6
⊡	16	6

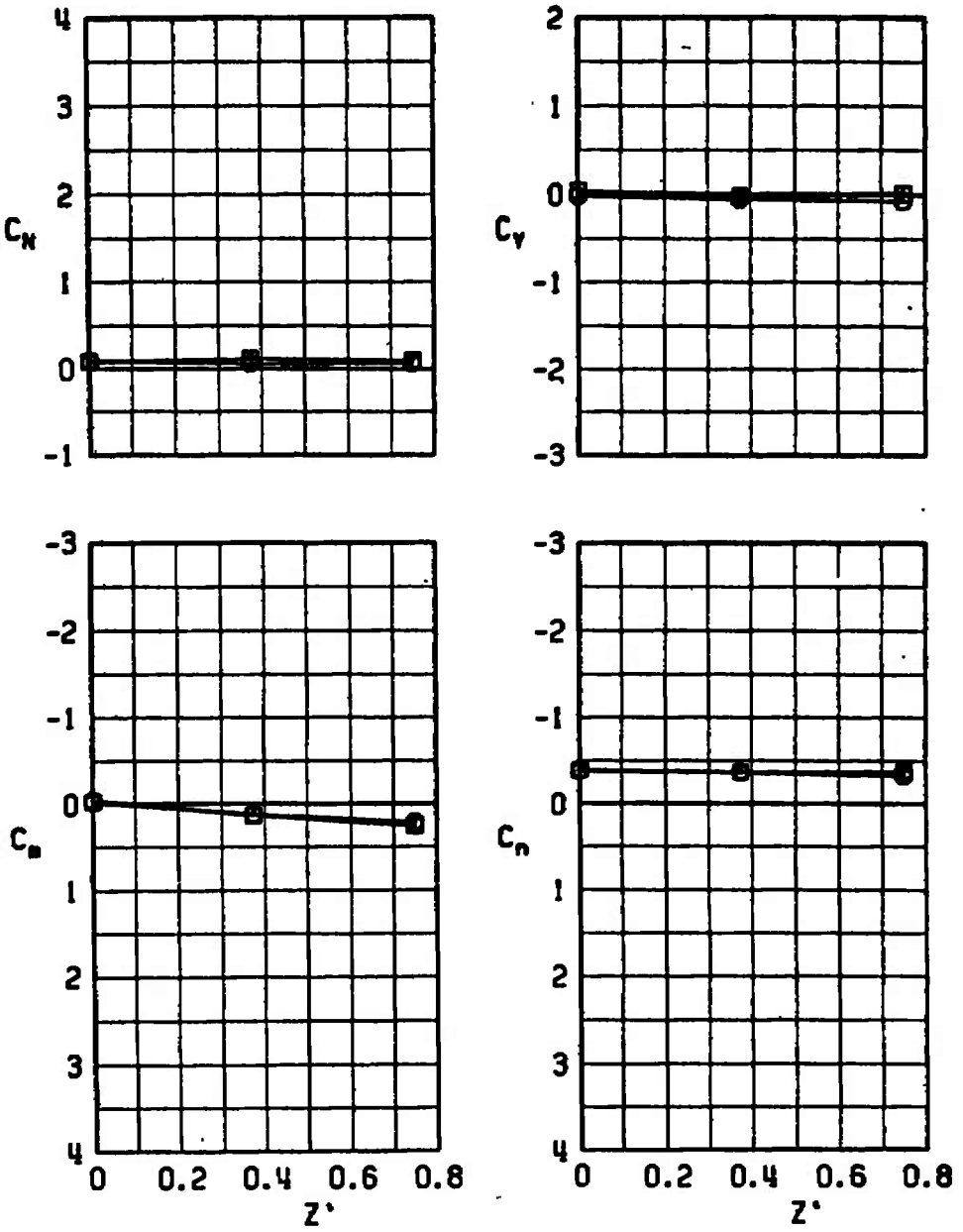

c. $\alpha = 6$, $Y' = 0$

Fig. 34 Continued

SYMBOL	CONF	α
○	15	6
□	16	6

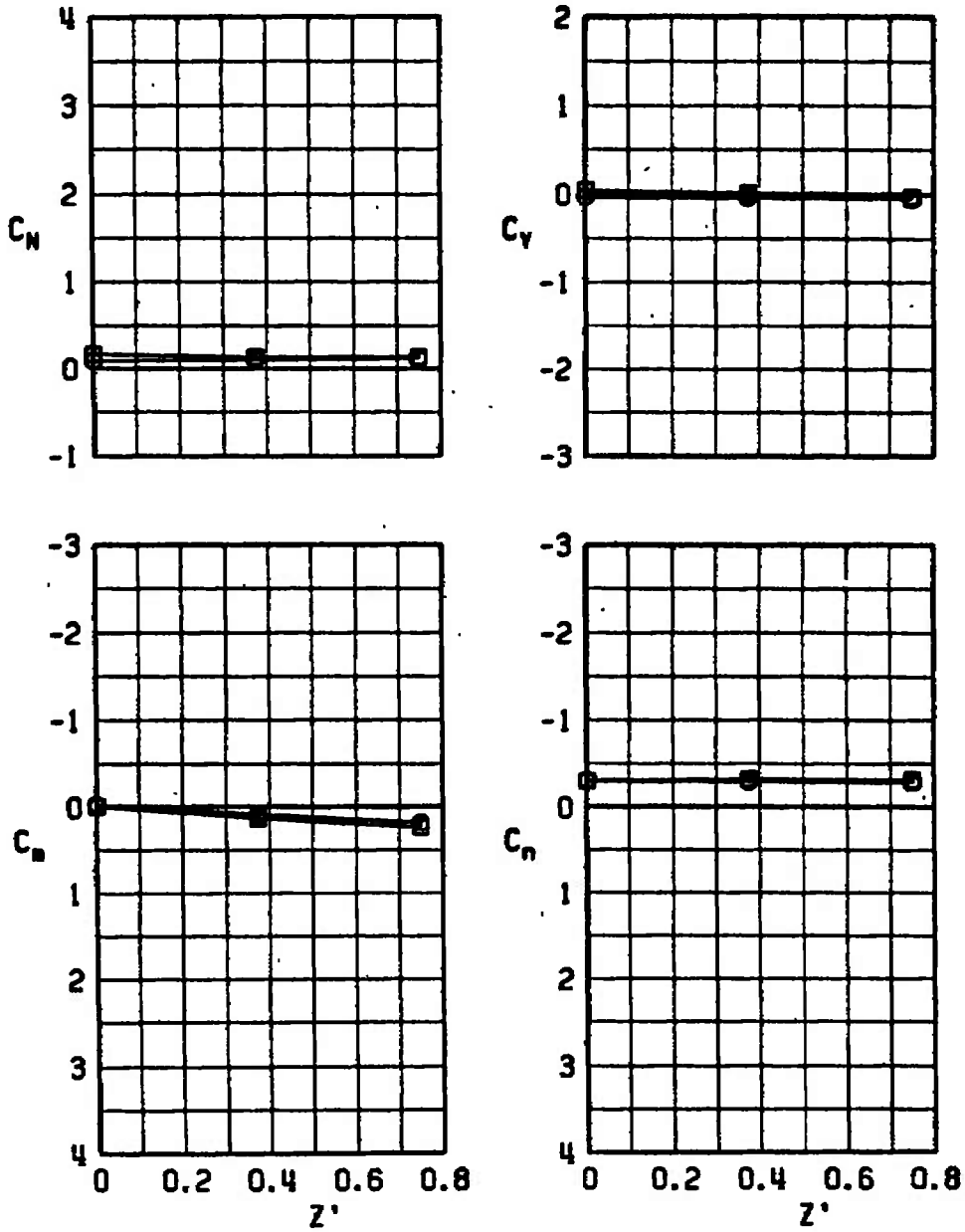

d. α = 6, Y' = -0.375
Fig. 34 Concluded

SYMBOL	CONF	α	ℓ_p
⊙	17	0	2.400
⊡	18	0	2.400

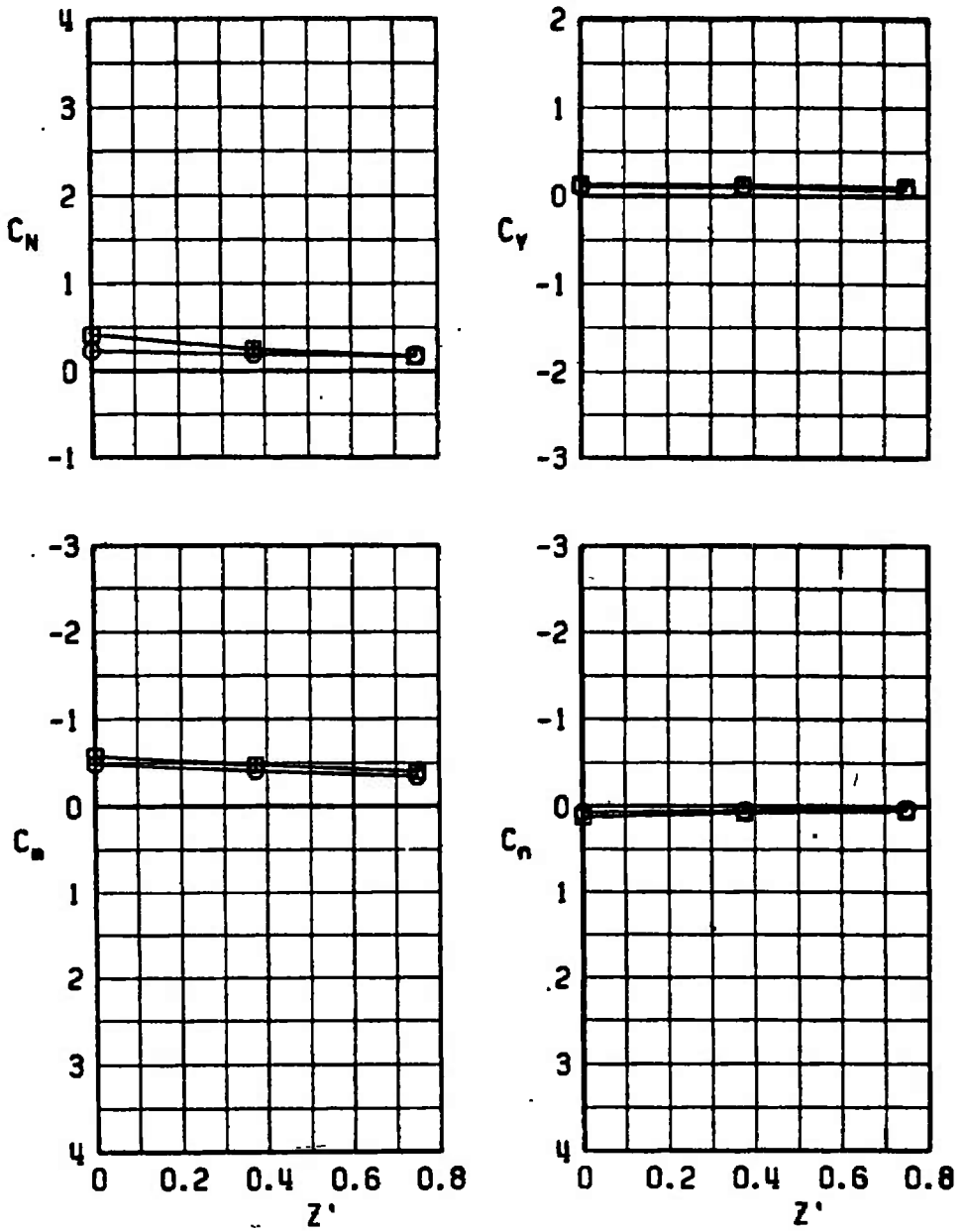

a. $\alpha = 0$, $Y' = 0$

Fig. 35 Force and Moment Coefficients for the Pressure Distribution Model at the Wing 1/3-Semispan Station, $N_1B_2WA_2D$ and $N_1B_2WP_{1/3}A_2D$, $M_\infty = 0.4$

SYMBOL	CONF	α	ℓ_p
⊙	17	0	2.400
⊡	18	0	2.400

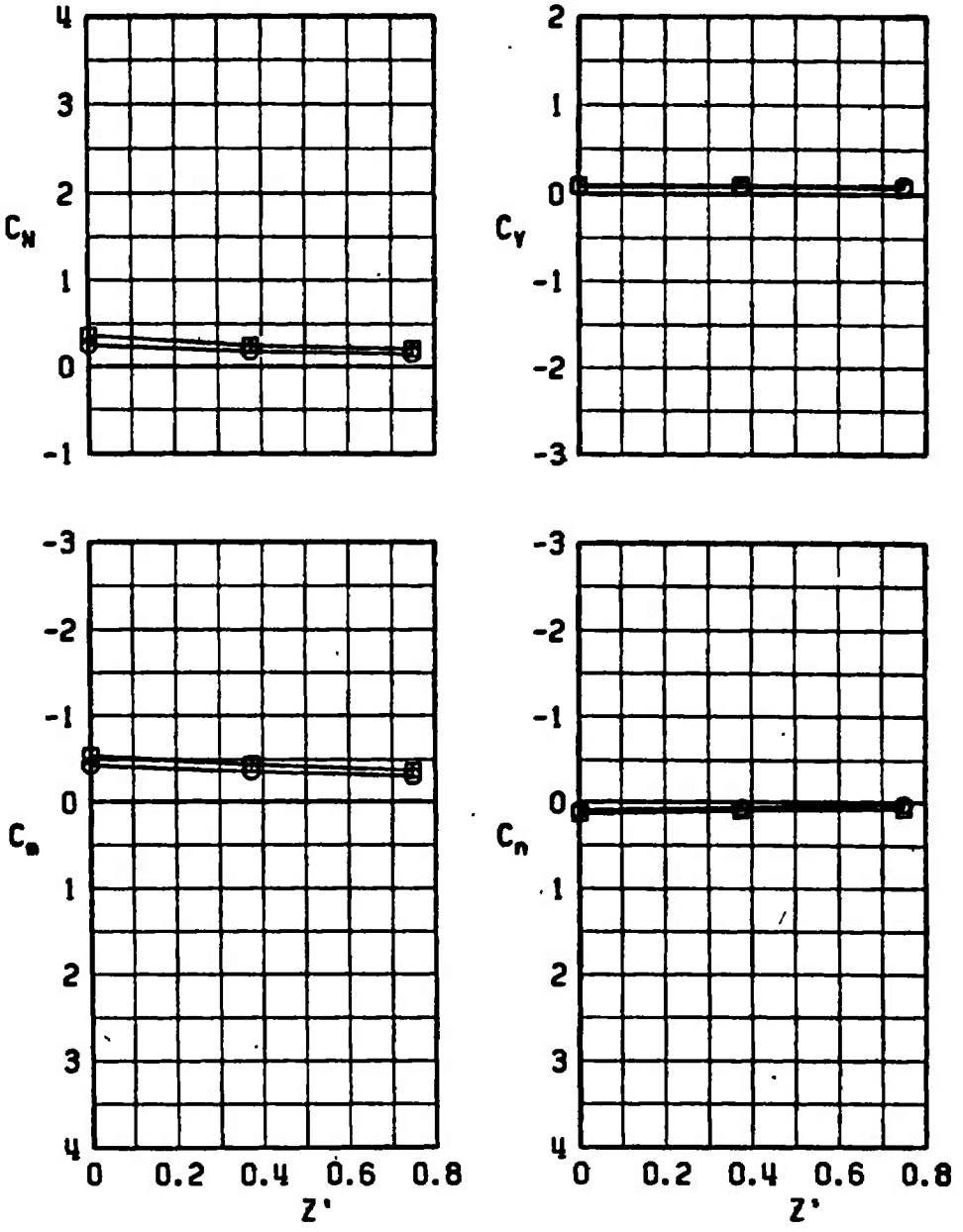

b. α = 0, Y' = -0.375

Fig. 35 Continued

SYMBOL	CONF	α	ℓ_p
⊙	17	6	2.400
⊡	18	6	2.400

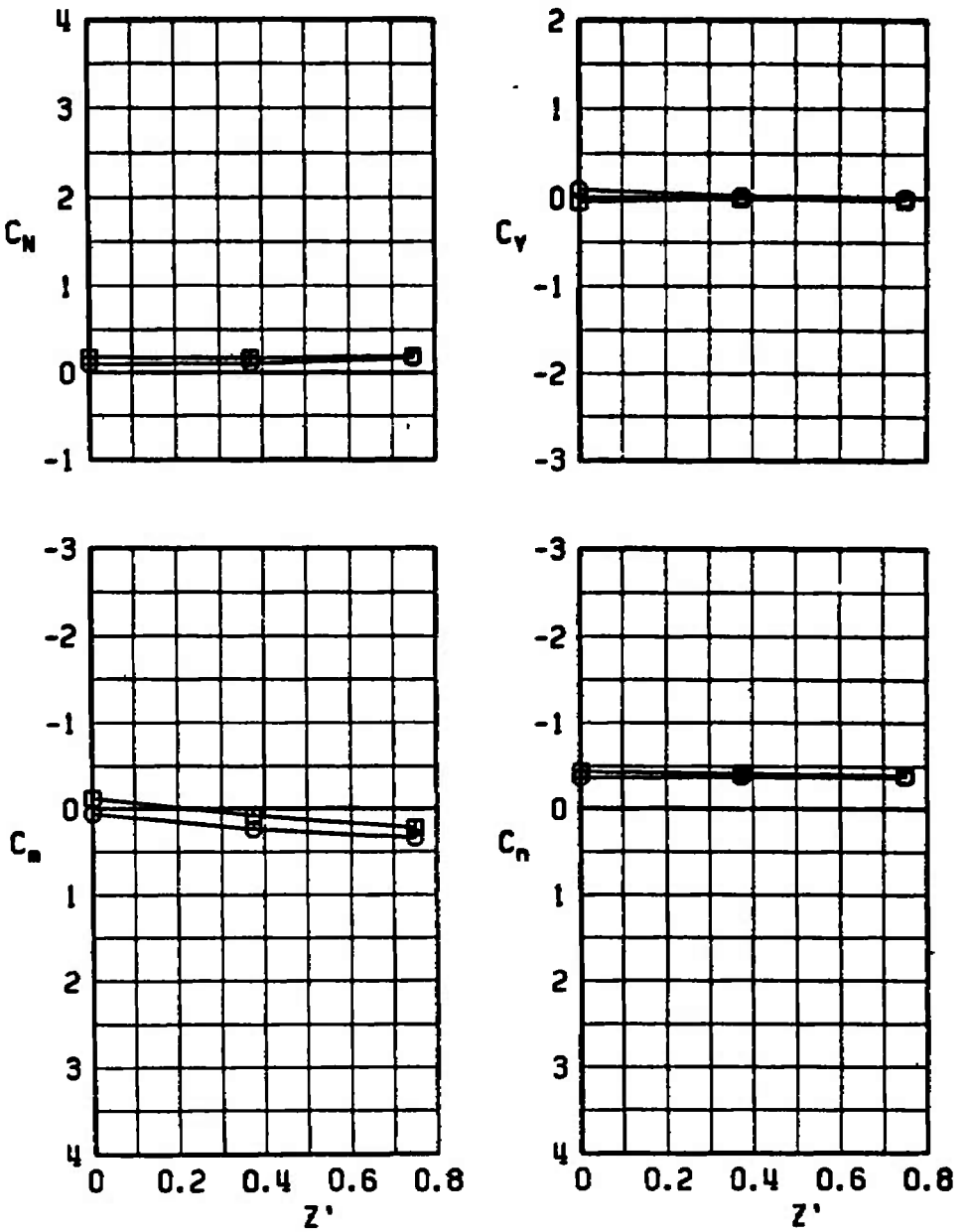

c. $\alpha = 6$, $Y' = 0$

Fig. 35 Continued

SYMBOL	CONF	α	ℓ_p
⊙	17	6	2.400
⊡	18	6	2.400

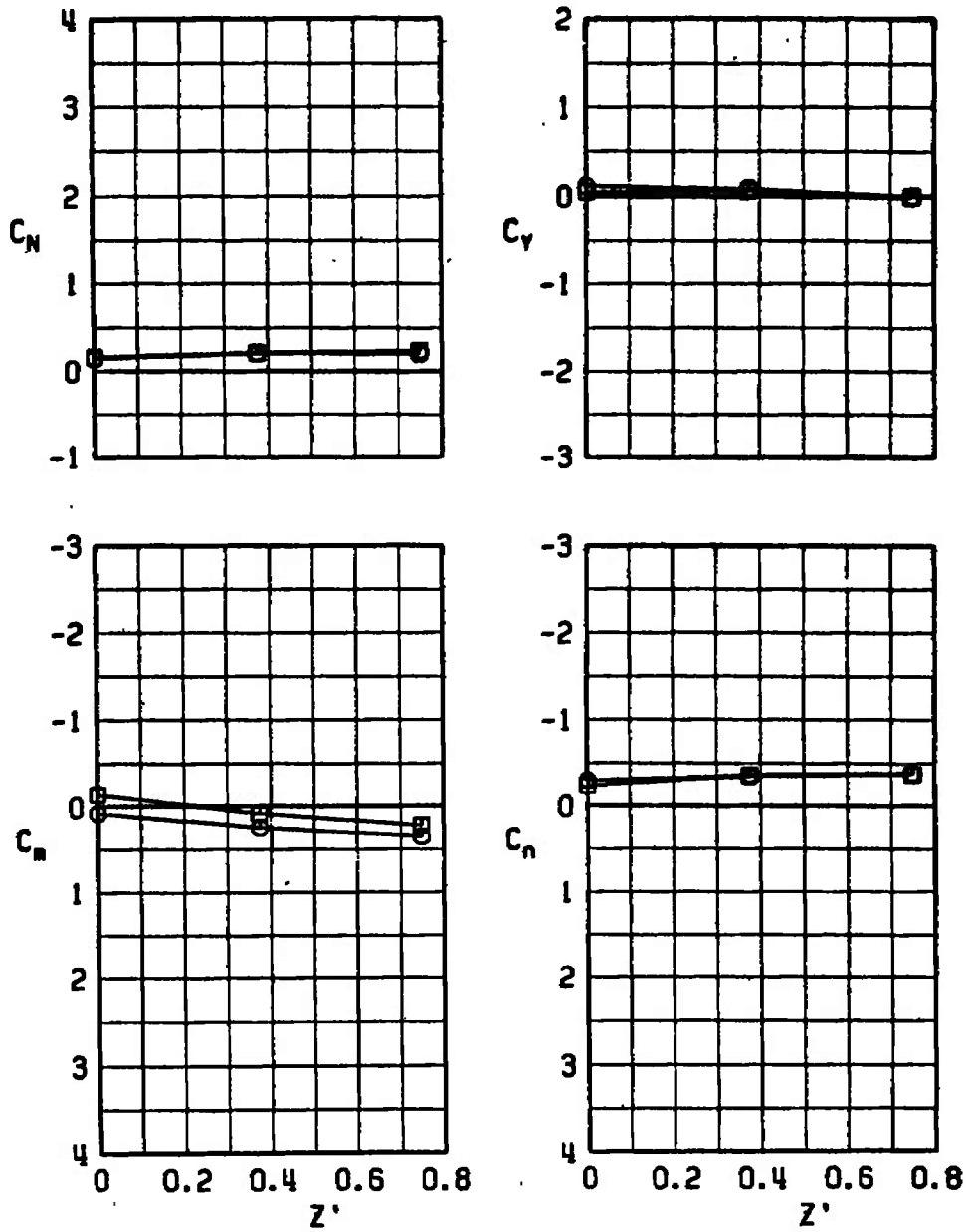

d. $\alpha = 6$, Y' = -0.375
Fig. 35 Concluded

SYMBOL	CONF	M_∞	α	WI	$\bar{m}$	ℓ_p
○	T-407	0.4	0	10	3.8825	0.375
□	T-407	0.4	0	10	3.8825	0.750
△	T-407	0.4	0	10	3.8825	2.400

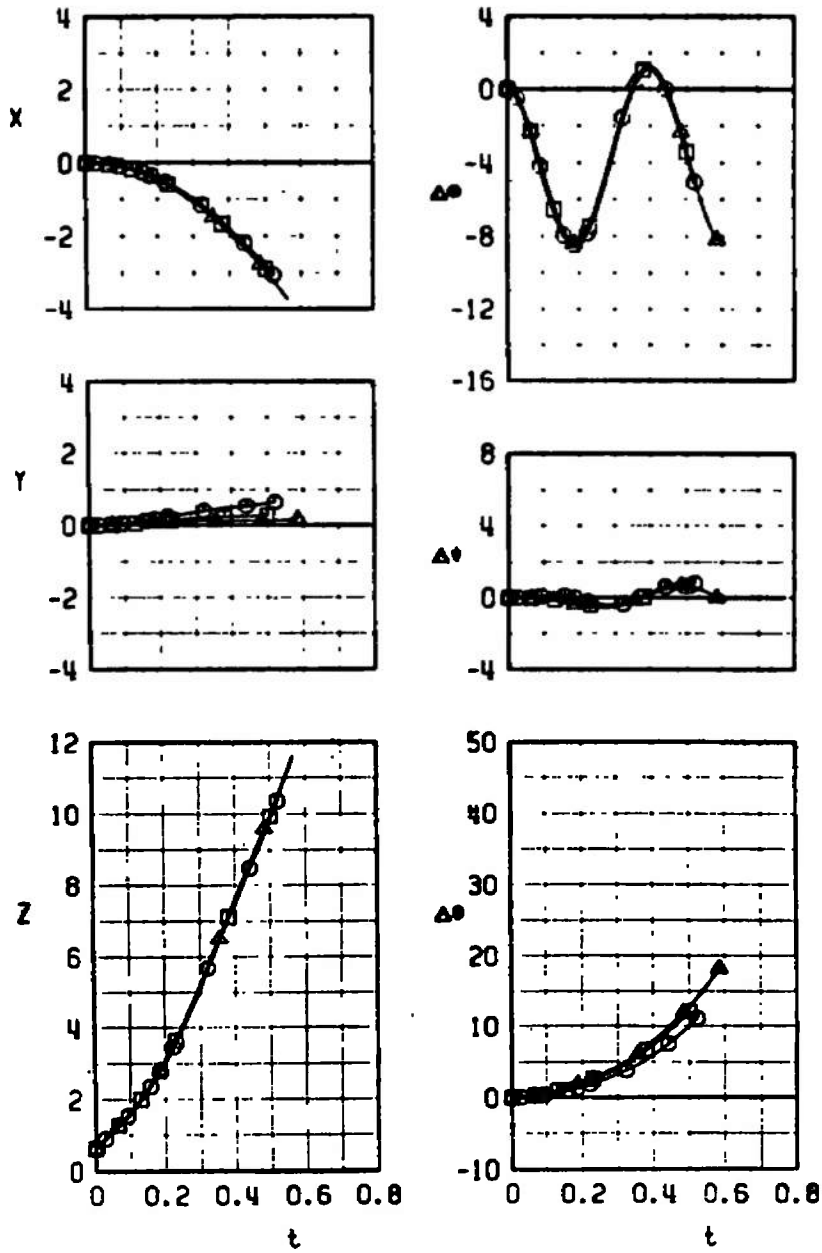

a. Configuration T-407

Fig. 36 Parent-Model Duct Flow Influence on Separation Trajectories of the Finned Large Model from the Wing 1/3-Semispan Pylon, α = 0 deg, M_∞ = 0.4

SYMBOL	CONF	M_∞	α	β	$\bar{m}$	ℓ_p
○	T-409	0.4	0	0	15.5300	0.375
□	T-409	0.4	0	0	15.5300	0.750
△	T-409	0.4	0	0	15.5300	2.400

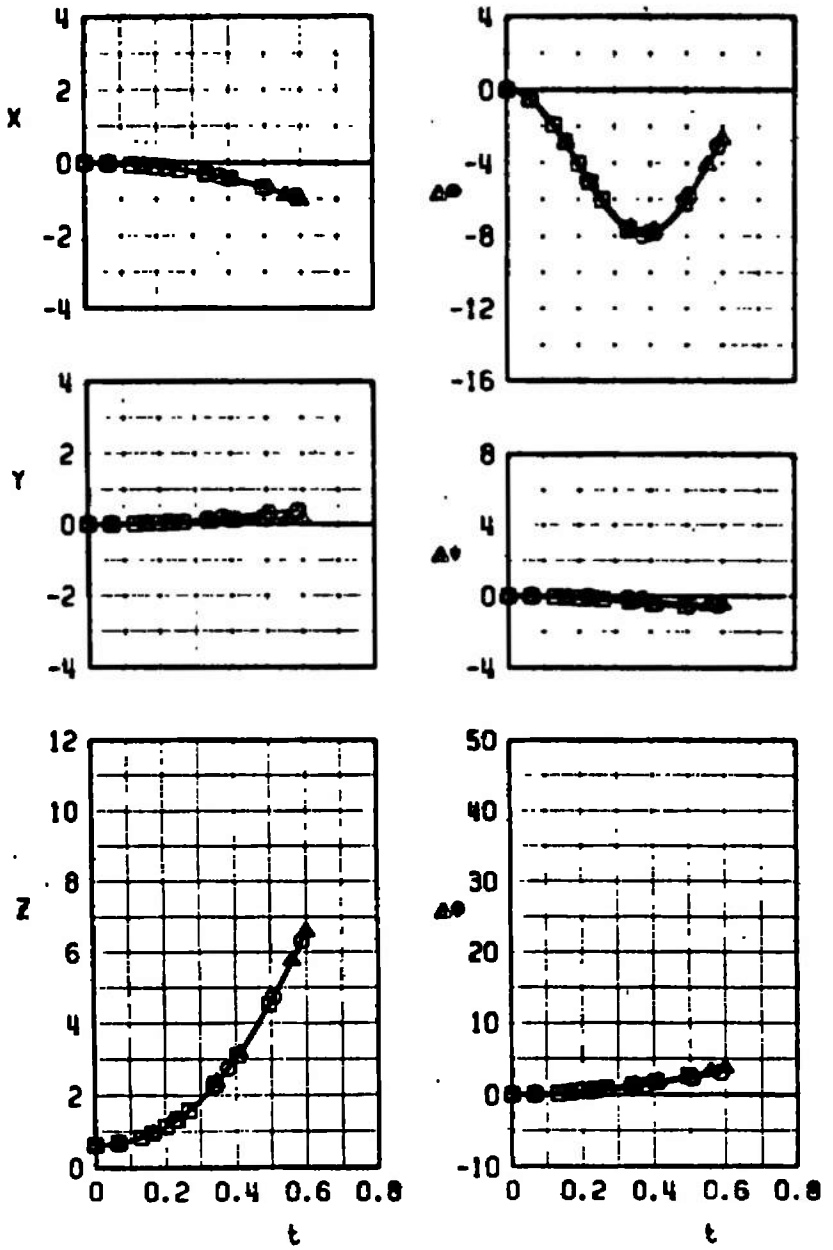

b. Configuration T-409
Fig. 36 Continued

SYMBOL	CONF	M_∞	α	WI	$\bar{m}$	ℓ_p
○	T-410	0.4	0	10	15.5300	0.375
□	T-410	0.4	0	10	15.5300	0.750
△	T-410	0.4	0	10	15.5300	2.400

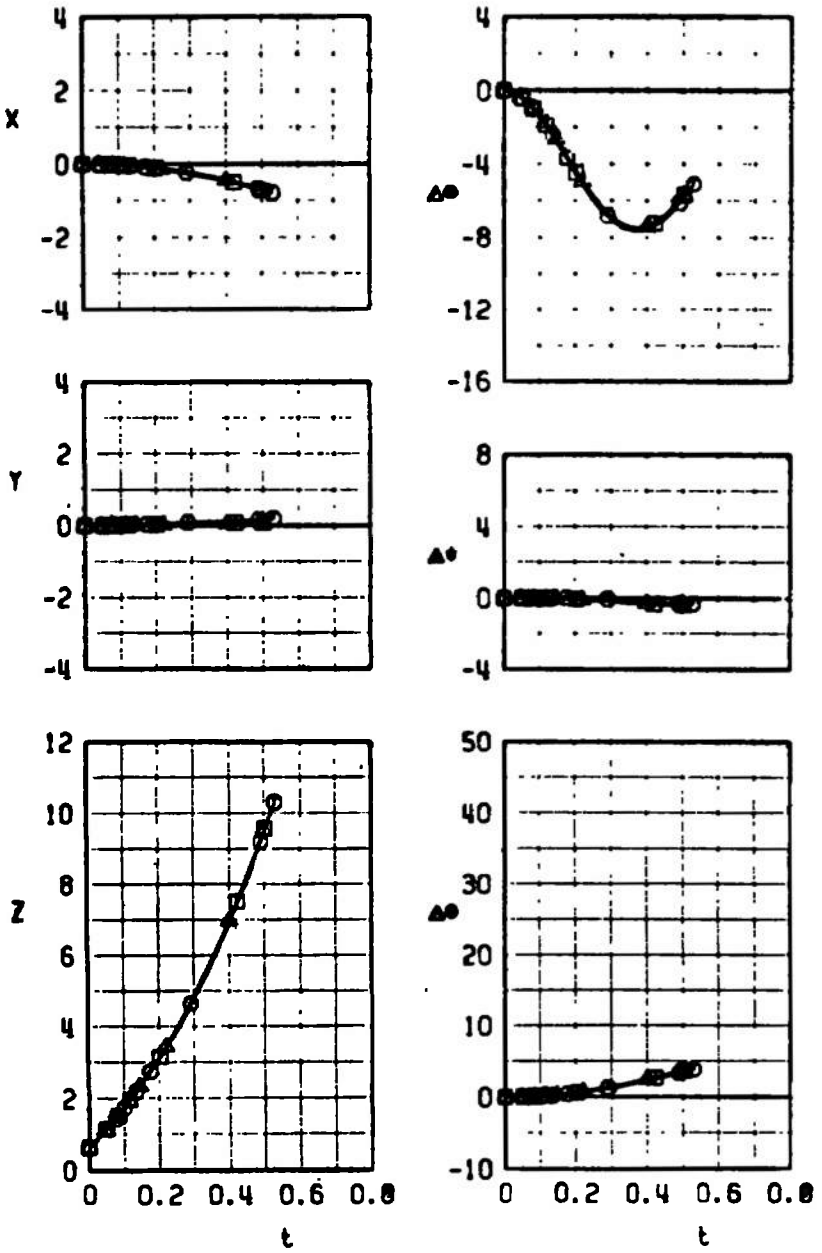

c. Configuration T-410
Fig. 36 Concluded

SYMBOL	CONF	M_∞	α	WI	$\bar{m}$	ℓ_p
○	T-408	0.4	6	10	3.8825	0.375
□	T-411	0.4	6	0	3.8825	0.750
△	T-412	0.4	6	10	3.8825	2.400

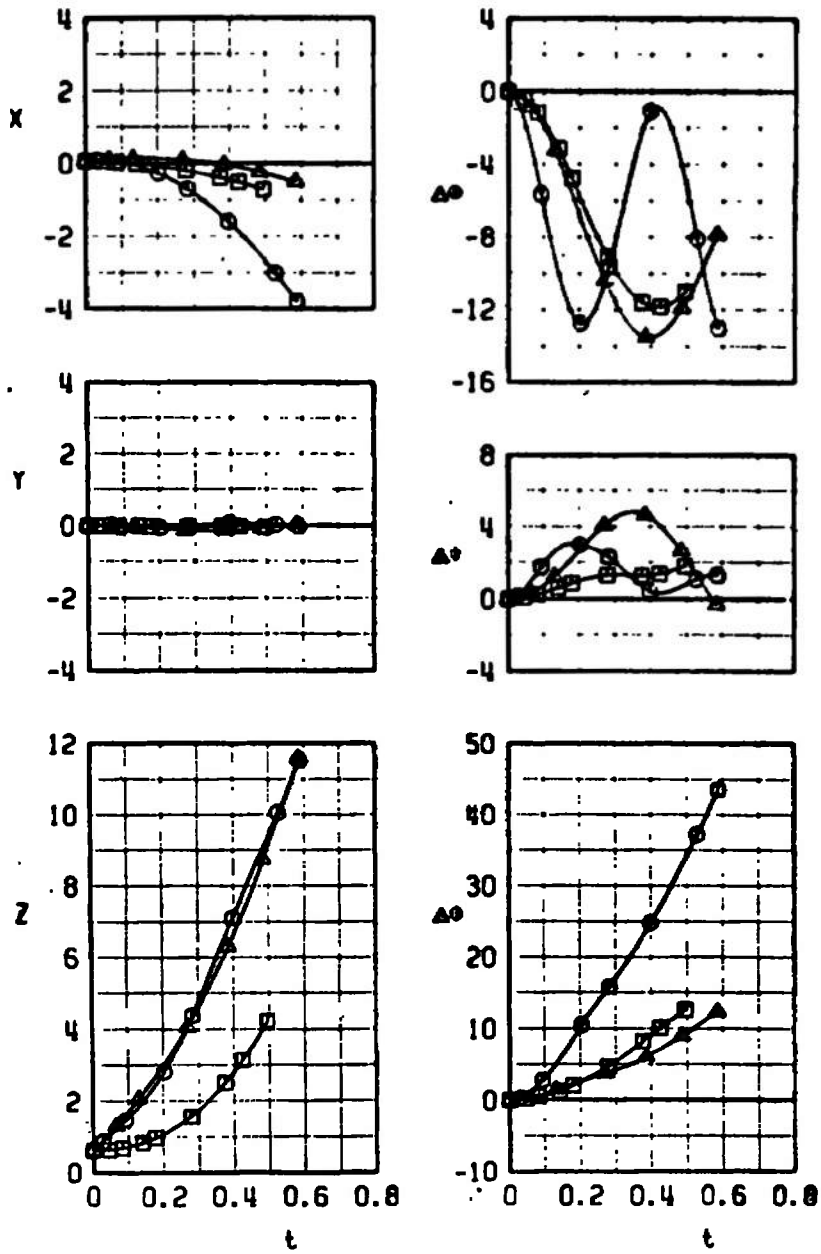

a. Configuration T-408

Fig. 37 Parent-Model Duct Flow Influence on Separation Trajectories of the Finned Large Model from the Wing 1/3-Semispan Pylon, α = 6 deg, M_∞ = 0.4

SYMBOL	CONF	M_∞	=	M1	$\bar{m}$	ℓ_p
○	T-411	0.4	6	0	15.5300	0.375
□	T-411	0.4	6	0	15.5300	0.750
△	T-411	0.4	6	0	15.5300	2.400

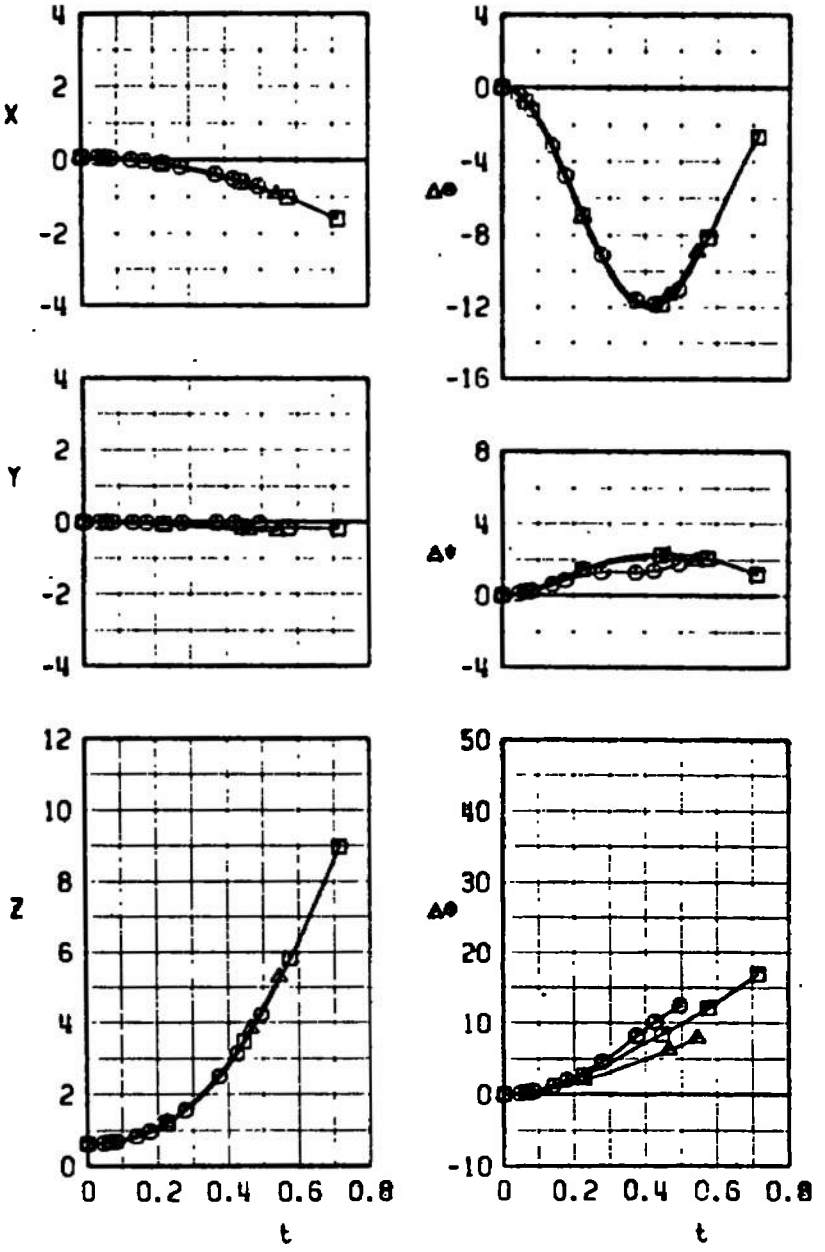

b. Configuration T-411
Fig. 37 Continued

SYMBOL	CONF	M_∞	α	M1	$\bar{m}$	ℓ_p
○	T-412	0.4	6	10	3.6825	2.4
□	T-412	0.4	6	10	15.5300	2.4
△	T-412	0.4	6	10	15.5300	2.4

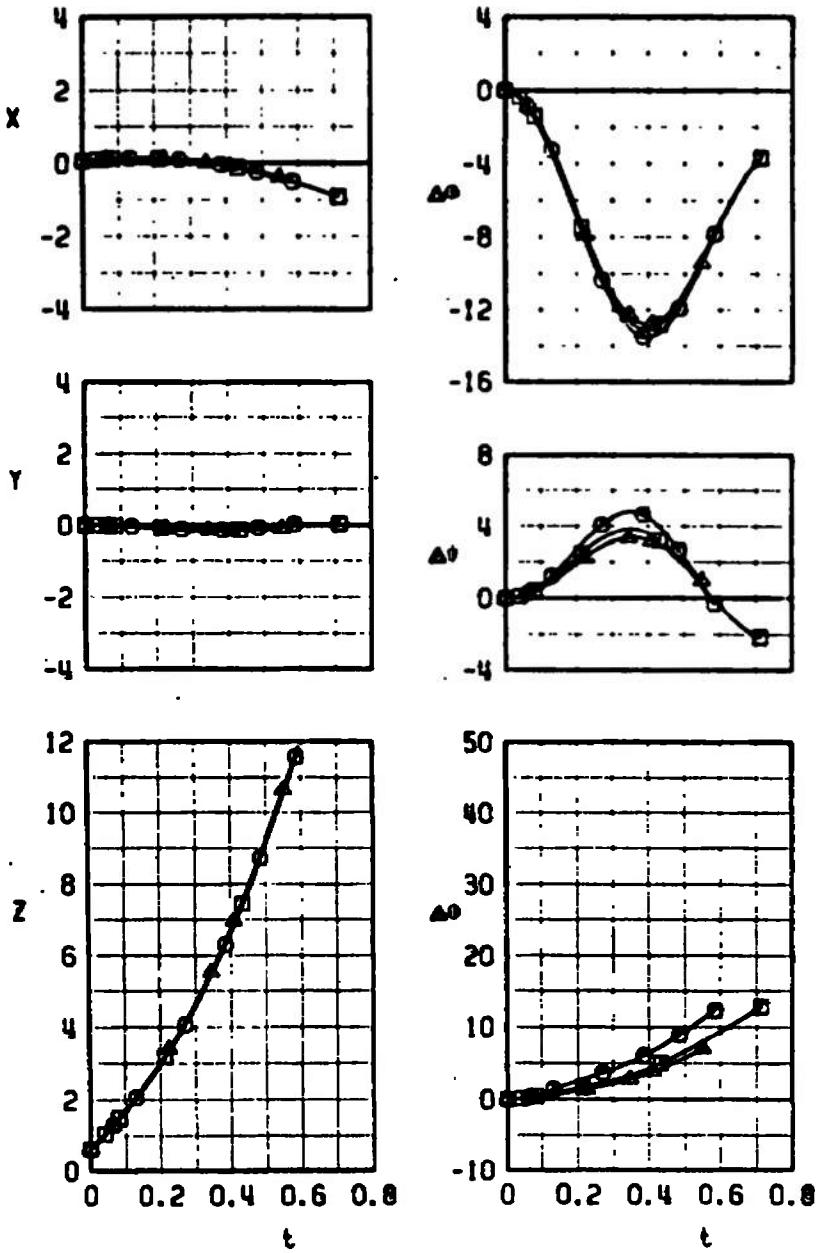

c. Configuration T-412
Fig. 37 Concluded

SYMBOL	CONF	M_∞	α	M1	$\bar{m}$	ℓ_p
○	T-413	0.7	6	10	15.5300	0.375
□	T-413	0.7	6	10	15.5300	0.750
△	T-413	0.7	6	10	15.5300	2.400

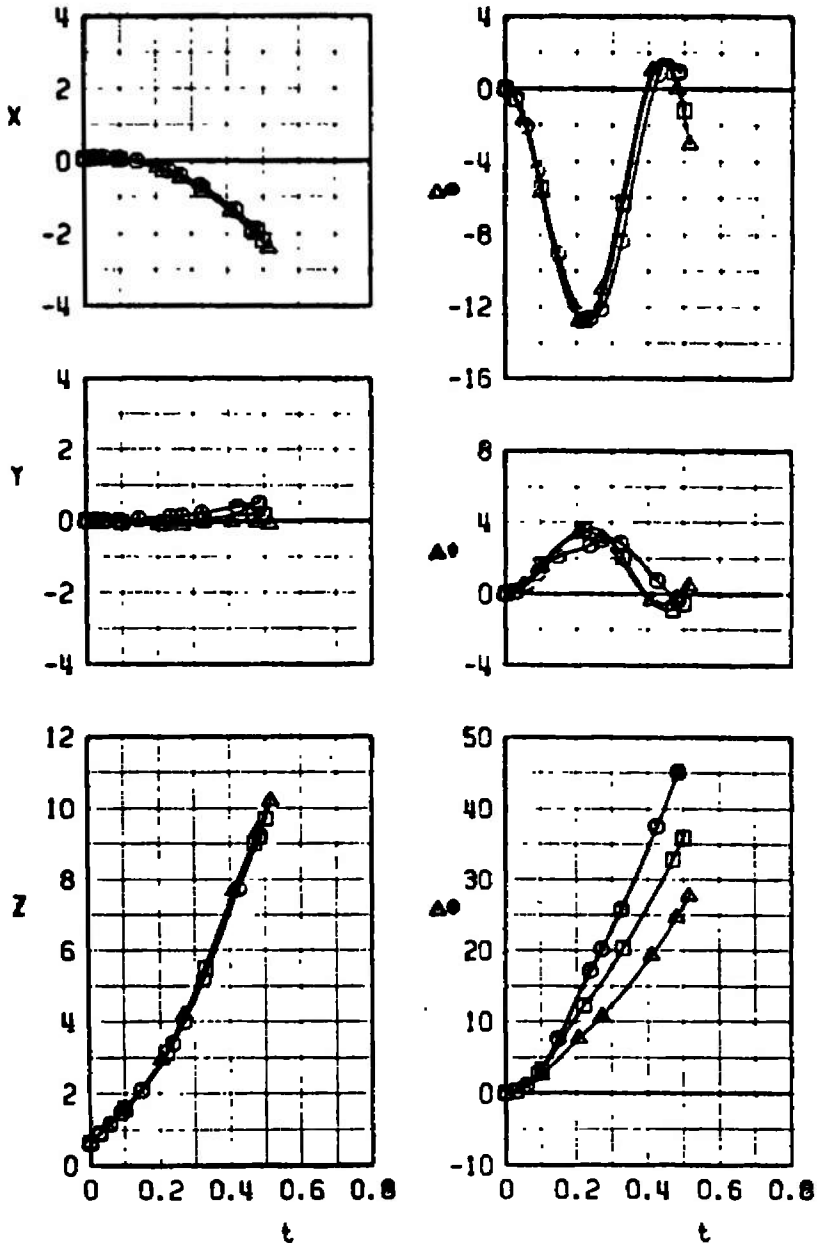

Fig. 38 Parent-Model Duct Flow Influence on Separation Trajectories of the Finned Large Model from the Wing 1/3-Semispan Pylon, α = 6 deg, M_∞ = 0.7

SYMBOL	CONF	M_∞	α	M1	m
○	T-412	0.4	6	10	15.5300
□	T-413	0.7	6	10	15.5300

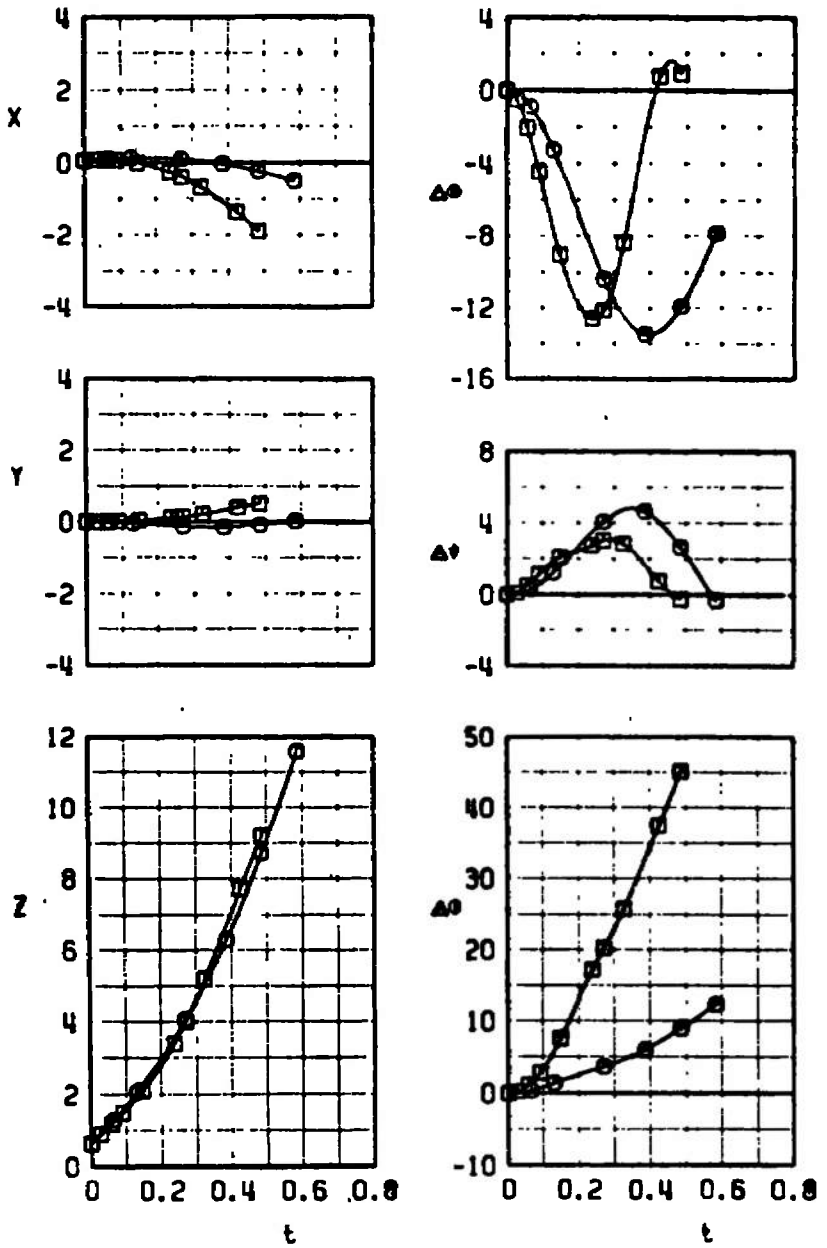

a. $\ell_p = 0.375$

Fig. 39 Comparison of Separation Trajectories of the Finned Large Model at M_∞ = 0.4 and 0.7 from the Wing 1/3-Semispan Pylon, α = 6 deg

SYMBOL	CONF	M_∞	α	M1	$\bar{m}$
○	T-412	0.4	6	10	15.5300
□	T-413	0.7	6	10	15.5300

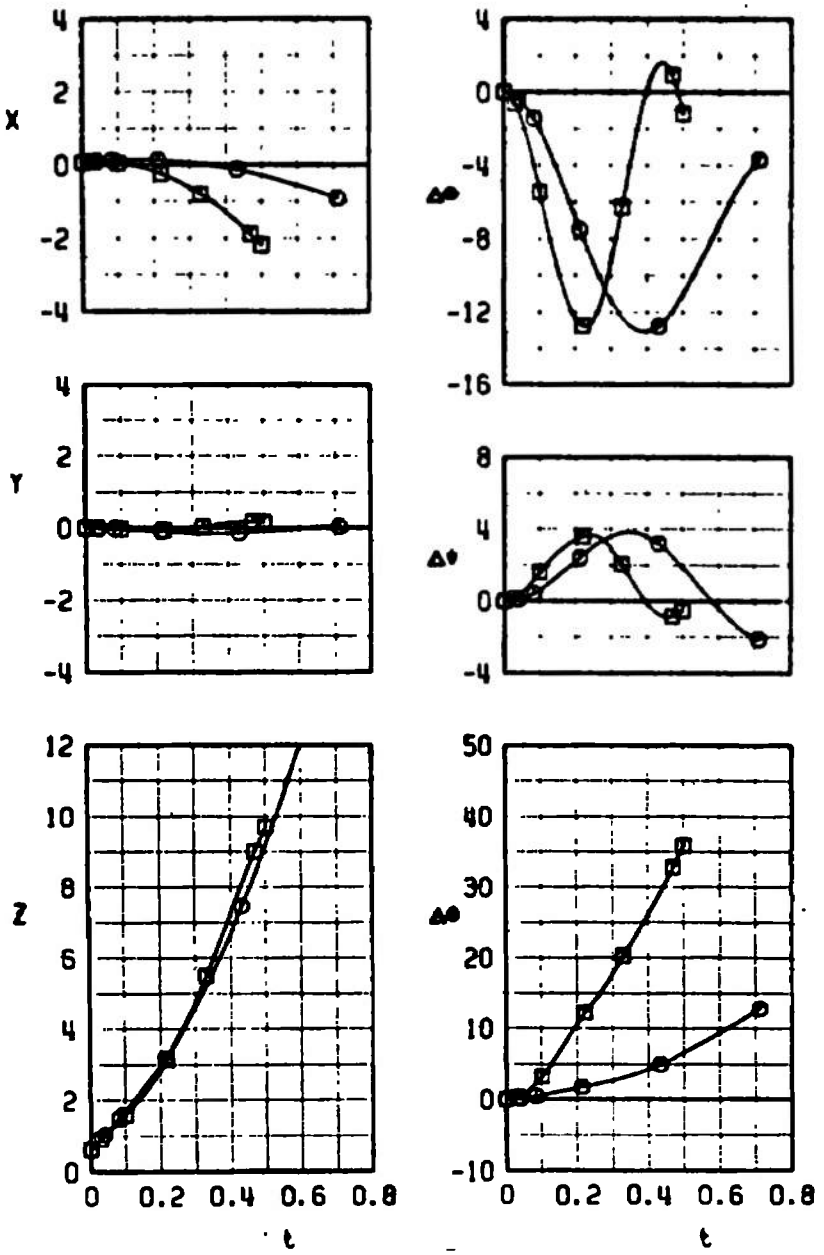

b. $\ell_p = 0.750$

Fig. 39 Continued

SYMBOL	CONF	M_∞	α	MI	$\bar{m}$
○	T-412	0.4	6	10	15.5300
□	T-413	0.7	6	10	15.5300

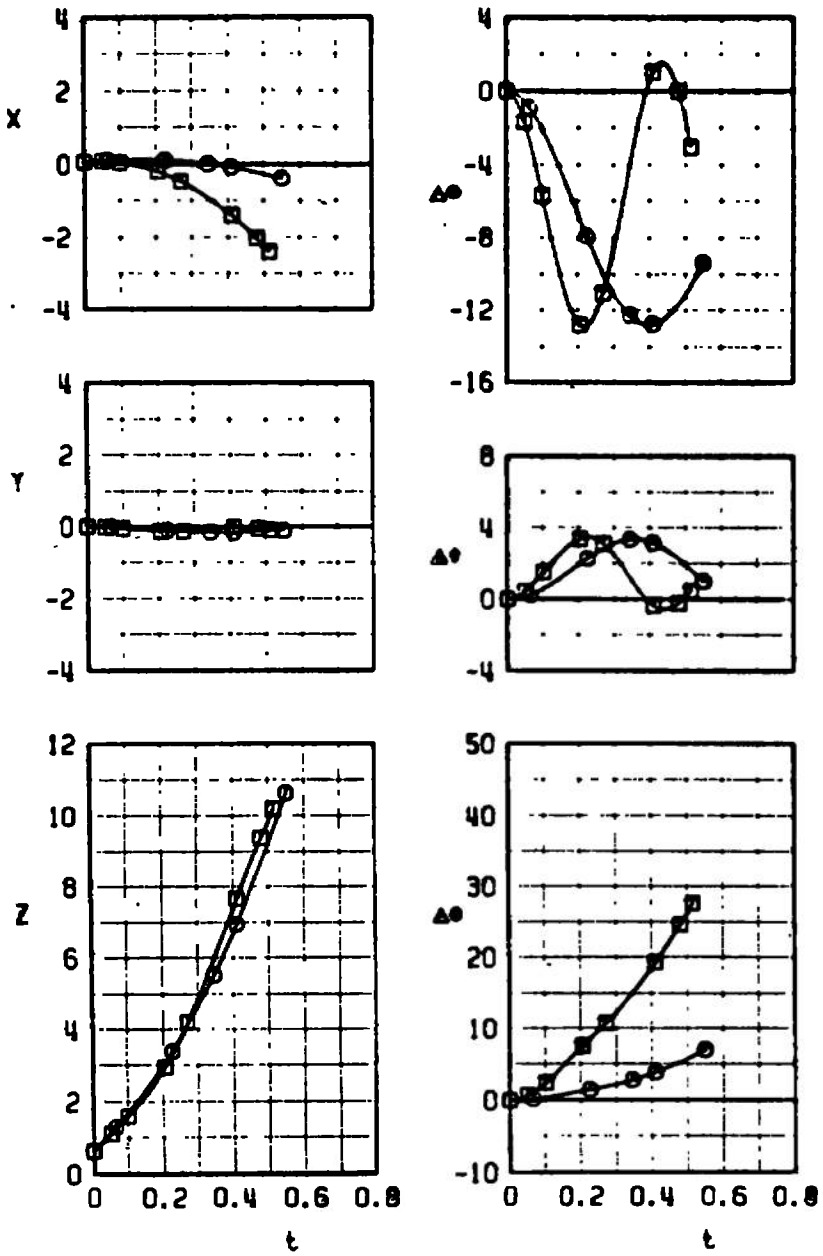

c. ℓ_p = 2.40

Fig. 39 Continued

SYMBOL	CONF	M_∞	α	WI	$\bar{m}$
○	T-405	0.4	6	10	15.5300
□	T-405	0.7	6	10	15.5300

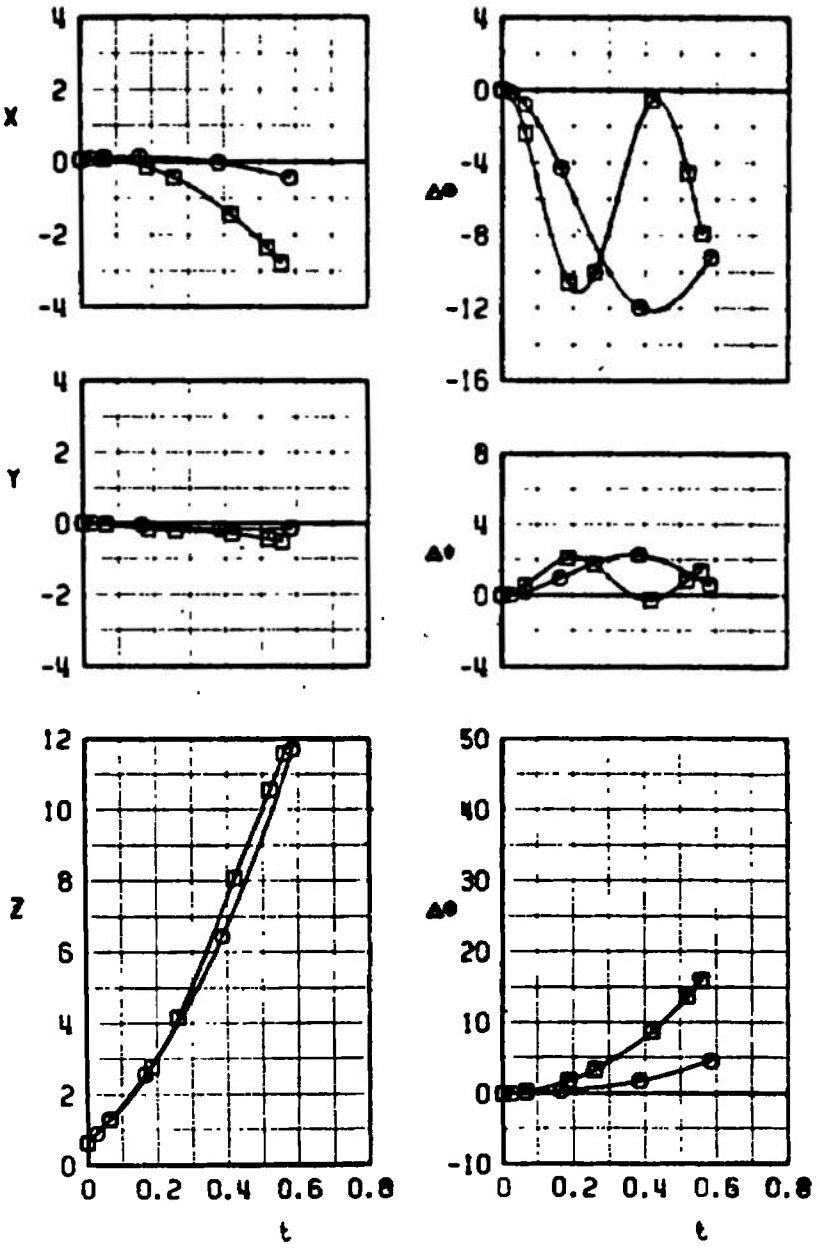

d. Without Ducts
Fig. 39 Concluded

SYMBOL	CONF	M_∞	α	MI	$\bar{m}$	ℓ_p
○	T-407	0.4	0	10	3.8825	2.4
□	T-409	0.4	0	0	15.5300	2.4
△	T-410	0.4	0	10	15.5300	2.4

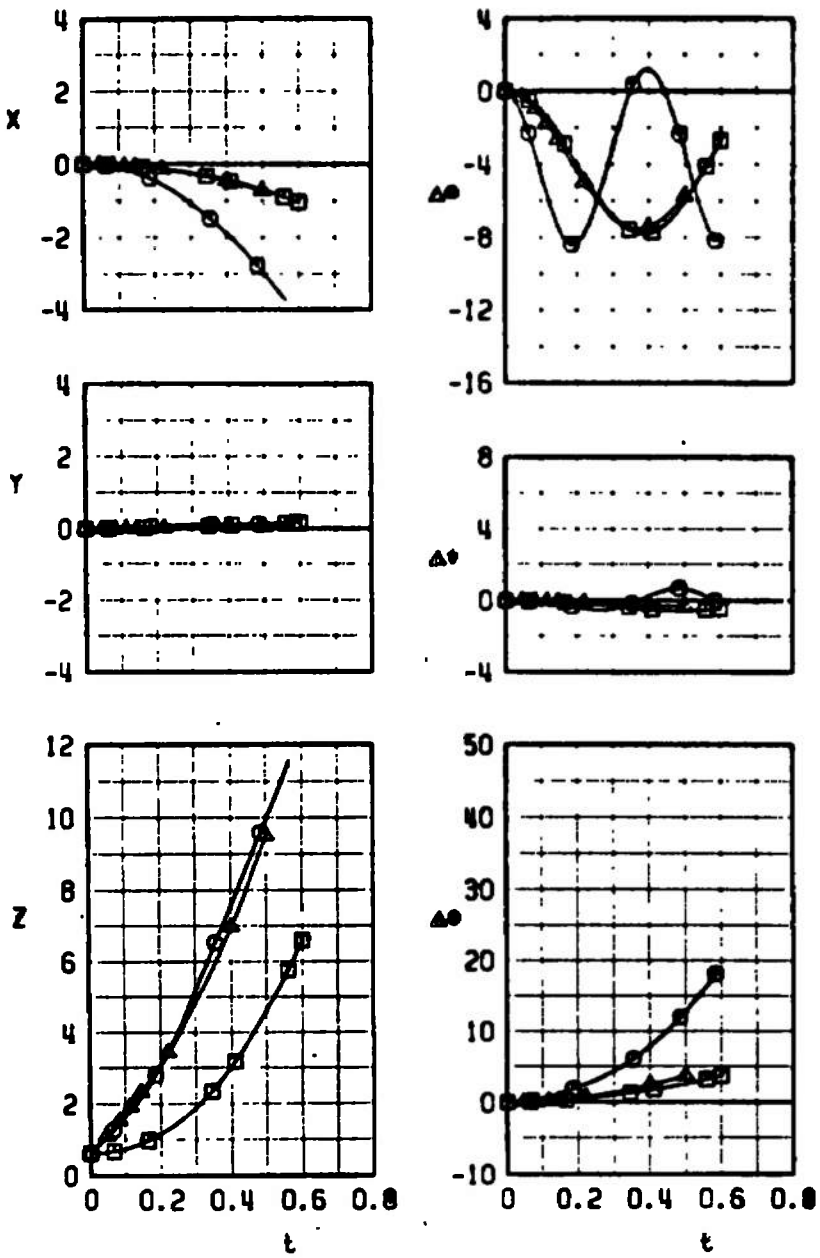

a. $N_1B_2WP_{1/3}A_2D$, $\alpha = 0$

Fig. 40 Separation Trajectories of the Finned Large Model from the 1/3-Semispan Pylon, $M_\infty = 0.4$

SYMBOL	CONF	M_∞	α	MI	$\bar{m}$	δ_p
○	T-408	0.4	6	10	3.8825	2.4
□	T-411	0.4	6	0	15.5300	2.4
△	T-412	0.4	6	10	15.5300	2.4

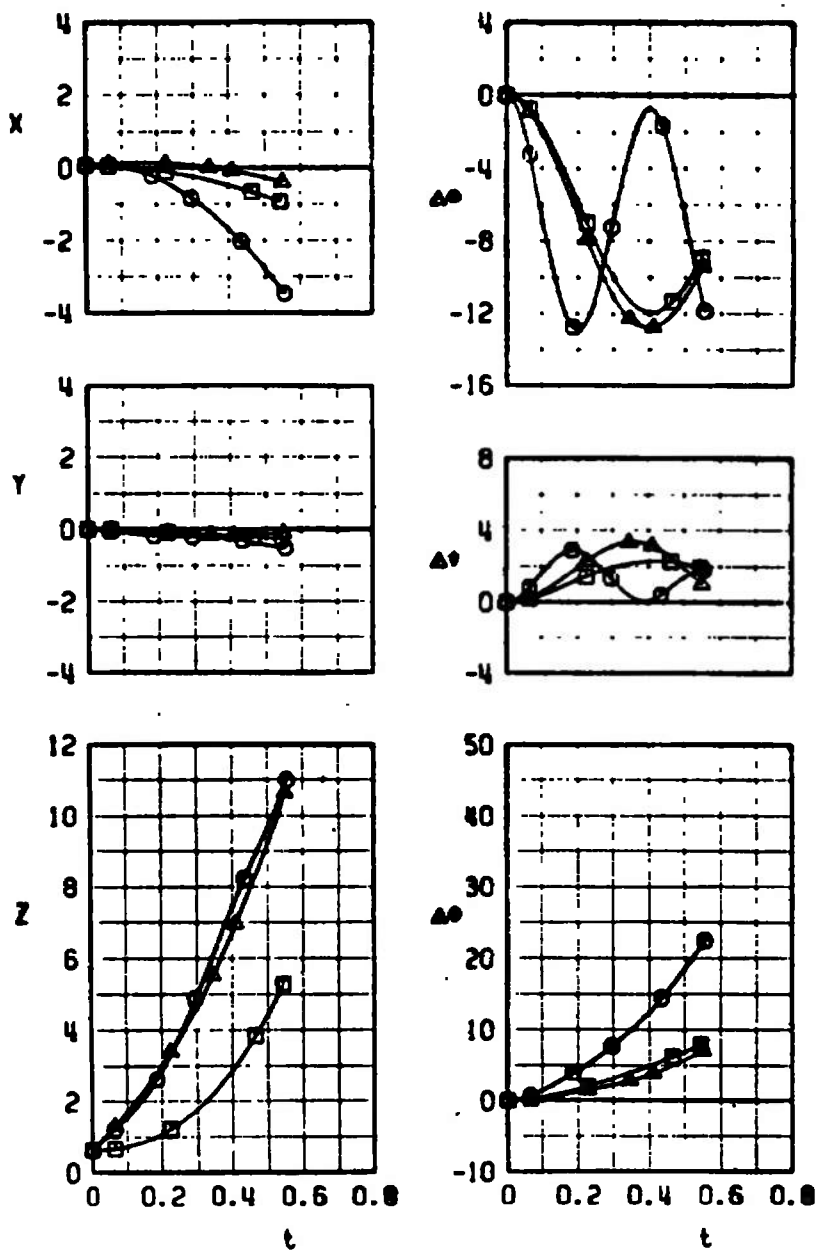

b. $N_1B_2WP_{1/3}A_2D$, $\alpha = 6$

Fig. 40 Continued

SYMBOL	CONF	M_∞	α	M1	$\bar{m}$
○	T-400	0.4	0	10	3.8825
□	T-402	0.4	0	0	15.5300
△	T-403	0.4	0	10	15.5300

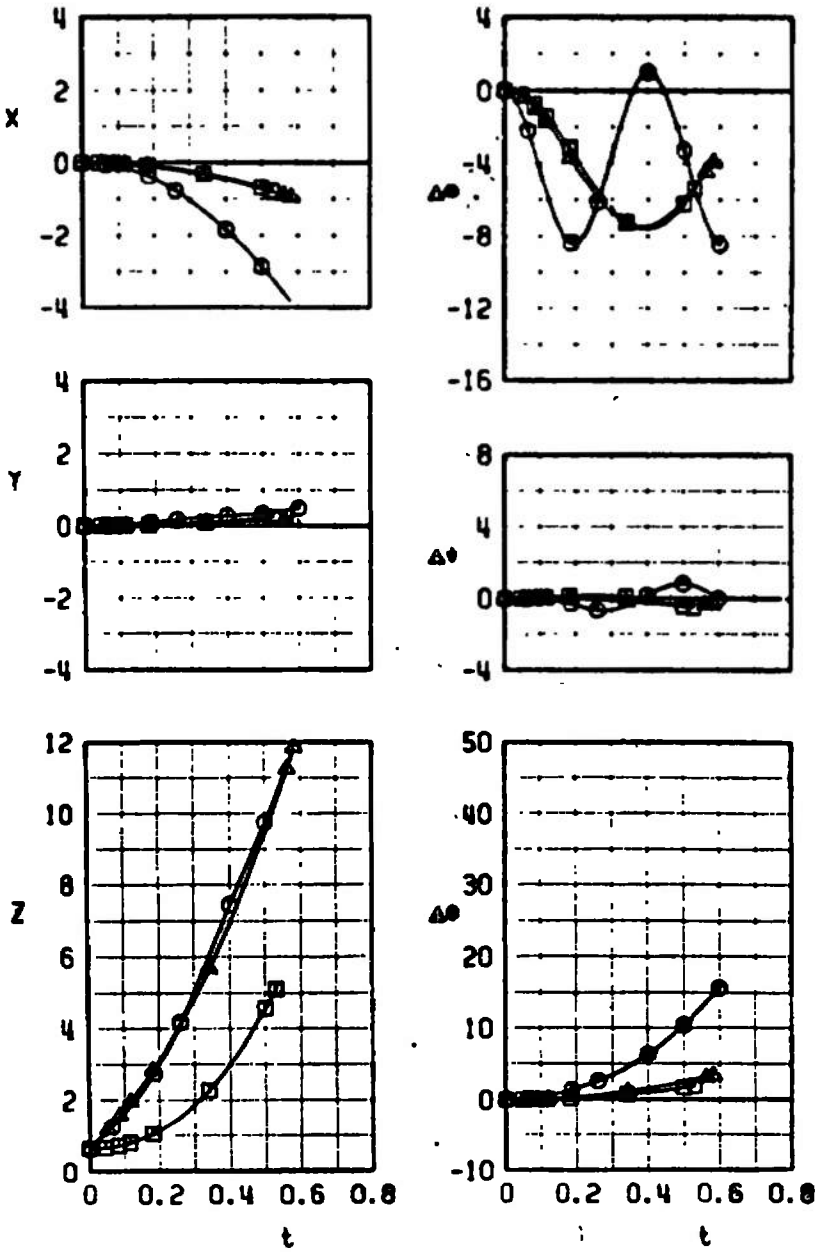

c. $N_1 B_2 WP_{1/3}$, $\alpha = 0$
Fig. 40 Continued

SYMBOL	CONF	M_∞	α	WI	$\bar{m}$
○	T-401	0.4	6	10	3.8825
□	T-404	0.4	6	0	15.5300
△	T-405	0.4	6	10	15.5300

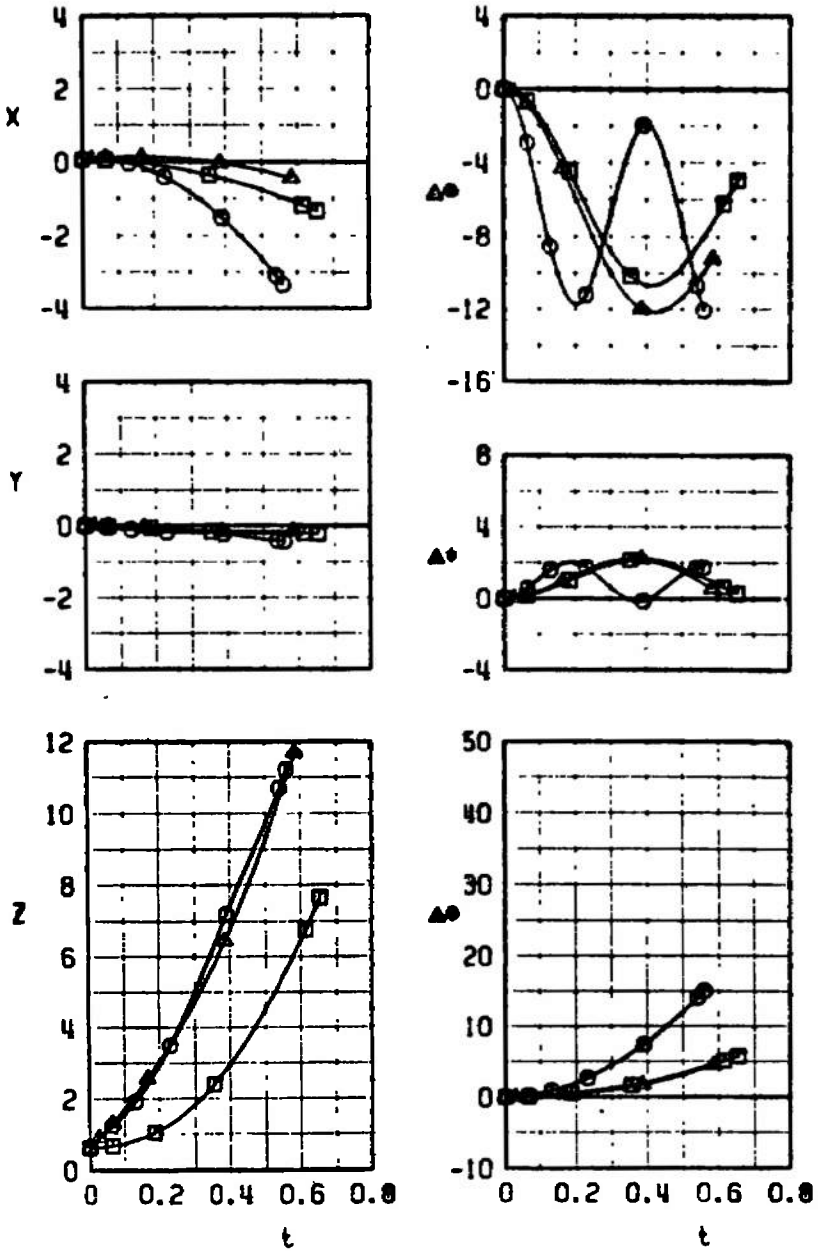

d. $N_1B_2WP_{1/3}$, $\alpha = 6$

Fig. 40 Concluded

TABLE I
FULL-SCALE STORE INITIAL CONDITIONS FOR CAPTIVE TRAJECTORY TESTING

Aircraft Position and Motion at Start of Trajectories					Store Initial Conditions Relative to the Carriage Position on the Pylon		
Aircraft Configuration	Duct Plug Position, ℓ_p, in.	Altitude, h, ft	Mach Number, M_∞	Angle of Attack, α, deg	Horizontal Forward Displacement, ft	Vertical Downward Displacement, ft	Vertical Downward Velocity, ft/sec
$N_1B_2WP_{1/3}$	N.A.	5,000	0.4	0	0	0.625	0 and 10
↓	↓	↓	0.4	6	0.06533	0.62158	0 and 10
↓	↓	↓	0.7	6	0.06533	0.62158	10
$N_1B_2WP_{1/3}A_2D$	0.375, 0.750, 2.40	↓	0.4	0	0	0.625	0 and 10
↓	↓	↓	0.4	6	0.06533	0.62158	0 and 10
↓	↓	↓	0.7	6	0.06533	0.62158	10

TABLE II
FULL-SCALE STORE PARAMETERS FOR CAPTIVE TRAJECTORY TESTING WITH THE FINNED LARGE FORCE MODEL (S_{LFF})

Parameter	Values
Model Scale Factor, λ	0.05
$\bar{m}$	3.8825 and 15.530
X_{cg}	5.31
S	1.228
d	1.25
I_{xx}	2.0 and 8.0
I_{yy}	20.0 and 80.0
I_{zz}	20.0 and 80.0
Pitch, Yaw, and Roll Damping Coefficients	0

TABLE III
BASIC CONFIGURATION NOMENCLATURE

Parent Aircraft

A_1	Body add-on without ducts
A_2	Body add-on with ducts
B_1	Short body
B_2	Long body
C_1	Canopy for N_1
D	Duct-flow controller assembly
N_1	Uncambered Nose
N_2	Cambered Nose
W	Wing

Pylons

$P_{1/3}$	1/3-semispan pylon
P_c	Fuselage centerline pylon

Stores

Probe	Flow-field probe
S_p	Pressure distribution store
S_{LFN}	Large force and moment store - no fins
S_{LFF}	Large force and moment store - with fins
S_{SUU-41}	Noncircular-cross-section dispenser type store
$S_{ESUU-41}$	Equivalent, axisymmetric store with area distribution of S_{SUU-41}

TABLE IV
CONFIGURATION IDENTIFICATION

Flow-Field Test

Conf. No.	Re/ft x 10^{-6}	M_∞	α, deg	Probe Movement X_p	Probe Movement Y_p	Probe Movement Z_p	ℓ_p, in.
FF1	3.6	0.4	0 to 15	14.66 to 18.66	3.2 and 4.0	0.99 to 2.492	0 to 2.4
FF1	↓	↓	↓	17.66 to 25.66	0 to 5.0	0.52 to 4.0	0 to 2.4
FF2				↓	↓	↓	NA
FF3							↓
FF4			0 to 12	14.66 to 25.66	0 to 4.0	0 to 4.0	
FF5			↓	4.0 to 13.0	2.2 to 4.0	0 to 1.0	
FF5				14.66 to 26.66	2.0 to 6.0	0	
FF6			0 to 15	14.66 to 26.66	2.0 to 6.0	0	
FF6			0 to 12	0 to 16.0	0 to 6.0	0 to 4.0	
FF6			↓	14.66 to 25.66	0 to 4.0	↓	
FF7				0 to 16.0	0 to 6.0		
FF8	↓	↓	0 to 15	14.66 to 26.66	2.0 to 6.0	0	↓

Force and Moment Tests

Conf. No.	Re/ft x 10^{-6}	M_∞	α, deg	Initial Store Position	Store Movement X′	Store Movement Y′	Store Movement Z′	ℓ_p, in.
1	3.6	0.4	-15 to 15	Tunnel ℄	NA	NA	NA	NA
2			-15 to 15	Tunnel ℄	NA	NA	NA	
3			0 to 15	1/3-Semispan Pylon	0	0	0 to 0.75	
4						0		
5						0 and -0.375		
6								
7								0.375, 0.750 and 2.40
8		0.4 and 0.7						
9		0.4		Fuselage ℄ Pylon		0		
10				1/3-Semispan Pylon		0 and -0.375		NA
11								NA
12								0.375, 0.750, and 2.40
13		0.4 and 0.7						
14	↓	0.4	↓	Fuselage ℄ Pylon	↓	0	↓	↓

TABLE IV (Concluded)

Pressure Tests									
Conf. No.	Re/ft x 10^{-6}	M_∞	α, deg	Initial Store Position	Store Movement				ℓ_p, in.
					X′	Y′	Z′	Roll	
15	3.6	0.4	0 and 6	1/3-Semispan Pylon	0	0 and -0.375	0 to +0.75	-175 to 175	NA
16									NA
17									0.375, 0.75, and 2.40
18		0.4 and 0.7							
19		0.4		Fuselage ℄ Pylon		0			
Trajectory Tests									
Conf. No.	Re/ft x 10^{-6}	M_∞	α, deg	Initial Store Position	Store Mass		W_1, ft/sec		ℓ_p, in.
T-400	3.6	0.4	0	1/3-Semispan Pylon	3.88		10		NA
T-401			6		3.88		10		
T-402			0		15.53		0		
T-403			0				10		
T-404			6				0		
T-405			6				10		
T-406		0.7	6						
T-407		0.4	0		3.88				0.375, 0.750, and 2.40
T-408			6		3.88				
T-409			0		15.53		0		
T-410			0				10		
T-411			6				0		
T-412			6				10		
T-413		0.7	6				10		

TABLE V
TEST SUMMARY

Configuration Number	Store Model	Basic Configuration
Flow-Field Tests		
FF-1	Probe	$N_1B_2WA_2D$
FF-2	↓	$N_1B_2WA_1$
FF-3	↓	N_1B_2W
FF-4	↓	$N_1B_1A_1$
FF-5	↓	$N_1B_1C_1$
FF-6	↓	N_1B_1
FF-7	↓	N_2B_1
FF-8	↓	Tunnel Empty
Force and Moment Tests		
1	S_{SUU-41}	Tunnel Empty
2	$S_{ESUU-41}$	Tunnel Empty
3	S_{SUU-41}	$N_1B_2WP_{1/3}$
4	$S_{ESUU-41}$	$N_1B_2WP_{1/3}$
5	S_{LFN}	N_1B_2W
6	↓	$N_1B_2WA_1$
7	↓	$N_1B_2WA_2D$
8	↓	$N_1B_2WP_{1/3}A_2D$
9	↓	$N_1B_2WP_cA_2D$
10	S_{LFF}	N_1B_2W
11	↓	$N_1B_2WA_1$
12	↓	$N_1B_2WA_2D$
13	↓	$N_1B_2WP_{1/3}A_2D$
14	↓	$N_1B_2WP_cA_2D$
Pressure Tests		
15	S_p	N_1B_2W
16	↓	$N_1B_2WA_1$
17	↓	$N_1B_2WA_2D$
18	↓	$N_1B_2WP_{1/3}A_2D$
19	↓	$N_1B_2WP_cA_2D$
Trajectory Tests		
T-400 to T-406	S_{LFF}	$N_1B_2WP_{1/3}$
T-407 to T-413	S_{LFF}	$N_1B_2WP_{1/3}A_2D$

UNCLASSIFIED

Security Classification

DOCUMENT CONTROL DATA - R & D

(Security classification of title, body of abstract and indexing annotation must be entered when the overall report is classified)

1 ORIGINATING ACTIVITY (Corporate author) Arnold Engineering Development Center Arnold Air Force Station, Tennessee 37389	2a. REPORT SECURITY CLASSIFICATION UNCLASSIFIED 2b GROUP N/A

3 REPORT TITLE

FLOW-FIELD CHARACTERISTICS AND AERODYNAMIC LOADS ON EXTERNAL STORES NEAR THE FUSELAGE AND WING PYLON POSITIONS OF A SWEPT-WING/FUSELAGE MODEL AT MACH NUMBERS OF 0.40 AND 0.70 - PHASE IV

4 DESCRIPTIVE NOTES (Type of report and inclusive dates)

Final Report - July 13, 1972 to February 10, 1973

5 AUTHORIS: (First name, middle initial, last name)

R. H. Roberts and J. R. Myers, ARO, Inc.

6 REPORT DATE March 1974	7a TOTAL NO OF PAGES 144	7b. NO OF REFS 0
8a CONTRACT OR GRANT NO b PROJECT NO 8219 c Program Element 62201F d	9a. ORIGINATOR'S REPORT NUMBER(S) AEDC-TR-73-87 9b. OTHER REPORT NO(S) (Any other numbers that may be assigned this report) ARO-PWT-TR-73-43	

10 DISTRIBUTION STATEMENT

Approved for public release; distribution unlimited.

11 SUPPLEMENTARY NOTES Available in DDC	12 SPONSORING MILITARY ACTIVITY Air Force Flight Dynamics Laboratory (AFFDL/FGC), Wright-Patterson AFB, OH 45433

13 ABSTRACT Experimental data were obtained to aid in the prediction of aerodynamic loads and separation-trajectory characteristics on stores under the influence of an aircraft flow field. Four types of data were obtained in the vicinity of a generalized aircraft model: (1) flow field surveys, using a 40-deg cone probe, to determine the local velocity field, (2) force and moment data on four store models, (3) pressure distribution data on an ogive-cylinder model, and (4) captive-trajectory store separation data on one store model. The generalized aircraft model consisted of a swept-wing/fuselage combination with rectangular, flow-through engine ducts. Pylon locations were on the fuselage centerline and at the wing 1/3-semispan. The effect of a systematic variation of duct flow was investigated in each phase of testing. Testing was accomplished at Mach numbers 0.4 and 0.7, a Reynolds number of 3.6 million per foot, and aircraft and store angles of attack varying from 0 to 15 deg. Results of the test show that duct flow had little effect on the parameters investigated on all phases of testing, except at the higher Mach number where small variations in the coefficients or trajectories were evident. In general, the variations of parameters investigated for all test configurations followed an orderly pattern and should be amenable to the formulation of a generalized analytical store separation prediction method.

DD FORM 1 NOV 65 1473

UNCLASSIFIED

Security Classification

14. KEY WORDS	LINK A		LINK B		LINK C	
	ROLE	WT	ROLE	WT	ROLE	WT
jet aircraft						
external stores						
subsonic flow						
wind tunnel tests						
aerodynamic loads						
flow distribution						
separation characteristics						
ducts						
duct flow						